Yin Liu
Kurt–Schumacher-Str. 46
D–67663 Kaiserslautern
Gebourtsort: Beijing/China

Modelling and Simulation of Service Area Based OFDM Air Interfaces for Beyond 3G Mobile Radio Systems

deutscher Titel:

Modellierung und Simulation von OFDM–Luftschnittstellen für Mobilfunksysteme jenseits der dritten Generation auf der Basis von Service–Gebieten

Vom Fachbereich Elektrotechnik und Informationstechnik

der Technischen Universität Kaiserslautern

zur Verleihung des akademischen Grades

Doktor der Ingenieurwissenschaften (Dr.–Ing.)

genehmigte Dissertation

von

M.Sc. Yin Liu

D 386

Tag der Einreichung:	2. Dezember 2004
Tag der mündlichen Prüfung:	11. Februar 2005
Dekan des Fachbereichs Elektrotechnik:	Prof. Dr.–Ing. G. Huth
Vorsitzender der Prüfungskommission:	Prof. Dr.–Ing. habil. A. Potchinkov
1. Berichterstatter:	Prof. Dr.–Ing. habil. Dr.–Ing. E. h. P.W. Baier
2. Berichterstatter:	Prof. Dr.–Ing. R. Zengerle

Vorwort

Die vorliegende Arbeit entstand in der Zeit von November 2001 bis Februar 2005 im Rahmen meiner Tätigkeit als wissenschaftliche Mitarbeiterin Prof. Dr.–Ing. habil. Dr.–Ing. E. h. P. W. Baiers am Lehrstuhl für hochfrequente Signalübertragung und –verarbeitung der Technischen Universität Kaiserslautern. Ich möchte all jenen danken, die mich bei der Entstehung dieser Arbeit unterstützt haben.

Mein besonderer Dank ergeht an Herrn Prof. Baier für die Anregung, die Betreuung und die Förderung meiner Arbeit. Durch seine stete Diskussionsbereitschaft sowie durch zahlreiche Ratschläge und Hinweise hat er wesentlich zum Gelingen dieser Arbeit beigetragen.

Herrn Prof. Dr.–Ing. R. Zengerle danke ich für zahlreiche sehr hilfreiche Hinweise für die kritisch–kooperative Durchsicht der Dissertation und für die Übernahme des Korreferats. Weiterhin danke ich dem Vorsitzenden der Promotionskommission, Herrn Prof. Dr.–Ing. habil. A. Potchinkov. Im Rahmen meiner wissenschaftlichen Arbeit entstand auch eine enge Kooperation mit der Arbeitsgruppe Prof. Dr. H. Rohlings, TU Hamburg-Harburg, aus der wichtige Anregungen und Hinweise für meine Arbeit resultierten.

Den jetzigen und den ehemaligen Kollegen am Lehrstuhl für hochfrequente Signal–übertragung und –verarbeitung danke ich für die angenehme Arbeitsatmosphäre und für viele fruchtbare Diskussionen, die mir oftmals weitergeholfen haben. Ein besonderer Dank ergeht an Herrn Dr.–Ing. habil. T. Weber für die Betreuung und die Unterstützung beim Einarbeiten in das JOINT–Konzept und für die freundschaftliche Zusammenarbeit in gemeinsamen Projekten. Weiterhin bedanke ich mich herzlich bei den Herren Dr.–Ing. A. Sklavos und Dr.–Ing. I. Maniatis für die gute Zusammenarbeit.

Mein Dank gebührt auch der Siemens AG, insbesondere den Herren Dr.–Ing. E. Schulz und Dipl.–Ing. W. Zirwas, für die Förderung meiner Arbeit und viele fruchtbare Diskussionen.

Der Technischen Universität Kaiserslautern danke ich für die Möglichkeit die leistungsfähigen Rechner des Regionalen Hochschulrechenzentrums Kaiserslautern (RHRK) zu benutzen. Den Mitarbeitern des RHRK danke ich für die Beratung und die Hilfestellung in Rechnerfragen.

Ein weiterer Dank ergeht an alle Studenten, die im Rahmen ihrer Studien–, Diplom– und Masterarbeiten sowie als wissenschaftliche Hilfskräfte unter meiner Anleitung

Beiträge zu dieser Arbeit geleistet haben.

Nicht zuletzt möchte ich mich bei meinem Mann Tao Tang und meiner Schwester Yi Liu bedanken, die mir immer ein großer Rückhalt waren. Ganz besonders herzlich danke ich meiner Mutter Liqin Lin und meinem Vater Tonglin Liu. Sie haben mir das Studium der Elektrotechnik ermöglicht und mich immer nach besten Kräften unterstützt. Ihnen ist diese Arbeit gewidmet.

在此，我要感谢我的父亲刘桐林先生、母亲林丽钦女士以及我的姐姐刘怡女士，特别还有我的丈夫汤涛先生。是他们一直以来对我无私的关爱与支持，令我能够顺利完成博士的学业与工作。

Kaiserslautern, im Februar 2005

Yin Liu

Contents

Chapter 1
Introduction

1.1 Service area based architectures versus cellular architectures

Even though 3G mobile radio networks up to now have not yet come widely into operation, already today research activities directed towards the definition and design of Beyond 3G (B3G) systems are being started in many parts of the world [WM02, Nat03, EKLG$^+$03]. According to the observations made in connection with the emergence of 2G and 3G systems, the time, which elapses from the first system considerations until eventually system operation commences, easily reaches one decade. Therefore, today's activities towards B3G systems are far from being premature. Among the various demands put by operators and potential users on B3G systems, the flexible support support of data rates significantly above those typical of 2G and 3G systems is of paramount importance [TNA$^+$01]. Because also in the future the available and allotted frequency bands will be a scarce resource, the support of high data rates requires system designs which make optimum use of the assigned frequency spectrum and thus guarantee a high spectrum efficiency. Spectrum efficiency can be enhanced by measures on different layers of the ISO/OSI reference model [EF86]. Basically, we can discern between measures on the physical layer, which beneficially exploit the phenomena of wave propagation, and measures on higher layers, which aim at making optimum use of the resources offered by the physical layer by assigning them advantageously to the different communication links. In a balanced system design, measures on all layers would interplay in such a way that spectrum efficiency is maximized. As a basis for such a maximization, the physical layer deserves special attention. This thesis deals with a novel architecture of the physical layer suitable for B3G systems.

As a rule, in conventional 2G [RW95, EV97, Wal98] cellular architectures mobile terminals (MTs) of each cell are radio linked exclusively to the base station (BS) of their individual cell. This is also true for 3G [ETS97a, Wal98] cellular architectures with the exception of the few MTs being in soft handoff. The straightforward assignment of MTs to BSs is advantageous with respect to the signalling requirements, but it has the following drawbacks:

- In the uplink (UL), the signals radiated by the MTs not only impinge at their own BS as desired signals, but also at the BSs of other cells as undesired signals.
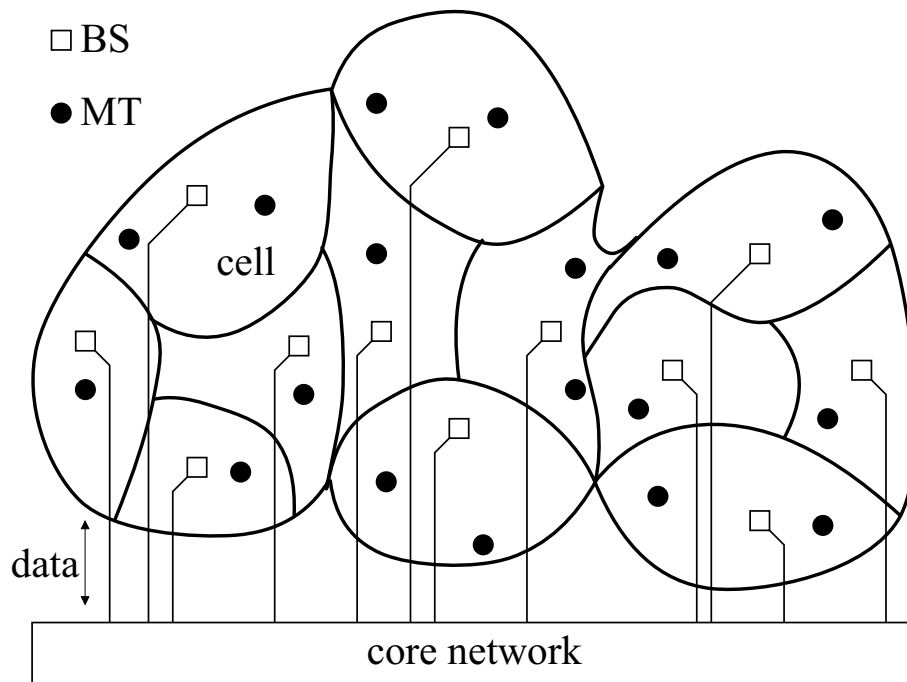
Fig. 1.1. Conventional cellular architecture, example with 12 cells

- In the downlink (DL), the signals radiated by the BS not only impinge at their own MTs as desired signals, but also at MTs of other cells as undesired signals.

The mentioned undesired signals act as interference instead of being constructively utilized. This detrimental effect is particularly pronounced if rather high transmit powers are required in order to compensate the high propagation losses in the case of MTs being far away from their BS or suffering from heavy shadowing.

In the novel architecture proposed in this thesis, instead of individual BSs access points (APs) are introduced with groups of such APs being linked to a central unit (CU). Each such group defines a service area (SA), and the MTs of each SA can communicate with the SA–specific CU via all APs of the SA. By means of Figs. 1.1 and 1.2 the conventional cellular architecture [MD79, DB96, Gib99, Wes02] and the novel SA based architecture [WMSL02] are compared with each other. Fig. 1.1 shows a conventional cellular architecture. Each cell contains a BS, and the MTs of each cell communicate solely with this BS. All BSs are connected to a central entity termed core network in Fig. 1.1, which, in the case of GSM, consists of the base station controllers and the mobile switching centers [RW95, EV97, Wal98]. The core network can be considered the data source and data sink in the communication with the MTs. Fig. 1.2 shows the novel SA based architecture. Instead of a number of cells – each with a BS – of
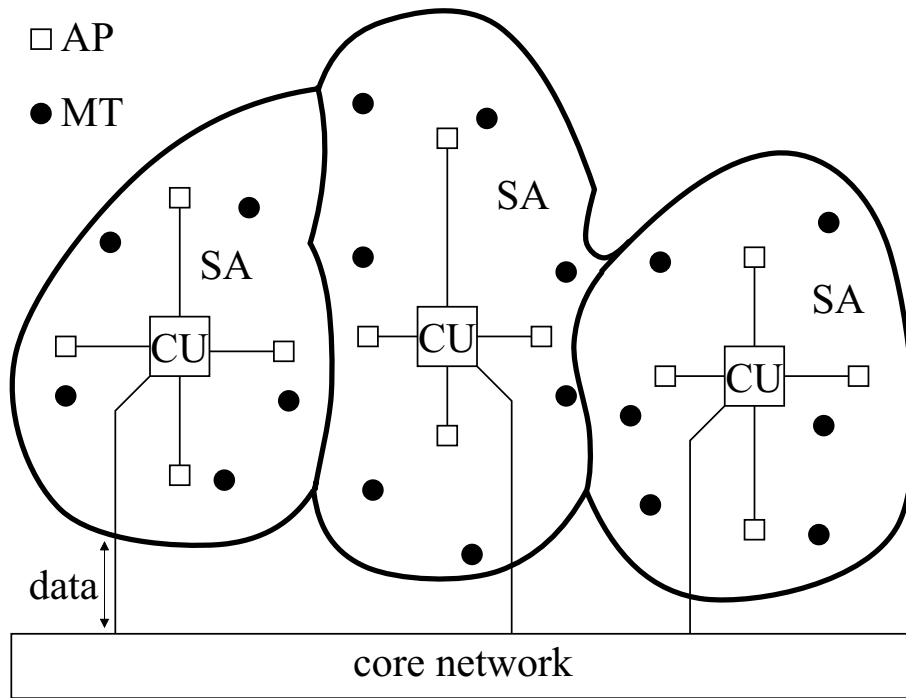
Fig. 1.2. Novel SA-based architecture, example with three SAs

conventional cellular architectures we now have a SA with a number of APs, which are connected to a CU. The CUs in their turn are connected to the core network. In the conventional cellular architecture, see Fig. 1.1, each cell constitutes a multipoint–to–point structure in the UL and a point–to–multipoint structure in the DL. In contrast to this, see Fig. 1.2, each SA of the SA-based architecture constitutes a multipoint–to–multipoint structure both in the UL and in the DL.

The basic way of operation of the SA-based architecture as shown in Fig. 1.2 is the following:

- In the UL the transmit signals of the MTs of a SA are received by all APs of the SA and fed to the CU, where they are jointly processed. The aim of this joint processing consists in exploiting the energies of all signals received by the APs of the SA in such a way that the required total transmit energy in the SA is minimized and that the complexity of the MTs can be kept low. An UL transmission scheme which allows to reach these goals is joint detection (JD) published in [Kle96, Skl04].

- In the DL, each MT of a SA is supported by transmit signals radiated by all APs of the SA. These signals are jointly generated in the CU based on the data for each MT of the SA in such a way that the required total transmit energy

in the SA is minimized, and that the complexity of the MTs can be kept low. A DL transmission scheme which allows to reach these goals is the scheme joint transmission (JT) published in [MBW$^+$00, TWMB01, Skl04].

Because JD and JT are important features of the proposed architecture, the designation "Joint Transmission and Detection Integrated Network" (JOINT) has been coined for this architecture. The rationale of JOINT can be applied both in conglomerates of SAs as shown in Fig. 1.2 and in single, that is isolated SAs.

In the case of the conventional cellular architecture the MTs of each cell form a group of MTs which can be supported without causing mutual interference [Kle96, Ver98, Pap00], that is intracell interference may be eliminated. In the case of the SA based architecture the MTs of each SA form such a group of MTs which can be supported without causing mutual interference [WMSL02, Skl04], that is intra–SA interference can be eliminated. A look at Figs. 1.1 and 1.2 shows that in the case of the SA based architecture the groups of MTs which can be supported without mutual interference are larger than in the case of the conventional cell architecture. Therefore, in the SA based architecture the interference problems are relaxed as compared to those in the case of the conventional cellular architecture. This relation is expected to entail in capacity increase.

1.2 Basic features of JOINT as considered in the thesis

In the framework of the basic architecture of JOINT described in Section 1.1 and illustrated in Fig. 1.2, many degrees of freedom exist for the system designer as for instance with respect to the design criteria

- multiple access (MA) scheme (FDMA, TDMA, CDMA, SDMA),

- transmission mode (single carrier, multi–carrier),

- duplexing scheme (TDD, FDD), and

- antenna arrangements at the APs and the MTs (single–element antennas, multi–element antennas).

Considering these freedoms, the following choices are made in this thesis:

- MA scheme: SDMA,

- transmission mode: Multi–carrier, specifically OFDM,

- duplexing scheme: TDD, and

- antenna arrangements: Single–element antennas at the APs, single–element antennas at the MTs.

In what follows, these choices are briefly motivated. The MA scheme SDMA is an obvious separation scheme for spatially dislocated MTs which communicate with a number of spatially dislocated APs, as it is the case in JOINT. Of course SDMA could be combined with other MA schemes, which, however, is not in the scope of this thesis. The choice of OFDM is made with respect to the advantages of this transmission mode as for instance suitability for high data rates, flexibility, low transmitter and receiver complexity [WE71, Bin90, Pra98, vNP00, KS01, RGG01] etc. As opposed to the duplexing scheme FDD, the selected scheme TDD facilitates the flexible support of highly different data rates in UL and DL, and allows to exploit the reciprocity of UL and DL channels in the context of channel estimation. At the MTs single–element antennas are chosen with a view to keep the MT complexity low. This argument does not count so much for the APs, where, in addition to single–element antennas, also multi–element antennas are considered with a view to performance enhancements.

In addition to the above mentioned design criteria also criteria like

- splitting up of the signal processing effort between the APs and the CU of a SA,

- implementation of the links between the APs and the CU of a SA (base band, RF band, coaxial wire, optical fibre, radio relay etc.),

- geometrical definition of SAs and placement of APs, and

- algorithms to perform JD and JT

could be considered. However, these criteria do not play a major role in the context of this thesis.

1.3 Importance of modelling and simulation of JOINT

The rapidly increasing demand for a higher capacity of mobile radio systems and for good quality of service (QoS) pushes the development of mobile radio system solutions for the future networks. The process of designing and developing such future mobile radio systems, like the JOINT system, is a very ambitious task due to the inherent complexity and the manifold external factors of limitation. Without the facility of measurements in existing systems, simulations based on the accurate modelling of the system and of the investigation scenarios are the most feasible way to determine the potential increase in the system capacity and/or the system performance under development costs as low as possible.

In mobile radio systems as for instance the SA based system JOINT, numerous MTs transmit and receive information–carrying signals over time variant mobile radio channels. Multiple access interference (MAI) is the main limiting factor to the capacity and the performance of the mobile radio system. In the UL of JOINT, as mentioned in the previous section, the MTs transmit their signals using the entire available bandwidth B simultaneously. During the UL transmissions, different kinds of interferences occur, which degrade the system performance. On the way to the receiver, the signal radiated by a MT becomes a victim of multipath propagation [Pro95, Gib99], i.e., a number of echoes of the original signal overlap at the receiver causing intersymbol interference (ISI). At the same time, the signals transmitted by the remaining MTs simultaneously active in the considered SA cause intra–SA MAI at the receiver. Furthermore, expanding our considerations from the single SA to multiple adjacent co–channel SAs, it is obvious that the transmissions in these SAs will cause inter–SA MAI to each other. In the DL of JOINT, the CU designs the desired signals which are then transmitted from all APs to all MTs simultaneously active in the considered SA. The mentioned ISI, intra–SA MAI and inter–SA MAI also occur during the DL transmission. These interferences limit the system performance and lead to the problem that the mobile radio system is obliged to take the trade–off between QoS and the system load. In order to study these interferences analytically and numerically only comprehensive simulations are reasonable means. One key prerequisite for the simulation is the accurate modelling of the system.

The task of interference reduction is processed in the CU of each SA. Multiuser detection in the UL of JOINT is performed by means of JD [Ver98, Kle96] so that the interference in the resulting data estimates becomes as low as possible. The CU applies JT [MBW+00, BMWT00, TWMB01] in the DL, i.e., it designs the transmit signals

based on the premises that the resulting estimates at the MTs are free from interferences and the necessary transmit energy at the APs is minimized, see also Section 1.2. JD and JT presuppose the knowledge of mobile radio channels, which is estimated by a pilot–aided channel estimation technique termed joint channel estimation (JCE) [SMWB01, MWSL02] in the JOINT system. Investigations through modelling and simulations, concerning the performances in the UL and the DL of JOINT, respectively, will show that these techniques are able to combat interferences and enhance the system performance.

Besides the mentioned technologies applied at the CU in each SA, there are still many other aspects which will influence the system performance of JOINT as for example time variance of mobile radio channels. Static channel realizations might be suitable for the investigation on special features of signal processing algorithms. However, due to mobility of MTs and versatile dynamic properties of the system, a more realistic and reliable analysis can be only obtained based on the realtime modelling and simulation of time variant channels, taking all important phenomena into account.

1.4   Open questions

The rapid development of mobile radio communications technologies not only paves the way towards the commercialization of 3G mobile radio networks nowadays, but also encourages the research on beyond 3G or other future mobile radio systems. Many efforts have been taken to enhance and/or develop the technologies aiming at improving the efficiency of the data transmission and estimation, for instance JD [Kle96, Ver98] in the UL, JT [MBW+00, BMWT00, TWMB01] in the DL, and JCE [SMWB01, MWSL02] offering the channel knowledge for JD and JT. The novel air interface solution JOINT, integrating these technologies into a SA based OFDM system, is proposed for the future networks, as mentioned in the previous sections. Yet there are some open questions concerning this integrated system concept.

Firstly, the concept of JOINT has been created, while the detailed and accurate modelling of JOINT is not available up to now. Moreover, the key algorithms, like e.g., JD and JT, have not been specified for the SA concept in the OFDM system, which are crucial for the proposed system JOINT. The channel model, which is very important for the investigation since the system behaves significantly differently in different channel environments, is also vacant and should be described and modelled.

Secondly, there is yet no feasible simulation platform for JOINT. Some current simulation softwares, like e.g., Matlab, have their respective advantages in scientific calcu-

lations and are suitable for implementing detailed algorithms. However, the computational efforts increase dramatically if all the important aspects of JOINT are realized. A good simulation platform is to be found and the simulation chain of JOINT should be implemented on it with high simulation efficiency but low cost of computational effort.

Thirdly, the question whether the proposed system JOINT can really improve the system performance compared to that of 3G cellular systems is to be answered. Furthermore, improvements or refinements of JOINT are expected in order to defend the novel proposal against other competing candidates. In detail the following topics concerning the physical layer are important:

- Performances of JOINT in the UL and in the DL with perfect channel knowledge,

- impact of non perfect channel knowledge on JD and JT,

- system level simulations of JOINT,

- joint link and system level simulations JOINT.

One of the main goals of JOINT is to increase the system capacity. The advantage of the SA based system JOINT in system capacity compared to 3G cellular systems and WLAN systems as for instance IEEE 802.11 is expected and needs to be illustrated. On the other hand, some disadvantages, e.g., a considerably large crest factor, an inherent drawback in the OFDM system, will degrade the performance of JOINT. How to handle it is also an interesting topic.

1.5   Goals and structure of the thesis

The goals of this thesis, corresponding to the open questions formulated in Section 1.4, are described in the following:

- Completing the system design of JOINT,

- optimizing the existing algorithms and building accurate modules of the proposed system JOINT, including the key components, e.g., JD, JT and JCE at the CU, and channel models for different scenarios,

- implementing the simulation chain of JOINT in an efficient simulation platform, and

- evaluating the performance of the proposed system JOINT based on the simulation results.

Corresponding to the above four goals the thesis comprises 10 chapters. Chapters 2 to 6 focus on modelling the JOINT concept, including the channel models and the key technologies applied in JOINT. Chapter 7 concerns the implementation of the JOINT simulation chain. Chapters 8 and 9 focus on performance evaluations based on the simulation results. Finally Chapter 10 summarizes the thesis.

Chapter 2 describes the channel models applied in the investigation in this thesis.

In Chapter 3, the SA based air interface JOINT, see Section 1.2, is described and modelled in detail. The basic characteristics of OFDM are described. The parametrization of JOINT is introduced based on the application of OFDM. A system model based on the SA concept is developed with a matrix–vector formalism in the frequency domain.

Chapter 4 tackles briefly the theory of JCE applied in JOINT. JCE solves the important problem of offering the channel estimation for JD in the UL and JT in the DL, respectively.

In Chapter 5, a linear zero–forcing (ZF) JD algorithm applied in the UL of JOINT is elaborated. A performance criterion termed signal–to–noise–ratio (SNR) degradation is introduced, which reveals the price, in terms of SNR, to be paid for the MAI elimination.

In Chapter 6, a linear ZF JT algorithm applied in the DL of JOINT is addressed. Aiming at obtaining interference–free data estimates at the receiver side, i.e., the MTs, the modulation process at the CU is designed carefully. However, more energy, which can be illustrated by the term transmission efficiency, has to be spent at the transmitter side, i.e., the APs at the CU, to combat the intra–SA MAI.

Chapter 7 gives an introduction to the implementation of the JOINT simulation chain. With MLDesigner [MT03], which is an advantageous simulation software fulfilling the requirements mentioned in the previous section, the key algorithms of JD, JT and JCE are implemented. Moreover, a number of channel models are generated according to different investigation scenarios. Flexibility is one of the characteristics of the JOINT simulation chain, e.g., replacing functionalities can be easily handled by adding or removing modules. Some problems, like e.g., synchronization and simulation efficiency, which have once hurdled the implementation process, and their solutions are mentioned at the end of Chapter 7.

Chapter 8 evaluates the UL and DL performances of JOINT in a single–SA scenario obtained through the simulations. Furthermore, the impact of imperfect channel knowledge on the performance of JOINT is studied.

Chapter 9 focuses on the performance of JOINT in a multiple–SA scenario, in which the noise, the intra–SA MAI and the inter–SA MAI are all taken into account. The simulation results in terms of the average bit error rate (BER), and the BER statistics are presented. Based on the simulation results, the spectrum efficiency is analyzed. A comparison of the spectrum efficiencies of the SA based system JOINT and conventional cellular systems shows the advantage of JOINT in improving the system capacity, which is one of the main goals of JOINT.

Finally, the thesis is summarized in Chapter 10.

Chapter 2
Channel models

2.1 Preliminary remarks

The system design and performance heavily depend on the characteristics of the channels for which the system has to work. Therefore, the channel information is necessary for the investigation and evaluation of the system performance. Unlike the wired communication channel, mobile radio channels are indeterministic and variable. Generally, there are two possible ways to obtain the required channel information, namely

- by measurements or

- by channel models, which should not be too far from the real world.

In this thesis the mobile radio channels are modelled based on a stochastic process with parameters, some of which are determined according to measured channel properties.

Simulations on computers can be only performed in the time discrete or the frequency discrete manner. Moreover, the discrete modelling of signals and channels can bring much simplification to the implementation of signal processing. Therefore, for the following considerations, the equivalent discrete lowpass representation of channel impulse responses (CIRs) and channel transfer functions (CTFs) is used [SJ67, Pro95]. In what follows complex quantities are underlined, and vectors and matrices are printed in boldface. Vectors and matrices referring to the frequency domain carry a tilde, whereas vectors and matrices referring to the time domain have no further distinguishing marks. Estimates of the corresponding signals are addressed with a hat. Furthermore, $(\cdot)^*$ and $(\cdot)^{\mathrm{T}}$ designate the complex conjugate and the transposition, respectively. The following operators are used to address an individual element and a submatrix of the matrix in brackets: The operator $[\cdot]_{x,y}$ yields the element in the x–th row and the y–th column, and the operator $[\cdot]_{x_2,y_2}^{x_1,y_1}$ yields the submatrix bounded by the rows x_1 and x_2 and the columns y_1 and y_2.

2.2 Modelling in both time and frequency domains

With respect to a time instant t, a mobile radio channel between a transmitter and a receiver can be characterized by a CIR vector [SMWB01]

$$\underline{\mathbf{h}}(t) = (\underline{h}_1(t) \ldots \underline{h}_W(t))^{\mathrm{T}} \tag{2.1}$$

of dimension W, where the time instant t belongs to a discrete set of observation time instants, i.e.,

$$t \in \{t_1, \ldots, t_n, \ldots\}, \, n \in \mathbb{N}. \tag{2.2}$$

Correspondingly in the frequency domain, an $N_F \times 1$ CTF vector [SMWB01]

$$\tilde{\underline{h}}(t) = \left(\tilde{\underline{h}}_1(t) \ldots \tilde{\underline{h}}_{N_F}(t) \right)^{\mathrm{T}} \tag{2.3}$$

is used to describe the CTFs on all the N_F subcarriers for the time instant t. (2.3) and (2.1) can be related to each other by discrete Fourier transform (DFT) and inverse DFT (IDFT) [OW97]. If we assume that W of (2.1) and N_F of (2.3) fulfill [SMWB01, MWSL02]

$$W \leq N_F, \tag{2.4}$$

then we can zeropad the vector $\underline{h}(t)$ of (2.1) to obtain the vector

$$\underline{h}_{\mathrm{ZP}}(t) = \left(\underline{h}(t)^{\mathrm{T}} \underbrace{0 \cdots 0}_{N_F - W} \right)^{\mathrm{T}}. \tag{2.5}$$

Now with $\tilde{\boldsymbol{\mathcal{F}}}$ denoting the $N_F \times N_F$ Fourier matrix whose elements are

$$[\tilde{\boldsymbol{\mathcal{F}}}]_{m,n} = e^{-j \frac{2\pi}{N_F}(m-1)(n-1)}, m = 1 \ldots N_F, n = 1 \ldots N_F, \tag{2.6}$$

the relations

$$\tilde{\underline{h}}(t) = \tilde{\boldsymbol{\mathcal{F}}} \cdot \underline{h}_{\mathrm{ZP}}(t) \tag{2.7}$$

and

$$\underline{h}_{\mathrm{ZP}}(t) = \tilde{\boldsymbol{\mathcal{F}}}^{-1} \cdot \tilde{\underline{h}}(t) \tag{2.8}$$

are valid [SMWB01, MWSL02]. With the dimension–reduced Fourier matrix $[\tilde{\boldsymbol{\mathcal{F}}}]_{N_F,W}^{1,1}$, consisting of the first W columns of the Fourier matrix $\tilde{\boldsymbol{\mathcal{F}}}$, (2.7) can be simplified as [SMWB01, MWSL02]

$$\tilde{\underline{h}}(t) = [\tilde{\boldsymbol{\mathcal{F}}}]_{N_F,W}^{1,1} \underline{h}(t). \tag{2.9}$$

2.3 Characteristics of the channel

2.3.1 Fast fading

When a transmitter or a receiver moves on a small scale, multipath [Pro95] fading or fast fading is addressed to characterize the channel. In a mobile radio system, the
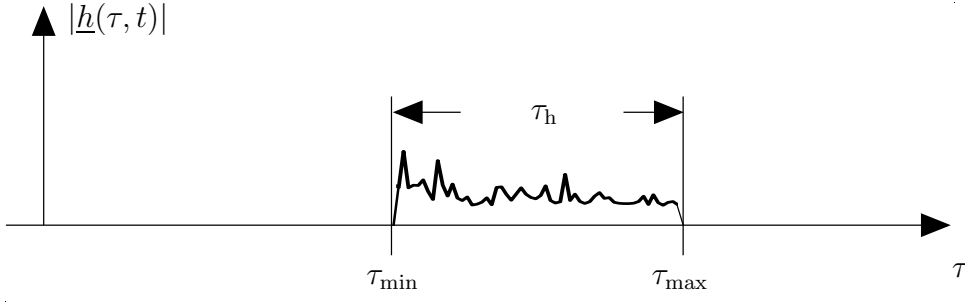
Fig. 2.1. Schematic run of the magnitude $|\underline{h}(\tau, t)|$ of a CIR $\underline{h}(\tau, t)$ at the time instant t

signals in general reach the receiver via a multitude of paths. One direct line–of–sight (LoS) path may exist or not, and the other paths are non–LoS (NLoS) paths. Due to reflection, scattering or diffraction by obstacles, the multipath [Pro95] signals reach the receiver each with a different intensity, zero phase and delay. With P denoting the number of the paths, the signals are delayed by delays $\tau_p, p = 1 \ldots P$, and changed in phases with phase shifts $\varphi_p, p = 1 \ldots P$. The motion of the MT results in Doppler shifts $f_{\mathrm{d},p}, p = 1 \ldots P$, of the corresponding propagation paths. Therefore, a CIR

$$\underline{h}(\tau, t) = \frac{1}{\sqrt{P}} \sum_{p=1}^{P} \exp(\mathrm{j}\varphi_p) \exp(\mathrm{j}2\pi f_{\mathrm{d},p} t) \, \delta(\tau - \tau_p) \tag{2.10}$$

with respect to τ at a time instant t can be obtained [COS89]. Fig. 2.1 shows schematically the CIR magnitude $|\underline{h}(\tau, t)|$ versus the delay τ at the time instant t. Such a CIR $\underline{h}(\tau, t)$ can be characterized by

- its minimum delay $\tau_{\min}$,

- its maximum delay $\tau_{\max}$, and

- its duration or excess delay

$$\tau_{\mathrm{h}} = \tau_{\max} - \tau_{\min}. \tag{2.11}$$

$\underline{h}(\tau, t)$ of (2.10) is usually not band–limited. Filtered by a band–pass filter with bandwidth B, which is also the bandwidth of the transmission system, follows the CIR [COS89]

$$
\begin{aligned}
\underline{h}_{\mathrm{BP}}(\tau, t) &= \underline{h}(\tau, t) * \mathrm{sinc}(B\tau) \\
&= \frac{1}{\sqrt{P}} \sum_{p=1}^{P} \exp(\mathrm{j}\varphi_p) \exp(\mathrm{j}2\pi f_{\mathrm{d},p} t) \, \mathrm{sinc}(B(\tau - \tau_p)),
\end{aligned} \tag{2.12}
$$

a)

b)
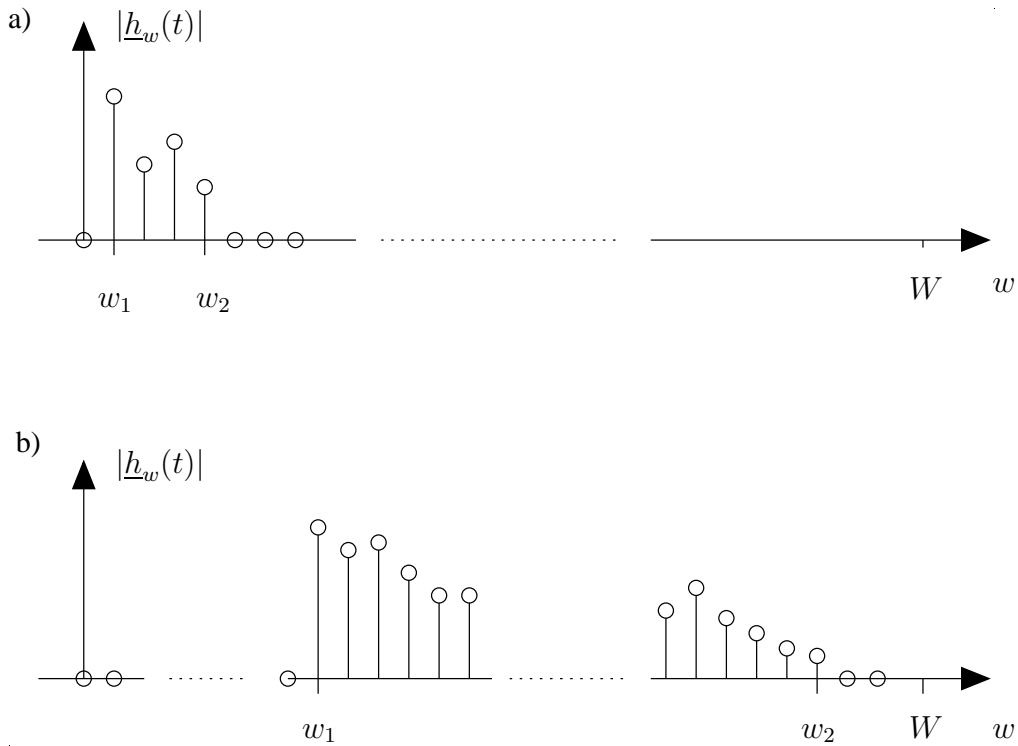
Fig. 2.2. Schematic run of the magnitude $|\underline{h}_w(t)|$ of a CIR $\underline{h}_w(t)$ at the time
   instant t, with w_1 corresponding to the minimum delay $\tau_{\min}$ and w_2
   corresponding to the maximum delay $\tau_{\max}$, respectively,
   a) indoor case,
   b) outdoor case

which is now band–limited. Then, by sampling (2.12) with the bandwidth B and
truncating the discrete sequence to the dimension W [COS89], the obtained CIR

$$
\begin{aligned}
\underline{h}_w(t) &= \underline{h}_{\mathrm{BP}}(\tau,t)\big|_{\tau=(w-1)\cdot\frac{1}{B}} \\
&= \frac{1}{\sqrt{P}}\sum_{p=1}^{P}\exp(\mathrm{j}\varphi_p)\exp(\mathrm{j}2\pi f_{\mathrm{d},p}t)\operatorname{sinc}(w-1-B\tau_p). \qquad (2.13)
\end{aligned}
$$

is just the corresponding w–th element $\underline{h}_w(t)$ of (2.1). The larger the CIR dimension
W is, the closer the (2.1) gets to the real channel.

Usually the discrete band–pass CIRs $\underline{h}_w(t)$ of (2.13) of a point–to–point channel link
start with a number of zero–valued samples. For a multipoint–to–multipoint channel
applied in JOINT, the numbers of these zero–valued samples at the front of the CIRs
$\underline{h}_w(t)$ of different links are different. Omitting the front zero–valued $\underline{h}_w(t)$ samples
brings only a phase shift to the receive signals in the case of data estimation and does
not much influence the performance of the data estimation. Therefore, for the data

estimation the zeros at the front of the CIRs $\underline{h}_w(t)$ can be omitted and then the CIRs $\underline{h}_w(t)$ of different channel links are well synchronized.

However, the above asynchronous phenomenon of different channel links will bring troubles to the channel estimation. The sampled CIRs $\underline{h}_w(t)$, as depicted in Fig. 2.2, behave differently in the indoor and in the outdoor scenarios. It is seen that in the indoor scenarios, both w_1 and w_2, which correspond to the minimum delay τ_{min} and the maximum delay τ_{max}, respectively, are very small. That means, the sequence of the zeros at the front of the $\underline{h}_w(t)$ samples and the sequence of the non–zero–valued $\underline{h}_w(t)$ samples are both very short. In contrast to this situation, both w_1 and w_2 are very large in the outdoor scenarios. That means, the sequence of the zeros at the front of the $\underline{h}_w(t)$ samples and the sequence of the non–zero–valued $\underline{h}_w(t)$ samples are both very long. In the case of the channel estimation in the indoor scenarios, omitting few zeros at the front of the CIRs $\underline{h}_w(t)$ and shifting the other non–zero–valued samples to the left will not cause great changes to the CIRs $\underline{h}_w(t)$. However, in the outdoor scenarios, omitting a large number of zeros at the front of the CIRs $\underline{h}_w(t)$ and shifting many non–zero–valued samples to the left will bring significant influences to the estimation results of the CIRs $\underline{h}_w(t)$. Hence, the synchronization problem cannot be solved in this way. The aspect concerning the synchronization problem will be elaborated in the next chapter.

According to the explanation given above, for the case of the data estimation and for the case of the channel estimation in the indoor scenarios it is feasible to assume that the CIRs $\underline{h}_w(t)$ start with non–zero–valued samples. However, for the case of the channel estimation in the outdoor scenarios, the CIRs $\underline{h}_w(t)$ cannot be assumed to be starting with the non–zero–valued samples. In this thesis the system performance of data estimation in JOINT is focused, whereas the theory and implementation of JCE will be only briefly touched. The key investigations are based on the assumption that the CIRs and the CTFs are perfectly known at the CU for the data estimation in the UL and in the DL. Hence, for the sake of simplicity, a frequently used channel model, usually a Rayleigh fading channel with an exponential power delay profile and a Jakes Doppler spectrum [Ste92, Pro95, LR99], whose CIRs start with the non–zero–valued samples, is introduced in the following.

The quantities of the phase shifts φ_p, the delays τ_p and the Doppler shifts $f_{d,p}$, $p = 1 \ldots P$, of (2.13) are randomly generated and are assumed to be invariable during a transmission frame including N discrete time instants $t = t_1 \ldots t_N$, if N is not too large. For each new transmission frame, φ_p, τ_p and $f_{d,p}$ have to be anew generated. Probability density functions (PDFs) of φ_p, τ_p and $f_{d,p}$ make the channel realization correspond to given statistical properties of the model, for instance, the Rayleigh fading channel with

an exponential power delay profile and a Jakes Doppler spectrum [Ste92, Pro95, LR99]. Generally, the phase shifts φ_p are independent realizations of the random variable φ with a uniform distribution in $[0,2\pi)$, i.e., the PDF of φ in [Ste92]

$$p_\varphi(\varphi) = \begin{cases} \frac{1}{2\pi} & \text{for } \varphi \in [0, 2\pi), \\ 0 & \text{else.} \end{cases} \tag{2.14}$$

For the widely–used exponentially decreasing power delay profile [COS89], if a denotes the exponent of the power delay profile and can be determined by

$$a = \frac{3\ln 10}{\tau_{\max}}, \tag{2.15}$$

the delays τ_p are independent realizations of a random variable τ with the PDF [Ste92]

$$p_\tau(\tau) = \begin{cases} \frac{a}{1-\exp(-a\tau_{\max})}\exp\left(-a\tau\right) & \text{for } 0 \le \tau < \tau_{\max}, \\ 0 & \text{else.} \end{cases} \tag{2.16}$$

If the multipath signals are received from all directions with equal probabilities, with $f_{\text{d,max}}$ denoting the maximum Doppler shift, the Doppler shifts $f_{\text{d},p}$ are independent realizations of a random variable f_d with a Jakes PDF [Ste92, Pro95, LR99]

$$p_{f_\text{d}}(f_\text{d}) = \begin{cases} \dfrac{1}{\pi f_{\text{d,max}}\sqrt{1-\left(\frac{f_\text{d}}{f_{\text{d,max}}}\right)^2}} & \text{for } |f_\text{d}| \le f_{\text{d,max}}, \\ 0 & \text{else.} \end{cases} \tag{2.17}$$

Following (2.14), (2.16) and (2.17), the phase shifts φ_p, the excess delays τ_p and the Doppler shifts $f_{\text{d},p}$ are generated so that the CIR vector $\underline{\mathbf{h}}(t)$ and CTF vector $\tilde{\underline{\mathbf{h}}}(t)$ can be realized to describe the Rayleigh fading channel with an exponential power delay profile and a Jakes Doppler spectrum [Ste92, Pro95, LR99], which is to be applied in the data estimation for the scenarios in which the transmitter or the receivers make small–scale movement in this thesis.

2.3.2   Slow fading

Due to the shadowing effect during the propagation, the power received fluctuates with time slowly as the transmitter or the receiver moves in a large scale [Par92, LR99, Pro95]. This phenomenon is termed slow fading or large–scale fading. Generally the log–normal fading is suitable for modelling shadowing effects caused by obstacles during the propagation [Par92, Pro95, LR99]. Therefore, slow fading can be also termed log–normal fading.
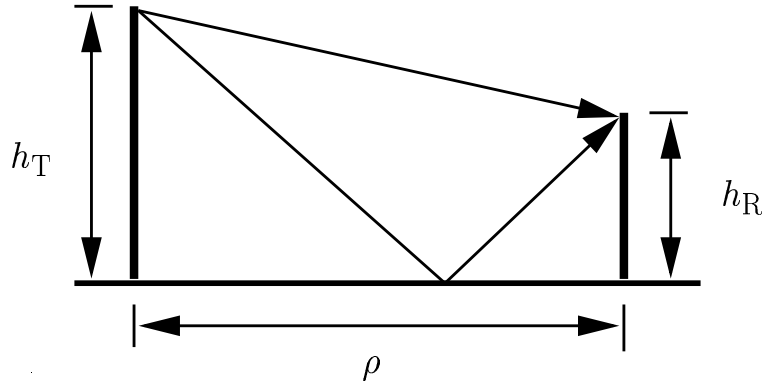
Fig. 2.3. Two–ray model

For the power $P_t(t)$ transmitted at the time instant t, the power $P_r(t)$ received is given by [Par92, Pro95, LR99]

$$P_r(t) = g(t) \cdot P_t(t), \tag{2.18}$$

where $g(t)$ is the linear path gain of the corresponding propagation channel. The linear path gain $g(t)$ obeys approximately a log–normal distribution [Par92, Pro95, LR99], i.e., the logarithm

$$G(t) = 10 \log_{10} g(t) \tag{2.19}$$

can be approximated as a Gaussian variable with a standard deviation σ_G and a mean value $\bar{G}$.

In reality the standard deviation σ_G usually takes values between $0 \ldots 10$ dB according to the environment [COS91, Par92, BARY96, DB96, LR99].

The average logarithmic path gain $\bar{G}$, which depends on the distance ρ between the transmitter and the receiver, has to be determined according to the considered scenario. There are many outdoor path loss models [COS91, Par92, BARY96, DB96, LR99] to describe the average logarithmic path gain $\bar{G}$, on the basis of either theoretical analysis or on measurement results in different propagation scenarios. Some of these models are introduced briefly in the following:

- The free space model [Par92]: The average logarithmic path gain $\bar{G}$ decreases in the free space at a decay rate of 20 dB/decade [Par92, LR99], i.e., $\bar{G}$ drops 20 dB as ρ gets ten times larger.

- The two–ray model depicted in Fig. 2.1: Since one reflected path is taken into account [Par92] beyond one direct path from the transmitter to the receiver, the average logarithmic path gain $\bar{G}$ drops at a decay rate of about 40 dB/decade [Par92].
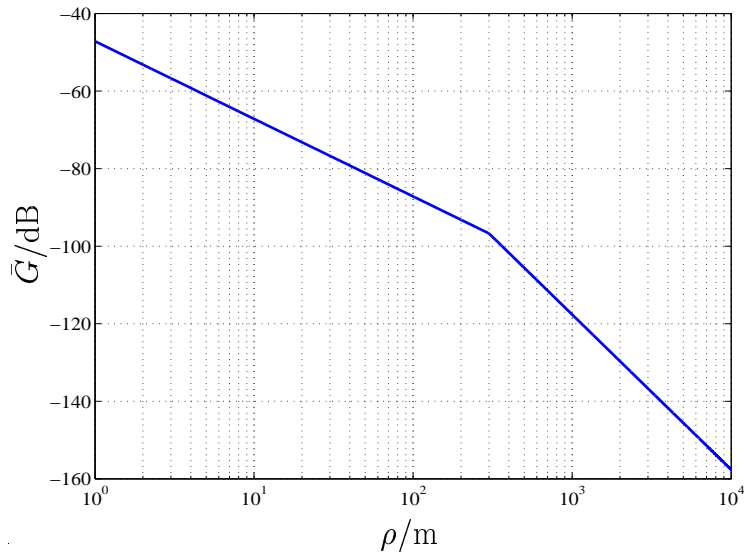
Fig. 2.4. An example of the dual–slope model, when, e.g., $g_{\mathrm{T}} = g_{\mathrm{R}} = 1, \alpha_1 = 2.0, \alpha_2 = 4.0$ and $\rho_{\mathrm{B}} = 300$m hold

- The COST–231–Hata model and COST–231–Walfish–Ikegami model [COS91]: These two models are the results of experiments performed under the conditions described in [COS91].

All the models mentioned above have one point in common: The average logarithmic path gain $\bar{G}$ drops versus the distance ρ with a constant decay rate. However, more and more measurement results [HN80, Ste92, XBMLS92] indicate that in most outdoor environments the decay rate of the average logarithmic path gain $\bar{G}$ versus the distance ρ is not a constant value, in other words, this decay rate depends on the distance ρ [XBMLS92]. In order to model the channel more accurately, a dual–slope model is proposed with the concept of the break–even–point distance ρ_{B} [XBMLS92]. With α_1 and α_2 denoting the two different attenuation exponents, respectively, which describe the two different decay rates, and with λ denoting the wavelength, the average logarithmic path gain $\bar{G}$ versus the distance ρ is given by

$$
\bar{G}/\mathrm{dB} = \begin{cases} -10\alpha_1 \log_{10}\left(\frac{4\pi\rho}{\lambda}\right) + 10\log_{10}\left(g_{\mathrm{T}}g_{\mathrm{R}}\right) & \text{for } 0 \leq \rho < \rho_{\mathrm{B}}, \\ -10\alpha_1 \log_{10}\left(\frac{4\pi\rho_{\mathrm{B}}}{\lambda}\right) + 10\log_{10}\left(g_{\mathrm{T}}g_{\mathrm{R}}\right) - 10\alpha_2 \log_{10}\left(\frac{\rho}{\rho_{\mathrm{B}}}\right) & \text{for } \rho \geq \rho_{\mathrm{B}}, \end{cases}
$$
(2.20)

where g_{T} and g_{R} denote the antenna gains of the transmit antenna and the receive antenna, respectively [XBMLS92]. According to (2.20) the average logarithmic path gain $\bar{G}$ decreases with the decay rate equal to $10\alpha_1$ dB/decade within the break–even–point range, that is for $\rho < \rho_{\mathrm{B}}$, and with the decay rate equal to $10\alpha_2$ dB/decade out

of the break–even–point range, that is for $\rho \geq \rho_\mathrm{B}$, where $\alpha_1 < \alpha_2$ holds, as depicted in Fig. 2.4. The values of the attenuation exponents α_1, α_2 and of the break–even–point distance ρ_B should be chosen according to the indicated scenario.

For the resultant of two independent stochastic processes, fast fading and slow fading, the modified CIR vector $\underline{\mathbf{h}}'(t)$ can be obtained by multiplying the CIR vector $\underline{\mathbf{h}}(t)$ of (2.1) with a factor $\sqrt{g(t)}$, that is

$$\underline{\mathbf{h}}'(t) = \sqrt{g(t)} \cdot \underline{\mathbf{h}}(t). \tag{2.21}$$

Consequently, the modified CTF vector $\tilde{\underline{\mathbf{h}}}'(t)$ can be obtained by multiplying the CTF vector $\tilde{\underline{\mathbf{h}}}(t)$ of (2.3) also with the factor $\sqrt{g(t)}$

$$\tilde{\underline{\mathbf{h}}}'(t) = \sqrt{g(t)} \cdot \tilde{\underline{\mathbf{h}}}(t). \tag{2.22}$$

This modified channel model including the Rayleigh fading mentioned in Subsection 2.3.1 and the log–normal fading described in this subsection is applied in the data estimation for the outdoor urban scenarios considered in this thesis.

Chapter 3
JOINT: A multipoint–to–multipoint OFDM system

3.1 Motivation

In order to generate a solid basis for the considerations in the following chapters, in the present Chapter 3 an expansion from the conventional point–to–point OFDM transmission [Doe57, WE71, PR80, Bin90, Pra98, KS01, FK03] to the multipoint–to–multipoint OFDM transmission, which is applied in JOINT, is first discussed in Section 3.2. The problem of time synchronization in JOINT is basically addressed in Section 3.3. Finally the parameter values to be applied in the numerical simulations of JOINT are given in Section 3.4. In what follows, the consideration is with respect to the time instant t. Therefore, for the sake of simplicity, t will be omitted in the notation if it is not declared otherwise.

3.2 OFDM transmission technique

OFDM is a multiplexing and modulation technique gaining considerable interest in recent years. Moreover, OFDM is applied in numerous communications systems over the world [ETS97b, ETS97c, RCLF89, RS95, TL97, Cim85, Bin91, CTC91, Jon95, IEE99, CWKS97, vNAM^{+}99, ETS96, ETS99]. The advantages and disadvantages of the OFDM transmission technique have been elaborated in lots of publications, e. g. [Bin90, Pra98, vNP00, KS01]. In the following the application of OFDM in JOINT is addressed.

Generally, a mobile radio system can be described by a linear transmission structure (LTS) as the one illustrated in Fig. 3.1.a. The mobile radio channels considered in this thesis are assumed to be linear. Here, the LTS consists of the modulator in the transmitter, the linearly modelled mobile radio channel and the demodulator at the receiver. At the input of the LTS, the vector

$$\underline{\mathbf{x}} = \left(\underline{x}^{(1)} \ldots \underline{x}^{(N)} \right)^{\mathrm{T}} \tag{3.1}$$

containing N complex values of the input signal is fed into the LTS. At the receiver, i. e., the output of the LTS, the vector

$$\underline{\mathbf{y}} = \left(\underline{y}^{(1)} \ldots \underline{y}^{(M)} \right)^{\mathrm{T}} \tag{3.2}$$

a)

$$\mathbf{\underline{x}} = \begin{pmatrix} \underline{x}^{(1)} \\ \vdots \\ \underline{x}^{(N)} \end{pmatrix} \quad \vdots \quad \boxed{\begin{array}{c} \text{linear} \\ \text{transmission} \\ \text{system} \\ \text{(modulator-} \\ \text{channel-} \\ \text{demodulator)} \end{array}} \quad \vdots \quad \begin{pmatrix} \underline{y}^{(1)} \\ \vdots \\ \underline{y}^{(M)} \end{pmatrix} = \mathbf{\underline{y}}$$

b)

$$\mathbf{\underline{\tilde{s}}} = \begin{pmatrix} \underline{\tilde{s}}^{(1)} \\ \vdots \\ \underline{\tilde{s}}^{(N_\mathrm{F})} \end{pmatrix} \quad \vdots \quad \boxed{\begin{array}{c} \text{OFDM} \\ \text{(modulator-} \\ \text{channel-} \\ \text{demodulator)} \end{array}} \quad \vdots \quad \begin{pmatrix} \underline{\tilde{e}}^{(1)} \\ \vdots \\ \underline{\tilde{e}}^{(N_\mathrm{F})} \end{pmatrix} = \mathbf{\underline{\tilde{e}}}$$
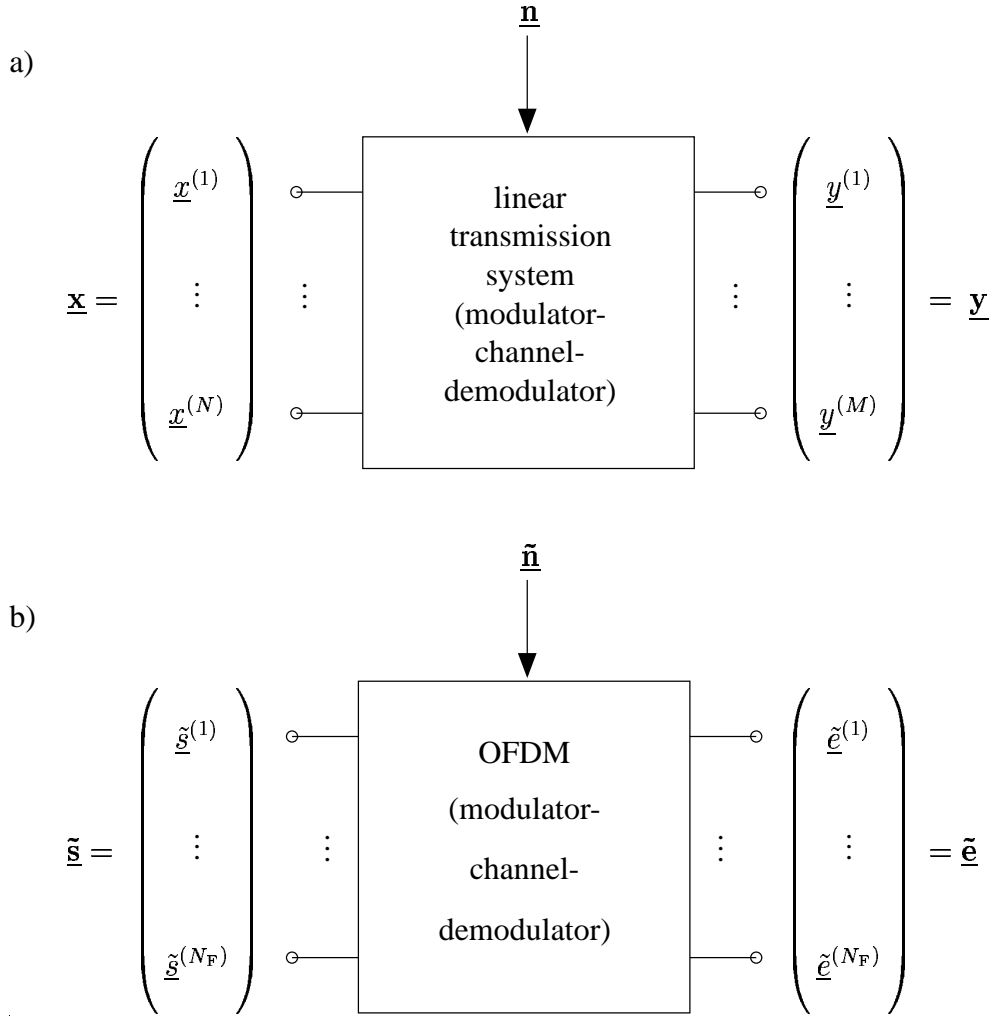
Fig. 3.1. Linear transmission structure describing a mobile radio transmission system
a) general case,
b) special case: OFDM point–to–point transmission system

of dimension M is obtained. With the matrix

$$\mathbf{\underline{B}} = \begin{pmatrix} \underline{b}_{11} & \cdots & \underline{b}_{1N} \\ \vdots & & \vdots \\ \underline{b}_{M1} & \cdots & \underline{b}_{MN} \end{pmatrix} \tag{3.3}$$

of dimensions $M \times N$, which describes the impact of the LTS on the input signal represented by the vector $\mathbf{\underline{x}}$ of (3.1), and the vector

$$\mathbf{\underline{n}} = \left(\underline{n}^{(1)} \dots \underline{n}^{(M)} \right)^{\mathrm{T}} \tag{3.4}$$

of dimension M representing the noise received, the relation

$$\mathbf{\underline{y}} = \mathbf{\underline{B}}\, \mathbf{\underline{x}} + \mathbf{\underline{n}} \tag{3.5}$$

holds between the input vector $\underline{\mathbf{x}}$ of (3.1) and the output vector $\underline{\mathbf{y}}$ of (3.2) of the LTS. As it can be observed from the structure of the matrix $\underline{\mathbf{B}}$ of (3.3), in general relations exist between each of the elements of $\underline{\mathbf{x}}$ on the one side and $\underline{\mathbf{y}}$ on the other side, which constitute a challenge for the equalization at the receiver of the LTS.

One special case of a LTS is illustrated in Fig. 3.1.b, where a point–to–point OFDM transmission system is presented in the frequency domain. In the case of OFDM, both the input vector

$$\underline{\tilde{\mathbf{s}}} = \left(\underline{\tilde{s}}_1 \ldots \underline{\tilde{s}}_{N_\mathrm{F}}\right)^{\mathrm{T}} \tag{3.6}$$

and the output vector

$$\underline{\tilde{\mathbf{e}}} = \left(\underline{\tilde{e}}_1 \ldots \underline{\tilde{e}}_{N_\mathrm{F}}\right)^{\mathrm{T}} \tag{3.7}$$

consist of N_F complex amplitudes, where N_F denotes the number of subcarriers. With the noise vector

$$\underline{\tilde{\mathbf{n}}} = \left(\underline{\tilde{n}}_1 \ldots \underline{\tilde{n}}_{N_\mathrm{F}}\right)^{\mathrm{T}}, \tag{3.8}$$

(3.5) is rewritten as

$$\underline{\tilde{\mathbf{e}}} = \underline{\mathbf{B}}\,\underline{\tilde{\mathbf{s}}} + \underline{\tilde{\mathbf{n}}}. \tag{3.9}$$

The speciality of OFDM lies in the structure of the matrix $\underline{\mathbf{B}}$ of (3.3) and (3.9). It can be seen from (3.6), (3.7) and (3.9) that for the typical OFDM point–to–point transmission the matrix $\underline{\mathbf{B}}$ is square. Further, in the OFDM applying LTS of Fig. 3.1.b, the structure modulator – channel – demodulator is represented by the structure inverse fast Fourier transform (IFFT) – cyclic prefix addition – channel – cyclic prefix removal – FFT [WE71, Bin90, Pra98]. Due to this special LTS structure in the case of OFDM,

$$\underline{b}_{mn} = \begin{cases} \underline{b}_{n_\mathrm{F}} & \text{for } n = m, \; n_\mathrm{F} = 1 \ldots N_\mathrm{F}, \\ 0 & \text{else} \end{cases} \tag{3.10}$$

holds for the elements of $\underline{\mathbf{B}}$, i.e., $\underline{\mathbf{B}}$ is a diagonal matrix. Therefore, the equalization task at the receiver of the LTS [Bin90, Pra98, FK03] can be facilitated. Due to the fact that the matrix $\underline{\mathbf{B}}$ of (3.3) becomes diagonal for the OFDM applying LTS of Fig. 3.1.b, the relation between the vector $\underline{\tilde{\mathbf{s}}}$ of the transmitted signal of (3.6) and the vector $\underline{\tilde{\mathbf{e}}}$ of the receive signal of (3.7) can be examined subcarrierwise.

Extending these considerations to JOINT, the structure depicted in Fig. 3.1.b represents the link between an arbitrary pair of an MT and an AP in the considered SA. Therefore, JOINT is a multipoint–to–multipoint OFDM system. For instance, in the UL of JOINT it is assumed that in the SA there are K_B APs distributed and K MTs simultaneously active, each being equipped with a single antenna. In this case, the matrix $\underline{\mathbf{B}}$ in (3.9), is represented by the channel matrix

$$\underline{\tilde{\mathbf{H}}}^{(k, \; k_\mathrm{B})} = \begin{pmatrix} \underline{\tilde{h}}_1^{(k,k_\mathrm{B})} & \cdots & 0 \\ \vdots & \ddots & \vdots \\ 0 & \cdots & \underline{\tilde{h}}_{N_\mathrm{F}}^{(k,k_\mathrm{B})} \end{pmatrix} \in \mathbb{C}^{N_\mathrm{F} \times N_\mathrm{F}}, \tag{3.11}$$

between the MT $k, k = 1 \ldots K$, and the AP $k_\mathrm{B}, k_\mathrm{B} = 1 \ldots K_\mathrm{B}$, where the values $\tilde{\underline{h}}_{n_\mathrm{F}}^{(k,k_\mathrm{B})}$, $n_\mathrm{F} = 1 \ldots N_\mathrm{F}$, denote the CTFs of the subcarriers between the MT k and the AP k_B. With (3.11), (3.5) is rewritten as

$$\tilde{\underline{e}}_\mathrm{u}^{(k_\mathrm{B})} = \tilde{\underline{H}}^{(k,\ k_\mathrm{B})}\, \tilde{\underline{s}}_\mathrm{u}^{(k)} +\ \tilde{\underline{n}}_\mathrm{u}^{(k_\mathrm{B})}. \tag{3.12}$$

For such a multiple–MT and multiple–AP scenario the total channel matrix contains several diagonal submatrices describing the mobile radio channels between each MT k, $k = 1 \ldots K$, and each AP k_B, $k_\mathrm{B} = 1 \ldots K_\mathrm{B}$, i.e.,

$$\tilde{\underline{H}}_\mathrm{u} = \begin{pmatrix} \tilde{\underline{H}}^{(1,1)} & \cdots & \tilde{\underline{H}}^{(K,1)} \\ \vdots & & \vdots \\ \tilde{\underline{H}}^{(1,K_\mathrm{B})} & \cdots & \tilde{\underline{H}}^{(K,K_\mathrm{B})} \end{pmatrix} \tag{3.13}$$

holds. With (3.13), with the total vector

$$\tilde{\underline{s}}_\mathrm{u} = \left(\tilde{\underline{s}}_\mathrm{u}^{(1)\mathrm{T}} \ldots \tilde{\underline{s}}_\mathrm{u}^{(K)\mathrm{T}} \right)^\mathrm{T} \tag{3.14}$$

of the transmitted signals of dimension KN_F, with the total vector

$$\tilde{\underline{e}}_\mathrm{u} = \left(\tilde{\underline{e}}_\mathrm{u}^{(1)\mathrm{T}} \ldots \tilde{\underline{e}}_\mathrm{u}^{(K_\mathrm{B})\mathrm{T}} \right)^\mathrm{T} \tag{3.15}$$

of the receive signals of dimension $K_\mathrm{B}N_\mathrm{F}$ and with the total vector

$$\tilde{\underline{n}}_\mathrm{u} = \left(\tilde{\underline{n}}_\mathrm{u}^{(1)\mathrm{T}} \ldots \tilde{\underline{n}}_\mathrm{u}^{(K_\mathrm{B})\mathrm{T}} \right)^\mathrm{T} \tag{3.16}$$

of the noise vector of dimension $K_\mathrm{B}N_\mathrm{F}$, (3.12) takes the form

$$\tilde{\underline{e}}_\mathrm{u} = \tilde{\underline{H}}_\mathrm{u}\, \tilde{\underline{s}}_\mathrm{u} +\ \tilde{\underline{n}}_\mathrm{u} \tag{3.17}$$

for the multiple–MT and multiple–AP scenario in the UL of JOINT. With the application of the simple OFDM transmitter at the MTs $\tilde{\underline{s}}_\mathrm{u}$ is either the transmitted data vector

$$\tilde{\underline{d}}_\mathrm{u} = \left(\tilde{\underline{d}}_{\mathrm{u},1}^{(1)} \ldots \tilde{\underline{d}}_{\mathrm{u},N_\mathrm{F}}^{(1)} \ldots \tilde{\underline{d}}_{\mathrm{u},1}^{(K)} \ldots \tilde{\underline{d}}_{\mathrm{u},N_\mathrm{F}}^{(K)} \right)^\mathrm{T} \tag{3.18}$$

of dimension KN_F for the data transmission or the pilot vector

$$\tilde{\underline{p}} = \left(\tilde{\underline{p}}_1^{(1)} \ldots \tilde{\underline{p}}_{N_\mathrm{F}}^{(1)} \ldots \tilde{\underline{p}}_1^{(K)} \ldots \tilde{\underline{p}}_{N_\mathrm{F}}^{(K)} \right)^\mathrm{T} \tag{3.19}$$

of dimension KN_F for JCE.

With (3.11), (3.13) and (3.17) it becomes obvious that due to the application of OFDM, the subcarrierwise investigation is feasible in the multiple–MT and multiple–AP case of JOINT and results in a relaxed computational effort in data estimation at the CU.

Therefore, a subcarrierwise representation is favorable, if data estimation is considered, i.e.,

$$
\underbrace{\begin{pmatrix} \underline{\tilde{e}}_{u,n_F}^{(1)} \\ \vdots \\ \underline{\tilde{e}}_{u,n_F}^{(K_B)} \end{pmatrix}}_{\underline{\tilde{\mathbf{e}}}_{u,n_F}} = \underbrace{\begin{pmatrix} \underline{\tilde{h}}_{n_F}^{(1,1)} & \cdots & \underline{\tilde{h}}_{n_F}^{(K,1)} \\ \vdots & & \vdots \\ \underline{\tilde{h}}_{n_F}^{(1,K_B)} & \cdots & \underline{\tilde{h}}_{n_F}^{(K,K_B)} \end{pmatrix}}_{\underline{\tilde{\mathbf{H}}}_{u,n_F}} \cdot \underbrace{\begin{pmatrix} \underline{\tilde{s}}_{u,n_F}^{(1)} \\ \vdots \\ \underline{\tilde{s}}_{u,n_F}^{(K)} \end{pmatrix}}_{\underline{\tilde{\mathbf{s}}}_{u,n_F}} + \underbrace{\begin{pmatrix} \underline{\tilde{n}}_{u,n_F}^{(1)} \\ \vdots \\ \underline{\tilde{n}}_{u,n_F}^{(K_B)} \end{pmatrix}}_{\underline{\tilde{\mathbf{n}}}_{u,n_F}}
\tag{3.20}
$$

holds for the corresponding subcarrier n_F, $n_F = 1 \ldots N_F$.

In the DL, with (3.11) (3.5) can be rewritten as

$$
\underline{\tilde{\mathbf{e}}}_d^{(k)} = \underline{\tilde{\mathbf{H}}}^{(k,\ k_B)}\, \underline{\tilde{\mathbf{s}}}_d^{(k_B)} +\ \underline{\tilde{\mathbf{n}}}_d^{(k)}
\tag{3.21}
$$

for the DL transmission. Due to the reciprocity of the UL and the DL channel in the application of TDD, the total channel matrix in the DL

$$
\underline{\tilde{\mathbf{H}}}_d = \underline{\tilde{\mathbf{H}}}_u^{\mathrm{T}} = \begin{pmatrix} \underline{\tilde{\mathbf{H}}}^{(1,1)} & \cdots & \underline{\tilde{\mathbf{H}}}^{(1,K_B)} \\ \vdots & & \vdots \\ \underline{\tilde{\mathbf{H}}}^{(K,1)} & \cdots & \underline{\tilde{\mathbf{H}}}^{(K,K_B)} \end{pmatrix}
\tag{3.22}
$$

holds. With (3.22), with the total vector

$$
\underline{\tilde{\mathbf{s}}}_d = \left(\underline{\tilde{\mathbf{s}}}_d^{(1)\mathrm{T}} \ldots \underline{\tilde{\mathbf{s}}}_d^{(K_B)\mathrm{T}} \right)^{\mathrm{T}}
\tag{3.23}
$$

of the transmitted signals of dimension $K_B N_F$, with the total vector

$$
\underline{\tilde{\mathbf{e}}}_d = \left(\underline{\tilde{\mathbf{e}}}_d^{(1)\mathrm{T}} \ldots \underline{\tilde{\mathbf{e}}}_d^{(K)\mathrm{T}} \right)^{\mathrm{T}}
\tag{3.24}
$$

of the receive signals of dimension $K N_F$ and with the total vector

$$
\underline{\tilde{\mathbf{n}}}_d = \left(\underline{\tilde{\mathbf{n}}}_d^{(1)\mathrm{T}} \ldots \underline{\tilde{\mathbf{n}}}_d^{(K)\mathrm{T}} \right)^{\mathrm{T}}
\tag{3.25}
$$

of the noise vector of dimension $K N_F$, (3.21) takes the form

$$
\underline{\tilde{\mathbf{e}}}_d = \underline{\tilde{\mathbf{H}}}_d\, \underline{\tilde{\mathbf{s}}}_d +\ \underline{\tilde{\mathbf{n}}}_d
\tag{3.26}
$$

for the multiple–MT and multiple–AP scenario in the DL of JOINT, where $\underline{\tilde{\mathbf{s}}}_d$ is the designed on the basis of the transmitted data vector

$$
\underline{\tilde{\mathbf{d}}}_d = \left(\underline{\tilde{d}}_{d,1}^{(1)} \ldots \underline{\tilde{d}}_{d,N_F}^{(1)} \ldots \underline{\tilde{d}}_{d,1}^{(K)} \ldots \underline{\tilde{d}}_{d,N_F}^{(K)} \right)^{\mathrm{T}}
\tag{3.27}
$$

of dimension $K N_F$.
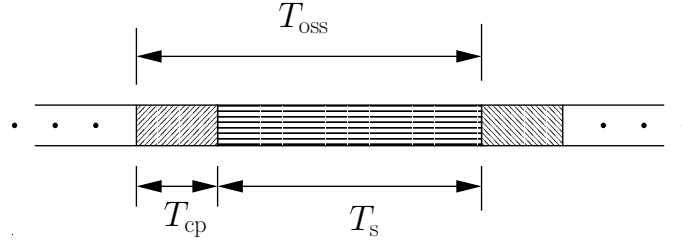
Fig. 3.2. Temporal structure of an OFDM slot

Moreover, the subcarrierwise DL transmission of JOINT reads

$$
\underbrace{\begin{pmatrix} \tilde{\underline{e}}_{\mathrm{d},n_{\mathrm{F}}}^{(1)} \\ \vdots \\ \tilde{\underline{e}}_{\mathrm{d},n_{\mathrm{F}}}^{(K)} \end{pmatrix}}_{\tilde{\underline{\mathbf{e}}}_{\mathrm{d},n_{\mathrm{F}}}} = \underbrace{\begin{pmatrix} \tilde{\underline{h}}_{n_{\mathrm{F}}}^{(1,1)} & \cdots & \tilde{\underline{h}}_{n_{\mathrm{F}}}^{(1,K_{\mathrm{B}})} \\ \vdots & & \vdots \\ \tilde{\underline{h}}_{n_{\mathrm{F}}}^{(K,1)} & \cdots & \tilde{\underline{h}}_{n_{\mathrm{F}}}^{(K,K_{\mathrm{B}})} \end{pmatrix}}_{\tilde{\underline{\mathbf{H}}}_{\mathrm{d},n_{\mathrm{F}}} = \tilde{\underline{\mathbf{H}}}_{\mathrm{u},n_{\mathrm{F}}}^{\mathrm{T}}} \cdot \underbrace{\begin{pmatrix} \tilde{\underline{s}}_{\mathrm{d},n_{\mathrm{F}}}^{(1)} \\ \vdots \\ \tilde{\underline{s}}_{\mathrm{d},n_{\mathrm{F}}}^{(K_{\mathrm{B}})} \end{pmatrix}}_{\tilde{\underline{\mathbf{s}}}_{\mathrm{d},n_{\mathrm{F}}}} + \underbrace{\begin{pmatrix} \tilde{\underline{n}}_{\mathrm{d},n_{\mathrm{F}}}^{(1)} \\ \vdots \\ \tilde{\underline{n}}_{\mathrm{d},n_{\mathrm{F}}}^{(K)} \end{pmatrix}}_{\tilde{\underline{\mathbf{n}}}_{\mathrm{d},n_{\mathrm{F}}}} . \tag{3.28}
$$

3.3   Time synchronization

A crucial task in OFDM systems are time and frequency synchronization [KMH98, vNP00, FK03]. In this section we consider the time synchronization problem. As the point–to–point OFDM system is extended to the multipoint–to–multipoint OFDM system a new problem of time synchronization arises, which will be explained and solved in the following. Before we go deeper into the topic, it is necessary to briefly introduce some basics, e.g., on the OFDM symbol structure.

Each OFDM symbol slot consists of two parts [Pra98, vNP00, FK03]:

- The OFDM symbol of duration T_{s}, which contains the data or the pilots to be transmitted by being mapped on the subcarriers, and

- the above mentioned cyclic prefix of duration T_{cp}, which contains a cyclic extension of the OFDM symbol [PR80, vNP00].

Consequently,

$$
T_{\mathrm{oss}} = T_{\mathrm{s}} + T_{\mathrm{cp}} \tag{3.29}
$$

holds for the duration of the OFDM symbol slot, as depicted in Fig.3.2.

a)

b)
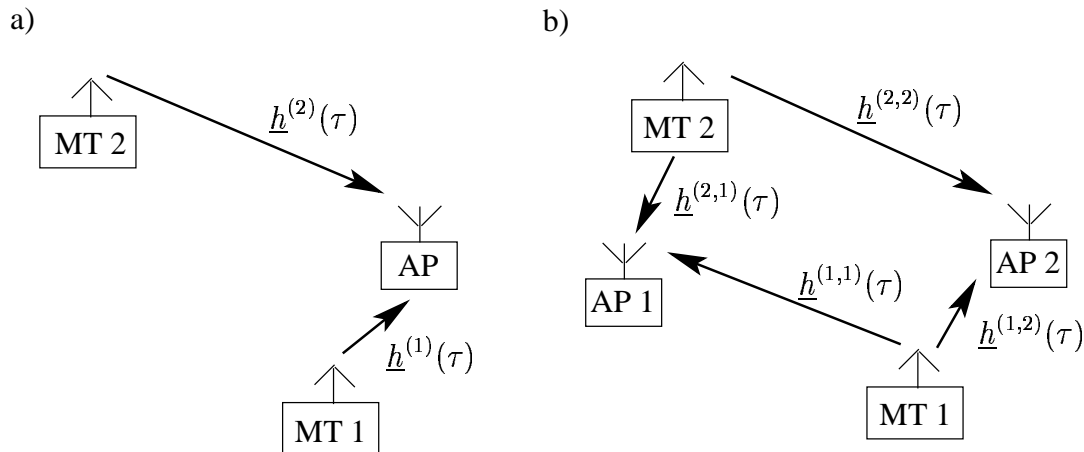
Fig. 3.3. Time synchronization issues in the UL
   a) multipoint–to–point transmission
   b) multipoint–to–multipoint transmission as in JOINT

In the case of point–to–point OFDM transmission systems time synchronization is a well studied problem which can be solved by controlling the timing reference of e.g., the transmitter [vNP00, FK03].

If we extend such a point–to–point system to a multipoint–to–point system as shown in Fig. 3.3a with different time delays between the MTs and the APs, there are also well known solutions to the time synchronization problem [KMH98, vdBBB$^+$99]. Totally different is the situation in the case of JOINT, see Fig. 3.3b, where we have a multipoint–to–multipoint system. In such a system, in the example of Fig. 3.3b we consider the case K equal to two, it is generally impossible to achieve that the signals of MT 1 and MT 2 arrive synchronously both at AP 1 and AP 2. An exception would be the particular situation that all distances between APs and MTs would be equal. In what follows we will briefly show how time synchronization of JOINT can be achieved in situations as the one shown in Fig.3.3b.

Fig. 3.4 shows schematically the magnitudes of the four CIRs $\underline{h}^{(k,\ k_\mathrm{B})}(\tau)$, k, $k_\mathrm{B} \in \{1,\ 2\}$ introduced in Fig. 3.3b. In this example the smallest possible value of T_cp would be given by

$$T_\mathrm{cp,min} = \tau_\mathrm{max}^{(1,1)} - \tau_\mathrm{min}^{(1,2)} = \tau_\mathrm{sup} - \tau_\mathrm{min}^{(1,2)}. \tag{3.30}$$

τ_sup denotes the supremum of the maximum delays. Therefore with respect to the time synchronization problem in JOINT we propose to choose

$$T_\mathrm{cp} \geq \tau_\mathrm{sup}. \tag{3.31}$$
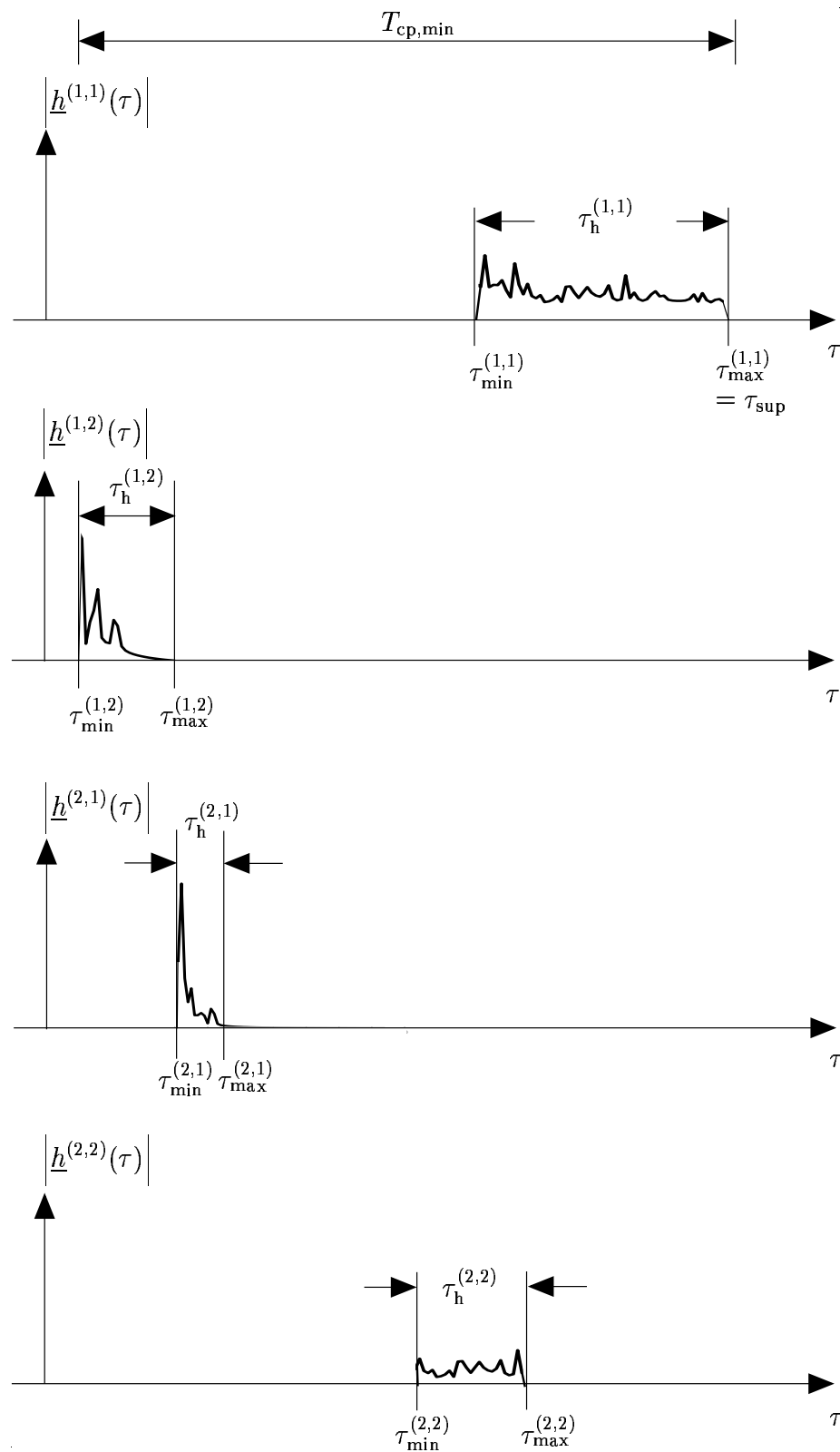
Fig. 3.4. Choice of the duration T_{cp} of the cyclic prefix in JOINT
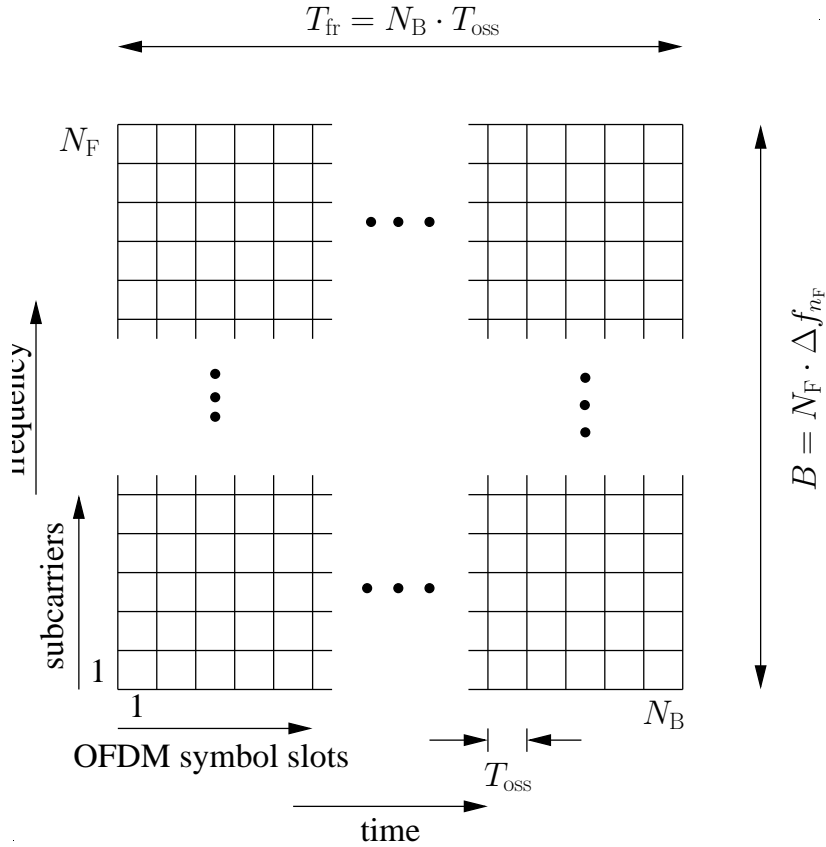
Fig. 3.5. Time–frequency representation of an OFDM frame

3.4   Parametrization of JOINT

The design of an OFDM based system like JOINT demands a trade–off between various system requirements and channel properties, which, into the bargain, often conflict with each other. This section presents important parameters and relations between them in order to achieve a proper design of JOINT.

Fig. 3.5 illustrates the time–frequency representation of an OFDM frame as applied in JOINT. In the time direction, one OFDM frame stretches out over a total of N_B OFDM symbol slots. Each OFDM symbol slot n_B, $n_\mathrm{B} = 1 \ldots N_\mathrm{B}$, covers the N_F available subcarriers in the frequency direction. Adjacent subcarriers are spaced by Δf_{n_F} apart. The duration T_fr of an OFDM frame is given by the product of the number N_B of OFDM symbol slots and the duration T_oss of one OFDM symbol slot, i. e.,

$$T_\mathrm{fr} = N_\mathrm{B} \cdot T_\mathrm{oss}, \tag{3.32}$$

whereas the product of the number N_F of available subcarriers and the subcarrier

spacing $\Delta f_{n_{\mathrm{F}}}$ gives the system bandwidth B, i. e.,

$$B = N_{\mathrm{F}} \cdot \Delta f_{n_{\mathrm{F}}}. \tag{3.33}$$

Now, following the well known rationale of OFDM [WE71, Bin90, vNP00, FK03], certain relations have to be fulfilled between the quantities of, such as, the subcarrier spacing $\Delta f_{n_{\mathrm{F}}}$, the OFDN symbol duration T_{s}, the supremum τ_{sup} of the maximum delays and the cyclic prefix duration T_{cp}.

In order to achieve the orthogonality between the adjacent subcarriers typical for OFDM [Bin90, vNP00, FK03],

$$T_{\mathrm{s}} \cdot \Delta f_{n_{\mathrm{F}}} = 1 \tag{3.34}$$

has to be valid. The cyclic prefix duration T_{cp} must be chosen in such a way that it at least exceeds the supremum of the maximum delay τ_{sup} of the CIR, which is approximately the reverse of the coherence bandwidth B_{c} of the channel, to overcome the frequency selectivity, i.e.,

$$T_{\mathrm{cp}} \geq \frac{1}{B_{\mathrm{c}}} \approx \tau_{\mathrm{sup}} \tag{3.35}$$

is to be met. Providing a cyclic prefix of the required non–zero duration T_{cp} reduces transmission capacity and is the price to be paid for enabling low cost signal processing at the receiver by FFT also in the case of radio channels exhibiting a non–zero delay spread [PR80, Bin90, Pra98, vNP00, FK03]. This price can be quantified by a quantity $T_{\mathrm{cp}}/T_{\mathrm{s}}$ termed overhead. Usually, in OFDM systems

$$T_{\mathrm{cp}}/T_{\mathrm{s}} = 0.1 \ \ldots \ 0.25 \tag{3.36}$$

holds for the overhead [PR80, Bin90, Pra98, vNP00, FK03] so that the overhead $T_{\mathrm{cp}}/T_{\mathrm{s}}$ introduced by the insertion of the cyclic prefix is kept as low as possible. According to (3.33), (3.34) and (3.36) the subcarrier spacing $\Delta f_{n_{\mathrm{F}}}$ is given by

$$\Delta f_{n_{\mathrm{F}}} = \frac{B}{N_{\mathrm{F}}} = \frac{1}{T_{\mathrm{s}}} = \frac{1}{4 \ \ldots \ 10 \, T_{\mathrm{cp}}}. \tag{3.37}$$

With (3.35) and (3.37) follows

$$B_{\mathrm{c}} \approx \frac{1}{\tau_{\mathrm{sup}}} \approx \frac{1}{T_{\mathrm{cp}}} = 4 \ \ldots \ 10 \, \Delta f_{n_{\mathrm{F}}}. \tag{3.38}$$

One of the drawbacks of the OFDM transmission technique is its sensitivity to Doppler shifts [vNP00, KS01, FK03]. A measure for the Doppler shift is the maximum Doppler frequency $f_{\mathrm{d,max}}$. With the carrier frequency f_{c}, the maximum relative velocity v_{max} between transmitter and receiver and the speed c_0 of light

$$f_{\mathrm{d,max}} = f_{\mathrm{c}} \frac{v_{\mathrm{max}}}{c_0}, \tag{3.39}$$

Table 3.1. System parametrization of JOINT

Parameter	Value
supremum of maximum delays	$\tau_{\mathrm{sup}} = 5\ \mu\mathrm{s}$
coherence bandwidth	$B_{\mathrm{c}} = 200\ \mathrm{kHz}$
carrier frequency	$f_{\mathrm{c}} = 5.5\ \mathrm{GHz}$
maximum speed	$v_{\mathrm{max}} = 200\ \mathrm{km/h}$
maximum Doppler frequency	$f_{\mathrm{d,max}} = 1.018\ \mathrm{kHz}$
break–even–point distance	$\rho_{\mathrm{B}} = 300\ \mathrm{m}$
attenuation exponents	$\alpha_1 = 2.0$ and $\alpha_2 = 4.0$
antenna gains	$g_{\mathrm{T}} = g_{\mathrm{R}} = 1$
system bandwidth	$B = 20\ \mathrm{MHz}$
OFDM symbol duration	$T_{\mathrm{s}} = 25.6\ \mu\mathrm{s}$
cyclic prefix duration	$T_{\mathrm{cp}} = 6.4\ \mu\mathrm{s}$
OFDM symbol slot duration	$T_{\mathrm{oss}} = 32\ \mu\mathrm{s}$
number of subcarriers (FFT length)	$N_{\mathrm{F}} = 512$
subcarrier spacing	$\Delta f_{n_{\mathrm{F}}} = 39.063\ \mathrm{kHz}$
modulation	QAM

holds [Kam96, Hay01]. The sensitivity of OFDM to Doppler shifts is negligible if

$$\Delta f_{n_{\mathrm{F}}} \gg f_{\mathrm{d,max}} \tag{3.40}$$

holds as a requirement to be observed in OFDM system design.

To describe the log–normal fading the break–even–point distance ρ_{B} of (2.20) is assumed to be 300 m for the typical outdoor environment. The two attenuation exponents α_1 and α_2 of (2.20) are assumed to be equal to 2.0 and 4.0, respectively. Moreover, the antenna gains g_{T} and g_{R} of the transmit antenna and the receive antenna are both assumed to be one.

In order to illustrate the theoretical considerations of this thesis by quantitative examples, a certain parameter set of JOINT should be chosen. Table 3.1 gives the chosen system parametrization of JOINT.

Chapter 4

Maximum–likelihood joint channel estimation in the uplink of JOINT

4.1 Preliminary remarks

An important presupposition of the data detection and transmission of JOINT is that channel state information (CSI) is known at the CU. The task to estimate the CIRs and the CTFs is performed by JCE at the CU in the UL of JOINT. JCE, a pilot–aided multiuser channel estimation technique [SMWB01, MWSL02], aims at estimating all the CTFs between MTs and APs in a SA simultaneously with the aid of the pilot signals in the UL, which have special properties known both at the transmitters and receivers. In JOINT it is assumed that the pilot symbols are transmitted once in the middle of an OFDM frame, which contains a number of symbol slots assigned to the UL and the DL symbols.

4.2 System model

The pilot symbols radiated by MT $k, k = 1 \ldots K$, can be either stacked in an MT–specific pilot vector

$$\underline{\tilde{\mathbf{p}}}^{(k)} = \left(\underline{\tilde{p}}_1^{(k)} \ldots \underline{\tilde{p}}_{N_{\mathrm{F}}}^{(k)} \right)^{\mathrm{T}} \tag{4.1}$$

of dimension N_{F}, which forms a part of the total pilot vector of (3.19), or in an $N_{\mathrm{F}} \times N_{\mathrm{F}}$ diagonal pilot matrix [SMWB01, MWSL02]

$$\underline{\tilde{\mathbf{P}}}^{(k)} = \begin{pmatrix} \underline{\tilde{p}}_1^{(k)} & \cdots & 0 \\ \vdots & \ddots & \vdots \\ 0 & \cdots & \underline{\tilde{p}}_{N_{\mathrm{F}}}^{(k)} \end{pmatrix} . \tag{4.2}$$

With $\underline{\tilde{\mathbf{P}}}^{(k)}$ of (4.2) the total pilot matrix

$$\underline{\tilde{\mathbf{P}}} = \left(\begin{array}{ccc} \underline{\tilde{\mathbf{P}}}^{(1)} & \ldots & \underline{\tilde{\mathbf{P}}}^{(K)} \end{array} \right) \tag{4.3}$$

of dimensions $N_{\mathrm{F}} \times (K N_{\mathrm{F}})$ can be established [SMWB01, MWSL02]. According to (2.1) and (2.3), the K unknown CIR vectors

$$\underline{\mathbf{h}}^{(k,k_{\mathrm{B}})} = \left(\underline{h}_1^{(k,k_{\mathrm{B}})} \ldots \underline{h}_W^{(k,k_{\mathrm{B}})} \right)^{\mathrm{T}} \tag{4.4}$$

valid for AP $k_{\mathrm{B}}, k_{\mathrm{B}} = 1 \ldots K_{\mathrm{B}}$, can be stacked in an AP–specific CIR vector

$$\underline{\mathbf{h}}^{(k_{\mathrm{B}})} = \left(\underline{\mathbf{h}}^{(1,k_{\mathrm{B}})\mathrm{T}} \ \ldots \ \underline{\mathbf{h}}^{(K,k_{\mathrm{B}})\mathrm{T}} \right)^{\mathrm{T}} \tag{4.5}$$

of dimension KW, and the K unknown CTF vectors

$$\underline{\tilde{\mathbf{h}}}^{(k,k_{\mathrm{B}})} = \left(\underline{\tilde{h}}_1^{(k,k_{\mathrm{B}})} \ \ldots \underline{\tilde{h}}_{N_{\mathrm{F}}}^{(k,k_{\mathrm{B}})} \right)^{\mathrm{T}} \tag{4.6}$$

valid for the AP k_{B} can be stacked in an AP–specific CTF vector

$$\underline{\tilde{\mathbf{h}}}^{(k_{\mathrm{B}})} = \left(\underline{\tilde{\mathbf{h}}}^{(1,k_{\mathrm{B}})\mathrm{T}} \ \ldots \ \underline{\tilde{\mathbf{h}}}^{(K,k_{\mathrm{B}})\mathrm{T}} \right)^{\mathrm{T}} \tag{4.7}$$

of dimension KN_{F}. It is assumed that at the AP k_{B} the AP–specific receive vector

$$\underline{\tilde{\mathbf{e}}}_{\mathrm{h}}^{(k_{\mathrm{B}})} = \left(\underline{\tilde{e}}_{\mathrm{h},1}^{(k_{\mathrm{B}})} \ \ldots \ \underline{\tilde{e}}_{\mathrm{h},N_{\mathrm{F}}}^{(k_{\mathrm{B}})} \right)^{\mathrm{T}} \tag{4.8}$$

of dimension N_{F} is corrupted by the noise vector

$$\underline{\tilde{\mathbf{n}}}_{\mathrm{h}}^{(k_{\mathrm{B}})} = \left(\underline{\tilde{n}}_{\mathrm{h},1}^{(k_{\mathrm{B}})} \ \ldots \ \underline{\tilde{n}}_{\mathrm{h},N_{\mathrm{F}}}^{(k_{\mathrm{B}})} \right)^{\mathrm{T}} \tag{4.9}$$

of dimension N_{F}. With (4.3), (4.7) and (4.9)

$$\underline{\tilde{\mathbf{e}}}_{\mathrm{h}}^{(k_{\mathrm{B}})} = \underline{\tilde{\mathbf{P}}} \, \underline{\tilde{\mathbf{h}}}^{(k_{\mathrm{B}})} + \underline{\tilde{\mathbf{n}}}_{\mathrm{h}}^{(k_{\mathrm{B}})} \tag{4.10}$$

holds for the AP–specific receive vector of (4.8) [SMWB01, MWSL02], where the $K \, N_{\mathrm{F}}$ unknown elements of the AP–specific CTF vector $\underline{\tilde{\mathbf{h}}}^{(k_{\mathrm{B}})}$ of (4.7) have to be determined.

During the time slot for the pilot transmission in the UL, the pilot energies

$$E_{\mathrm{p},n_{\mathrm{F}}}^{(k)} = \frac{1}{2} |\underline{\tilde{p}}_{-n_{\mathrm{F}}}^{(k)}|^2 = E_{\mathrm{p}}, k = 1 \ldots K, \ n_{\mathrm{F}} = 1 \ldots N_{\mathrm{F}}, \tag{4.11}$$

invested for the pilot symbols $\underline{\tilde{p}}_{-n_{\mathrm{F}}}^{(k)}$ of (4.1) are assumed to be equal. If $\underline{\tilde{\mathbf{n}}}_{\mathrm{h}}^{(k_{\mathrm{B}})}$ of (4.9) is uncorrelated,

$$\mathrm{E} \left\{ \underline{\tilde{\mathbf{n}}}_{\mathrm{h}}^{(k_{\mathrm{B}})} \ \underline{\tilde{\mathbf{n}}}_{\mathrm{h}}^{(k_{\mathrm{B}})*\mathrm{T}} \right\} = 2\sigma^2 \mathbf{I}^{N_{\mathrm{F}}}, k_{\mathrm{B}} = 1 \ldots K_{\mathrm{B}}, \tag{4.12}$$

follows for the covariance matrix of $\underline{\tilde{\mathbf{n}}}_{\mathrm{h}}^{(k_{\mathrm{B}})}$ with σ^2 denoting the variance of the real and the imaginary parts of the components of $\underline{\tilde{\mathbf{n}}}_{\mathrm{h}}^{(k_{\mathrm{B}})}$. In the SA full system load is assumed to hold in the following, that is

$$N_{\mathrm{F}} = K \cdot W. \tag{4.13}$$

4.3   Algorithm of joint channel estimation

The goal of JCE is to obtain the CTF estimates on the basis of the information of the AP–specific receive vector $\tilde{\underline{\mathbf{e}}}_{\mathrm{h}}^{(k_{\mathrm{B}})}$, $k_{\mathrm{B}} = 1 \ldots K_{\mathrm{B}}$, of (4.10) and the total pilot matrix $\tilde{\underline{\mathbf{P}}}$ of (4.3).

With a $(KN_{\mathrm{F}}) \times (KW)$ block–diagonal matrix [SMWB01, MWSL02]

$$
\tilde{\underline{\boldsymbol{\mathcal{F}}}}_{W,\mathrm{tot}} = \begin{pmatrix} [\tilde{\underline{\boldsymbol{\mathcal{F}}}}]_{N_{\mathrm{F}},W}^{1,1} & \cdots & 0 \\ \vdots & \ddots & \vdots \\ 0 & \cdots & [\tilde{\underline{\boldsymbol{\mathcal{F}}}}]_{N_{\mathrm{F}},W}^{1,1} \end{pmatrix}, \tag{4.14}
$$

whose diagonal submatrices are the dimension–reduced Fourier matrices $[\tilde{\underline{\boldsymbol{\mathcal{F}}}}]_{N_{\mathrm{F}},W}^{1,1}$ of (2.9), and with the AP–specific CIR vector $\underline{\mathbf{h}}^{(k_{\mathrm{B}})}$ of (4.5), (2.9) is rewritten as

$$
\tilde{\underline{\mathbf{h}}}^{(k_{\mathrm{B}})} = \tilde{\underline{\boldsymbol{\mathcal{F}}}}_{W,\mathrm{tot}} \underline{\mathbf{h}}^{(k_{\mathrm{B}})} \tag{4.15}
$$

for the multiple–MT and multiple–AP scenario with respect to the AP k_{B}. With (4.15) (4.10) can be rewritten as [SMWB01, MWSL02]

$$
\tilde{\underline{\mathbf{e}}}_{\mathrm{h}}^{(k_{\mathrm{B}})} = \underbrace{\tilde{\underline{\mathbf{P}}} \, \tilde{\underline{\boldsymbol{\mathcal{F}}}}_{W,\mathrm{tot}}}_{\tilde{\underline{\boldsymbol{\mathcal{G}}}}} \underline{\mathbf{h}}^{(k_{\mathrm{B}})} + \tilde{\underline{\mathbf{n}}}_{\mathrm{h}}^{(k_{\mathrm{B}})}. \tag{4.16}
$$

In order to minimize the mean square error $\mathrm{E}\left\{||\tilde{\underline{\mathbf{e}}}_{\mathrm{h}}^{(k_{\mathrm{B}})} - \tilde{\underline{\boldsymbol{\mathcal{G}}}} \, \hat{\underline{\mathbf{h}}}^{(k_{\mathrm{B}})}||^2\right\}$ the estimate

$$
\hat{\underline{\mathbf{h}}}^{(k_{\mathrm{B}})} = \left(\tilde{\underline{\boldsymbol{\mathcal{G}}}}^{*\mathrm{T}} \tilde{\underline{\boldsymbol{\mathcal{G}}}}\right)^{-1} \tilde{\underline{\boldsymbol{\mathcal{G}}}}^{*\mathrm{T}} \tilde{\underline{\mathbf{e}}}_{\mathrm{h}}^{(k_{\mathrm{B}})} \tag{4.17}
$$

of the AP–specific CIR vector $\underline{\mathbf{h}}^{(k_{\mathrm{B}})}$ of (4.5) can be obtained [SMWB01, MWSL02]. If the white noise $\tilde{\underline{\mathbf{n}}}_{\mathrm{h}}^{(k_{\mathrm{B}})}$ of (4.9) also yields to Gaussian distribution, the estimate $\hat{\underline{\mathbf{h}}}^{(k_{\mathrm{B}})}$ of (4.17) is the maximum–likelihood (ML) estimate. Obviously, $\tilde{\underline{\boldsymbol{\mathcal{F}}}}_{W,\mathrm{tot}}$ is known once N_{F} and W are chosen. The number of the unknowns concerning the AP–specific channels is reduced from KN_{F} to KW. With (4.15) and (4.17) the unbiased estimate of the AP–specific CTF vector $\tilde{\underline{\mathbf{h}}}^{(k_{\mathrm{B}})}$ is given by [SMWB01, MWSL02]

$$
\begin{aligned} \hat{\tilde{\underline{\mathbf{h}}}}^{(k_{\mathrm{B}})} &= \underbrace{\tilde{\underline{\boldsymbol{\mathcal{F}}}}_{W,\mathrm{tot}} \left(\tilde{\underline{\boldsymbol{\mathcal{G}}}}^{*\mathrm{T}} \tilde{\underline{\boldsymbol{\mathcal{G}}}}\right)^{-1} \tilde{\underline{\boldsymbol{\mathcal{G}}}}^{*\mathrm{T}}}_{\tilde{\underline{\mathbf{Z}}}} \tilde{\underline{\mathbf{e}}}_{\mathrm{h}}^{(k_{\mathrm{B}})} \\ &= \tilde{\underline{\mathbf{h}}}^{(k_{\mathrm{B}})} + \tilde{\underline{\mathbf{Z}}} \, \tilde{\underline{\mathbf{n}}}_{\mathrm{h}}^{(k_{\mathrm{B}})}. \end{aligned} \tag{4.18}
$$

(4.16) and (4.18) show that either the matrix $\tilde{\underline{\boldsymbol{\mathcal{G}}}}$ or the matrix $\tilde{\underline{\mathbf{Z}}}$ contains the matrix $\tilde{\underline{\boldsymbol{\mathcal{F}}}}_{W,\mathrm{tot}}$, i.e., the receive signals on all the subcarriers have to be processed jointly.

Therefore, JCE is not a subcarrierwise process. Once the pilot matrix $\tilde{\underline{\mathbf{P}}}$ is chosen for the transmission, the matrices $\tilde{\underline{\boldsymbol{\mathcal{G}}}}$ and $\tilde{\underline{\mathbf{Z}}}$ are fixed, since the matrix $\tilde{\underline{\boldsymbol{\mathcal{F}}}}_{W,\text{tot}}$ is constant for the given K, W and N_F. Moreover, for all the APs the matrices $\tilde{\underline{\boldsymbol{\mathcal{G}}}}$ and $\tilde{\underline{\mathbf{Z}}}$ are the same because the design of the pilot matrix $\tilde{\underline{\mathbf{P}}}$ is regardless of the APs. These facts can be utilized in the implementation of the algorithm.

4.4   Choice of the pilot vectors

As stated previously, the pilot vectors are not only known both at the MTs and the CU, but also have some special properties so that the estimates $\hat{\tilde{\underline{\mathbf{h}}}}^{(k_\text{B})}$ of the $\tilde{\underline{\mathbf{h}}}^{(k_\text{B})}$ of (4.18) with good performances can be obtained without too much effort. Now a question arises: Which kind of vectors can be chosen as the pilot vectors $\tilde{\underline{\mathbf{p}}}^{(k)}$ of (4.1)?

To answer the above question, the performance evaluation criterion of JCE is first discussed. In [SMWB01, MWSL02] the signal–to–noise–ratio (SNR) degradation is introduced as an evaluation criterion for JCE in the presence of the noise. The SNR degradation is defined as the ratio of the SNR obtained in a reference case and the SNR obtained by JCE. The single MT case is chosen as the reference case [SMWB01, MWSL02], where the MT k uses all the N_F available subcarriers for the pilot transmission, e.g., the pilot vector

$$\tilde{\underline{\mathbf{p}}}_\text{ref}^{(k)} = \sqrt{2E_\text{p}} \left(\underbrace{1 \ldots 1}_{N_\text{F}} \right)^\text{T} \tag{4.19}$$

for the considered MT k is transmitted. Then the reference SNR

$$\gamma_{\text{ref},n_\text{F}}^{(k,k_\text{B})} = \frac{E_\text{p} N_\text{F}}{2\sigma^2 W} \left| \tilde{\underline{h}}_{n_\text{F}}^{(k,k_\text{B})} \right|^2 \tag{4.20}$$

for the estimate $\hat{\tilde{\underline{h}}}_{n_\text{F}}^{(k,k_\text{B})}$ of the CTF $\tilde{\underline{h}}_{n_\text{F}}^{(k,k_\text{B})}$ at the output of the joint channel estimator is obtained [SMWB01, MWSL02]. With (4.18) follows the SNR

$$\begin{aligned}
\gamma_{n_\text{F}}^{(k,k_\text{B})} &= \frac{\left| \tilde{\underline{h}}_{n_\text{F}}^{(k,k_\text{B})} \right|^2}{\left| \tilde{\underline{h}}_{n_\text{F}}^{(k,k_\text{B})} - \hat{\tilde{\underline{h}}}_{n_\text{F}}^{(k,k_\text{B})} \right|^2} \\
&= \frac{\left| \tilde{\underline{h}}_{n_\text{F}}^{(k,k_\text{B})} \right|^2}{2\sigma^2 \left[\tilde{\underline{\mathbf{Z}}} \, \tilde{\underline{\mathbf{Z}}}^{*\text{T}} \right]_{i,i}}, i = (k-1)N_\text{F} + n_\text{F}, \tag{4.21}
\end{aligned}$$

of the estimate $\hat{\tilde{\underline{h}}}_{n_{\mathrm{F}}}^{(k,k_{\mathrm{B}})}$ of the CTF $\tilde{\underline{h}}_{n_{\mathrm{F}}}^{(k,k_{\mathrm{B}})}$ [SMWB01, MWSL02]. Consequently, with (4.20) and (4.21) the SNR degradation

$$
\begin{aligned}
\delta_{n_{\mathrm{F}}}^{(k,k_{\mathrm{B}})} &= \frac{\gamma_{\mathrm{ref},n_{\mathrm{F}}}^{(k,k_{\mathrm{B}})}}{\gamma_{n_{\mathrm{F}}}^{(k,k_{\mathrm{B}})}} \\
&= \frac{E_{\mathrm{p}} N_{\mathrm{F}}}{W}[\,\tilde{\underline{\mathbf{Z}}}\,\tilde{\underline{\mathbf{Z}}}^{*\mathrm{T}}]_{i,i}, i = (k-1)N_{\mathrm{F}} + n_{\mathrm{F}},
\end{aligned} \tag{4.22}
$$

can be obtained [SMWB01, MWSL02]. In (4.22) the diagonal elements of $\tilde{\underline{\mathbf{Z}}}\,\tilde{\underline{\mathbf{Z}}}^{*\mathrm{T}}$ are anti–proportional to the pilot energy E_{p} so that the SNR degradations $\delta_{n_{\mathrm{F}}}^{(k,k_{\mathrm{B}})}$ do not depend on the pilot energy E_{p} [SMWB01, MWSL02]. With (4.16), (4.18) and (4.22) it is seen that for a given scenario where the parameters E_{p}, W, K and N_{F} are chosen, the matrix product $\tilde{\underline{\mathbf{Z}}}\,\tilde{\underline{\mathbf{Z}}}^{*\mathrm{T}}$ and the SNR degradations $\delta_{n_{\mathrm{F}}}^{(k,k_{\mathrm{B}})}$ of (4.22) depend only on the chosen pilot vectors $\tilde{\underline{\mathbf{p}}}^{(k)}$ of (4.1)[SMWB01, MWSL02].

The goal to design the pilot vectors $\tilde{\underline{\mathbf{p}}}^{(k)}$ of (4.1) for JCE is to obtain the SNR degradations $\delta_{n_{\mathrm{F}}}^{(k,k_{\mathrm{B}})}$ of (4.22) as small as possible [SMWB01, MWSL02]. A good example of the pilot vectors is designed on the basis of the well known Walsh codes [Pro95, MWSL02], whose SNR degradations $\delta_{n_{\mathrm{F}}}^{(k,k_{\mathrm{B}})}$ at the output of the joint channel estimator are equal to 1. In the frequency domain, the Walsh codes to be assigned to the MTs as pilots are chosen from the columns of the $N_{\mathrm{F}} \times N_{\mathrm{F}}$ Hadamard matrix [Pro95]. E.g., for $N_{\mathrm{F}} = 8$ follows the 8×8 Hadamard matrix

$$
\tilde{\mathbf{W}}_8 = \begin{pmatrix}
1 & 1 & 1 & 1 & 1 & 1 & 1 & 1 \\
1 & -1 & 1 & -1 & 1 & -1 & 1 & -1 \\
1 & 1 & -1 & -1 & 1 & 1 & -1 & -1 \\
1 & -1 & -1 & 1 & 1 & -1 & -1 & 1 \\
1 & 1 & 1 & 1 & -1 & -1 & -1 & -1 \\
1 & -1 & 1 & -1 & -1 & 1 & -1 & 1 \\
1 & 1 & -1 & -1 & -1 & -1 & 1 & 1 \\
1 & -1 & -1 & 1 & -1 & 1 & 1 & -1
\end{pmatrix}. \tag{4.23}
$$

According to (4.23) it is seen that if the pilots based on the Walsh codes are applied for JCE, all the N_{F} subcarriers are utilized simultaneously for the MTs and there may exist many different sets of pilots, since $K \leq N_{\mathrm{F}}$ is always valid in JOINT.

In this thesis, the pilot vectors based on the Walsh codes are applied for JCE.

Chapter 5

Linear zero–forcing joint detection in the uplink of JOINT

5.1 Preliminary remarks

As mentioned in Chapter 1 the CU minimizes the intra–SA MAI among the various simultaneously active links in the considered SA in the UL through JD, which belongs to the category of multiuser detection (MUD) [Ver98]. There are some optimum MUD approaches, e.g., the maximum a posteriori (MAP) sequence estimation [Ver86] and the maximum–likelihood (ML) sequence estimation [For72, Ver98] algorithms. However, such search processes for the data estimates are too computation–consuming and limit their application. Some suboptimum linear JD algorithms [Kle96, Ver98, Bla98] exist, which form a compromise between the system performance and the computational complexity, e.g., the zero–forcing (ZF) [Kle96, Ver98, Bla98, Skl04] JD and the minimum–mean–square–error (MMSE) [Kle96, Skl04] JD. In JOINT, the applied JD algorithm can be chosen from various options. For the sake of simplicity the linear receive–ZF (RxZF) JD is focused on in this thesis.

A subcarrierwise investigation of the data detection in the uplink is feasible due to the application of OFDM according to Chapter 3. Therefore, in the following sections the subcarierwise representations are used.

5.2 System model in the uplink of JOINT

For the OFDM based UL of JOINT, the subcarrierwise data transmission is illustrated in Fig.5.1. In a SA, K_B APs are fixedly located and connected to the CU, and K MTs are simultaneously active. For the subcarrier $n_\mathrm{F}, n_\mathrm{F} = 1 \ldots N_\mathrm{F}$, the data symbols $\underline{\tilde{d}}^{(k)}_{\mathrm{u},n_\mathrm{F}}$ of the MT $k, k = 1 \ldots K$, which can be stacked in a vector

$$\underline{\tilde{\mathbf{d}}}_{\mathrm{u},n_\mathrm{F}} = \left(\underline{\tilde{d}}^{(1)}_{\mathrm{u},n_\mathrm{F}} \ldots \underline{\tilde{d}}^{(K)}_{\mathrm{u},n_\mathrm{F}} \right)^{\mathrm{T}} \tag{5.1}$$

of dimension K, are handled and transmitted simultaneously into the multiport–to–multiport channel. The distorted signals are received by the APs and collected at the CU, where JD is performed. This yields the data estimate vector

$$\underline{\hat{\tilde{\mathbf{d}}}}_{\mathrm{u},n_\mathrm{F}} = \left(\underline{\hat{\tilde{d}}}^{(1)}_{\mathrm{u},n_\mathrm{F}} \ldots \underline{\hat{\tilde{d}}}^{(K)}_{\mathrm{u},n_\mathrm{F}} \right)^{\mathrm{T}}, \tag{5.2}$$
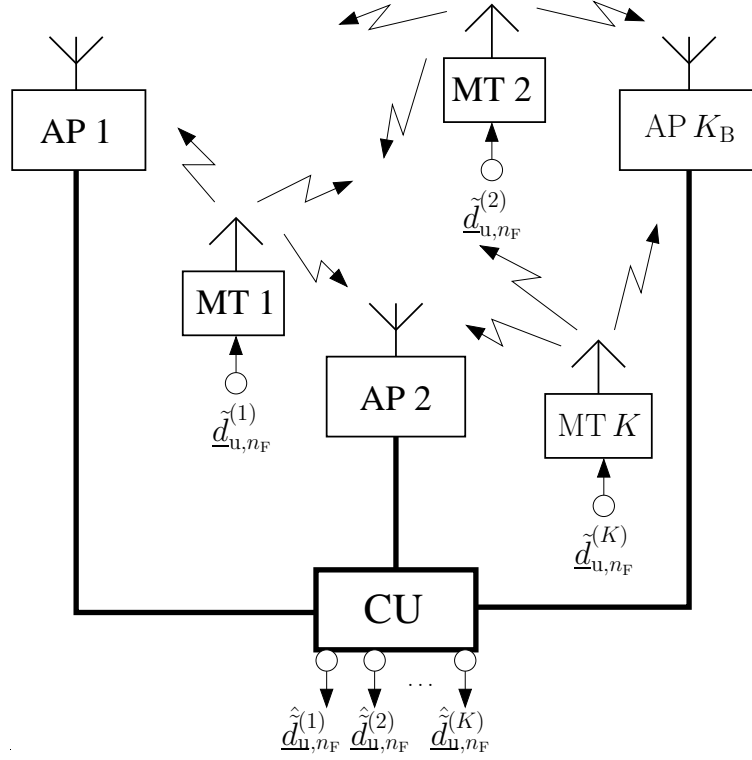
Fig. 5.1. Subcarrierwise system model of the UL of JOINT

which consists of K estimates $\hat{\tilde{\underline{d}}}_{\mathrm{u},n_\mathrm{F}}^{(k)}$ of the data symbols $\tilde{\underline{d}}_{\mathrm{u},n_\mathrm{F}}^{(k)}$ of (5.1).

Since one goal of JOINT is keeping the MT structure as simple as possible, simple OFDM transmitters are applied at the MTs. Therefore, the transmit vector $\tilde{\underline{\mathbf{s}}}_{\mathrm{u},n_\mathrm{F}}$ of (3.20) of dimension K in the UL is just equal to the data vector $\tilde{\underline{\mathbf{d}}}_{\mathrm{u},n_\mathrm{F}}$ of (5.1), i.e.,

$$\tilde{\underline{\mathbf{s}}}_{\mathrm{u},n_\mathrm{F}} = \tilde{\underline{\mathbf{d}}}_{\mathrm{u},n_\mathrm{F}}. \tag{5.3}$$

Consequently, (3.20) can be rewritten as

$$\tilde{\underline{\mathbf{e}}}_{\mathrm{u},n_\mathrm{F}} = \tilde{\underline{\mathbf{H}}}_{\mathrm{u},n_\mathrm{F}} \cdot \tilde{\underline{\mathbf{d}}}_{\mathrm{u},n_\mathrm{F}} + \tilde{\underline{\mathbf{n}}}_{\mathrm{u},n_\mathrm{F}}. \tag{5.4}$$

For the assumption of equal transmit energies

$$E_\mathrm{d} = \frac{1}{2}|\tilde{\underline{d}}_{\mathrm{u},n_\mathrm{F}}^{(k)}|^2, \tag{5.5}$$

and the independent data symbols $\tilde{\underline{d}}_{\mathrm{u},n_\mathrm{F}}^{(k)}$ of (5.1) the covariance matrix

$$\underline{\mathbf{R}}_{\mathrm{d,u}} = \mathrm{E}\left\{\tilde{\underline{\mathbf{d}}}_{\mathrm{u},n_\mathrm{F}} \tilde{\underline{\mathbf{d}}}_{\mathrm{u},n_\mathrm{F}}^{*\mathrm{T}}\right\} = 2E_\mathrm{d}\mathbf{I}^K \tag{5.6}$$

of the transmit data vector $\tilde{\underline{\mathbf{d}}}_{\mathrm{u},n_{\mathrm{F}}}$ is obtained. If the noise $\tilde{\underline{\mathbf{n}}}_{\mathrm{u},n_{\mathrm{F}}}$ of (3.20) is white with the variance σ^2 of the real and imaginary parts [Pro95],

$$\underline{\mathbf{R}}_{\mathrm{n},\mathrm{u}} = \mathrm{E}\left\{\ \tilde{\underline{\mathbf{n}}}_{\mathrm{u},n_{\mathrm{F}}}\ \tilde{\underline{\mathbf{n}}}_{\mathrm{u},n_{\mathrm{F}}}^{*\mathrm{T}}\right\} = 2\sigma^2 \mathbf{I}^{K_{\mathrm{B}}} \tag{5.7}$$

follows for the covariance matrix of the noise vector $\tilde{\underline{\mathbf{n}}}_{\mathrm{u},n_{\mathrm{F}}}$ of (3.20).

5.3 Algorithm of linear zero–forcing joint detection

5.3.1 Reference system: matched filter

The matched filter (MF) has a relatively simple structure including several correlators to match the corresponding channels. The MF delivers a biased data estimation vector [Kle96, Skl04]

$$
\begin{aligned}
\hat{\tilde{\underline{\mathbf{d}}}}_{\mathrm{u},n_{\mathrm{F}}} &= \left[\mathrm{diag}\left(\tilde{\underline{\mathbf{H}}}_{\mathrm{u},n_{\mathrm{F}}}^{*\mathrm{T}}\tilde{\underline{\mathbf{H}}}_{\mathrm{u},n_{\mathrm{F}}}\right)\right]^{-1}\tilde{\underline{\mathbf{H}}}_{\mathrm{u},n_{\mathrm{F}}}^{*\mathrm{T}}\tilde{\underline{\mathbf{e}}}_{\mathrm{u},n_{\mathrm{F}}}\\
&= \tilde{\underline{\mathbf{d}}}_{\mathrm{u},n_{\mathrm{F}}} + \mathrm{MAI\ part} + \mathrm{noise\ part} \tag{5.8}
\end{aligned}
$$

at the output. Ignoring the intra–SA MAI, in the SA based system the MF maximizes the SNR [Kle96, Skl04]

$$\gamma_{\mathrm{MF},n_{\mathrm{F}}}^{(k)} = \frac{E_{\mathrm{d}}}{\sigma^2}\left[\tilde{\underline{\mathbf{H}}}_{\mathrm{u},n_{\mathrm{F}}}^{*\mathrm{T}}\ \tilde{\underline{\mathbf{H}}}_{\mathrm{u},n_{\mathrm{F}}}\right]_{k,k},\ k = 1\ldots K, \tag{5.9}$$

of the data symbol $\tilde{\underline{d}}_{\mathrm{u},n_{\mathrm{F}}}^{(k)}$ of (5.1). Therefore, the MF is usually chosen as the reference system, which yields the optimum SNR.

5.3.2 Zero forcing

The idea of ZF comes out by multiplying the receive signal vector by a matrix, which can counteract the influence of the MAI. To find the solution to the linear equation system of (5.4) valid for the UL of JOINT, the number K of the unknowns $(\tilde{\underline{d}}_{\mathrm{u},n_{\mathrm{F}}}^{(k)})$ should not exceed the number K_{B} of the equations, i.e., the condition

$$K \le K_{\mathrm{B}} \tag{5.10}$$

must be satisfied. In such cases, the unbiased estimation vector [Kle96, Skl04]

$$
\begin{aligned}
\hat{\tilde{\underline{\mathbf{d}}}}_{\mathrm{u},n_{\mathrm{F}}} &= \left(\tilde{\underline{\mathbf{H}}}_{\mathrm{u},n_{\mathrm{F}}}^{*\mathrm{T}}\tilde{\underline{\mathbf{H}}}_{\mathrm{u},n_{\mathrm{F}}}\right)^{-1}\tilde{\underline{\mathbf{H}}}_{\mathrm{u},n_{\mathrm{F}}}^{*\mathrm{T}}\tilde{\underline{\mathbf{e}}}_{\mathrm{u},n_{\mathrm{F}}}\\
&= \tilde{\underline{\mathbf{d}}}_{\mathrm{u},n_{\mathrm{F}}} + \left(\tilde{\underline{\mathbf{H}}}_{\mathrm{u},n_{\mathrm{F}}}^{*\mathrm{T}}\tilde{\underline{\mathbf{H}}}_{\mathrm{u},n_{\mathrm{F}}}\right)^{-1}\tilde{\underline{\mathbf{H}}}_{\mathrm{u},n_{\mathrm{F}}}^{*\mathrm{T}}\ \tilde{\underline{\mathbf{n}}}_{\mathrm{u},n_{\mathrm{F}}} \tag{5.11}
\end{aligned}
$$

of the data vector $\tilde{\underline{\mathbf{d}}}_{\mathrm{u},n_{\mathrm{F}}}$ of (5.1) can be obtained. On the basis of the MF part $\tilde{\underline{\mathbf{H}}}_{\mathrm{u},n_{\mathrm{F}}}^{*\mathrm{T}}\tilde{\underline{\mathbf{e}}}_{\mathrm{u},n_{\mathrm{F}}}$, the leading part $\left(\tilde{\underline{\mathbf{H}}}_{\mathrm{u},n_{\mathrm{F}}}^{*\mathrm{T}}\tilde{\underline{\mathbf{H}}}_{\mathrm{u},n_{\mathrm{F}}}\right)^{-1}$ eliminates the intra–SA MAI [Kle96, Skl04]. Such an unbiased estimation is realized at the price of the enhanced noise $\left(\tilde{\underline{\mathbf{H}}}_{\mathrm{u},n_{\mathrm{F}}}^{*\mathrm{T}}\tilde{\underline{\mathbf{H}}}_{\mathrm{u},n_{\mathrm{F}}}\right)^{-1}\tilde{\underline{\mathbf{H}}}_{\mathrm{u},n_{\mathrm{F}}}^{*\mathrm{T}}\tilde{\underline{\mathbf{n}}}_{\mathrm{u},n_{\mathrm{F}}}$ [Kle96, Skl04]. Therefore, the SNR

$$\gamma_{\mathrm{ZF},n_{\mathrm{F}}}^{(k)} = \frac{E_{\mathrm{d}}}{\sigma^2\left[\left(\tilde{\underline{\mathbf{H}}}_{\mathrm{u},n_{\mathrm{F}}}^{*\mathrm{T}}\tilde{\underline{\mathbf{H}}}_{\mathrm{u},n_{\mathrm{F}}}\right)^{-1}\right]_{k,k}}, k = 1\ldots K, \tag{5.12}$$

is generally larger than the SNR $\gamma_{\mathrm{MF},n_{\mathrm{F}}}^{(k)}$ of (5.9) of the MF system.

5.3.3 Signal–to–noise–ratio degradation

As introduced for JCE in Chapter 4, the SNR degradation is a performance criterion. For the RxZF JD in the UL, the SNR degradation indicates how much the system performance is degraded in terms of SNR due to the effort to eliminate the intra–SA MAI compared to the MF based reference system, which has the optimum SNR, see (5.9).

With (5.9) and (5.12) the SNR degradation

$$\begin{aligned}\delta_{n_{\mathrm{F}}}^{(k)} &= \frac{\gamma_{\mathrm{MF},n_{\mathrm{F}}}^{(k)}}{\gamma_{\mathrm{ZF},n_{\mathrm{F}}}^{(k)}}\\ &= \left[\left(\tilde{\underline{\mathbf{H}}}_{\mathrm{u},n_{\mathrm{F}}}^{*\mathrm{T}}\tilde{\underline{\mathbf{H}}}_{\mathrm{u},n_{\mathrm{F}}}\right)^{-1}\right]_{k,k}\left[\tilde{\underline{\mathbf{H}}}_{\mathrm{u},n_{\mathrm{F}}}^{*\mathrm{T}}\tilde{\underline{\mathbf{H}}}_{\mathrm{u},n_{\mathrm{F}}}\right]_{k,k}\end{aligned} \tag{5.13}$$

can be computed on the basis of the channel matrix $\tilde{\underline{\mathbf{H}}}_{\mathrm{u},n_{\mathrm{F}}}$. The SNR degradation $\delta_{n_{\mathrm{F}}}^{(k)}$ of (5.13) is equal to or greater than one [Kle96, Skl04]. If the columns of $\tilde{\underline{\mathbf{H}}}_{\mathrm{u},n_{\mathrm{F}}}$ are orthogonal to each other, i.e., the matrix $\tilde{\underline{\mathbf{H}}}_{\mathrm{u},n_{\mathrm{F}}}^{*\mathrm{T}}\tilde{\underline{\mathbf{H}}}_{\mathrm{u},n_{\mathrm{F}}}$ becomes a diagonal matrix., then, the numerator and the denominator of (5.13) become equal, and the SNR degradation $\delta_{n_{\mathrm{F}}}^{(k)}$ of (5.13) becomes one, which is the best case. If the rank of the channel matrix $\tilde{\underline{\mathbf{H}}}_{\mathrm{u},n_{\mathrm{F}}}$ is not full, i.e., if some columns of $\tilde{\underline{\mathbf{H}}}_{\mathrm{u},n_{\mathrm{F}}}$ are correlated, the SNR degradation $\delta_{n_{\mathrm{F}}}^{(k)}$ of (5.13) will converge to ∞, which corresponds to the worst case.

Chapter 6

Linear zero–forcing joint transmission in the downlink of JOINT

6.1 Preliminary remarks

The basic idea of JT [MBW$^+$00, TWMB01, Skl04] is to design the transmit signals in such a way that interferences in the data symbols received are a priori avoided. The perfect channel knowledge is assumed to be available on the transmitter side. In practical systems the mentioned channel knowledge could be obtained by JCE in the uplink, because the channel reciprocity can be exploited in the case that TDD is used. Transmit matched filtering (TxMF) and transmit zero forcing (TxZF) are the two basic linear JT algorithms. In what follows the linear TxZF JT is focused on.

A subcarrierwise investigation of JT in the downlink is feasible due to the application of OFDM according to Chapter 3. Therefore, in the following sections the subcarrierwise representations are used.

6.2 System model in the downlink of JOINT

For the OFDM based DL of JOINT, the subcarrierwise data transmission is illustrated in Fig.6.1. In a SA, K_B APs are at fixed locations and connected to the CU, and K MTs are simultaneously active. For the subcarrier $n_\mathrm{F}, n_\mathrm{F} = 1 \ldots N_\mathrm{F}$, the data symbols $\tilde{\underline{d}}_{\mathrm{d},n_\mathrm{F}}^{(k)}$ to be transmitted to the MTs k can be stacked in a vector

$$\tilde{\underline{\mathbf{d}}}_{\mathrm{d},n_\mathrm{F}} = \left(\tilde{\underline{d}}_{\mathrm{d},n_\mathrm{F}}^{(1)} \ldots \tilde{\underline{d}}_{\mathrm{d},n_\mathrm{F}}^{(K)} \right)^\mathrm{T} \tag{6.1}$$

of dimension K. These data symbols are jointly processed by the TxZF JT at the CU. The $K_\mathrm{B} \times 1$ transmit vector $\tilde{\underline{\mathbf{s}}}_{\mathrm{d},n_\mathrm{F}}$ of (3.28) in the DL can be obtained by multiplying the modulator matrix $\tilde{\underline{\mathbf{M}}}_{n_\mathrm{F}}$ of dimensions $K \times K_\mathrm{B}$ by the data vector $\tilde{\underline{\mathbf{d}}}_{\mathrm{d},n_\mathrm{F}}$ of (6.1), i.e.,

$$\tilde{\underline{\mathbf{s}}}_{\mathrm{d},n_\mathrm{F}} = \tilde{\underline{\mathbf{M}}}_{\mathrm{d},n_\mathrm{F}} \tilde{\underline{\mathbf{d}}}_{\mathrm{d},n_\mathrm{F}}. \tag{6.2}$$

Consequently, (3.28) can be rewritten as

$$\begin{aligned} \tilde{\underline{\mathbf{e}}}_{\mathrm{d},n_\mathrm{F}} &= \tilde{\underline{\mathbf{H}}}_{\mathrm{d},n_\mathrm{F}} \, \tilde{\underline{\mathbf{s}}}_{\mathrm{d},n_\mathrm{F}} + \tilde{\underline{\mathbf{n}}}_{\mathrm{d},n_\mathrm{F}} \\ &= \tilde{\underline{\mathbf{H}}}_{\mathrm{d},n_\mathrm{F}} \tilde{\underline{\mathbf{M}}}_{\mathrm{d},n_\mathrm{F}} \tilde{\underline{\mathbf{d}}}_{\mathrm{d},n_\mathrm{F}} + \tilde{\underline{\mathbf{n}}}_{\mathrm{d},n_\mathrm{F}}. \end{aligned} \tag{6.3}$$
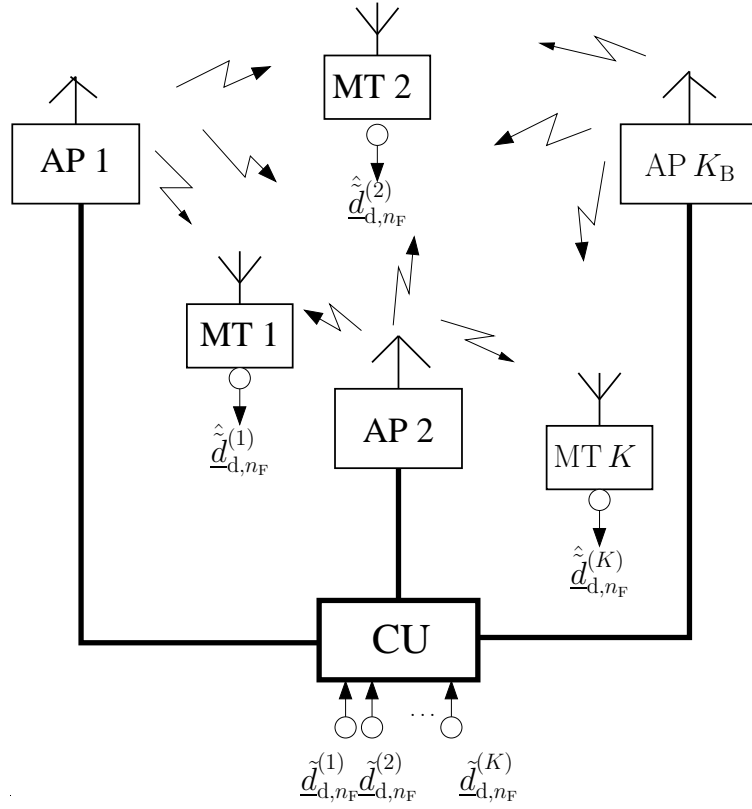
Fig. 6.1. Subcarrierwise data transmission in the DL of JOINT

The estimates $\hat{\tilde{\underline{d}}}_{\mathrm{d},n_{\mathrm{F}}}^{(k)}$ of the data symbols $\tilde{\underline{d}}_{\mathrm{d},n_{\mathrm{F}}}^{(k)}$ of (6.1) are stacked into a vector

$$\hat{\tilde{\underline{\mathbf{d}}}}_{\mathrm{d},n_{\mathrm{F}}} = \left(\hat{\tilde{\underline{d}}}_{\mathrm{d},n_{\mathrm{F}}}^{(1)} \ldots \hat{\tilde{\underline{d}}}_{\mathrm{d},n_{\mathrm{F}}}^{(K)} \right)^{\mathrm{T}} \tag{6.4}$$

of dimension K. It is assumed that the data symbols $\tilde{\underline{d}}_{\mathrm{d},n_{\mathrm{F}}}^{(k)}$ of (6.1), which have the equal energies

$$E_{\mathrm{d}} = \frac{1}{2} |\tilde{\underline{d}}_{\mathrm{d},n_{\mathrm{F}}}^{(k)}|^{2}, \tag{6.5}$$

are uncorrelated to each other. Therefore, the covariance matrix

$$\underline{\mathbf{R}}_{\mathrm{d},\mathrm{d}} = \mathrm{E} \left\{ \tilde{\underline{\mathbf{d}}}_{\mathrm{d},n_{\mathrm{F}}} \, \tilde{\underline{\mathbf{d}}}_{\mathrm{d},n_{\mathrm{F}}}^{*\mathrm{T}} \right\} = 2E_{\mathrm{d}}\mathbf{I}^{K} \tag{6.6}$$

of the transmit data vector $\tilde{\underline{\mathbf{d}}}_{\mathrm{d},n_{\mathrm{F}}}$ of (6.1) is obtained. If the noise $\tilde{\underline{\mathbf{n}}}_{\mathrm{d},n_{\mathrm{F}}}$ of (6.3) is white with the variance σ^{2} of the real and imaginary parts [Pro95], for the covariance matrix follows

$$\underline{\mathbf{R}}_{\mathrm{n},\mathrm{d}} = \mathrm{E} \left\{ \tilde{\underline{\mathbf{n}}}_{\mathrm{d},n_{\mathrm{F}}} \, \tilde{\underline{\mathbf{n}}}_{\mathrm{d},n_{\mathrm{F}}}^{*\mathrm{T}} \right\} = 2\sigma^{2}\mathbf{I}^{K}. \tag{6.7}$$

With (6.2) and (6.5) the total transmit energy [TWMB01, WMZ04, Skl04] reads

$$
\begin{aligned}
T_{\mathrm{d}} &= \frac{1}{2}\, \underline{\tilde{\mathbf{s}}}_{\mathrm{d},n_{\mathrm{F}}}^{*\mathrm{T}}\, \underline{\tilde{\mathbf{s}}}_{\mathrm{d},n_{\mathrm{F}}} \\
&= \frac{1}{2}\, \underline{\tilde{\mathbf{d}}}_{\mathrm{d},n_{\mathrm{F}}}^{*\mathrm{T}} \underline{\tilde{\mathbf{M}}}_{\mathrm{d},n_{\mathrm{F}}}^{*\mathrm{T}} \underline{\tilde{\mathbf{M}}}_{\mathrm{d},n_{\mathrm{F}}} \underline{\tilde{\mathbf{d}}}_{\mathrm{d},n_{\mathrm{F}}} \\
&= E_{\mathrm{d}} \cdot \operatorname{trace}\left\{ \underline{\tilde{\mathbf{M}}}_{\mathrm{d},n_{\mathrm{F}}}^{*\mathrm{T}} \underline{\tilde{\mathbf{M}}}_{\mathrm{d},n_{\mathrm{F}}} \right\}.
\end{aligned} \tag{6.8}
$$

The transmit vector $\underline{\tilde{\mathbf{s}}}_{\mathrm{d},n_{\mathrm{F}}}$ of (6.2) is the superposition of partial transmit vectors $\underline{\tilde{\mathbf{s}}}_{\mathrm{d},n_{\mathrm{F}}}^{(k)}$ each containing the information on the specific data symbol $\underline{\tilde{d}}_{\mathrm{d},n_{\mathrm{F}}}^{(k)}$ of (6.1) [TWMB01, WMZ04, Skl04], i.e.,

$$
\begin{aligned}
\underline{\tilde{\mathbf{s}}}_{\mathrm{d},n_{\mathrm{F}}} &= \sum_{k=1}^{K} \underline{\tilde{\mathbf{s}}}_{\mathrm{d},n_{\mathrm{F}}}^{(k)} \\
&= \sum_{k=1}^{K} \left[\underline{\tilde{\mathbf{M}}}_{\mathrm{d},n_{\mathrm{F}}} \right]_{K_{\mathrm{B}},k}^{1,k} \underline{\tilde{d}}_{\mathrm{d},n_{\mathrm{F}}}^{(k)}
\end{aligned} \tag{6.9}
$$

holds. The partial transmit energy is transmitted

$$
\begin{aligned}
T_{\mathrm{d},n_{\mathrm{F}}}^{(k)} &= \frac{1}{2}\, \underline{\tilde{\mathbf{s}}}_{\mathrm{d},n_{\mathrm{F}}}^{(k)\ *\mathrm{T}}\, \underline{\tilde{\mathbf{s}}}_{\mathrm{d},n_{\mathrm{F}}}^{(k)} \\
&= E_{\mathrm{d}} \cdot \left[\underline{\tilde{\mathbf{M}}}_{\mathrm{d},n_{\mathrm{F}}} \right]_{K_{\mathrm{B}},k}^{1,k\ *\mathrm{T}} \left[\underline{\tilde{\mathbf{M}}}_{\mathrm{d},n_{\mathrm{F}}} \right]_{K_{\mathrm{B}},k}^{1,k} \\
&= E_{\mathrm{d}} \cdot \left[\underline{\tilde{\mathbf{M}}}_{\mathrm{d},n_{\mathrm{F}}}^{*\mathrm{T}} \underline{\tilde{\mathbf{M}}}_{\mathrm{d},n_{\mathrm{F}}} \right]_{k,k},
\end{aligned} \tag{6.10}
$$

for the specific data symbol $\underline{\tilde{d}}_{\mathrm{d},n_{\mathrm{F}}}^{(k)}$ of (6.1)[TWMB01, WMZ04, Skl04]. The receive vector $\underline{\tilde{\mathbf{e}}}_{\mathrm{d},n_{\mathrm{F}}}$ of (6.3) is the superposition of partial receive vectors $\underline{\tilde{\mathbf{e}}}_{\mathrm{d},n_{\mathrm{F}}}^{(k)}$ each containing the information on the specific data symbol $\underline{\tilde{d}}_{\mathrm{d},n_{\mathrm{F}}}^{(k)}$ of (6.1) [TWMB01, WMZ04, Skl04], i.e.,

$$
\begin{aligned}
\underline{\tilde{\mathbf{e}}}_{\mathrm{d},n_{\mathrm{F}}} &= \sum_{k=1}^{K} \underline{\tilde{\mathbf{e}}}_{\mathrm{d},n_{\mathrm{F}}}^{(k)} \\
&= \sum_{k=1}^{K} \left[\underline{\tilde{\mathbf{H}}}_{\mathrm{d},n_{\mathrm{F}}} \right]_{k,K_{\mathrm{B}}}^{k,1} \left[\underline{\tilde{\mathbf{M}}}_{\mathrm{d},n_{\mathrm{F}}} \right]_{K_{\mathrm{B}},k}^{1,k} \underline{\tilde{d}}_{\mathrm{d},n_{\mathrm{F}}}^{(k)}
\end{aligned} \tag{6.11}
$$

holds. With (6.11) the corresponding useful energy [TWMB01, WMZ04, Skl04]

$$
\begin{aligned}
R_{\mathrm{d},n_{\mathrm{F}}}^{(k)} &= \frac{1}{2} \underline{\tilde{\mathbf{e}}}_{\mathrm{d},n_{\mathrm{F}}}^{(k)\ *\mathrm{T}} \underline{\tilde{\mathbf{e}}}_{\mathrm{d},n_{\mathrm{F}}}^{(k)} \\
&= \frac{1}{2} |\underline{\tilde{d}}_{\mathrm{d},n_{\mathrm{F}}}^{(k)}|^{2} \left[\left(\underline{\tilde{\mathbf{H}}}_{\mathrm{d},n_{\mathrm{F}}} \underline{\tilde{\mathbf{M}}}_{\mathrm{d},n_{\mathrm{F}}} \right)^{*\mathrm{T}} \left(\underline{\tilde{\mathbf{H}}}_{\mathrm{d},n_{\mathrm{F}}} \underline{\tilde{\mathbf{M}}}_{\mathrm{d},n_{\mathrm{F}}} \right) \right]_{k,k} \\
&= E_{\mathrm{d}} \cdot \left[\left(\underline{\tilde{\mathbf{H}}}_{\mathrm{d},n_{\mathrm{F}}} \underline{\tilde{\mathbf{M}}}_{\mathrm{d},n_{\mathrm{F}}} \right)^{*\mathrm{T}} \left(\underline{\tilde{\mathbf{H}}}_{\mathrm{d},n_{\mathrm{F}}} \underline{\tilde{\mathbf{M}}}_{\mathrm{d},n_{\mathrm{F}}} \right) \right]_{k,k}
\end{aligned} \tag{6.12}
$$

for the specific data symbol $\underline{\tilde{d}}_{\mathrm{d},n_{\mathrm{F}}}^{(k)}$ of (6.1)[TWMB01, WMZ04, Skl04] is received.

6.3 Algorithm of linear zero–forcing joint transmission

6.3.1 Reference system: matched filter

The aim of the TxMF JT is to minimize the partial transmit energy $T_{\mathrm{d},n_{\mathrm{F}}}^{(k)}$ of (6.10) required for the data symbol $\underline{\tilde{d}}_{\mathrm{d},n_{\mathrm{F}}}^{(k)}$ of (6.1) if the intra–MAI is neglected, i.e., each column vector $\left[\underline{\tilde{\mathbf{M}}}_{\mathrm{d},n_{\mathrm{F}}}\right]_{K_{\mathrm{B}},k}^{1,k}$ of (6.10) is optimized separately. From this rationale the modulator matrix

$$\underline{\tilde{\mathbf{M}}}_{\mathrm{TxMF},n_{\mathrm{F}}} = \underline{\tilde{\mathbf{H}}}_{\mathrm{d},n_{\mathrm{F}}}^{*\mathrm{T}} \left(\mathrm{diag}\left(\underline{\tilde{\mathbf{H}}}_{\mathrm{d},n_{\mathrm{F}}} \underline{\tilde{\mathbf{H}}}_{\mathrm{d},n_{\mathrm{F}}}^{*\mathrm{T}} \right) \right)^{-1} \tag{6.13}$$

follows for the TxMF JT. With (6.10), (6.12) and (6.13), the partial transmit energy

$$\begin{aligned} T_{\mathrm{TxMF},n_{\mathrm{F}}}^{(k)} &= E_{\mathrm{d}} \cdot \left[\underline{\tilde{\mathbf{M}}}_{\mathrm{TxMF},n_{\mathrm{F}}}^{*\mathrm{T}} \underline{\tilde{\mathbf{M}}}_{\mathrm{TxMF},n_{\mathrm{F}}} \right]_{k,k} \\ &= \frac{E_{\mathrm{d}}}{\left[\underline{\tilde{\mathbf{H}}}_{\mathrm{d},n_{\mathrm{F}}} \underline{\tilde{\mathbf{H}}}_{\mathrm{d},n_{\mathrm{F}}}^{*\mathrm{T}} \right]_{k,k}} \end{aligned} \tag{6.14}$$

and the corresponding useful energy

$$\begin{aligned} R_{\mathrm{TxMF},n_{\mathrm{F}}}^{(k)} &= E_{\mathrm{d}} \cdot \left[\left(\underline{\tilde{\mathbf{H}}}_{\mathrm{d},n_{\mathrm{F}}} \underline{\tilde{\mathbf{M}}}_{\mathrm{TxMF},n_{\mathrm{F}}} \right)^{*\mathrm{T}} \left(\underline{\tilde{\mathbf{H}}}_{\mathrm{d},n_{\mathrm{F}}} \underline{\tilde{\mathbf{M}}}_{\mathrm{TxMF},n_{\mathrm{F}}} \right) \right]_{k,k} \\ &= E_{\mathrm{d}} \end{aligned} \tag{6.15}$$

received can be obtained for the data symbol $\underline{\tilde{d}}_{\mathrm{d},n_{\mathrm{F}}}^{(k)}$ of (6.1) in the case of TxMF. With (6.14) and (6.15) the ratio

$$\begin{aligned} \frac{R_{\mathrm{TxMF},n_{\mathrm{F}}}^{(k)}}{T_{\mathrm{TxMF},n_{\mathrm{F}}}^{(k)}} &= \frac{E_{\mathrm{d}}}{E_{\mathrm{d}} \big/ \left[\underline{\tilde{\mathbf{H}}}_{\mathrm{d},n_{\mathrm{F}}} \underline{\tilde{\mathbf{H}}}_{\mathrm{d},n_{\mathrm{F}}}^{*\mathrm{T}} \right]_{k,k}} \\ &= \left[\underline{\tilde{\mathbf{H}}}_{\mathrm{d},n_{\mathrm{F}}} \underline{\tilde{\mathbf{H}}}_{\mathrm{d},n_{\mathrm{F}}}^{*\mathrm{T}} \right]_{k,k} \end{aligned} \tag{6.16}$$

indicates how much transmit energy $T_{\mathrm{TxMF},n_{\mathrm{F}}}^{(k)}$ of (6.14) is converted to the useful receive energy $R_{\mathrm{TxMF},n_{\mathrm{F}}}^{(k)}$ of (6.15) with respect to TxMF.

6.3.2 Transmit zero forcing

The idea behind the TxZF JT is to eliminate the intra–SA MAI and to minimize the required transmit energy $T_{\mathrm{d},n_{\mathrm{F}}}^{(k)}$ of (6.10) at the same time. In order to receive interference–free estimate

$$\underline{\hat{\tilde{\mathbf{d}}}}_{\mathrm{d},n_{\mathrm{F}}} = \underline{\tilde{\mathbf{e}}}_{\mathrm{d},n_{\mathrm{F}}} = \underline{\tilde{\mathbf{d}}}_{\mathrm{d},n_{\mathrm{F}}} \tag{6.17}$$

at the receivers of the MTs in the absence of the noise, the modulator matrix

$$\underline{\tilde{\mathbf{M}}}_{\mathrm{TxZF},n_{\mathrm{F}}} = \underline{\tilde{\mathbf{H}}}_{\mathrm{d},n_{\mathrm{F}}}^{*\mathrm{T}} \left(\underline{\tilde{\mathbf{H}}}_{\mathrm{d},n_{\mathrm{F}}} \underline{\tilde{\mathbf{H}}}_{\mathrm{d},n_{\mathrm{F}}}^{*\mathrm{T}} \right)^{-1} \tag{6.18}$$

is obtained for the TxZF JT. With (6.10), (6.12) and (6.18), the partial transmit energy

$$
\begin{aligned}
T_{\mathrm{TxZF},n_{\mathrm{F}}}^{(k)} &= E_{\mathrm{d}} \cdot \left[\underline{\tilde{\mathbf{M}}}_{\mathrm{TxZF},n_{\mathrm{F}}}^{*\mathrm{T}} \underline{\tilde{\mathbf{M}}}_{\mathrm{TxZF},n_{\mathrm{F}}} \right]_{k,k} \\
&= E_{\mathrm{d}} \cdot \left[\left(\underline{\tilde{\mathbf{H}}}_{\mathrm{d},n_{\mathrm{F}}} \underline{\tilde{\mathbf{H}}}_{\mathrm{d},n_{\mathrm{F}}}^{*\mathrm{T}} \right)^{-1} \right]_{k,k}
\end{aligned} \tag{6.19}
$$

and the corresponding useful energy

$$
\begin{aligned}
R_{\mathrm{TxZF},n_{\mathrm{F}}}^{(k)} &= E_{\mathrm{d}} \cdot \left[\left(\underline{\tilde{\mathbf{H}}}_{\mathrm{d},n_{\mathrm{F}}}^{(k)} \underline{\tilde{\mathbf{M}}}_{\mathrm{TxZF},n_{\mathrm{F}}}^{(k)} \right)^{*\mathrm{T}} \left(\underline{\tilde{\mathbf{H}}}_{\mathrm{d},n_{\mathrm{F}}}^{(k)} \underline{\tilde{\mathbf{M}}}_{\mathrm{TxZF},n_{\mathrm{F}}}^{(k)} \right) \right]_{k,k} \\
&= E_{\mathrm{d}}
\end{aligned} \tag{6.20}
$$

received can be obtained for the data symbol $\underline{\tilde{d}}_{\mathrm{d},n_{\mathrm{F}}}^{(k)}$ of (6.1) in the case of TxZF. With (6.19) and (6.20) the ratio

$$
\begin{aligned}
\frac{R_{\mathrm{TxZF},n_{\mathrm{F}}}^{(k)}}{T_{\mathrm{TxZF},n_{\mathrm{F}}}^{(k)}} &= \frac{E_{\mathrm{d}}}{E_{\mathrm{d}} \cdot \left[\left(\underline{\tilde{\mathbf{H}}}_{\mathrm{d},n_{\mathrm{F}}} \underline{\tilde{\mathbf{H}}}_{\mathrm{d},n_{\mathrm{F}}}^{*\mathrm{T}} \right)^{-1} \right]_{k,k}} \\
&= \frac{1}{\left[\left(\underline{\tilde{\mathbf{H}}}_{\mathrm{d},n_{\mathrm{F}}} \underline{\tilde{\mathbf{H}}}_{\mathrm{d},n_{\mathrm{F}}}^{*\mathrm{T}} \right)^{-1} \right]_{k,k}}
\end{aligned} \tag{6.21}
$$

indicates how much transmit energy $T_{\mathrm{TxZF},n_{\mathrm{F}}}^{(k)}$ of (6.19) is converted to the useful receive energy $R_{\mathrm{TxZF},n_{\mathrm{F}}}^{(k)}$ of (6.20) with respect to TxZF.

6.3.3 Transmission efficiency

The price to be paid for the elimination of the intra–MAI by the TxZF JT is an increase of the average transmit energy T_{d} of (6.8) as compared to the TxMF JT. Therefore, how efficiently the energy $T_{\mathrm{d},n_{\mathrm{F}}}^{(k)}$ is invested for the data symbol $\underline{\tilde{d}}_{\mathrm{d},n_{\mathrm{F}}}^{(k)}$ of (6.1) is an important measure to evaluate the performance of the JT algorithms. Now, we introduce the concept of transmission efficiency [TWMB01, WMZ04, Skl04]. The transmission efficiency $\eta_{n_{\mathrm{F}}}^{(k)}$ for the data symbol $\underline{\tilde{d}}_{\mathrm{d},n_{\mathrm{F}}}^{(k)}$ of (6.1) is defined as the ratio of

the ratio $\frac{R^{(k)}_{\mathrm{TxZF},n_{\mathrm{F}}}}{T^{(k)}_{\mathrm{TxZF},n_{\mathrm{F}}}}$ of (6.21) and the ratio $\frac{R^{(k)}_{\mathrm{TxMF},n_{\mathrm{F}}}}{T^{(k)}_{\mathrm{TxMF},n_{\mathrm{F}}}}$ of (6.16) [TWMB01, WMZ04, Skl04]:

$$
\begin{aligned}
\eta^{(k)}_{n_{\mathrm{F}}} &= \frac{R^{(k)}_{\mathrm{TxZF},n_{\mathrm{F}}}/T^{(k)}_{\mathrm{TxZF},n_{\mathrm{F}}}}{R^{(k)}_{\mathrm{TxMF},n_{\mathrm{F}}}/T^{(k)}_{\mathrm{TxMF},n_{\mathrm{F}}}} \\
&= \frac{T^{(k)}_{\mathrm{TxMF},n_{\mathrm{F}}}}{T^{(k)}_{\mathrm{TxZF},n_{\mathrm{F}}}} \\
&= \frac{1}{\left[\left(\underline{\tilde{\mathbf{H}}}_{\mathrm{d},n_{\mathrm{F}}}\,\underline{\tilde{\mathbf{H}}}^{*\mathrm{T}}_{\mathrm{d},n_{\mathrm{F}}}\right)^{-1}\right]_{k,k}\left[\underline{\tilde{\mathbf{H}}}_{\mathrm{d},n_{\mathrm{F}}}\,\underline{\tilde{\mathbf{H}}}^{*\mathrm{T}}_{\mathrm{d},n_{\mathrm{F}}}\right]_{k,k}}.
\end{aligned}
\tag{6.22}
$$

The transmission efficiency $\eta^{(k)}_{n_{\mathrm{F}}}$ of (6.22) takes the values from zero to one, with one being the optimum.

Chapter 7
Implementation of the JOINT simulation chain

7.1 Preliminary remarks

In previous chapters channel models and key processes, e.g., JCE, JD and JT of JOINT, are introduced. In order to evaluate the performance of JOINT, the implementation of a JOINT simulation chain is necessary. A possible simulation tool is MLDesigner [MT03], which is a software system for the design of missions, systems, products and chips [MT03]. Implementing the JOINT simulation chain is a very complicated process. Up to now nearly ten thousand lines of codes have been accomplished by the author. To see what has been done, we can refer to the programs. It would be too much to include all these contents in this thesis. In order to explain the basics of the work, the author only focuses on some key issues involved in the implementation of the JOINT simulation chain. In the present chapter the fundamentals of software engineering and a brief introduction to MLDesigner are given for a better understanding. The implementation of the key functional modules, e.g., channel models, JCE, JD and JT, is elaborated. After that, the JOINT simulation chain is described. Finally, some experiences accumulated during the implementation, which are valuable for future work, are presented.

7.2 Fundamentals of software engineering

The definitions of programming, software development and software engineering are three basic concepts in software engineering, which are defined [Rom95] as follows:

- **Programming.** Programming indicates the construction of a program, of a part of a program or of a component according to the desired specifications [Rom95]. Generally the programming is basic for the project to be implemented. The goal of the programming is to realize some sole functionalities of the components.

- **Software development.** Software development aims at constructing the programs to solve some problems, which may be not clearly specified [Rom95]. The software development can be distinguished from the programming by a higher complexity. In one word, programming is a part of software development.

- **Software engineering.** Software engineering indicates an entire process of definition, implementation, optimization and verification of principles, methods and other aspects of the software project [Rom95]. Software engineering has the highest complexity among the three mentioned concepts.

In order to accomplish the JOINT simulation chain, a number of aspects, including e.g., requirement definitions, algorithm implementations and verifications, have to be considered.

From the inception of an idea for a software system until it is implemented, and even after the start of being utilized by users, the system undergoes updates and evolutions. So does the JOINT simulation chain. The software is said to have a life cycle [GJM91] composed of several phases. A typical waterfall life cycle model [GJM91] as depicted in Fig.7.1 comprises the following phases:

- **Requirement analysis and specification.** The requirement analysis is usually the first phase of a large–scale software project, as e.g., the JOINT simulation chain. It is undertaken after a feasibility study [GJM91], which defines the precise cost and benefits of the software project. The purpose of this phase is to identify and specify the exact requirements for the system, i.e., the issue "what is the problem" is to be addressed here. For JOINT with SAs being the architectural entities, the goal is to construct a link level simulation chain of JOINT based on a single–SA scenario and on a multi–SA scenario.

- **Design and specification.** Once all the requirements for the system are documented, both the overall system structure design and the detailed module design can be dealt with in the design and specification phase. The purpose of this phase is to specify a particular software system, which meets the requirements proposed in the previous phase, i.e., the issue "how to solve the problem" is stated. For the JOINT simulation chain, data flows of the system are specified. Moreover, ports, parameters and functionalities of all modules of JOINT should be clearly defined.

- **Coding and module testing.** In this phase the actual code for the individual modules is produced by programming and tested. Each module of JOINT, simple or complex, is indispensable. Testing is absolutely required as well, since the exact realization of each module is the guarantee of the reliability of the simulation results.

- **Integration and system testing.** All the modules developed and tested individually are put together and integrated in this phase and tested as a whole system, e.g., the JOINT simulation chain.

- **Maintenance.** Once the software system has passed all the tests, it can be used. Any modifications or updates of the system are usually performed in this phase.
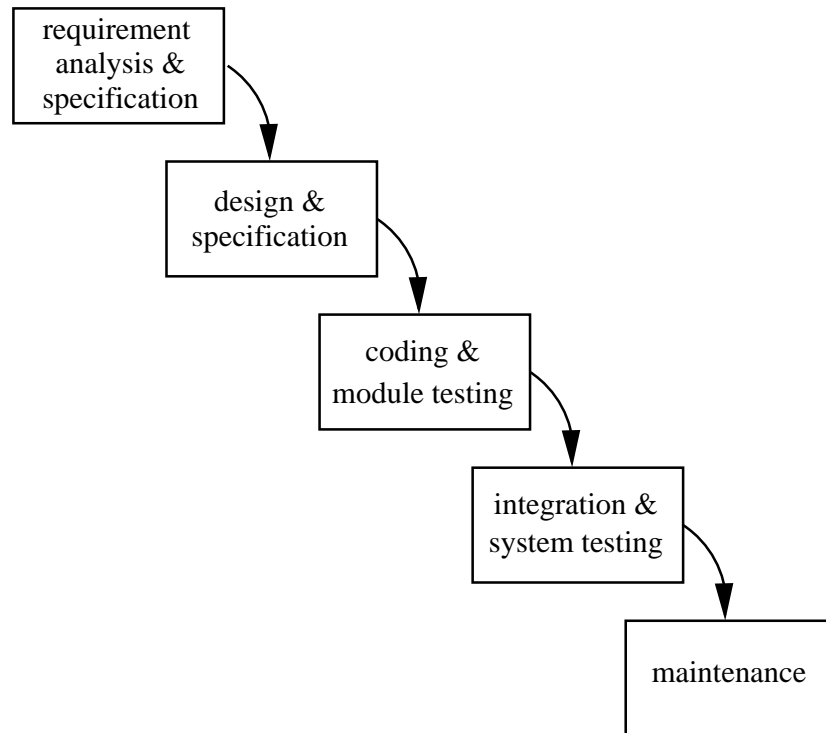
Fig. 7.1. The waterfall model of the general software life cycle

7.3   Introduction to MLDesigner

As already mentioned in Section 7.1 MLDesigner is a software system for the design of missions, systems, products, and chips [MT03]. It is a multi–domain simulator. MLDesigner can be used for the implementation and analysis of a broad range of applications, from complex systems like mobile/fixed communication networks, satellite communication/navigation/observation systems, performance and architecture trade-offs of electronic systems and chips, and automotive navigation/communication systems to simple logic designs [MT03]. MLDesigner consists of

- a multi–document graphical editor, including a parameter editor to create, edit and store graphical models of systems,

- the Ptolemy tool command language (PTCL) [Ous90, Ous94] environment to define complex systems that are too large to be defined by a graphical block diagram editor,

- an animation and plotting system to present simulation results and performance measures,

- integrated multi–domain simulators, including debugging animators,

- more than 1400 core modules and

- more than 260 example systems.

The functional modelling in MLDesigner is generally realized either by a network of embedded model components or by the programming code. A model component may define a number of ports or parameters as well as other model elements such as memories, events, and resources [MT03] to describe its external interfaces or behavior. External interfaces are needed for embedding the model component into the functional model of other model components. Embedding is realized by instantiating model instances, i.e., the model contains references to embedded model components. This type of hierarchical system model structure, as shown in Fig.7.2, allows embedding of modules from other domains. For a better understanding of the thesis, it is necessary to know the following terms:

- **Primitive.** Primitives are the model components of the lowest level in MLDesigner. The functionality of a primitive is realized by using the Ptolemy [Ous90, Ous94] language containing C++ code fragments. The model ports of a primitive component define its external interfaces, whereas the primitive source code written in the Ptolemy [Ous90, Ous94] language defines the behavior of the primitive. Primitives can have input/output ports and parameters for interfacing. They are called Stars in the Ptolemy vocabulary [Ous90, Ous94].

- **Module.** Modules are made up of connected embedded primitives or modules. Like primitives, modules can have input/output ports as well as parameters for interfacing. A module can be a simple structure with one level or a hierarchical structure with more levels of embedded modules. Modules are called Galaxies in the Ptolemy vocabulary [Ous90, Ous94].

- **System.** System is the top–level model and consists of a number of connected primitives or modules. A system does not have any input/output ports. Defined parameters are used to parameterize the system model. A system model is called a Universe in the Ptolemy vocabulary [Ous90, Ous94].

As already said, MLDesigner is a multi–domain simulator. Among the diverse domains Synchronous Data Flow (SDF) [MT03] is one of the most mature domains in
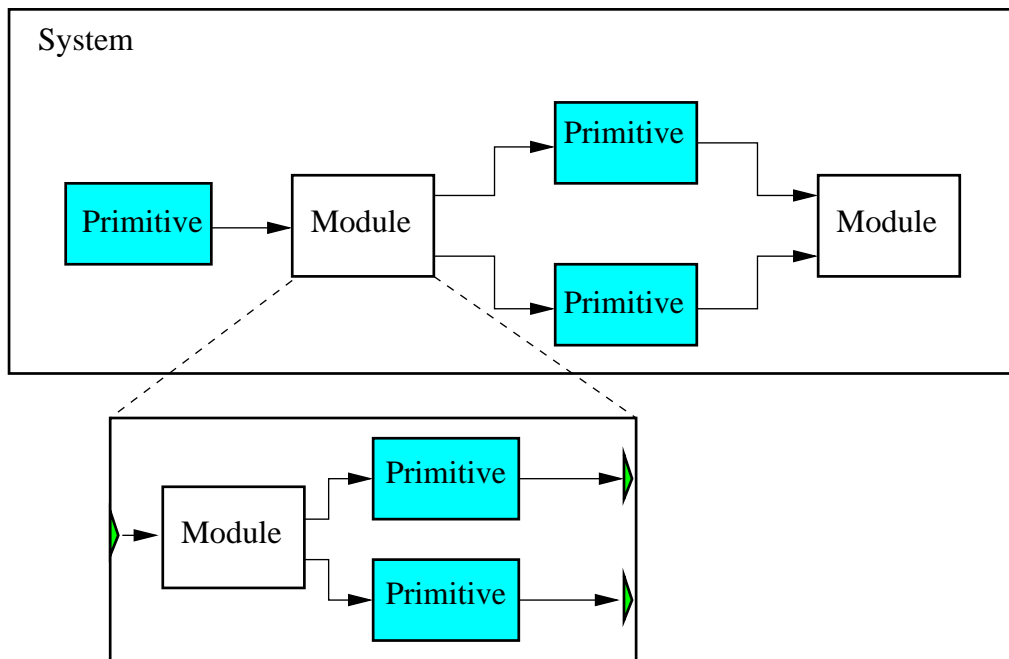
Fig. 7.2. Embedded structure of MLDesigner

MLDesigner, having a large amount of primitives and demo programs. Therefore, the JOINT simulation chain is implemented in this SDF domain. The SDF domain is a data–driven, statically scheduled domain. "Data–driven" means that the availability of particles at the inputs of a primitive enables the primitive. Primitives without any inputs are always enabled. "Statically scheduled" means that the firing order of the primitives is determined once during the start–up phase.

7.4   Implementation of key modules of the JOINT simulation chain

7.4.1   Preliminary remarks

In the present subsection the key primitives and modules of the JOINT simulation chain are described. For a first overview, the key primitives and the key modules, respectively, are listed in Tables 7.1 and 7.2.

Table 7.1. Key primitives of JOINT

Designation	Functionality
ChannelModels	Generator of CSI
BitSource	Generator of random binary information bits
Noise	Generator of the complex Gaussian noise
Pilot_gen	Generator of the pilots for the MTs
QPSK_Mod	QPSK modulator
QPSK_DeMod	QPSK demodulator
Mux	Multiplexer of the data and the pilots
Demux	De–multiplexer the receive data and the receive pilots
JointChannelEstimation	Estimator of CSI
sort_channels	Sorter of the CTF matrix for the subcarrierwise processing
JD_core	Detector with subcarierwise JD algorithms
JT_core	Transmitter with subcarierwise JT algorithms
BER	Calculator of BERs

7.4.2   Channel models

7.4.2.1   Features

CSI, which is required by the data transmission and estimation, see Chapters 5 and 6, is generated by the primitive "ChannelModels". The following requirements are met according to the system design:

- The primitive "ChannelModels" generates N_B slot–specific CSI data for N_B time slots of a frame each time when the primitive is triggered.

- According to different scenarios multiple channel models are available.

- Beyond the randomly generated CSI data, the primitive "ChannelModels" is able to load the static CSI data from an existing file, which may be obtained by other means. In other words, not only the living channels, but also the given snapshots of the channels can be offered according to the desired scenario.

7.4.2.2   Particular description

As depicted in Fig.7.3, the primitive "ChannelModels" has only one output port, which offers the complex CSI data sequently.

Table 7.2. Key modules of JOINT

Designation	Functionality	Components (primitives)
MT_Tx	Transmitter of the multiplexed UL signals, the modulated data or the pilots at the MT	QPSK_Mod, Pilot_gen, Multiplexer
JointDetetion	Data estimator exploiting the JD algorithms at the CU	sort_channels, JD_core
Cu_Rx	Demodulator of the UL data estimates at the CU	QPSK_DeMod
Cu_Tx	Modulator of the DL information bits at the CU	QPSK_Mod
JointTransmission	Data transmitter exploiting the JT algorithms at the CU	sort_channels, JT_core
MT_Rx	Receiver at the MT	QPSK_DeMod

Primitive "ChannelModels"
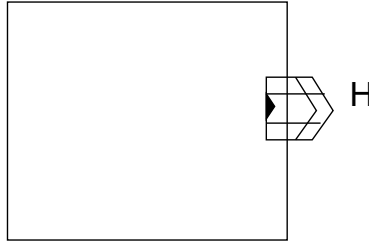
Fig. 7.3. Primitive "ChannelModels" implemented in MLDesigner

Each time when the primitive "ChannelModels" is triggered, a sequence of N_B CSI data, i.e., N_B slot–specific CTF matrices

$$\underline{\tilde{\mathbf{H}}}_{n_\mathrm{B}} = \left(\underline{\tilde{\mathbf{H}}}_{n_\mathrm{B},1} \ldots \underline{\tilde{\mathbf{H}}}_{n_\mathrm{B},N_\mathrm{F}} \right), n_\mathrm{B} = 1 \ldots N_\mathrm{B}, \tag{7.1}$$

for N_B OFDM symbol slots of one frame are generated, where

$$N_\mathrm{B} = N_\mathrm{BU} + N_\mathrm{BP} + N_\mathrm{BD} \tag{7.2}$$

holds. The first N_BU CTF matrices $\underline{\tilde{\mathbf{H}}}_{n_\mathrm{B}}, n_\mathrm{B} = 1 \ldots N_\mathrm{BU}$, are for the UL data transmission, the following N_BP equal to one matrix $\underline{\tilde{\mathbf{H}}}_{n_\mathrm{B}}, n_\mathrm{B} = N_\mathrm{BU} + 1$, is for the pilot

transmission in the UL, and the last N_{BD} CTF matrices $\tilde{\underline{\mathbf{H}}}_{n_{\mathrm{B}}}, n_{\mathrm{B}} = N_{\mathrm{BU}} + 2 \ldots N_{\mathrm{B}}$, are for the DL data transmission.

The slot–specific CTF matrix $\tilde{\underline{\mathbf{H}}}_{n_{\mathrm{B}}}$ of (7.1) consists of N_{F} subcarrier–specific submatrices $\tilde{\underline{\mathbf{H}}}_{n_{\mathrm{B}},n_{\mathrm{F}}}$, each of dimensions $N_{\mathrm{AP}} \times N_{\mathrm{MT}}$, where N_{AP} and N_{MT} represent the number of the considered APs and the number of the considered MTs in the co–channel SAs, respectively. With N_{SA} denoting the number of the co–channel SAs in the considered area and with the assumption of the same number K_{B} of APs and the same number K of MTs in each SA,

$$N_{\mathrm{AP}} = N_{\mathrm{SA}} \cdot K_{\mathrm{B}} \tag{7.3}$$

and

$$N_{\mathrm{MT}} = N_{\mathrm{SA}} \cdot K \tag{7.4}$$

hold. Consequently, the subcarrier–specific submatrix

$$\tilde{\underline{\mathbf{H}}}_{n_{\mathrm{B}},n_{\mathrm{F}}} = \begin{pmatrix} \tilde{\underline{\mathbf{H}}}_{n_{\mathrm{B}},n_{\mathrm{F}}}^{(1,1)} & \cdots & \tilde{\underline{\mathbf{H}}}_{n_{\mathrm{B}},n_{\mathrm{F}}}^{(1,N_{\mathrm{SA}})} \\ \vdots & & \vdots \\ \tilde{\underline{\mathbf{H}}}_{n_{\mathrm{B}},n_{\mathrm{F}}}^{(N_{\mathrm{SA}},1)} & \cdots & \tilde{\underline{\mathbf{H}}}_{n_{\mathrm{B}},n_{\mathrm{F}}}^{(N_{\mathrm{SA}},N_{\mathrm{SA}})} \end{pmatrix} \tag{7.5}$$

of (7.1) comprises $N_{\mathrm{SA}} \times N_{\mathrm{SA}}$ submatrices $\tilde{\underline{\mathbf{H}}}_{n_{\mathrm{B}},n_{\mathrm{F}}}^{(n_{\mathrm{SA}},n_{\mathrm{SA}})}$, each of dimensions $K_{\mathrm{B}} \times K$, describing all the co–channel CTFs in the considered area, which is covered by the multiple SAs. The submatrices $\tilde{\underline{\mathbf{H}}}_{n_{\mathrm{B}},n_{\mathrm{F}}}^{(n_{\mathrm{SA}},n_{\mathrm{SA}})}$ on the diagonal of (7.5) correspond to the subcarrier–specific matrix $\tilde{\underline{\mathbf{H}}}_{\mathrm{u},n_{\mathrm{F}}}$ of (3.20) in the UL or the transpose of the subcarrier–specific matrix $\tilde{\underline{\mathbf{H}}}_{\mathrm{d},n_{\mathrm{F}}}^{\mathrm{T}}$ of (3.28) in the DL in the corresponding SAs., i.e.,

$$\tilde{\underline{\mathbf{H}}}_{n_{\mathrm{B}},n_{\mathrm{F}}}^{(n_{\mathrm{SA}},n_{\mathrm{SA}})} = \tilde{\underline{\mathbf{H}}}_{\mathrm{u},n_{\mathrm{F}}} = \tilde{\underline{\mathbf{H}}}_{\mathrm{d},n_{\mathrm{F}}}^{\mathrm{T}}. \tag{7.6}$$

The single–SA scenario is a special case of N_{SA} equal to one. With (7.3) and (7.4)

$$N_{\mathrm{AP}} = K_{\mathrm{B}} \tag{7.7}$$

and

$$N_{\mathrm{MT}} = K \tag{7.8}$$

can be obtained for N_{SA} equal to one.

The elements of the slot–specific CTF matrix $\tilde{\underline{\mathbf{H}}}_{n_{\mathrm{B}}}$ of (7.1) can be generated according to the algorithms in Chapter 2 for different types of channel models. The types of the channel models can be chosen by setting the parameter "chan_type". Different integer values of "chan_type" correspond to the basic channel models, e.g., "1" representing for a non–cross–coupling channel model, in which

$$\tilde{\underline{\mathbf{H}}}_{n_{\mathrm{B}},n_{\mathrm{F}}} = \mathbf{I}^{K} \tag{7.9}$$

holds, "2" presenting a Rayleigh fading channel model with an exponential power delay profile and a Jakes Doppler spectrum [Ste92, Pro95, LR99] as introduced in Subsection 2.3.1, "3" representing a Rayleigh fading channel model with log–normal fading as described in Subsection 2.3.2, and "4" representing a channel model loaded from an existing file.

For the other parameters concerning the channel models and JOINT, which are consistent with the ones used in Chapters 2 and 3, refer to Table 3.1.

7.4.3   Joint channel estimation

7.4.3.1   Features

The task of the primitive "JointChannelEstimation" is to offer the desired CSI data for the data estimation in the UL and the data transmission in the DL, as stated in Chapter 4. The following requirements are met according to the system design:

- The primitive "JointChannelEstimation" delivers N_B slot–specific CSI data for N_B OFDM symbol slots of a frame each time when the primitive is triggered.

- For different purposes of investigations the primitive "JointChannelEstimation" is able to offer either the estimated CSI data or the true CSI data.

- Both single–SA scenarios and multiple–SA scenarios can be handled.

7.4.3.2   Particular description

The primitive "JointChannelEstimation" has two input ports, see Fig. 7.4. One input port is e, which is a multiple–input port for complex matrices. Therefore, N_F subcarrier–specific receive pilot vectors

$$\underline{\tilde{\mathbf{e}}}_{h,n_F} = \left(\underline{\tilde{e}}_{h,n_F}^{(1)} \ldots \underline{\tilde{e}}_{h,n_F}^{(N_{AP})} \right)^T, \tag{7.10}$$

each of dimension N_{AP}, can be collected in a parallel manner. As depicted in Fig.7.4, the other input port is H, which is a port for a single complex matrix. The total CTF matrix

$$\underline{\tilde{\mathbf{H}}} = \begin{pmatrix} \underline{\tilde{\mathbf{H}}}_1 \\ \vdots \\ \underline{\tilde{\mathbf{H}}}_{N_B} \end{pmatrix} \tag{7.11}$$

Primitive "JointChannelEstimation"
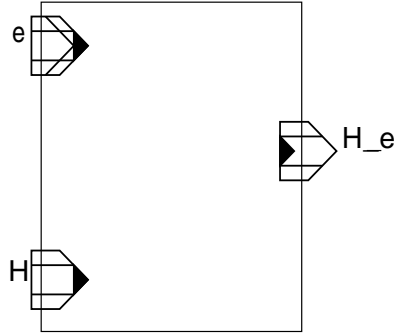
Fig. 7.4. Primitive "JointChannelEstimation" implemented in MLDesigner

of the whole frame, which consists of N_B slot–specific submatrices $\underline{\tilde{\mathbf{H}}}_{n_B}$ of (7.1), is received by the primitive "JointChannelEstimation". The primitive "JointChannelEstimation" has one output port H_e for a single complex matrix, which delivers N_B true slot–specific CTF matrices $\underline{\tilde{\mathbf{H}}}_{n_B}$ of (7.1) or N_B estimates $\underline{\hat{\tilde{\mathbf{H}}}}_{n_B}$ of the slot–specific CTF matrices $\underline{\tilde{\mathbf{H}}}_{n_B}$ of (7.1) sequently.

The primitive "JointChannelEstimation" is triggered once per frame. The primitive starts with a judgement, whether to deliver the true slot–specific CTF matrices $\underline{\tilde{\mathbf{H}}}_{n_B}$ of (7.1) or the CTF estimate matrices $\underline{\hat{\tilde{\mathbf{H}}}}_{n_B}$. This is determined by the parameter "OperationModeJCE", with integer values.

If "OperationModeJCE" is equal to "1", the algorithm of JCE is performed as follows:

- The N_F subcarrier–specific receive pilot vectors $\underline{\tilde{\mathbf{e}}}_{h,n_F}$ of (7.10) from the multiple–input are first sorted to $N_{SA}N_F$ partial subcarrier–specific vectors

$$\underline{\tilde{\mathbf{e}}}_{h,n_F}^{(n_{SA})} = \left(\underline{\tilde{e}}_{h,n_F}^{((n_{SA}-1)K_B+1)} \ldots \underline{\tilde{e}}_{h,n_F}^{((n_{SA}-1)K_B+K_B)} \right)^T, n_{SA} = 1 \ldots N_{SA}, \qquad (7.12)$$

each of dimension K_B. For the case of N_{SA} equal to one, e.g., the single–SA scenario, this step can be skipped over. Then, the $N_{SA}N_F$ partial subcarrier–specific vectors $\underline{\tilde{\mathbf{e}}}_{h,n_F}^{(n_{SA})}$ of (7.12) are sorted to $N_{SA}K_B$ SA–AP–specific vectors

$$\underline{\tilde{\mathbf{e}}}_h^{(k_B,n_{SA})} = \left(\underline{\tilde{e}}_{h,1}^{((n_{SA}-1)K_B+k_B)} \ldots \underline{\tilde{e}}_{h,N_F}^{((n_{SA}-1)K_B+k_B)} \right)^T, \qquad (7.13)$$

each of dimension N_F, which are equivalent to $\underline{\tilde{\mathbf{e}}}_h^{(k_B)}$ of (4.8) for the single–SA scenario.

- Secondly, the SA–AP–specific receive pilot vectors $\underline{\tilde{\mathbf{e}}}_{\mathrm{h}}^{(k_{\mathrm{B}}, n_{\mathrm{SA}})}$ of (7.13) are processed, respectively, for the corresponding SA $n_{\mathrm{SA}}, n_{\mathrm{SA}} = 1 \ldots N_{\mathrm{SA}}$, according to (4.16) to (4.18). Therefore, the SA–AP–specific CTF estimate vectors $\underline{\hat{\tilde{\mathbf{h}}}}^{(k_{\mathrm{B}}, n_{\mathrm{SA}})}$, which are equivalent to $\underline{\hat{\tilde{\mathbf{h}}}}^{(k_{\mathrm{B}})}$ of (4.18) in the case of the single–SA scenario, each of dimension $K N_{\mathrm{F}}$, can be obtained.

- Thirdly, the estimate $\underline{\hat{\tilde{\mathbf{H}}}}_{n_{\mathrm{B}}}$ of the slot–specific CTF matrix $\underline{\tilde{\mathbf{H}}}_{n_{\mathrm{B}}}$ of (7.1) for the time slot n_{B} equal to $N_{\mathrm{BU}} + 1$, which is reserved for the pilot transmission, can be constructed with the $N_{\mathrm{SA}} K_{\mathrm{B}}$ SA–AP–specific CTF estimate vectors $\underline{\hat{\tilde{\mathbf{h}}}}^{(k_{\mathrm{B}}, n_{\mathrm{SA}})}$. Since it is assumed that the channels are time invariant during one transmission frame, N_{B} replicas of the slot–specific CTF estimate matrix $\underline{\hat{\tilde{\mathbf{H}}}}_{N_{\mathrm{BU}}+1}$ at the time slot n_{B} equal to $N_{\mathrm{BU}} + 1$ are delivered sequently at the output port H_e.

If "OperationModeJCE" is equal to "0", the algorithm of JCE is not performed. The total CTF matrix $\underline{\tilde{\mathbf{H}}}$ of (7.11) is simply sorted into N_{B} sequent slot–specific CTF matrices $\underline{\tilde{\mathbf{H}}}_{n_{\mathrm{B}}}$ of (7.1). The N_{B} matrices $\underline{\tilde{\mathbf{H}}}_{n_{\mathrm{B}}}$ of (7.1), which may differ from each other, are delivered sequently at the output port H_e.

The parameter "PilotType" indicates which type of pilots is used, corresponding to the type of pilots applied in the MTs. Different integer values correspond to the different types of pilots. In the following investigations, the pilots based on Walsh codes, as introduced in Section 4.4, are considered. Concerning the other parameters related to JCE, e.g., the channel dimension W and the pilot energy E_{p}, these parameters are consistent with the ones used in Chapter 4.

7.4.4 Joint detection

7.4.4.1 Features

The whole task of the data estimation in the UL is undertaken by the module "Joint-Dection". The prerequisites of JD are the known CSI data in terms of the CTF matrices $\underline{\tilde{\mathbf{H}}}_{n_{\mathrm{B}}}$ of (7.1), which are offered by the primitive "JointChannelEstimation" as discussed in Subsection 7.4.3. The following requirements are met according to the system design:

- The linear JD algorithms are realized in the module "JointDection".

- Subcarrierwise processing for the linear JD algorithms is favored.

- The extension to some nonlinear JD algorithms is possible.

- Both single–SA scenarios and multiple–SA scenarios can be handled.

7.4.4.2 Particular description

The module "JointDection", consisting of two functional components, i.e., the primitive "sort_channel" and the primitive "JD_core", as depicted in Fig.7.5, is processed N_{BU} times per frame. The module "JointDection" has two input ports. One input port is e, which is a multiple–input port for complex matrices. Therefore, N_{F} slot–subcarrier– specific receive data vectors

$$\tilde{\underline{\mathbf{e}}}_{\mathrm{u},n_{\mathrm{B}},n_{\mathrm{F}}} = \left(\tilde{\underline{e}}_{\mathrm{u},n_{\mathrm{B}},n_{\mathrm{F}}}^{(1)} \cdots \tilde{\underline{e}}_{\mathrm{u},n_{\mathrm{B}},n_{\mathrm{F}}}^{(N_{\mathrm{AP}})} \right)^{\mathrm{T}}, \tag{7.14}$$

each of dimension N_{AP} equal to $N_{\mathrm{SA}}K_{\mathrm{B}}$, can be collected in parallel for the time slot n_{B}, $n_{\mathrm{B}} = 1 \ldots N_{\mathrm{BU}}$. In the case of N_{SA} equal to one, i.e., the single–SA scenario, the slot–subcarrier–specific receive data vectors $\tilde{\underline{\mathbf{e}}}_{\mathrm{u},n_{\mathrm{B}},n_{\mathrm{F}}}$ of (7.14) are equivalent to the subcarrier–specific receive data vectors $\tilde{\underline{\mathbf{e}}}_{\mathrm{u},n_{\mathrm{F}}}$ of (3.20), each of dimension K_{B}. The other input port is H, which is for a single complex matrix. Through the port H the slot–specific CTF matrices $\tilde{\underline{\mathbf{H}}}_{n_{\mathrm{B}}}$ of (7.1) are delivered sequently, for the corresponding time slot n_{B} in the UL transmissions. The module "JointDection" has one output port d_e, which is a multiple–output port for complex matrices. Through the port d_e N_{F} slot–subcarrier–specific data estimate vectors

$$\hat{\tilde{\underline{\mathbf{d}}}}_{\mathrm{u},n_{\mathrm{B}},n_{\mathrm{F}}} = \left(\hat{\tilde{\underline{d}}}_{\mathrm{u},n_{\mathrm{B}},n_{\mathrm{F}}}^{(1)} \cdots \hat{\tilde{\underline{d}}}_{\mathrm{u},n_{\mathrm{B}},n_{\mathrm{F}}}^{(N_{\mathrm{MT}})} \right)^{\mathrm{T}}, \tag{7.15}$$

each of dimension N_{MT} equal to $N_{\mathrm{SA}}K$, are delivered for the time slot n_{B}. In the case of N_{SA} equal to one, i.e., the single–SA scenario, $\hat{\tilde{\underline{\mathbf{d}}}}_{\mathrm{u},n_{\mathrm{B}},n_{\mathrm{F}}}$ of (7.15) is equivalent to the subcarrier–specific data estimate vectors $\hat{\tilde{\underline{\mathbf{d}}}}_{\mathrm{u},n_{\mathrm{F}}}$ of (5.2), each of dimension K.

The primitive "sort_channel" aims at sorting the slot–specific CTF matrix $\tilde{\underline{\mathbf{H}}}_{n_{\mathrm{B}}}$ of (7.1) into a slot–subcarrier–specific form $\tilde{\underline{\mathbf{H}}}_{n_{\mathrm{B}},n_{\mathrm{F}}}$ of (7.1), which are desired by the subcarrierwise JD algorithms, for the time slot n_{B}. The input port of the primitive "sort_channel" is connected to the input port H of the module "JointDetection". The output port of the primitive "sort_channel", which is a multiple–output port for complex matrices, is connected to one of the input ports of JD_core so that the N_{F} sorted slot–subcarrier–specific CTF matrices $\tilde{\underline{\mathbf{H}}}_{n_{\mathrm{B}},n_{\mathrm{F}}}$ of (7.1) are delivered in parallel to the primitive "JD_core" at the time slot n_{B}.

The primitive "JD_core" accomplishes the key JD algorithms. The primitive "JD_core" has two input ports. Both input ports are multiple–input ports for complex matrices. One input port is connected directly to the input port e of the module "JointDetection" to receive the N_{F} parallel slot–subcarrier–specific receive data vectors $\tilde{\underline{\mathbf{e}}}_{\mathrm{u},n_{\mathrm{B}},n_{\mathrm{F}}}$ of (7.14), each of dimension $N_{\mathrm{SA}}K_{\mathrm{B}}$. The other input port is connected to the output port of the primitive "sort_channel" for the N_{F} slot–subcarrier–specific CTF matrices $\tilde{\underline{\mathbf{H}}}_{n_{\mathrm{B}},n_{\mathrm{F}}}$

Module "JointDetection"
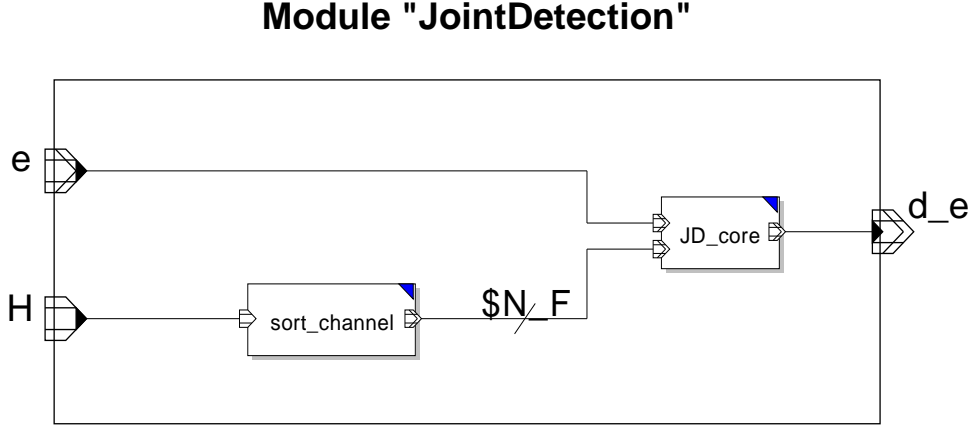
Fig. 7.5. Module "JointDection" implemented in MLDesigner

of (7.1). The output port d_e of the primitive "JD_core" is a multiple–output port for complex matrices. The primitive "JD_core" works as follows:

- Firstly, the N_{F} slot–subcarrier–specific receive data vectors $\underline{\tilde{\mathbf{e}}}_{\mathrm{u},n_{\mathrm{B}},n_{\mathrm{F}}}$ of (7.14) are sorted to $N_{\mathrm{SA}}N_{\mathrm{F}}$ partial slot–subcarrier–specific receive data vectors

$$\underline{\tilde{\mathbf{e}}}_{\mathrm{u},n_{\mathrm{B}},n_{\mathrm{F}}}^{(n_{\mathrm{SA}})} = \left(\underline{\tilde{e}}_{\mathrm{u},n_{\mathrm{B}},n_{\mathrm{F}}}^{((n_{\mathrm{SA}}-1)K_{\mathrm{B}}+1)} \ldots \underline{\tilde{e}}_{\mathrm{u},n_{\mathrm{B}},n_{\mathrm{F}}}^{((n_{\mathrm{SA}}-1)K_{\mathrm{B}}+K_{\mathrm{B}})}\right)^{\mathrm{T}}, \qquad (7.16)$$

each of dimension K_{B}.

- Then, the N_{F} slot–subcarrier–specific CTF matrices $\underline{\tilde{\mathbf{H}}}_{n_{\mathrm{B}},n_{\mathrm{F}}}$ of (7.1) are sorted so that $N_{\mathrm{SA}}N_{\mathrm{F}}$ SA–slot–subcarrier–specific CTF matrix $\underline{\tilde{\mathbf{H}}}_{n_{\mathrm{B}},n_{\mathrm{F}}}^{(n_{\mathrm{SA}},n_{\mathrm{SA}})}$ of (7.5), each of dimensions $K_{\mathrm{B}} \times K$, which are actually the diagonal submatrices of $\underline{\tilde{\mathbf{H}}}_{n_{\mathrm{B}},n_{\mathrm{F}}}$ of (7.5), are obtained.

- Thirdly, according to the JD algorithms discussed in Chapter 5, two options are available: the RxMF JD and the RxZF JD. The parameter "detector_type" determines which type of the joint detectors is applied. The SA–slot–subcarrier– specific data estimate vectors $\underline{\hat{\mathbf{d}}}_{\mathrm{u},n_{\mathrm{B}},n_{\mathrm{F}}}^{(n_{\mathrm{SA}})}$ can be obtained with (5.8) for the RxMF JD, or with (5.11) for the RxZF JD, respectively.

- The $N_{\mathrm{SA}}N_{\mathrm{F}}$ SA–slot–subcarrier–specific data estimate vectors $\hat{\underline{\hat{\mathbf{d}}}}_{\mathrm{u},n_{\mathrm{B}},n_{\mathrm{F}}}^{(n_{\mathrm{SA}})}$, each of dimension K, are sorted to N_{F} slot–subcarrier–specific data estimate vectors $\hat{\underline{\hat{\mathbf{d}}}}_{\mathrm{u},n_{\mathrm{B}},n_{\mathrm{F}}}$ of (7.15), each of dimension $N_{\mathrm{SA}}K$.

For single–SA scenarios, the process described above can be simplified by setting N_{SA} equal to one.

7.4.5 Joint transmission

7.4.5.1 Features

The task of the data transmission in the DL is undertaken by the module "Joint-Transmission". The prerequisites of JT are the known CSI data in terms of the CTF matrices $\underline{\tilde{\mathbf{H}}}_{n_{\mathrm{B}}}$ of (7.1), which are offered by the primitive "JointChannelEstimation" as discussed in Subsection 7.4.3. The following requirements are met according to the system design:

- The linear JT algorithms are realized in the module "JointTransmission".

- Subcarrierwise processing for the linear JT algorithms is favored.

- The extension to some nonlinear JT algorithms is possible.

- Both single–SA scenarios and multiple–SA scenarios can be handled.

7.4.5.2 Particular description

The module "JointTransmission", consisting of the primitive "sort_channel" and the primitive "JT_core", as depicted in Fig.7.6, is processed N_{BD} times per frame. The module "JointTransmission" has two input ports. One input port is d, which is a multiple–input port for complex matrices. Therefore, N_{F} slot–subcarrier–specific transmit data vectors

$$\underline{\tilde{\mathbf{d}}}_{\mathrm{d},n_{\mathrm{B}},n_{\mathrm{F}}} = \left(\underline{\tilde{d}}_{\mathrm{d},n_{\mathrm{B}},n_{\mathrm{F}}}^{(1)} \ldots \underline{\tilde{d}}_{\mathrm{d},n_{\mathrm{B}},n_{\mathrm{F}}}^{(N_{\mathrm{MT}})} \right)^{\mathrm{T}}, \tag{7.17}$$

each of dimension N_{MT}, can be sent in parallel for the time slot $n_{\mathrm{B}}, n_{\mathrm{B}} = N_{\mathrm{BU}}+2 \ldots N_{\mathrm{B}}$. In the case of N_{SA} equal to one, i.e., the single–SA scenario, the slot–subcarrier–specific transmit data vectors $\underline{\tilde{\mathbf{d}}}_{\mathrm{d},n_{\mathrm{B}},n_{\mathrm{F}}}$ of (7.17) are equivalent to the subcarrier–specific transmit data vector $\underline{\tilde{\mathbf{d}}}_{\mathrm{d},n_{\mathrm{F}}}$ of (6.1), each of dimension K. The other input port is H,

Module "JointTransmission"
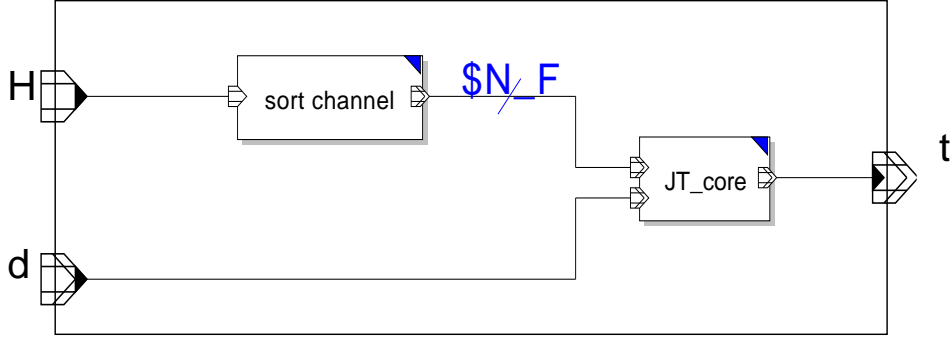
Fig. 7.6. Module "JointTransmission" implemented in MLDe-
signer

which is for a single complex matrix. Through the port H the DL slot–specific CTF matrices $\underline{\tilde{\mathbf{H}}}_{n_{\mathrm{B}}}^{\mathrm{T}}$ are delivered sequently at the time slot n_{B} for the DL transmissions. The module "JointTransmission" has one output port t, which is a multiple–output port for complex matrices. Through the port t N_{F} slot–subcarrier–specific transmit vectors

$$\underline{\tilde{\mathbf{s}}}_{\mathrm{d},n_{\mathrm{B}},n_{\mathrm{F}}} = \left(\underline{\tilde{s}}_{\mathrm{d},n_{\mathrm{B}},n_{\mathrm{F}}}^{(1)} \dots \underline{\tilde{s}}_{\mathrm{d},n_{\mathrm{B}},n_{\mathrm{F}}}^{(N_{\mathrm{AP}})} \right)^{\mathrm{T}}, \tag{7.18}$$

each of dimension N_{AP} equal to $N_{\mathrm{SA}} K_{\mathrm{B}}$, are delivered for the time slot n_{B}. In the case of N_{SA} equal to one, i.e., the single–SA scenario, $\underline{\tilde{\mathbf{s}}}_{\mathrm{d},n_{\mathrm{B}},n_{\mathrm{F}}}$ of (7.18) is equivalent to the subcarrier–specific transmit vector $\underline{\tilde{\mathbf{s}}}_{\mathrm{d},n_{\mathrm{F}}}$ of (3.28), each of dimension K_{B}.

The primitive "sort_channel" aims at sorting the DL slot–specific CTF matrix $\underline{\tilde{\mathbf{H}}}_{n_{\mathrm{B}}}^{\mathrm{T}}$ into a slot–subcarrier–specific form $\underline{\tilde{\mathbf{H}}}_{n_{\mathrm{B}},n_{\mathrm{F}}}^{\mathrm{T}}$, which is desired by the subcarrierwise JT algorithms for the time slot n_{B}. The input port of the primitive "sort_channel" is connected to the input port H of the module "JointTransmission". The output port of the primitive "sort_channel", which is a multiple–output port for complex matrices, is connected to one of the input ports of the primitive "JT_core" so that the N_{F} sorted DL slot–subcarrier–specific CTF matrices $\underline{\tilde{\mathbf{H}}}_{n_{\mathrm{B}},n_{\mathrm{F}}}^{\mathrm{T}}$ of (7.1) are delivered in parallel to the primitive "JT_core".

The primitive "JT_core" accomplishes the key JT algorithms. The primitive "JT_core" has two input ports. Both input ports are multiple–input ports for complex matrices. One input port is connected directly to the input port d of the module "JointTransmission" to receive N_F parallel slot–subcarrier–specific data vectors $\underline{\tilde{\mathbf{d}}}_{\mathrm{d},n_\mathrm{B},n_\mathrm{F}}$ of (7.17) to be transmitted, each of dimension $N_\mathrm{SA}K$. The other input is connected to the output port of the primitive "sort_channel" for the N_F slot–subcarrier–specific CTF matrices $\underline{\tilde{\mathbf{H}}}_{n_\mathrm{B},n_\mathrm{F}}^\mathrm{T}$. The output port t of the primitive "JT_core" is a multiple–output port, which delivers N_F slot–subcarrier–specific transmit vectors $\underline{\tilde{\mathbf{s}}}_{\mathrm{d},n_\mathrm{B},n_\mathrm{F}}$ of (7.18). The primitive "JT_core" works as follows:

- Firstly, the N_F slot–subcarrier–specific data vectors $\underline{\tilde{\mathbf{d}}}_{\mathrm{d},n_\mathrm{B},n_\mathrm{F}}$ of (7.17) to be transmitted are sorted to $N_\mathrm{SA}N_\mathrm{F}$ partial slot–subcarrier–specific data vectors

$$
\tilde{\underline{\mathbf{d}}}_{\mathrm{d},n_\mathrm{B},n_\mathrm{F}}^{(n_\mathrm{SA})} = \left(\tilde{\underline{d}}_{\mathrm{d},n_\mathrm{B},n_\mathrm{F}}^{((n_\mathrm{SA}-1)K+1)} \ \cdots \ \tilde{\underline{d}}_{\mathrm{d},n_\mathrm{B},n_\mathrm{F}}^{((n_\mathrm{SA}-1)K+K)} \right)^\mathrm{T}, \tag{7.19}
$$

each of dimension K.

- Then, the N_F slot–subcarrier–specific CTF matrices $\underline{\tilde{\mathbf{H}}}_{n_\mathrm{B},n_\mathrm{F}}^\mathrm{T}$ in the DL transmission are sorted so that $N_\mathrm{SA}N_\mathrm{F}$ SA–slot–subcarrier–specific CTF matrix $\underline{\tilde{\mathbf{H}}}_{n_\mathrm{B},n_\mathrm{F}}^{(n_\mathrm{SA},n_\mathrm{SA})\,\mathrm{T}}$ in the DL, each of dimensions $K \times K_\mathrm{B}$, which are actually the transpose of the diagonal submatrices of $\underline{\tilde{\mathbf{H}}}_{n_\mathrm{B},n_\mathrm{F}}$ of (7.5), are obtained.

- Thirdly, two options, the TxMF JT and the TxZF JT, are available according to the two JT algorithms discussed in Chapter 6. The parameter "transmitter_type" determines which type of the joint transmitters is applied. The SA–slot–subcarrier–specific modulator matrix $\underline{\tilde{\mathbf{M}}}_{n_\mathrm{B},n_\mathrm{F}}^{(n_\mathrm{SA})}$ can be obtained with (6.11) for the TxMF JT, or with (6.14) for the TxZF JT, respectively. Therefore, the SA–slot–subcarrier–specific transmit vectors

$$
\tilde{\underline{\mathbf{s}}}_{\mathrm{d},n_\mathrm{B},n_\mathrm{F}}^{(n_\mathrm{SA})} = \left(\tilde{\underline{s}}_{\mathrm{d},n_\mathrm{B},n_\mathrm{F}}^{((n_\mathrm{SA}-1)K_\mathrm{B}+1)} \ \cdots \ \tilde{\underline{s}}_{\mathrm{d},n_\mathrm{B},n_\mathrm{F}}^{((n_\mathrm{SA}-1)K_\mathrm{B}+K_\mathrm{B})} \right)^\mathrm{T}, \tag{7.20}
$$

each of dimension K_B, can be obtained.

- The $N_\mathrm{SA}N_\mathrm{F}$ SA–slot–subcarrier–specific transmit vectors $\tilde{\underline{\mathbf{s}}}_{\mathrm{d},n_\mathrm{B},n_\mathrm{F}}^{(n_\mathrm{SA})}$ of (7.20), are sorted to N_F slot–subcarrier–specific data estimate vectors $\underline{\tilde{\mathbf{s}}}_{\mathrm{d},n_\mathrm{B},n_\mathrm{F}}$ of (7.18).

For single–SA scenarios, the process described above can be simplified by setting N_SA equal to one.

7.5   Implementation of the JOINT simulation chain

Concerning the physical layer (PHY) investigation in conventional cellular systems, link level and system level performances [Ste96, Lu01] are usually jointly considered. However, in the SA based system JOINT, things become different and complicated, mainly in the system level investigation. For instance in the UL, since APs in a SA are distributed away from each other, the interferences received at the different APs differ from each other so that the signal–to–noise–and–interference ratios (SNIRs) at the different APs become variable as well, even when the noise power is given to be the same. On the other hand, in the DL the data transmission signals are strictly designed by the JT algorithms. Therefore, it is problematic to calculated the exact interferences at the MTs without the knowledge about the detailed transmission in other co–channel SAs. In one word, it is very difficult to do the system level simulations with power control schemes in the SA based system as compared in the conventional cellular system.

In this thesis, the end–to–end performance investigation of JOINT, in terms of BERs, is focused on. Therefore, a simulation chain of JOINT for the BER simulation is implemented, as depicted in Fig. 7.7. The JOINT simulation chain for the system level investigations is not included in the thesis. The link level JOINT simulation chain comprises the UL part and the DL part, which are associated by the reciprocal channels.

In the UL part, a complete link consists of

- the primitive "BitSource", an information–bit generator which generates the binary sequences in parallel for the multiple MTs,

- the module "MT_Tx", a transmitter of the MT which includes a modulator, a pilot generator and a data–pilot multiplexer for each MT,

- the primitive "Noise_UL", a noise generator which generates the Gaussian noise in the UL,

- the primitive "ChannelModels" introduced in Subsection 7.4.2,

- the primitive "Chan_UL", which realizes the UL process, in which signals are distorted by a linear transmission system and the noise,

- the primitive "Demux", a de–multiplexer which distinguishes the pilot and the data transmission for the following the primitive "JointChannelEstimation" and the module "JointDetection", introduced in Subsections 7.4.3 and 7.4.4, respectively,

- the module "CU_Rx", a demodulator and

- the primitive "BER", a BER calculator, which compares the estimate bits and the data bits and calculates the BERs for the corresponding MTs.

In the DL part, a complete link consists of

- the primitive "BitSource", an information–bit generator which is the same as the one in the UL part,

- the module "CU_Tx", a transmitter of the CU which realizes the signal modulation for each MT,

- the module "JointTransmission" as introduced in 7.4.5,

- the primitive "Noise_DL", a noise generator which generates the Gaussian noise in the DL,

- the primitive "Chan_DL", a primitive which realizes the DL process, in which signals are distorted by a linear transmission system and the noise,

- the module "MT_Rx", a demodulator and

- the primitive "BER", a BER calculator which compares the estimate bits and the data bits and calculates the BERs for the corresponding MTs.

There are some other primitives like e.g., "form"/ "re–form", "Park", "switchA"/ "switchB"/ "switchC" and "UL_2_DL", which realize the important roles forming the desired structures for input ports of the other functional primitives or modules without changing the values of the particles, where the particles indicate any data flowing through primitives and/or modules of a system, including e.g., data bits and data symbols in the form of scalars or of vectors/matrices [MT03].

By setting the proper parameters, the JOINT simulation chain, as shown in Fig.7.7, can be run for single–/multiple–SA scenarios, for different channel models, and for some other different system requirements.

7.6   Specific problems and solutions

7.6.1   Synchronization

The topic on synchronization of JOINT has been considered in Section 3.3. Here, the problem of synchronization among the modules and the primitives of the JOINT simulation chain is addressed.

As stated in Section 7.3, most of the primitives and modules are designed and implemented in the SDF domain. One basic principle in the SDF domain is the balance between the produced particles and the consumed particles [MT03].

Each port of an SDF primitive has an attribute that specifies the number of particles consumed for input ports or the number of particles produced for output ports [MT03]. When an input port is connected to an output port with an arc, the number of particles produced on the arc by the source primitive may not be the same as the number of particles consumed from that arc by the destination primitive. To maintain a balanced system, the scheduler must fire the source and destination primitives with different frequencies.

The primitive "JointChannelEstimaiton" is a good example to show how the balance is kept. The primitive "JointChannelEstimaiton" is processed once per frame exactly at the time slot n_{B} equal to $N_{\mathrm{BU}} + 1$ for the pilot transmission. However, the primitive "JointChannelEstimaiton" has to receive all the CSI data of the N_{B} time slots in the whole frame in order to fulfill the design requirement of delivering the true CSI data as well as the CSI estimates for JD in the UL and for JT in the DL. Such a confliction can be solved by some tricks to keep the system in balance. At the input port H of the primitive "JointChannelEstimaiton" the N_{B} slot–specific CTF matrices $\tilde{\underline{\mathbf{H}}}_{n_{\mathrm{B}}}$ of (7.1) should be be loaded together in the form of a new big matrix $\tilde{\underline{\mathbf{H}}}$ of (7.11) at the time slot n_{B} equal to $N_{\mathrm{BU}} + 1$ when the primitive "JointChannelEstimaiton" is triggered. This means between the channel model primitive and the primitive "JointChannelEstimaiton" there should exist a primitive named "Park", as depicted in Fig. 7.7, in which the sequent slot–specific CTF matrices $\tilde{\underline{\mathbf{H}}}_{n_{\mathrm{B}}}$ of (7.1) sent out at the output port H of the channel model primitive are detained and sorted into a big matrix $\tilde{\underline{\mathbf{H}}}$ of (7.11) delivered to the input port H of the primitive "JointChannelEstimaiton". On the other hand the N_{B} sequent slot–specific matrices $\tilde{\underline{\mathbf{H}}}_{n_{\mathrm{B}}}$ of (7.1) will be delivered from the output port $\mathsf{H\_e}$ of the primitive "JointChannelEstimaiton" to the output port H of the module "JointDetection" and to the output port H of the module "JointTransmission". However, only the first N_{BU} slot–specific CTF matrices $\tilde{\underline{\mathbf{H}}}_{n_{\mathrm{B}}}$ of (7.1) are required by the module "JointDetection", and the last N_{BD} slot–specific

CTF matrices $\tilde{\underline{\mathbf{H}}}_{n_{\mathrm{B}}}$ of (7.1) are required by the module "JointTransmission", respectively. Therefore, between the primitive "JointChannelEstimaiton" and the modules "JointDetection"/"JointTransmission", there should exist a primitive "Switch", as depicted in Fig. 7.7, in which the N_{B} sequent slot–specific CTF matrices $\tilde{\underline{\mathbf{H}}}_{n_{\mathrm{B}}}$ of (7.1) are handled so that the first N_{BU} slot–specific CTF matrices $\tilde{\underline{\mathbf{H}}}_{n_{\mathrm{B}}}$ of (7.1) and the last N_{BD} slot–specific CTF matrices $\tilde{\underline{\mathbf{H}}}_{n_{\mathrm{B}}}$ of (7.1) are delivered separately. This means one slot–specific CTF matrix $\tilde{\underline{\mathbf{H}}}_{n_{\mathrm{B}}}$ of (7.1) at the time slot n_{B} equal to $N_{\mathrm{BU}}+1$ is discarded.

7.6.2   Simulation efficiency

The JOINT simulation consists of many modules and primitives. Great amounts of calculations are carried out when simulations are running. Therefore, the CPU and memory of a computer system are greatly occupied during the simulations. Especially concerning the memory, if the memory consumption of the simulation chain is too high and exceeds the upper limit of the tolerance of the computer system, the simulation will be blocked or even cancelled. In order to avoid this, we have to carefully design the system to make an efficient use of the memory.

One way is to optimize the algorithms during the implementation. For instance in the JCE algorithm, the matrix $\tilde{\underline{\mathbf{Z}}}$ of (4.18), only depends on the pilot matrix $\tilde{\underline{\mathbf{P}}}$ of (4.16) and the matrix $\tilde{\boldsymbol{\mathcal{F}}}_{W,\mathrm{tot}}$ of (4.18), as discussed in Section 4.3. Meanwhile, the pilot matrix $\tilde{\underline{\mathbf{P}}}$ of (4.16) and the matrix $\tilde{\boldsymbol{\mathcal{F}}}_{W,\mathrm{tot}}$ of (4.18) are fixed once the parameters K, W and N_{F} are determined. Therefore, the matrix $\tilde{\underline{\mathbf{Z}}}$ of (4.18) is constant throughout the simulation once the parameters K, W and N_{F} are fixed. This means, that the matrix $\tilde{\underline{\mathbf{Z}}}$ of (4.18) needs to be calculated only once during the simulation in the optimized JCE algorithm. Such a modification can be achieved by putting the part of codes for the $\tilde{\underline{\mathbf{Z}}}$ calculation into the "begin" method in stead of the "go" method, where the term method is a term of C++ programs indicating a paragraph of codes for the given functionality. The method "begin" is to be executed only once at the very beginning after the total system is successfully compiled and properly scheduled. However, the method "go" is to be executed each time when the primitive is triggered. Consequently, the computational effort and the memory consumption are greatly reduced.

Another way to improve the memory efficiency is to avoid memory leaks. Most primitives deal with matrices. Therefore, allocating memory space to these matrices during the calculation is necessary. Memory leaks occur when new memory space is allocated dynamically and never deallocated. In C programs, new memory space is allocated by the functions "malloc" or "calloc", and deallocated by the function "free". In C++, new memory space is usually allocated by the operator "new" and deallocated by the

operator "delete". The problem with memory leaks is that the memory space, which is not deallocated after being used, accumulates over time and may cripple or even crash a program. The operator "cleanup" should be applied to variables containing dynamic memory. Some common mistakes may lead to memory leaks, like, e.g., the improper usage of the operator "delete" and overwriting a variable containing dynamic memory without freeing any existing memory first. Besides carefully checking the codes, the following two tricks can be used:

- In the method "constructor" of a primitive, the variables containing dynamic memory should be initialized to zero.

- By freeing memory apply the method "cleanup", which covers all possible cases of memory leaks during simulations.
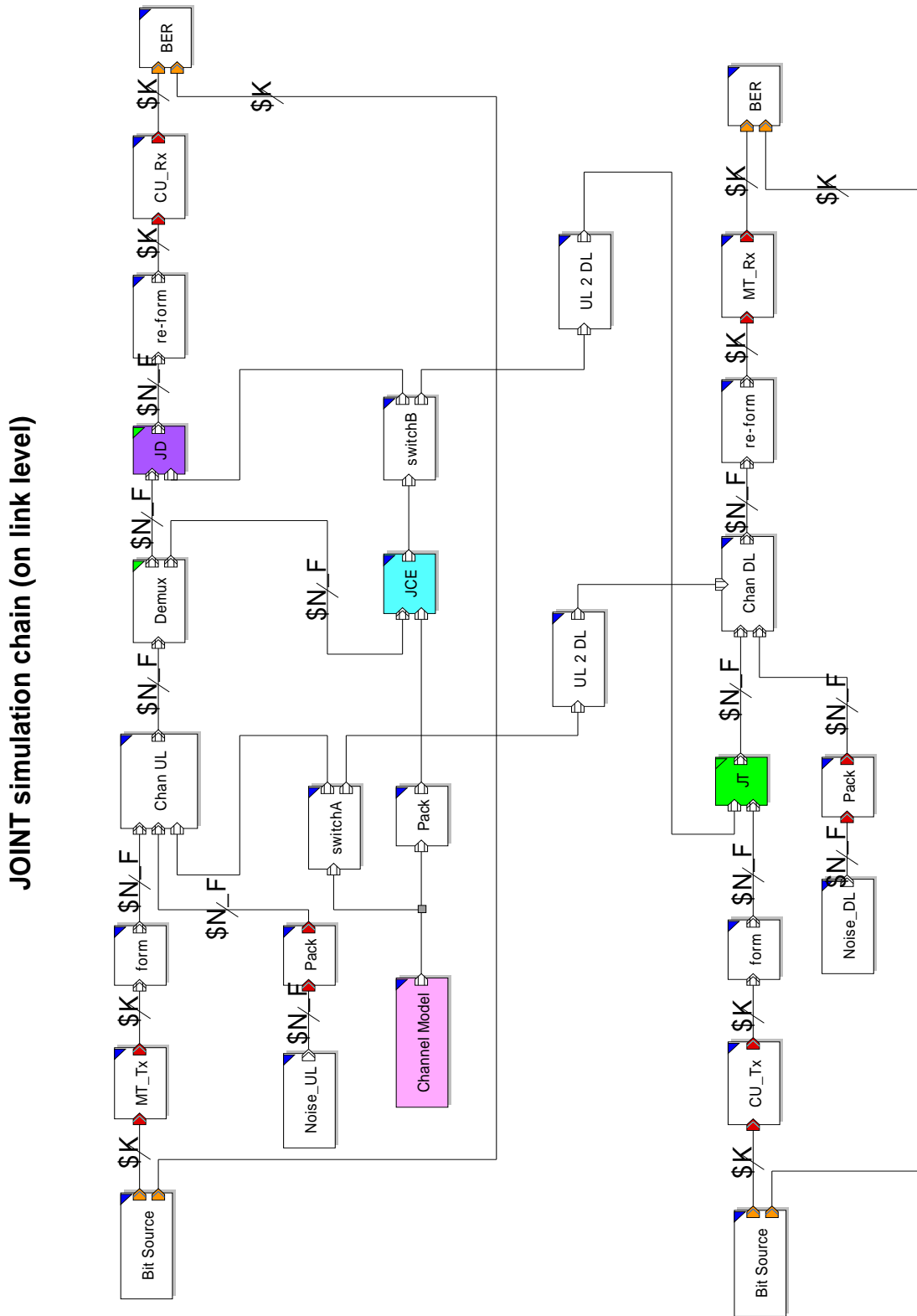
Fig. 7.7. JOINT simulation chain in MLDesigner

Chapter 8

Performance of JOINT in a single–service–area scenario

8.1   Preliminary remarks

The main advantage of the SA based JOINT compared to conventional cellular systems is that JOINT is capable to combat the intra–SA MAI and to improve the system performance, as explained in Chapter 1. In the present chapter, the system performance of JOINT will be evaluated in a single–SA scenario, in which the inter–SA MAI is temporarily ignored. Therefore, the performance of the data estimation technique and the data transmission technique of JOINT in the noise–limited case can be focused on.

In the present chapter, first the duality between the UL and the DL of JOINT is discussed under the assumption of perfect CSI. A general model of the linear data transmission is given. The UL performance and the DL performance, in terms of bit error probabilities, are compared on the basis of this general model so that the duality of the UL and the DL performances can be deduced. Moreover, this performance duality is also analyzed with respect to the efficiency of energy transmission.

CSI is the prerequisite for the data estimation in the UL and the data transmission in the DL. However, the CSI estimation errors are inevitable if JCE is applied. Two major factors, which lead to the CSI estimation errors, are analyzed. In the present chapter, the influences of the CSI estimation errors on the UL and the DL performances are also discussed.

Finally, numerical results obtained with the JOINT simulation chain introduced in Chapter 7 are given to demonstrate the aforementioned analysis.

8.2   Duality of the uplink and the downlink performances

8.2.1   General model of linear data transmission

In order to deeply understand the intrinsic relation between the UL transmission and the DL transmission of JOINT, it is necessary to study a more general linear data

transmission first, which covers all the common characteristics of the UL transmission and the DL transmission.
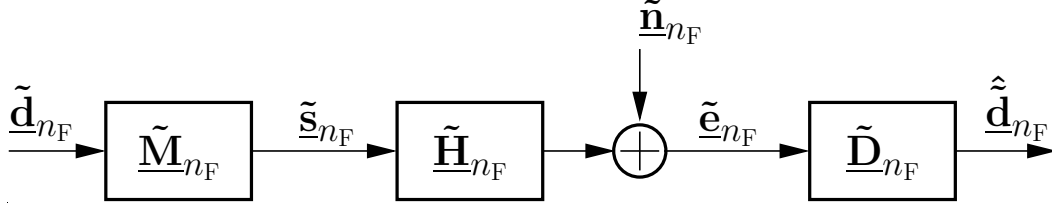
Fig. 8.1. General subcarrierwise model of a linear transmission

Fig. 8.1 shows such a general model of the linear data transmission in the frequency domain with respect to the subcarrier n_{F} [Skl04], regardless of the UL or the DL. The data vector

$$\underline{\tilde{\mathbf{d}}}_{n_{\mathrm{F}}} = \left(\underline{\tilde{d}}_{n_{\mathrm{F}}}^{(1)} \ldots \underline{\tilde{d}}_{n_{\mathrm{F}}}^{(K)} \right)^{\mathrm{T}} \tag{8.1}$$

of dimension K is first pre–processed by a linear modulator matrix $\underline{\tilde{\mathbf{M}}}_{n_{\mathrm{F}}}$ of dimensions $K_{\mathrm{I}} \times K$, where K_{I} denotes the number of the inputs of the MIMO channel. Therefore, the transmit vector

$$\underline{\tilde{\mathbf{s}}}_{n_{\mathrm{F}}} = \left(\underline{\tilde{s}}_{n_{\mathrm{F}}}^{(1)} \ldots \underline{\tilde{s}}_{n_{\mathrm{F}}}^{(K_{\mathrm{I}})} \right)^{\mathrm{T}} \tag{8.2}$$

of dimension K_{I} can be generated by multiplying the data vector $\underline{\tilde{\mathbf{d}}}_{n_{\mathrm{F}}}$ of (8.1) by the modulation matrix $\underline{\tilde{\mathbf{M}}}_{n_{\mathrm{F}}}$, i.e.,

$$\underline{\tilde{\mathbf{s}}}_{n_{\mathrm{F}}} = \underline{\tilde{\mathbf{M}}}_{n_{\mathrm{F}}} \underline{\tilde{\mathbf{d}}}_{n_{\mathrm{F}}}. \tag{8.3}$$

Then, the transmit vector $\underline{\tilde{\mathbf{s}}}_{n_{\mathrm{F}}}$ of (8.2) is fed into the MIMO channel denoted by the CTF matrix $\underline{\tilde{\mathbf{H}}}_{n_{\mathrm{F}}}$ of dimensions $K_{\mathrm{O}} \times K_{\mathrm{I}}$, where K_{O} denotes the number of the outputs of the MIMO channel. The transmit vector $\underline{\tilde{\mathbf{s}}}_{n_{\mathrm{F}}}$ of (8.2) is corrupted by the noise, which is denoted by the noise vector

$$\underline{\tilde{\mathbf{n}}}_{n_{\mathrm{F}}} = \left(\underline{\tilde{n}}_{n_{\mathrm{F}}}^{(1)} \ldots \underline{\tilde{n}}_{n_{\mathrm{F}}}^{(K_{\mathrm{O}})} \right)^{\mathrm{T}} \tag{8.4}$$

of dimension K_{O}. Therefore, the receive vector

$$\underline{\tilde{\mathbf{e}}}_{n_{\mathrm{F}}} = \left(\underline{\tilde{e}}_{n_{\mathrm{F}}}^{(1)} \ldots \underline{\tilde{e}}_{n_{\mathrm{F}}}^{(K_{\mathrm{O}})} \right)^{\mathrm{T}} \tag{8.5}$$

of dimension K_{O} can be obtained by

$$\underline{\tilde{\mathbf{e}}}_{n_{\mathrm{F}}} = \underline{\tilde{\mathbf{H}}}_{n_{\mathrm{F}}} \, \underline{\tilde{\mathbf{s}}}_{n_{\mathrm{F}}} + \, \underline{\tilde{\mathbf{n}}}_{n_{\mathrm{F}}}. \tag{8.6}$$

The receive vector $\underline{\tilde{\mathbf{e}}}_{n_{\mathrm{F}}}$ of (8.5) is processed by a linear detection process mathematically described by the detector matrix $\underline{\tilde{\mathbf{D}}}_{n_{\mathrm{F}}}$ of dimensions $K \times K_{\mathrm{O}}$ so that with (8.3) and (8.6) the data estimate vector

$$\underline{\hat{\tilde{\mathbf{d}}}}_{n_{\mathrm{F}}} = \left(\underline{\hat{\tilde{d}}}_{n_{\mathrm{F}}}^{(1)} \ldots \underline{\hat{\tilde{d}}}_{n_{\mathrm{F}}}^{(K)} \right)^{\mathrm{T}} \tag{8.7}$$

of dimension K is given by

$$
\begin{aligned}
\hat{\tilde{\underline{\mathbf{d}}}}_{n_{\mathrm{F}}} &= \tilde{\underline{\mathbf{D}}}_{n_{\mathrm{F}}} \tilde{\underline{\mathbf{e}}}_{n_{\mathrm{F}}} \\
&= \tilde{\underline{\mathbf{D}}}_{n_{\mathrm{F}}} \tilde{\underline{\mathbf{H}}}_{n_{\mathrm{F}}} \tilde{\underline{\mathbf{M}}}_{n_{\mathrm{F}}} \tilde{\underline{\mathbf{d}}}_{n_{\mathrm{F}}} + \tilde{\underline{\mathbf{D}}}_{n_{\mathrm{F}}} \, \tilde{\underline{\mathbf{n}}}_{n_{\mathrm{F}}}.
\end{aligned}
\tag{8.8}
$$

It is assumed that the uncorrelated data symbols $\tilde{\underline{d}}_{n_{\mathrm{F}}}^{(k)}$ have equal energies

$$
E_{\mathrm{d}} = \frac{1}{2} |\tilde{\underline{d}}_{n_{\mathrm{F}}}^{(k)}|^2, k, 1 \dots K.
\tag{8.9}
$$

For the covariance matrix of the data vector $\tilde{\underline{\mathbf{d}}}_{n_{\mathrm{F}}}$ of (8.1) follows

$$
\underline{\mathbf{R}}_{\mathbf{d}} = \mathrm{E}\left\{ \tilde{\underline{\mathbf{d}}}_{n_{\mathrm{F}}} \tilde{\underline{\mathbf{d}}}_{n_{\mathrm{F}}}^{*\mathrm{T}} \right\} = 2E_{\mathrm{d}} \cdot \mathbf{I}^{K}.
\tag{8.10}
$$

With σ^2 denoting the variance of real and imaginary parts of the uncorrelated noise elements $\tilde{\underline{n}}_{n_{\mathrm{F}}}^{(k_{\mathrm{O}})}$ of (8.4), the covariance matrix of the noise vector $\tilde{\underline{\mathbf{n}}}_{n_{\mathrm{F}}}$ of (8.4) reads

$$
\underline{\mathbf{R}}_{\mathbf{n}} = \mathrm{E}\left\{ \tilde{\underline{\mathbf{n}}}_{n_{\mathrm{F}}} \tilde{\underline{\mathbf{n}}}_{n_{\mathrm{F}}}^{*\mathrm{T}} \right\} = 2\sigma^2 \cdot \mathbf{I}^{K_{\mathrm{O}}}.
\tag{8.11}
$$

According to (6.10) the transmit energy

$$
\begin{aligned}
T_{n_{\mathrm{F}}}^{(k)} &= \frac{1}{2} |\tilde{\underline{d}}_{n_{\mathrm{F}}}^{(k)}|^2 \left[\tilde{\underline{\mathbf{M}}}_{n_{\mathrm{F}}}^{*\mathrm{T}} \tilde{\underline{\mathbf{M}}}_{n_{\mathrm{F}}} \right]_{k,k} \\
&= E_{\mathrm{d}} \cdot \left[\tilde{\underline{\mathbf{M}}}_{n_{\mathrm{F}}}^{*\mathrm{T}} \tilde{\underline{\mathbf{M}}}_{n_{\mathrm{F}}} \right]_{k,k}
\end{aligned}
\tag{8.12}
$$

invested for the data symbol $\tilde{\underline{d}}_{n_{\mathrm{F}}}^{(k)}$ of (8.1) is obtained. The ratio

$$
\frac{E_{\mathrm{d}}}{T_{n_{\mathrm{F}}}^{(k)}} = \frac{1}{\left[\tilde{\underline{\mathbf{M}}}_{n_{\mathrm{F}}}^{*\mathrm{T}} \tilde{\underline{\mathbf{M}}}_{n_{\mathrm{F}}} \right]_{k,k}}
\tag{8.13}
$$

of the desired energy E_{d} of (8.9) to the transmit energy $T_{n_{\mathrm{F}}}^{(k)}$ of (8.12) tells us how efficiently the energy $T_{n_{\mathrm{F}}}^{(k)}$ of (8.12) is transmitted for the data symbol $\tilde{\underline{d}}_{n_{\mathrm{F}}}^{(k)}$ of (8.1) with the energy E_{d} of (8.9). Generally, the ratio $E_{\mathrm{d}}/T_{n_{\mathrm{F}}}^{(k)}$ of (8.13) is a positive value no greater than one.

In order to obtain the unbiased data estimate $\hat{\tilde{\underline{\mathbf{d}}}}_{n_{\mathrm{F}}}$ of (8.8),

$$
\tilde{\underline{\mathbf{D}}}_{n_{\mathrm{F}}} \tilde{\underline{\mathbf{H}}}_{n_{\mathrm{F}}} \tilde{\underline{\mathbf{M}}}_{n_{\mathrm{F}}} = \mathbf{I}_{K}
\tag{8.14}
$$

has to be fulfilled so that (8.8) can be rewritten as

$$
\hat{\tilde{\underline{\mathbf{d}}}}_{n_{\mathrm{F}}} = \tilde{\underline{\mathbf{d}}}_{n_{\mathrm{F}}} + \tilde{\underline{\mathbf{D}}}_{n_{\mathrm{F}}} \, \tilde{\underline{\mathbf{n}}}_{n_{\mathrm{F}}}.
\tag{8.15}
$$

The filtered noise $\underline{\tilde{\mathbf{D}}}_{n_{\mathrm{F}}} \, \tilde{\underline{\mathbf{n}}}_{n_{\mathrm{F}}}$ accounts for the data estimation error

$$\underline{\boldsymbol{\Delta}}_{n_{\mathrm{F}}} = \hat{\tilde{\underline{\mathbf{d}}}}_{n_{\mathrm{F}}} - \tilde{\underline{\mathbf{d}}}_{n_{\mathrm{F}}} = \underline{\tilde{\mathbf{D}}}_{n_{\mathrm{F}}} \, \tilde{\underline{\mathbf{n}}}_{n_{\mathrm{F}}}. \tag{8.16}$$

With (8.10), (8.11) and the assumption that the data vector $\tilde{\underline{\mathbf{d}}}_{n_{\mathrm{F}}}$ of (8.1) and the noise vector $\tilde{\underline{\mathbf{n}}}_{n_{\mathrm{F}}}$ of (8.4) are statistically independent, the covariance matrix of the data estimation error $\underline{\boldsymbol{\Delta}}_{n_{\mathrm{F}}}$ of (8.16) reads

$$\underline{\mathbf{R}}_{\boldsymbol{\Delta}} = \mathrm{E}\left\{ \underline{\boldsymbol{\Delta}}_{n_{\mathrm{F}}} \underline{\boldsymbol{\Delta}}_{n_{\mathrm{F}}}^{*\mathrm{T}} \right\} = 2\sigma^2 \left(\underline{\tilde{\mathbf{D}}}_{n_{\mathrm{F}}} \underline{\tilde{\mathbf{D}}}_{n_{\mathrm{F}}}^{*\mathrm{T}} \right). \tag{8.17}$$

With (8.10) and (8.17) the SNR

$$\gamma_{n_{\mathrm{F}}}^{(k)} = \frac{\frac{1}{2}|\tilde{\underline{d}}_{n_{\mathrm{F}}}^{(k)}|^2}{\frac{1}{2}|\hat{\tilde{\underline{d}}}_{n_{\mathrm{F}}}^{(k)} - \tilde{\underline{d}}_{n_{\mathrm{F}}}^{(k)}|^2} = \frac{E_{\mathrm{d}}}{\sigma^2 \left[\underline{\tilde{\mathbf{D}}}_{n_{\mathrm{F}}} \underline{\tilde{\mathbf{D}}}_{n_{\mathrm{F}}}^{*\mathrm{T}} \right]_{k,k}} \tag{8.18}$$

of the data symbol $\tilde{\underline{d}}_{n_{\mathrm{F}}}^{(k)}$ of (8.1) can be obtained.

8.2.2 Bit error probability

In the UL of JOINT, since it is assumed that MTs and APs are equipped with single antennas,

$$K_{\mathrm{I}} = K \tag{8.19}$$

and

$$K_{\mathrm{O}} = K_{\mathrm{B}} \tag{8.20}$$

hold. From the viewpoint of the receiver side, i.e., at the CU, the modulator matrix $\underline{\tilde{\mathbf{M}}}_{n_{\mathrm{F}}}$ of (8.3) and the CTF matrix $\underline{\tilde{\mathbf{H}}}_{n_{\mathrm{F}}}$ of (8.6) are a priori known. To keep the MT structure as simple as possible is one target of the system design. Therefore, simple OFDM transmitters are assumed to be used at the MTs, i.e., the modulator matrix

$$\underline{\tilde{\mathbf{M}}}_{\mathrm{u},n_{\mathrm{F}}} = \mathbf{I}^K \tag{8.21}$$

holds for the UL. For the UL CTF matrix, refer to the CTF matrix $\underline{\tilde{\mathbf{H}}}_{\mathrm{u},n_{\mathrm{F}}}$ of (3.20) with dimensions $K_{\mathrm{B}} \times K$.

For the unbiased data estimation fulfilling (8.14), the linear RxZF JD [Kle96, Skl04] algorithm is applied at the CU in the UL of JOINT. The linear RxZF JD [Kle96, Skl04]

minimizes the square error $\|\tilde{\underline{\mathbf{e}}}_{\mathrm{u},n_{\mathrm{F}}} - \tilde{\underline{\mathbf{H}}}_{\mathrm{u},n_{\mathrm{F}}} \hat{\tilde{\underline{\mathbf{d}}}}_{\mathrm{u},n_{\mathrm{F}}}\|^2$ of the reconstructed receive signal $\tilde{\underline{\mathbf{H}}}_{\mathrm{u},n_{\mathrm{F}}} \hat{\tilde{\underline{\mathbf{d}}}}_{\mathrm{u},n_{\mathrm{F}}}$. Therefore, with (8.14) and (8.21) the UL detector matrix

$$
\begin{aligned}
\tilde{\underline{\mathbf{D}}}_{\mathrm{u},n_{\mathrm{F}}} &= \left(\left(\tilde{\underline{\mathbf{H}}}_{\mathrm{u},n_{\mathrm{F}}} \tilde{\underline{\mathbf{M}}}_{\mathrm{u},n_{\mathrm{F}}} \right)^{*\mathrm{T}} \left(\tilde{\underline{\mathbf{H}}}_{\mathrm{u},n_{\mathrm{F}}} \tilde{\underline{\mathbf{M}}}_{\mathrm{u},n_{\mathrm{F}}} \right) \right)^{-1} \left(\tilde{\underline{\mathbf{H}}}_{\mathrm{u},n_{\mathrm{F}}} \tilde{\underline{\mathbf{M}}}_{\mathrm{u},n_{\mathrm{F}}} \right)^{*\mathrm{T}} \\
&= \left(\tilde{\underline{\mathbf{M}}}_{\mathrm{u},n_{\mathrm{F}}}^{*\mathrm{T}} \tilde{\underline{\mathbf{H}}}_{\mathrm{u},n_{\mathrm{F}}}^{*\mathrm{T}} \tilde{\underline{\mathbf{H}}}_{\mathrm{u},n_{\mathrm{F}}} \tilde{\underline{\mathbf{M}}}_{\mathrm{u},n_{\mathrm{F}}} \right)^{-1} \tilde{\underline{\mathbf{M}}}_{\mathrm{u},n_{\mathrm{F}}}^{*\mathrm{T}} \tilde{\underline{\mathbf{H}}}_{\mathrm{u},n_{\mathrm{F}}}^{*\mathrm{T}} \\
&= \left(\tilde{\underline{\mathbf{H}}}_{\mathrm{u},n_{\mathrm{F}}}^{*\mathrm{T}} \tilde{\underline{\mathbf{H}}}_{\mathrm{u},n_{\mathrm{F}}} \right)^{-1} \tilde{\underline{\mathbf{H}}}_{\mathrm{u},n_{\mathrm{F}}}^{*\mathrm{T}}
\end{aligned}
\tag{8.22}
$$

can be derived. According to (8.12) and (8.21) the transmit energies

$$
T_{\mathrm{u},n_{\mathrm{F}}}^{(k)} = E_{\mathrm{d}}
\tag{8.23}
$$

invested for the data symbols $\tilde{\underline{d}}_{\mathrm{u},n_{\mathrm{F}}}^{(k)}$ of (8.1) in the UL are equal. With (8.18), (8.22) and (8.23) the SNR

$$
\begin{aligned}
\gamma_{\mathrm{u},n_{\mathrm{F}}}^{(k)} &= \frac{E_{\mathrm{d}}}{\sigma^2 \left[\tilde{\underline{\mathbf{D}}}_{\mathrm{u},n_{\mathrm{F}}} \tilde{\underline{\mathbf{D}}}_{\mathrm{u},n_{\mathrm{F}}}^{*\mathrm{T}} \right]_{k,k}} \\
&= \frac{T_{\mathrm{u},n_{\mathrm{F}}}^{(k)}}{\sigma^2 \left[\left(\tilde{\underline{\mathbf{H}}}_{\mathrm{u},n_{\mathrm{F}}}^{*\mathrm{T}} \tilde{\underline{\mathbf{H}}}_{\mathrm{u},n_{\mathrm{F}}} \right)^{-1} \right]_{k,k}}
\end{aligned}
\tag{8.24}
$$

of the data symbol $\tilde{\underline{d}}_{\mathrm{u},n_{\mathrm{F}}}^{(k)}$ of (8.1) in the UL is obtained. For the QPSK modulation, if the noise elements $\tilde{\underline{n}}_{\mathrm{u},n_{\mathrm{F}}}^{(k)}$ of (8.4) are complex Gaussian variables, the bit error probability

$$
P_{\mathrm{b},\mathrm{u},n_{\mathrm{F}}}^{(k)} = \frac{1}{2} \mathrm{erfc} \sqrt{\frac{\gamma_{\mathrm{u},n_{\mathrm{F}}}^{(k)}}{2}} = \frac{1}{2} \mathrm{erfc} \left(\sqrt{ \frac{\frac{T_{\mathrm{u},n_{\mathrm{F}}}^{(k)}}{\sigma^2}}{\left[\left(\tilde{\underline{\mathbf{H}}}_{\mathrm{u},n_{\mathrm{F}}}^{*\mathrm{T}} \tilde{\underline{\mathbf{H}}}_{\mathrm{u},n_{\mathrm{F}}} \right)^{-1} \right]_{k,k}} } \right)
\tag{8.25}
$$

of the data symbol $\tilde{\underline{d}}_{\mathrm{u},n_{\mathrm{F}}}^{(k)}$ of (8.1) in the UL is derived as a function of the pseudo SNR, i.e., the transmit–energy–to–noise–power ratio $T_{\mathrm{u},n_{\mathrm{F}}}^{(k)}/\sigma^2$ in the UL and the UL CTF matrix $\tilde{\underline{\mathbf{H}}}_{\mathrm{u},n_{\mathrm{F}}}$ of (3.20).

In the DL of JOINT, due to the application of single antennas on MTs and APs,

$$
K_{\mathrm{I}} = K_{\mathrm{B}}
\tag{8.26}
$$

and

$$
K_{\mathrm{O}} = K
\tag{8.27}
$$

hold. From the viewpoint of the transmitter side, i.e., at the CU, the detector matrix $\tilde{\underline{\mathbf{D}}}_{n_{\mathrm{F}}}$ of (8.7) and the CTF matrix $\tilde{\underline{\mathbf{H}}}_{n_{\mathrm{F}}}$ of (8.6) are a priori known. As in the UL, also

in the DL, the MT structure has to be kept as simple as possible. Therefore, simple OFDM receivers are assumed to be used at the MTs, i.e., for the DL detector matrix follows

$$\underline{\tilde{\mathbf{D}}}_{\mathrm{d},n_{\mathrm{F}}} = \mathbf{I}^K. \tag{8.28}$$

For the DL CTF matrix, refer to the CTF matrix $\underline{\tilde{\mathbf{H}}}_{\mathrm{d},n_{\mathrm{F}}}$ of (3.28) with dimensions $K \times K_{\mathrm{B}}$, which is the transpose of the UL CTF matrix $\underline{\tilde{\mathbf{H}}}_{\mathrm{u},n_{\mathrm{F}}}$ of (3.20).

For the unbiased data transmission fulfilling (8.14), the linear TxZF JT [MBW$^+$00, TWMB01, Skl04] algorithm is applied at the CU in the DL of JOINT. With (8.14) and (8.28) the DL modulator matrix

$$\begin{aligned}
\underline{\tilde{\mathbf{M}}}_{\mathrm{d},n_{\mathrm{F}}} &= \left(\underline{\tilde{\mathbf{D}}}_{\mathrm{d},n_{\mathrm{F}}}\underline{\tilde{\mathbf{H}}}_{\mathrm{d},n_{\mathrm{F}}}\right)^{*\mathrm{T}}\left(\left(\underline{\tilde{\mathbf{D}}}_{\mathrm{d},n_{\mathrm{F}}}\underline{\tilde{\mathbf{H}}}_{\mathrm{d},n_{\mathrm{F}}}\right)\left(\underline{\tilde{\mathbf{D}}}_{\mathrm{d},n_{\mathrm{F}}}\underline{\tilde{\mathbf{H}}}_{\mathrm{d},n_{\mathrm{F}}}\right)^{*\mathrm{T}}\right)^{-1} \\
&= \left(\underline{\tilde{\mathbf{H}}}_{\mathrm{d},n_{\mathrm{F}}}^{*\mathrm{T}}\underline{\tilde{\mathbf{D}}}_{\mathrm{d},n_{\mathrm{F}}}^{*\mathrm{T}}\right)\left(\underline{\tilde{\mathbf{D}}}_{\mathrm{d},n_{\mathrm{F}}}\underline{\tilde{\mathbf{H}}}_{\mathrm{d},n_{\mathrm{F}}}\underline{\tilde{\mathbf{H}}}_{\mathrm{d},n_{\mathrm{F}}}^{*\mathrm{T}}\underline{\tilde{\mathbf{D}}}_{\mathrm{d},n_{\mathrm{F}}}^{*\mathrm{T}}\right)^{-1} \\
&= \underline{\tilde{\mathbf{H}}}_{\mathrm{d},n_{\mathrm{F}}}^{*\mathrm{T}}\left(\underline{\tilde{\mathbf{H}}}_{\mathrm{d},n_{\mathrm{F}}}\underline{\tilde{\mathbf{H}}}_{\mathrm{d},n_{\mathrm{F}}}^{*\mathrm{T}}\right)^{-1}
\end{aligned} \tag{8.29}$$

is derived. According to (8.12) and (8.29) the transmit energy

$$\begin{aligned}
T_{\mathrm{d},n_{\mathrm{F}}}^{(k)} &= E_{\mathrm{d}}\left[\underline{\tilde{\mathbf{M}}}_{\mathrm{d},n_{\mathrm{F}}}^{*\mathrm{T}}\underline{\tilde{\mathbf{M}}}_{\mathrm{d},n_{\mathrm{F}}}\right]_{k,k} \\
&= E_{\mathrm{d}}\left[\left(\underline{\tilde{\mathbf{H}}}_{\mathrm{d},n_{\mathrm{F}}}\underline{\tilde{\mathbf{H}}}_{\mathrm{d},n_{\mathrm{F}}}^{*\mathrm{T}}\right)^{-1}\right]_{k,k}
\end{aligned} \tag{8.30}$$

invested for the data symbol $\underline{\tilde{d}}_{\mathrm{d},n_{\mathrm{F}}}^{(k)}$ of (8.1) in the DL can be obtained. With (8.18), (8.29) and (8.30) the SNR

$$\begin{aligned}
\gamma_{\mathrm{d},n_{\mathrm{F}}}^{(k)} &= \frac{E_{\mathrm{d}}}{\sigma^2\left[\underline{\tilde{\mathbf{M}}}_{\mathrm{d},n_{\mathrm{F}}}\underline{\tilde{\mathbf{M}}}_{\mathrm{d},n_{\mathrm{F}}}^{*\mathrm{T}}\right]_{k,k}} \\
&= \frac{T_{\mathrm{d},n_{\mathrm{F}}}^{(k)}}{\sigma^2\left[\left(\underline{\tilde{\mathbf{H}}}_{\mathrm{d},n_{\mathrm{F}}}\underline{\tilde{\mathbf{H}}}_{\mathrm{d},n_{\mathrm{F}}}^{*\mathrm{T}}\right)^{-1}\right]_{k,k}}
\end{aligned} \tag{8.31}$$

of the data symbol $\underline{\tilde{d}}_{\mathrm{d},n_{\mathrm{F}}}^{(k)}$ of (8.1) in the DL is obtained. For the QPSK modulation, if the noise elements $\tilde{\underline{n}}_{\mathrm{d},n_{\mathrm{F}}}^{(k)}$ of (8.4) are complex Gaussian variables, the bit error probability

$$P_{\mathrm{b},\mathrm{d},n_{\mathrm{F}}}^{(k)} = \frac{1}{2}\mathrm{erfc}\sqrt{\frac{\gamma_{\mathrm{d},n_{\mathrm{F}}}^{(k)}}{2}} = \frac{1}{2}\mathrm{erfc}\left(\sqrt{\frac{\frac{T_{\mathrm{d},n_{\mathrm{F}}}^{(k)}}{\sigma^2}}{\left[\left(\underline{\tilde{\mathbf{H}}}_{\mathrm{d},n_{\mathrm{F}}}\underline{\tilde{\mathbf{H}}}_{\mathrm{d},n_{\mathrm{F}}}^{*\mathrm{T}}\right)^{-1}\right]_{k,k}}}\right) \tag{8.32}$$

of the data symbol $\underline{\tilde{d}}_{\mathrm{d},n_{\mathrm{F}}}^{(k)}$ of (8.1) in the DL is derived as a function of the pseudo SNR $T_{\mathrm{d},n_{\mathrm{F}}}^{(k)}/\sigma^2$ in the DL and the DL CTF matrix $\underline{\tilde{\mathbf{H}}}_{\mathrm{d},n_{\mathrm{F}}}$ of (3.28).

If we carefully compare the bit error probabilities $P_{\mathrm{b,u},n_{\mathrm{F}}}^{(k)}$ of (8.25) in the UL and $P_{\mathrm{b,d},n_{\mathrm{F}}}^{(k)}$ of (8.32) in the DL, we can see that for equal pseudo SNRs

$$\frac{T_{\mathrm{u},n_{\mathrm{F}}}^{(k)}}{\sigma^2} = \frac{T_{\mathrm{d},n_{\mathrm{F}}}^{(k)}}{\sigma^2} \tag{8.33}$$

the relation

$$P_{\mathrm{b,u},n_{\mathrm{F}}}^{(k)} = P_{\mathrm{b,d},n_{\mathrm{F}}}^{(k)} \tag{8.34}$$

holds due to the reciprocity of the the UL and the DL channels. It can be seen that in order to combat the intra–SA MAI, the enhanced noise $\underline{\tilde{\mathbf{D}}}_{\mathrm{u},n_{\mathrm{F}}}\,\underline{\tilde{\mathbf{n}}}_{\mathrm{u},n_{\mathrm{F}}}$ of (8.16) caused by the application of the linear RxZF JD [Kle96, Skl04] in the UL degrades the system performance. On the other way, the enhanced transmit energy $T_{\mathrm{d},n_{\mathrm{F}}}^{(k)}$ of (8.30) is the price paid for the interference elimination with the application of the linear TxZF JT [MBW$^+$00, TWMB01, Skl04]. According to (8.34), for the same variance σ^2 of the noise the same energies have to be invested for the data symbols $\underline{\tilde{d}}_{\mathrm{u},n_{\mathrm{F}}}^{(k)}$ of (8.1) in the UL and $\underline{\tilde{d}}_{\mathrm{d},n_{\mathrm{F}}}^{(k)}$ of (8.1) in the DL, respectively, to obtain the same quality of performances. This is the duality of the UL and the DL with the application of the linear ZF [Kle96, Skl04].

8.2.3 Energy efficiency

As stated in Subsection 8.2.2, (8.34) shows the inherent consistency of the linear RxZF JD [Kle96, Skl04] and the linear TxZF JT [MBW$^+$00, TWMB01, Skl04] with respect to the interference elimination. In order to comprehensively evaluate the system performance of JOINT, it is necessary to look deeply inside the duality of the UL and the DL with the viewpoint of energy transmission.

To transmit energies efficiently at the given QoS is one target of future mobile radio systems. As already mentioned in Chapters 5 and 6, the MF realizes the optimum MT–specific energy transmission and the optimum MT–specific energy reception, respectively. Therefore, the MF system is chosen as the reference system.

The efficiency

$$\eta_{\mathrm{Tx},n_{\mathrm{F}}}^{(k)} = \frac{E_{\mathrm{d}}/T_{n_{\mathrm{F}}}^{(k)}}{\left(E_{\mathrm{d}}/T_{n_{\mathrm{F}}}^{(k)}\right)_{\mathrm{ref}}} \tag{8.35}$$

at the transmitter side is defined as the ratio of $E_{\mathrm{d}}/T_{n_{\mathrm{F}}}^{(k)}$ of (8.13) in the considered system to $\left(E_{\mathrm{d}}/T_{n_{\mathrm{F}}}^{(k)}\right)_{\mathrm{ref}}$ of (8.13) in the reference system. The efficiency [Ver98, WSLW03, Skl04]

$$\eta_{\mathrm{Rx},n_{\mathrm{F}}}^{(k)} = \frac{\gamma_{n_{\mathrm{F}}}^{(k)}}{\gamma_{\mathrm{ref},n_{\mathrm{F}}}^{(k)}} \tag{8.36}$$

at the receiver side is defined as the ratio of the SNR $\gamma_{n_F}^{(k)}$ of (5.9) in the considered system to the SNR $\gamma_{\mathrm{ref},n_F}^{(k)}$ of (5.9) in the reference MF system. The efficiency $\eta_{\mathrm{Tx},n_F}^{(k)}$ of (8.35) and the efficiency $\eta_{\mathrm{Rx},n_F}^{(k)}$ of (8.36) are two separate efficiency assessments of the transmitter and of the receiver, respectively. For the evaluation of the total link an overall energy efficiency

$$\varepsilon_{n_F}^{(k)} = \eta_{\mathrm{Tx},n_F}^{(k)} \cdot \eta_{\mathrm{Rx},n_F}^{(k)} \tag{8.37}$$

is defined as the product of the efficiency $\eta_{\mathrm{Tx},n_F}^{(k)}$ of (8.35) of the transmitter side and the efficiency $\eta_{\mathrm{Rx},n_F}^{(k)}$ of (8.36) of the receiver side.

In the UL, no special scheme has to be applied to combat the intra-SA MAI at the MTs. With (6.14), (8.13) and (8.21) and the efficiency

$$\eta_{\mathrm{Tx,u},n_F}^{(k)} = 1 \tag{8.38}$$

of (8.35) in the UL is optimum. At the receiver side of the CU, the linear RxZF JD is applied. With (5.9), (5.13), (8.18) and (8.22) the efficiency [Ver98, WSLW03, Skl04]

$$
\begin{aligned}
\eta_{\mathrm{Rx,u},n_F}^{(k)} &= \frac{1}{\left[\left(\underline{\tilde{\mathbf{H}}}_{\mathrm{u},n_F}^{*T} \underline{\tilde{\mathbf{H}}}_{\mathrm{u},n_F}\right)^{-1}\right]_{k,k} \left[\underline{\tilde{\mathbf{H}}}_{\mathrm{u},n_F}^{*T} \underline{\tilde{\mathbf{H}}}_{\mathrm{u},n_F}\right]_{k,k}} \\
&= \frac{1}{\delta_{n_F}^{(k)}}
\end{aligned}
\tag{8.39}
$$

of (8.36) is obtained for the UL receiver. This means that there is no energy loss at the transmitter side in the UL. The energy loss is only caused by the linear RxZF JD [Kle96, Skl04] at the CU. With (8.38) and (8.39) the overall energy efficiency

$$
\begin{aligned}
\varepsilon_{\mathrm{u},n_F}^{(k)} &= \eta_{\mathrm{Tx,u},n_F}^{(k)} \cdot \eta_{\mathrm{Rx,u},n_F}^{(k)} \\
&= \frac{1}{\left[\left(\underline{\tilde{\mathbf{H}}}_{\mathrm{u},n_F}^{*T} \underline{\tilde{\mathbf{H}}}_{\mathrm{u},n_F}\right)^{-1}\right]_{k,k} \left[\underline{\tilde{\mathbf{H}}}_{\mathrm{u},n_F}^{*T} \underline{\tilde{\mathbf{H}}}_{\mathrm{u},n_F}\right]_{k,k}}
\end{aligned}
\tag{8.40}
$$

of (8.37) in the UL holds.

In the DL the linear TxZF JT [MBW$^+$00, TWMB01, Skl04] is applied at the transmitter side of the CU. With (6.14) and (8.30) the efficiency

$$\eta_{\mathrm{Tx,d},n_F}^{(k)} = \frac{1}{\left[\left(\underline{\tilde{\mathbf{H}}}_{\mathrm{d},n_F} \underline{\tilde{\mathbf{H}}}_{\mathrm{d},n_F}^{*T}\right)^{-1}\right]_{k,k} \left[\underline{\tilde{\mathbf{H}}}_{\mathrm{d},n_F} \underline{\tilde{\mathbf{H}}}_{\mathrm{d},n_F}^{*T}\right]_{k,k}} \tag{8.41}$$

of (8.35) is obtained for the DL transmitter. At the receiver side of the DL, no special receiver scheme has to be applied to combat the MAI, see (8.28). Therefore, with (5.9), (8.31) and (8.28) the efficiency [Ver98, WSLW03, Skl04]

$$\eta_{\mathrm{Rx,d},n_F}^{(k)} = 1 \tag{8.42}$$

of (8.36) is obtained for the DL receiver. This means that there is no energy loss at the receiver side in the DL. The energy loss is only caused by the linear TxZF JT at the CU. With (8.41) and (8.42) the overall energy efficiency

$$
\begin{aligned}
\varepsilon_{\mathrm{d},n_{\mathrm{F}}}^{(k)} &= \eta_{\mathrm{Tx,d},n_{\mathrm{F}}}^{(k)} \cdot \eta_{\mathrm{Rx,d},n_{\mathrm{F}}}^{(k)} \\
&= \frac{1}{\left[\left(\tilde{\underline{\mathbf{H}}}_{\mathrm{d},n_{\mathrm{F}}} \tilde{\underline{\mathbf{H}}}_{\mathrm{d},n_{\mathrm{F}}}^{*\mathrm{T}}\right)^{-1}\right]_{k,k} \left[\tilde{\underline{\mathbf{H}}}_{\mathrm{d},n_{\mathrm{F}}} \tilde{\underline{\mathbf{H}}}_{\mathrm{ud},n_{\mathrm{F}}}^{*\mathrm{T}}\right]_{k,k}}
\end{aligned}
\tag{8.43}
$$

of (8.37) in the DL holds.

With (8.38) and (8.42) the equality of the efficiencies

$$
\eta_{\mathrm{Tx,u},n_{\mathrm{F}}}^{(k)} = \eta_{\mathrm{Rx,d},n_{\mathrm{F}}}^{(k)} = 1
\tag{8.44}
$$

holds. Similarly, with (8.39) and (8.41) the equality of the efficiencies

$$
\begin{aligned}
\eta_{\mathrm{Tx,d},n_{\mathrm{F}}}^{(k)} &= \eta_{\mathrm{Rx,u},n_{\mathrm{F}}}^{(k)} \\
&= \frac{1}{\left[\left(\tilde{\underline{\mathbf{H}}}_{\mathrm{u},n_{\mathrm{F}}}^{*\mathrm{T}} \tilde{\underline{\mathbf{H}}}_{\mathrm{u},n_{\mathrm{F}}}\right)^{-1}\right]_{k,k} \left[\tilde{\underline{\mathbf{H}}}_{\mathrm{u},n_{\mathrm{F}}}^{*\mathrm{T}} \tilde{\underline{\mathbf{H}}}_{\mathrm{u},n_{\mathrm{F}}}\right]_{k,k}}
\end{aligned}
\tag{8.45}
$$

is obtained due to the reciprocity of the UL and the DL channel described in (3.28). Consequently, the equality of the overall energy efficiencies

$$
\varepsilon_{\mathrm{u},n_{\mathrm{F}}}^{(k)} = \varepsilon_{\mathrm{d},n_{\mathrm{F}}}^{(k)} = \varepsilon_{n_{\mathrm{F}}}^{(k)}.
\tag{8.46}
$$

is obtained. (8.44), (8.45) and (8.46) show that the price paid for the interference elimination by the linear ZF [Kle96, Ver98, Bla98] is the same for either the UL or the DL [Skl04], and can well explain Equation (8.34).

8.3 Impact of imperfect channel state information

8.3.1 Sources of imperfect channel state information

8.3.1.1 Introduction

It is known that CSI is the prerequisite for JD and JT at the CU [Man04]. Therefore, the accuracy of the CSI estimation is a guarantee of the good performance of JOINT. CSI is estimated by JCE, see Chapter 4. However, it is inevitable that the channel estimation errors occur, i.e., only imperfect CSI is available for JD and JT. In the present subsection, we will trace to the two sources, the noise and the time variance of channels, which lead to the channel estimation errors, and investigate their impacts on JCE. Moreover, the impacts of the channel estimation errors on the UL and DL performances are to be discussed.

8.3.1.2   Channel estimation error due to noise

As already stated in Section 4.3, JCE is an ML estimation algorithm [Man04], i.e., for the noise–free case the perfect CSI can be obtained. In the case that the noise exists, the CTF estimation errors $\hat{\underline{\tilde{h}}}_{n_\mathrm{F}}^{(k,k_\mathrm{B})} - \underline{\tilde{h}}_{n_\mathrm{F}}^{(k,k_\mathrm{B})}$ of (4.21) occur. Therefore, the noise, which is an important factor influencing the JCE performance, is first considered. For the sake of simplicity the channel is assumed to be time–invariant temporarily.

With (4.15) to (4.18) the ML estimation of the AP–specific CTF vector $\underline{\tilde{\mathbf{h}}}^{(k_\mathrm{B})}$ of (4.18) reads

$$\hat{\underline{\tilde{\mathbf{h}}}}^{(k_\mathrm{B})} = \underline{\tilde{\mathbf{h}}}^{(k_\mathrm{B})} + \underline{\tilde{\mathbf{Z}}}\ \tilde{\mathbf{n}}_\mathrm{h}^{(k_\mathrm{B})}, \tag{8.47}$$

where the estimation matrix

$$\underline{\tilde{\mathbf{Z}}} = \tilde{\boldsymbol{\mathcal{F}}}_{W,\mathrm{tot}} \left(\left(\underline{\tilde{\mathbf{P}}}\,\tilde{\boldsymbol{\mathcal{F}}}_{W,\mathrm{tot}} \right)^{*\mathrm{T}} \left(\underline{\tilde{\mathbf{P}}}\,\tilde{\boldsymbol{\mathcal{F}}}_{W,\mathrm{tot}} \right) \right)^{-1} \left(\underline{\tilde{\mathbf{P}}}\,\tilde{\boldsymbol{\mathcal{F}}}_{W,\mathrm{tot}} \right)^{*\mathrm{T}} \tag{8.48}$$

holds with the total pilot matrix $\underline{\tilde{\mathbf{P}}}$ of (4.3) and the block–diagonal matrix $\tilde{\boldsymbol{\mathcal{F}}}_{W,\mathrm{tot}}$ of (4.14) [SMWB01, MWSL02]. In the case that the pilot vector $\underline{\tilde{\mathbf{p}}}^{(k)}$ of (4.1) is designed on the basis of Walsh codes, and the pilot energy E_p of (4.11) is equal to the data energy E_d of (8.9), the diagonal elements

$$\left[\underline{\tilde{\mathbf{Z}}}\ \underline{\tilde{\mathbf{Z}}}^{*\mathrm{T}} \right]_{i,i} = \frac{W}{E_\mathrm{p} N_\mathrm{F}}, i = 1 \ldots K N_\mathrm{F}, \tag{8.49}$$

of the matrix $\underline{\tilde{\mathbf{Z}}}\ \underline{\tilde{\mathbf{Z}}}^{*\mathrm{T}}$ are equal.

With (8.47) the CTF estimation error vector

$$\underline{\boldsymbol{\Delta}}_{\mathrm{h,n}}^{(k_\mathrm{B})} = \hat{\underline{\tilde{\mathbf{h}}}}^{(k_\mathrm{B})} - \underline{\tilde{\mathbf{h}}}^{(k_\mathrm{B})} = \underline{\tilde{\mathbf{Z}}}\ \tilde{\mathbf{n}}_\mathrm{h}^{(k_\mathrm{B})} \tag{8.50}$$

depends on the noise vector $\underline{\tilde{\mathbf{n}}}_\mathrm{h}^{(k_\mathrm{B})}$ of (4.9), the uncorrelated elements of which have the variance σ^2 of real and imaginary parts, and on the estimation matrix $\underline{\tilde{\mathbf{Z}}}$ of (8.48). For the covariance matrix of the CTF estimation error vector $\underline{\boldsymbol{\Delta}}_{\mathrm{h,n}}^{(k_\mathrm{B})}$ of (8.50) follows

$$\begin{aligned}
\underline{\mathbf{R}}_{\boldsymbol{\Delta}_{\mathrm{h,n}}} &= \mathrm{E}\left\{ \underline{\boldsymbol{\Delta}}_{\mathrm{h,n}}^{(k_\mathrm{B})} \underline{\boldsymbol{\Delta}}_{\mathrm{h,n}}^{(k_\mathrm{B})*\mathrm{T}} \right\} = \mathrm{E}\left\{ \underline{\tilde{\mathbf{Z}}}\ \tilde{\mathbf{n}}_\mathrm{h}^{(k_\mathrm{B})}\ \tilde{\mathbf{n}}_\mathrm{h}^{(k_\mathrm{B})*\mathrm{T}}\ \underline{\tilde{\mathbf{Z}}}^{*\mathrm{T}} \right\} \\
&= 2\sigma^2 \cdot \mathrm{diag}\left(\underline{\tilde{\mathbf{Z}}}\ \underline{\tilde{\mathbf{Z}}}^{*\mathrm{T}} \right) = \frac{2\sigma^2 W}{E_\mathrm{p} N_\mathrm{F}} \mathbf{I}^{K N_\mathrm{F}} = 2\sigma_{\mathrm{h,n}}^2\ \mathbf{I}^{K N_\mathrm{F}}. \tag{8.51}
\end{aligned}$$

It can be seen from (8.51) that the elements of $\underline{\boldsymbol{\Delta}}_{\mathrm{h,n}}^{(k_\mathrm{B})}$ of (8.50) are also uncorrelated and have the variance $\sigma_{\mathrm{h,n}}^2$ of real and imaginary parts. Regardless of the time variance of the channels, the CTF estimation error vector $\underline{\boldsymbol{\Delta}}_{\mathrm{h,n}}^{(k_\mathrm{B})}$ of (8.50) results only from the noise vector $\underline{\tilde{\mathbf{n}}}_\mathrm{h}^{(k_\mathrm{B})}$. Moreover, the variance $\sigma_{\mathrm{h,n}}^2$ of the CTF estimation error vector $\underline{\boldsymbol{\Delta}}_{\mathrm{h,n}}^{(k_\mathrm{B})}$ of (8.50) is proportional to the variance σ^2 of the noise.

8.3.1.3 Channel estimation error due to time variant channels

In reality the channels are time-variant due to the motions of the MTs. For the sake of clarity the subscript n_B denoting the index of the time slot is added to all the notations in the rest of the chapter. JCE is only performed once during the frame, and the estimated CSI will be used by JD and JT. The time–variant channels lead to the errors between the realtime CTFs $\tilde{\underline{h}}_{n_\mathrm{B},n_\mathrm{F}}^{(k,k_\mathrm{B})}$ in the time slots n_B of the data transmission and estimation, and the CTF estimates $\hat{\tilde{\underline{h}}}_{n_\mathrm{B},n_\mathrm{F}}^{(k,k_\mathrm{B})}$, which are all equal to the CTF estimate $\hat{\tilde{\underline{h}}}_{n'_\mathrm{B},n_\mathrm{F}}^{(k,k_\mathrm{B})}$ obtained at the time slot n'_B by JCE, even if the CTF estimate $\hat{\tilde{\underline{h}}}_{n'_\mathrm{B},n_\mathrm{F}}^{(k,k_\mathrm{B})}$ is perfectly estimated by JCE in the noise–free case.

When the time–variant channels are considered, and the noise–free case is assumed when performing JCE, i.e., at the time slot n'_B when JCE is performed, with the slot–AP–specific CTF vector

$$\tilde{\underline{\mathbf{h}}}_{n'_\mathrm{B}}^{(k_\mathrm{B})} = \left(\tilde{\underline{h}}_{n'_\mathrm{B},1}^{(1,k_\mathrm{B})}, \ldots \tilde{\underline{h}}_{n'_\mathrm{B},N_\mathrm{F}}^{(K,k_\mathrm{B})} \right)^\mathrm{T} \tag{8.52}$$

of dimension KN_F, the equal slot–AP–specific CTF estimate vectors

$$\hat{\tilde{\underline{\mathbf{h}}}}_{n_\mathrm{B}}^{(k_\mathrm{B})} = \tilde{\underline{\mathbf{h}}}_{n'_\mathrm{B}}^{(k_\mathrm{B})}, n_\mathrm{B} = 1 \ldots N_\mathrm{B}, \tag{8.53}$$

are obtained. With (8.53) the CTF estimation error vector

$$\underline{\boldsymbol{\Delta}}_{\mathrm{h},n_\mathrm{B}}^{(k_\mathrm{B})} = \hat{\tilde{\underline{\mathbf{h}}}}_{n_\mathrm{B}}^{(k_\mathrm{B})} - \tilde{\underline{\mathbf{h}}}_{n_\mathrm{B}}^{(k_\mathrm{B})} = \tilde{\underline{\mathbf{h}}}_{n'_\mathrm{B}}^{(k_\mathrm{B})} - \tilde{\underline{\mathbf{h}}}_{n_\mathrm{B}}^{(k_\mathrm{B})} \tag{8.54}$$

corresponding to the time slot n_B is obtained. For the covariance matrix of the CTF estimation error vector $\underline{\boldsymbol{\Delta}}_{\mathrm{h},n_\mathrm{B}}^{(k_\mathrm{B})}$ of (8.54) follows

$$\begin{aligned} \underline{\mathbf{R}}_{\boldsymbol{\Delta}_{\mathrm{h,tv}}} &= \mathrm{E}\left\{ \underline{\boldsymbol{\Delta}}_{\mathrm{h},n_\mathrm{B}}^{(k_\mathrm{B})} \underline{\boldsymbol{\Delta}}_{\mathrm{h},n_\mathrm{B}}^{(k_\mathrm{B})\,*\mathrm{T}} \right\} = \mathrm{E}\left\{ \left(\tilde{\underline{\mathbf{h}}}_{n'_\mathrm{B}}^{(k_\mathrm{B})} - \tilde{\underline{\mathbf{h}}}_{n_\mathrm{B}}^{(k_\mathrm{B})} \right) \left(\tilde{\underline{\mathbf{h}}}_{n'_\mathrm{B}}^{(k_\mathrm{B})} - \tilde{\underline{\mathbf{h}}}_{n_\mathrm{B}}^{(k_\mathrm{B})} \right)^{*\mathrm{T}} \right\} \\ &= \mathrm{E}\left\{ \|\tilde{\underline{\mathbf{h}}}_{n'_\mathrm{B}}^{(k_\mathrm{B})}\|^2 \right\} + \mathrm{E}\left\{ \|\tilde{\underline{\mathbf{h}}}_{n_\mathrm{B}}^{(k_\mathrm{B})}\|^2 \right\} - \mathrm{E}\left\{ \tilde{\underline{\mathbf{h}}}_{n'_\mathrm{B}}^{(k_\mathrm{B})} \tilde{\underline{\mathbf{h}}}_{n_\mathrm{B}}^{(k_\mathrm{B})\,*\mathrm{T}} \right\} - \mathrm{E}\left\{ \tilde{\underline{\mathbf{h}}}_{n_\mathrm{B}}^{(k_\mathrm{B})} \tilde{\underline{\mathbf{h}}}_{n'_\mathrm{B}}^{(k_\mathrm{B})\,*\mathrm{T}} \right\}. \end{aligned} \tag{8.55}$$

According to [Pro95], with the time difference

$$\Delta t = (n'_\mathrm{B} - n_\mathrm{B}) \cdot T_\mathrm{oss} \tag{8.56}$$

between the time slots n_B and n'_B the space–time correlation function

$$\underline{\rho}_\mathrm{F}(0, \Delta t) = \frac{1}{2}\mathrm{E}\left\{ \tilde{\underline{h}}_{n_\mathrm{B},n_\mathrm{F}}^{(k,k_\mathrm{B})} \cdot \tilde{\underline{h}}_{n'_\mathrm{B},n_\mathrm{F}}^{(k,k_\mathrm{B})*} \right\} \tag{8.57}$$

holds. With (8.57) and the assumption that the CTFs $\tilde{\underline{h}}_{n_\mathrm{B},n_\mathrm{F}}^{(k,k_\mathrm{B})}$ are uncorrelated to each other, (8.55) can be rewritten as

$$
\begin{aligned}
\underline{\mathbf{R}}_{\mathbf{\Delta}_\mathrm{h,tv}} &= \left(4\underline{\rho}_\mathrm{F}\left(0,0\right) - 2\underline{\rho}_\mathrm{F}\left(0,-\Delta t\right) - 2\underline{\rho}_\mathrm{F}\left(0,\Delta t\right) \right) \cdot \mathbf{I}^{KN_\mathrm{F}} \\
&= \left(4\underline{\rho}_\mathrm{F}\left(0,0\right) - 2\underline{\rho}_\mathrm{F}^{*}\left(0,\Delta t\right) - 2\underline{\rho}_\mathrm{F}\left(0,\Delta t\right) \right) \cdot \mathbf{I}^{KN_\mathrm{F}} \\
&= \left(4\underline{\rho}_\mathrm{F}\left(0,0\right) - 4\mathrm{Re}\left\{ \underline{\rho}_\mathrm{F}^{*}\left(0,\Delta t\right) \right\} \right) \cdot \mathbf{I}^{KN_\mathrm{F}}.
\end{aligned}
\tag{8.58}
$$

As introduced in Section 2.3, a Jakes Doppler spectrum [Ste92, Pro95, LR99] is assumed to describe the stochastic channel. It is known that the Jakes Doppler power spectrum [Ste92, Pro95, LR99]

$$
S_\mathrm{c}(0,f_\mathrm{d}) = \begin{cases} \dfrac{\frac{1}{\pi f_\mathrm{d,max}}}{\sqrt{1 - \left(\frac{f_\mathrm{d}}{f_\mathrm{d,max}}\right)^2}}, & \text{for } |f_\mathrm{d}| \leq f_\mathrm{d,max}, \\[2ex] 0, & \text{else,} \end{cases}
\tag{8.59}
$$

is the Fourier transform of the space–time correlation function $\underline{\rho}_\mathrm{F}\left(0,\Delta t\right)$ of (8.57) [Pro95]. In other words, the space–time correlation function $\underline{\rho}_\mathrm{F}\left(0,\Delta t\right)$ of (8.57) can be obtained by the inverse Fourier transform of the Doppler power spectrum $S_\mathrm{c}(0,f_\mathrm{d})$ of (8.59). With (8.59) the space–time correlation function $\underline{\rho}_\mathrm{F}\left(0,\Delta t\right)$ of (8.57) can be derived as

$$
\begin{aligned}
\underline{\rho}_\mathrm{F}\left(0,\Delta t\right) &= \int_{-\infty}^{+\infty} S_\mathrm{c}(0,f_\mathrm{d}) \cdot e^{j\,2\pi\,f_\mathrm{d}\Delta t}\,\mathrm{d}f_\mathrm{d} \\
&= \int_{-f_\mathrm{d,max}}^{+f_\mathrm{d,max}} \frac{\frac{1}{\pi f_\mathrm{d,max}}}{\sqrt{1 - \left(\frac{f_\mathrm{d}}{f_\mathrm{d,max}}\right)^2}} \cdot e^{j\,2\pi\,f_\mathrm{d}\Delta t}\,\mathrm{d}f_\mathrm{d} \\
&= \frac{1}{\pi f_\mathrm{d,max}} \cdot f_\mathrm{d,max} \cdot \int_{-f_\mathrm{d,max}}^{+f_\mathrm{d,max}} \frac{1}{\sqrt{f_\mathrm{d,max}^2 - f_\mathrm{d}^2}} \cdot e^{j2\pi f_\mathrm{d}\Delta t}\,\mathrm{d}f_\mathrm{d} \\
&= \frac{1}{\pi} \cdot \int_{+f_\mathrm{d,max}}^{-f_\mathrm{d,max}} \frac{1}{\sqrt{f_\mathrm{d,max}^2 - f_\mathrm{d}^2}} \cdot e^{-j2\pi f_\mathrm{d}\Delta t}\,\mathrm{d}(-f_\mathrm{d}) \\
&= \frac{1}{\pi} \cdot \int_{-f_\mathrm{d,max}}^{+f_\mathrm{d,max}} \frac{1}{\sqrt{f_\mathrm{d,max}^2 - f_\mathrm{d}^2}} \cdot e^{-j2\pi f_\mathrm{d}\Delta t}\,\mathrm{d}(f_\mathrm{d}) \\
&= 2\frac{1}{\pi} \cdot \int_{0}^{+f_\mathrm{d,max}} \frac{1}{\sqrt{f_\mathrm{d,max}^2 - f_\mathrm{d}^2}} \cdot \cos(2\pi f_\mathrm{d}\Delta t)\,\mathrm{d}(f_\mathrm{d}) \\
&= J_0(2\pi f_\mathrm{d,max}\Delta t),
\end{aligned}
\tag{8.60}
$$

where $J_0(\cdot)$ represents the zero–order Bessel function of the first kind [Pro95]. It can be seen that the space–time correlation function $\underline{\rho}_\mathrm{F}\left(0,\Delta t\right)$ of (8.60) is real. Therefore,

$$
\mathrm{Re}\left\{ \underline{\rho}_\mathrm{F}\left(0,\Delta t\right) \right\} = \underline{\rho}_\mathrm{F}\left(0,\Delta t\right)
\tag{8.61}
$$

holds. With

$$J_0(0) = 1, \tag{8.62}$$

(8.60) and (8.61) the covariance matrix $\underline{\mathbf{R}}_{\boldsymbol{\Delta}_{\mathrm{h,tv}}}$ of (8.58) can be written as

$$\underline{\mathbf{R}}_{\boldsymbol{\Delta}_{\mathrm{h,tv}}} = 2\sigma_{\mathrm{h,tv}}^2 \cdot \mathbf{I}^{KN_{\mathrm{F}}} = 2\left(1 - J_0(2\pi f_{\mathrm{d,max}}\Delta t)\right) \cdot \mathbf{I}^{KN_{\mathrm{F}}}. \tag{8.63}$$

The correlation duration [WLM$^+$03]

$$T_{\mathrm{k}} = \frac{3c_0}{4\pi f_{\mathrm{c}} v_{\mathrm{max}}}. \tag{8.64}$$

is a very important parameter to describe the stochastic property of the channels. With (3.39), (8.63) and (8.64) the variance of the elements of the CTF estimation error vector $\boldsymbol{\Delta}_{\mathrm{h},n_{\mathrm{B}}}^{(k_{\mathrm{B}})}$ of (8.54) caused by the time–variant channels reads

$$\sigma_{\mathrm{h,tv}}^2 = 1 - J_0(2\frac{v_{\mathrm{max}}}{c_0} \cdot f_{\mathrm{c}} \cdot \pi\Delta t) = 1 - J_0\left(\frac{3}{2} \cdot \frac{\Delta t}{T_{\mathrm{k}}}\right). \tag{8.65}$$

Fig. 8.2 shows the normalized variance $2\sigma_{\mathrm{h,tv}}^2 / \mathrm{E}\left\{|\underline{\tilde{h}}_{n_{\mathrm{B}},n_{\mathrm{F}}}^{(k,k_{\mathrm{B}})}|^2\right\}$ of the CTF estimation error vector $\boldsymbol{\Delta}_{\mathrm{h},n_{\mathrm{B}}}^{(k_{\mathrm{B}})}$ of (8.54) due to the time–variant channels. It can be seen that the normalized variance $2\sigma_{\mathrm{h,tv}}^2 / \mathrm{E}\left\{|\underline{\tilde{h}}_{n_{\mathrm{B}},n_{\mathrm{F}}}^{(k,k_{\mathrm{B}})}|^2\right\}$ is only a function of $\Delta t/T_{\mathrm{k}}$. Only when

$$\frac{\Delta t}{T_{\mathrm{k}}} \ll 1. \tag{8.66}$$

holds, the normalized variance $2\sigma_{\mathrm{h,tv}}^2 / \mathrm{E}\left\{|\underline{\tilde{h}}_{n_{\mathrm{B}},n_{\mathrm{F}}}^{(k,k_{\mathrm{B}})}|^2\right\}$ is small, and the CTF estimation error vector $\boldsymbol{\Delta}_{\mathrm{h},n_{\mathrm{B}}}^{(k_{\mathrm{B}})}$ of (8.54) can be ignored so that the channels can be considered as time–invariant.

8.3.2　Impact of imperfect channel state information

8.3.2.1　Imperfect channel state information

In Subsection 8.3.1 the different properties of imperfect CSI caused by the two major factors have been analyzed. In general the CTF estimation matrix

$$\hat{\underline{\tilde{\mathbf{H}}}}_{\mathrm{u},n_{\mathrm{B}},n_{\mathrm{F}}} = \underline{\tilde{\mathbf{H}}}_{\mathrm{u},n_{\mathrm{B}},n_{\mathrm{F}}} + \underline{\tilde{\mathbf{E}}}_{n_{\mathrm{B}},n_{\mathrm{F}}} = \hat{\underline{\tilde{\mathbf{H}}}}_{\mathrm{u},n_{\mathrm{F}}} \tag{8.67}$$

consists of the true CTF matrix $\underline{\tilde{\mathbf{H}}}_{\mathrm{u},n_{\mathrm{B}},n_{\mathrm{F}}}$ of the time slot n_{B} and the corresponding error matrix $\underline{\tilde{\mathbf{E}}}_{n_{\mathrm{B}},n_{\mathrm{F}}}$, each of dimensions $K_{\mathrm{B}} \times K$. During the frame, all the CTF estimation matrices $\hat{\underline{\tilde{\mathbf{H}}}}_{\mathrm{u},n_{\mathrm{B}},n_{\mathrm{F}}}$ are equal, while the true CTF matrices $\underline{\tilde{\mathbf{H}}}_{\mathrm{u},n_{\mathrm{B}},n_{\mathrm{F}}}$ vary. Since the two
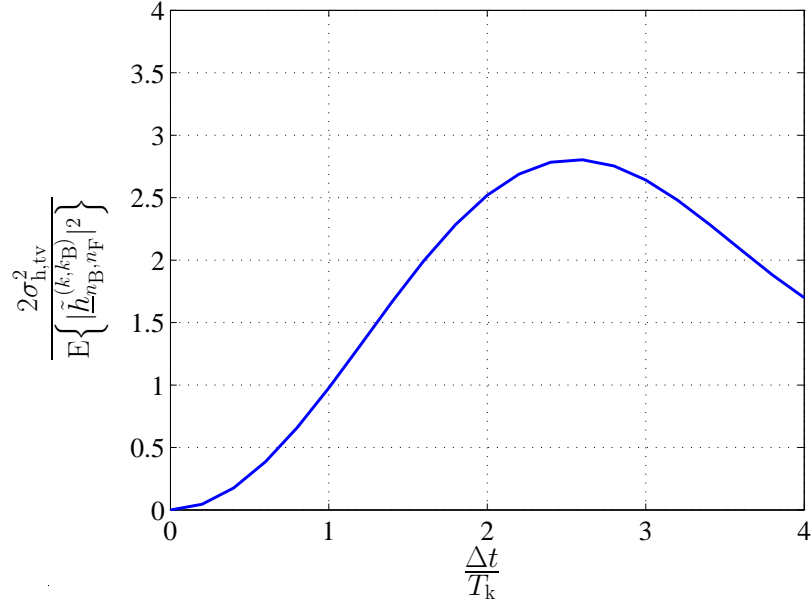
Fig. 8.2. Normalized variance $2\sigma_{\text{h,tv}}^2/\text{E}\left\{|\tilde{\underline{h}}_{n_\text{B},n_\text{F}}^{(k,k_\text{B})}|^2\right\}$, versus $\Delta t/T_\text{k}$

factors, the noise and the time variance of the channels, are independent of each other, with (8.51) and (8.65) the elements of the error matrix $\underline{\tilde{\mathbf{E}}}_{n_\text{B},n_\text{F}}$ of (8.67) are uncorrelated complex Gaussian variables with the variance

$$\sigma_\text{h}^2 = f\left(\sigma_{\text{h,n}}^2, \sigma_{\text{h,tv}}^2\right) \approx \sigma_{\text{h,n}}^2 + \sigma_{\text{h,tv}}^2 \tag{8.68}$$

of their real and imaginary parts.

8.3.2.2 Impact on the uplink data estimation

At the CU only the CTF estimation matrix $\hat{\tilde{\underline{\mathbf{H}}}}_{\text{u},n_\text{B},n_\text{F}}$ of (8.67) is available. Therefore, the detection matrix $\tilde{\underline{\mathbf{D}}}_{\text{u},n_\text{B},n_\text{F}}$ of (8.22) of the time slot $n_\text{B}, n_\text{B} \neq n_\text{B}'$, has to be constructed with the CTF estimation matrix $\hat{\tilde{\underline{\mathbf{H}}}}_{\text{u},n_\text{B},n_\text{F}}$ of (8.67), i.e.,

$$\tilde{\underline{\mathbf{D}}}_{\text{u},n_\text{B},n_\text{F}} = \left(\hat{\tilde{\underline{\mathbf{H}}}}_{\text{u},n_\text{B},n_\text{F}}^{*\text{T}} \hat{\tilde{\underline{\mathbf{H}}}}_{\text{u},n_\text{B},n_\text{F}}\right)^{-1} \hat{\tilde{\underline{\mathbf{H}}}}_{\text{u},n_\text{B},n_\text{F}}^{*\text{T}}. \tag{8.69}$$

With (8.67) and (8.69) the UL data estimation vector

$$\begin{aligned}
\hat{\tilde{\underline{\mathbf{d}}}}_{n_\text{B},n_\text{F}} &= \tilde{\underline{\mathbf{D}}}_{\text{u},n_\text{B},n_\text{F}} \tilde{\underline{\mathbf{e}}}_{\text{u},n_\text{B},n_\text{F}} \\
&= \left(\left(\tilde{\underline{\mathbf{H}}}_{\text{u},n_\text{B},n_\text{F}} + \tilde{\underline{\mathbf{E}}}_{n_\text{B},n_\text{F}}\right)^{*\text{T}} \left(\tilde{\underline{\mathbf{H}}}_{\text{u},n_\text{B},n_\text{F}} + \tilde{\underline{\mathbf{E}}}_{n_\text{B},n_\text{F}}\right)\right)^{-1} \\
&\quad \cdot \left(\tilde{\underline{\mathbf{H}}}_{\text{u},n_\text{B},n_\text{F}} + \tilde{\underline{\mathbf{E}}}_{n_\text{B},n_\text{F}}\right)^{*\text{T}} \tilde{\underline{\mathbf{e}}}_{\text{u},n_\text{B},n_\text{F}}
\end{aligned} \tag{8.70}$$

of the corresponding time slot n_B is obtained. Due to the existence of the error matrix $\underline{\tilde{\mathbf{E}}}_{n_\mathrm{B},n_\mathrm{F}}$ the UL data estimation vector $\underline{\hat{\tilde{\mathbf{d}}}}_{n_\mathrm{B},n_\mathrm{F}}$ is not unbiased any more. The UL data estimation error vector reads

$$
\begin{aligned}
\boldsymbol{\Delta}_{\mathrm{u},n_\mathrm{B},n_\mathrm{F}} &= \underline{\hat{\tilde{\mathbf{d}}}}_{n_\mathrm{B},n_\mathrm{F}} - \underline{\tilde{\mathbf{d}}}_{n_\mathrm{B},n_\mathrm{F}} \\
&= \left(\left(\underline{\tilde{\mathbf{H}}}_{\mathrm{u},n_\mathrm{B},n_\mathrm{F}} + \underline{\tilde{\mathbf{E}}}_{n_\mathrm{B},n_\mathrm{F}} \right)^{*\mathrm{T}} \left(\underline{\tilde{\mathbf{H}}}_{\mathrm{u},n_\mathrm{B},n_\mathrm{F}} + \underline{\tilde{\mathbf{E}}}_{n_\mathrm{B},n_\mathrm{F}} \right) \right)^{-1} \\
&\quad \cdot \left(\underline{\tilde{\mathbf{H}}}_{\mathrm{u},n_\mathrm{B},n_\mathrm{F}} + \underline{\tilde{\mathbf{E}}}_{n_\mathrm{B},n_\mathrm{F}} \right)^{*\mathrm{T}} \left(-\underline{\tilde{\mathbf{E}}}_{n_\mathrm{B},n_\mathrm{F}} \underline{\tilde{\mathbf{d}}}_{n_\mathrm{B},n_\mathrm{F}} + \tilde{\mathbf{n}}_{\mathrm{u},n_\mathrm{B},n_\mathrm{F}} \right) \\
&= -\left(\left(\underline{\tilde{\mathbf{H}}}_{\mathrm{u},n_\mathrm{B},n_\mathrm{F}} + \underline{\tilde{\mathbf{E}}}_{n_\mathrm{B},n_\mathrm{F}} \right)^{*\mathrm{T}} \left(\underline{\tilde{\mathbf{H}}}_{\mathrm{u},n_\mathrm{B},n_\mathrm{F}} + \underline{\tilde{\mathbf{E}}}_{n_\mathrm{B},n_\mathrm{F}} \right) \right)^{-1} \\
&\quad \cdot \left(\underline{\tilde{\mathbf{H}}}_{\mathrm{u},n_\mathrm{B},n_\mathrm{F}} + \underline{\tilde{\mathbf{E}}}_{n_\mathrm{B},n_\mathrm{F}} \right)^{*\mathrm{T}} \underline{\tilde{\mathbf{E}}}_{n_\mathrm{B},n_\mathrm{F}} \underline{\tilde{\mathbf{d}}}_{n_\mathrm{B},n_\mathrm{F}} \\
&\quad + \left(\left(\underline{\tilde{\mathbf{H}}}_{\mathrm{u},n_\mathrm{B},n_\mathrm{F}} + \underline{\tilde{\mathbf{E}}}_{n_\mathrm{B},n_\mathrm{F}} \right)^{*\mathrm{T}} \left(\underline{\tilde{\mathbf{H}}}_{\mathrm{u},n_\mathrm{B},n_\mathrm{F}} + \underline{\tilde{\mathbf{E}}}_{n_\mathrm{B},n_\mathrm{F}} \right) \right)^{-1} \\
&\quad \cdot \left(\underline{\tilde{\mathbf{H}}}_{\mathrm{u},n_\mathrm{B},n_\mathrm{F}} + \underline{\tilde{\mathbf{E}}}_{n_\mathrm{B},n_\mathrm{F}} \right)^{*\mathrm{T}} \tilde{\mathbf{n}}_{\mathrm{u},n_\mathrm{B},n_\mathrm{F}} \\
&= \underline{\tilde{\mathbf{X}}} \, \underline{\tilde{\mathbf{d}}}_{n_\mathrm{B},n_\mathrm{F}} + \underline{\tilde{\mathbf{Y}}} \, \tilde{\mathbf{n}}_{\mathrm{u},n_\mathrm{B},n_\mathrm{F}}.
\end{aligned}
\tag{8.71}
$$

It can been seen that the elements of the UL data estimation error vector $\boldsymbol{\Delta}_{\mathrm{u},n_\mathrm{B},n_\mathrm{F}}$ of (8.71) are nonlinear functions of the elements of the error matrix $\underline{\tilde{\mathbf{E}}}_{n_\mathrm{B},n_\mathrm{F}}$ of (8.67). Under the assumption of small CTF estimation errors $\left[\underline{\tilde{\mathbf{E}}}_{n_\mathrm{B},n_\mathrm{F}} \right]_{k_\mathrm{B},k}$, i.e., the variance σ_h^2 of (8.68) is very small, the nonlinear functions can be approximated by truncating the Taylor series of the UL data estimation error vector $\boldsymbol{\Delta}_{\mathrm{u},n_\mathrm{B},n_\mathrm{F}}$ of (8.71) after the linear terms [WM03], i.e.,

$$
\begin{aligned}
\boldsymbol{\Delta}_{\mathrm{u},n_\mathrm{B},n_\mathrm{F}} &\approx \left[\sum_{k_\mathrm{B}=1}^{K_\mathrm{B}} \sum_{k=1}^{K} \frac{\partial \underline{\tilde{\mathbf{X}}}}{\partial \mathrm{Re}\left\{ \left[\underline{\tilde{\mathbf{E}}}_{n_\mathrm{B},n_\mathrm{F}} \right]_{k_\mathrm{B},k} \right\}} \Bigg|_{\underline{\tilde{\mathbf{E}}}_{n_\mathrm{B},n_\mathrm{F}}=0} \mathrm{Re}\left\{ \left[\underline{\tilde{\mathbf{E}}}_{n_\mathrm{B},n_\mathrm{F}} \right]_{k_\mathrm{B},k} \right\} \right. \\
&\quad + \left. \sum_{k_\mathrm{B}=1}^{K_\mathrm{B}} \sum_{k=1}^{K} \frac{\partial \underline{\tilde{\mathbf{X}}}}{\partial \mathrm{Im}\left\{ \left[\underline{\tilde{\mathbf{E}}}_{n_\mathrm{B},n_\mathrm{F}} \right]_{k_\mathrm{B},k} \right\}} \Bigg|_{\underline{\tilde{\mathbf{E}}}_{n_\mathrm{B},n_\mathrm{F}}=0} \mathrm{Im}\left\{ \left[\underline{\tilde{\mathbf{E}}}_{n_\mathrm{B},n_\mathrm{F}} \right]_{k_\mathrm{B},k} \right\} \right] \underline{\tilde{\mathbf{d}}}_{n_\mathrm{B},n_\mathrm{F}} \\
&\quad + \left[\left(\underline{\tilde{\mathbf{H}}}_{\mathrm{u},n_\mathrm{B},n_\mathrm{F}}^{*\mathrm{T}} \underline{\tilde{\mathbf{H}}}_{\mathrm{u},n_\mathrm{B},n_\mathrm{F}} \right)^{-1} \underline{\tilde{\mathbf{H}}}_{\mathrm{u},n_\mathrm{B},n_\mathrm{F}}^{*\mathrm{T}} \right. \\
&\quad + \sum_{k_\mathrm{B}=1}^{K_\mathrm{B}} \sum_{k=1}^{K} \frac{\partial \underline{\tilde{\mathbf{Y}}}}{\partial \mathrm{Re}\left\{ \left[\underline{\tilde{\mathbf{E}}}_{n_\mathrm{B},n_\mathrm{F}} \right]_{k_\mathrm{B},k} \right\}} \Bigg|_{\underline{\tilde{\mathbf{E}}}_{n_\mathrm{B},n_\mathrm{F}}=0} \mathrm{Re}\left\{ \left[\underline{\tilde{\mathbf{E}}}_{n_\mathrm{B},n_\mathrm{F}} \right]_{k_\mathrm{B},k} \right\} \\
&\quad + \left. \sum_{k_\mathrm{B}=1}^{K_\mathrm{B}} \sum_{k=1}^{K} \frac{\partial \underline{\tilde{\mathbf{Y}}}}{\partial \mathrm{Im}\left\{ \left[\underline{\tilde{\mathbf{E}}}_{n_\mathrm{B},n_\mathrm{F}} \right]_{k_\mathrm{B},k} \right\}} \Bigg|_{\underline{\tilde{\mathbf{E}}}_{n_\mathrm{B},n_\mathrm{F}}=0} \mathrm{Im}\left\{ \left[\underline{\tilde{\mathbf{E}}}_{n_\mathrm{B},n_\mathrm{F}} \right]_{k_\mathrm{B},k} \right\} \right] \tilde{\mathbf{n}}_{\mathrm{u},n_\mathrm{B},n_\mathrm{F}}.
\end{aligned}
\tag{8.72}
$$

After some simplifications we obtain from (8.72)

$$
\begin{aligned}
\underline{\mathbf{\Delta}}_{\mathrm{u},n_{\mathrm{B}},n_{\mathrm{F}}} &\approx -\left(\underline{\tilde{\mathbf{H}}}_{\mathrm{u},n_{\mathrm{B}},n_{\mathrm{F}}}^{*\mathrm{T}}\underline{\tilde{\mathbf{H}}}_{\mathrm{u},n_{\mathrm{B}},n_{\mathrm{F}}}\right)^{-1}\underline{\tilde{\mathbf{H}}}_{\mathrm{u},n_{\mathrm{B}},n_{\mathrm{F}}}^{*\mathrm{T}}\underline{\tilde{\mathbf{E}}}_{n_{\mathrm{B}},n_{\mathrm{F}}}\underline{\tilde{\mathbf{d}}}_{n_{\mathrm{B}},n_{\mathrm{F}}} \\
&\quad+\left(\underline{\tilde{\mathbf{H}}}_{\mathrm{u},n_{\mathrm{B}},n_{\mathrm{F}}}^{*\mathrm{T}}\underline{\tilde{\mathbf{H}}}_{\mathrm{u},n_{\mathrm{B}},n_{\mathrm{F}}}\right)^{-1}\underline{\tilde{\mathbf{H}}}_{\mathrm{u},n_{\mathrm{B}},n_{\mathrm{F}}}^{*\mathrm{T}}\ \underline{\tilde{\mathbf{n}}}_{\mathrm{u},n_{\mathrm{B}},n_{\mathrm{F}}} \\
&\quad+\left(\underline{\tilde{\mathbf{H}}}_{\mathrm{u},n_{\mathrm{B}},n_{\mathrm{F}}}^{*\mathrm{T}}\underline{\tilde{\mathbf{H}}}_{\mathrm{u},n_{\mathrm{B}},n_{\mathrm{F}}}\right)^{-1}\underline{\tilde{\mathbf{E}}}_{\mathrm{u},n_{\mathrm{B}},n_{\mathrm{F}}}^{*\mathrm{T}}\ \underline{\tilde{\mathbf{n}}}_{\mathrm{u},n_{\mathrm{B}},n_{\mathrm{F}}} \\
&\quad-\left(\underline{\tilde{\mathbf{H}}}_{\mathrm{u},n_{\mathrm{B}},n_{\mathrm{F}}}^{*\mathrm{T}}\underline{\tilde{\mathbf{H}}}_{\mathrm{u},n_{\mathrm{B}},n_{\mathrm{F}}}\right)^{-1}\left(\underline{\tilde{\mathbf{H}}}_{\mathrm{u},n_{\mathrm{B}},n_{\mathrm{F}}}^{*\mathrm{T}}\underline{\tilde{\mathbf{E}}}_{\mathrm{u},n_{\mathrm{B}},n_{\mathrm{F}}}+\underline{\tilde{\mathbf{E}}}_{\mathrm{u},n_{\mathrm{B}},n_{\mathrm{F}}}^{*\mathrm{T}}\underline{\tilde{\mathbf{H}}}_{\mathrm{u},n_{\mathrm{B}},n_{\mathrm{F}}}\right) \\
&\quad\cdot\left(\underline{\tilde{\mathbf{H}}}_{\mathrm{u},n_{\mathrm{B}},n_{\mathrm{F}}}^{*\mathrm{T}}\underline{\tilde{\mathbf{H}}}_{\mathrm{u},n_{\mathrm{B}},n_{\mathrm{F}}}\right)^{-1}\underline{\tilde{\mathbf{H}}}_{\mathrm{u},n_{\mathrm{B}},n_{\mathrm{F}}}^{*\mathrm{T}}\ \underline{\tilde{\mathbf{n}}}_{\mathrm{u},n_{\mathrm{B}},n_{\mathrm{F}}}.
\end{aligned}
\tag{8.73}
$$

With (8.10) and (8.11) the covariance matrix of the UL data estimation error vector $\underline{\mathbf{\Delta}}_{\mathrm{u},n_{\mathrm{B}},n_{\mathrm{F}}}$ of (8.71) reads

$$
\begin{aligned}
\mathbf{R}_{\mathbf{\Delta}_{\mathrm{u}}} &= \mathrm{E}\left\{\left(\hat{\underline{\tilde{\mathbf{d}}}}_{n_{\mathrm{B}},n_{\mathrm{F}}}-\underline{\tilde{\mathbf{d}}}_{n_{\mathrm{B}},n_{\mathrm{F}}}\right)\left(\hat{\underline{\tilde{\mathbf{d}}}}_{n_{\mathrm{B}},n_{\mathrm{F}}}-\underline{\tilde{\mathbf{d}}}_{n_{\mathrm{B}},n_{\mathrm{F}}}\right)^{*\mathrm{T}}\right\} \\
&\approx 2\sigma^2\left(\underline{\tilde{\mathbf{H}}}_{\mathrm{u},n_{\mathrm{B}},n_{\mathrm{F}}}^{*\mathrm{T}}\underline{\tilde{\mathbf{H}}}_{\mathrm{u},n_{\mathrm{B}},n_{\mathrm{F}}}\right)^{-1}+2E_{\mathrm{d}}\cdot2\sigma_{\mathrm{h}}^2\cdot K\left(\underline{\tilde{\mathbf{H}}}_{\mathrm{u},n_{\mathrm{B}},n_{\mathrm{F}}}^{*\mathrm{T}}\underline{\tilde{\mathbf{H}}}_{\mathrm{u},n_{\mathrm{B}},n_{\mathrm{F}}}\right)^{-1} \\
&\quad+2\sigma^2\cdot2\sigma_{\mathrm{h}}^2\mathrm{trace}\left\{\left(\underline{\tilde{\mathbf{H}}}_{\mathrm{u},n_{\mathrm{B}},n_{\mathrm{F}}}^{*\mathrm{T}}\underline{\tilde{\mathbf{H}}}_{\mathrm{u},n_{\mathrm{B}},n_{\mathrm{F}}}\right)^{-1}\right\}\left(\underline{\tilde{\mathbf{H}}}_{\mathrm{u},n_{\mathrm{B}},n_{\mathrm{F}}}^{*\mathrm{T}}\underline{\tilde{\mathbf{H}}}_{\mathrm{u},n_{\mathrm{B}},n_{\mathrm{F}}}\right)^{-1} \\
&\quad+2\sigma^2\cdot2\sigma_{\mathrm{h}}^2\left(K_{\mathrm{B}}-K\right)\left(\underline{\tilde{\mathbf{H}}}_{\mathrm{u},n_{\mathrm{B}},n_{\mathrm{F}}}^{*\mathrm{T}}\underline{\tilde{\mathbf{H}}}_{\mathrm{u},n_{\mathrm{B}},n_{\mathrm{F}}}\right)^{-2} \\
&= 2\sigma^2\left(\underline{\tilde{\mathbf{H}}}_{\mathrm{u},n_{\mathrm{B}},n_{\mathrm{F}}}^{*\mathrm{T}}\underline{\tilde{\mathbf{H}}}_{\mathrm{u},n_{\mathrm{B}},n_{\mathrm{F}}}\right)^{-1} \\
&\quad\cdot\left(1+\frac{2E_{\mathrm{d}}\cdot2\sigma_{\mathrm{h}}^2\cdot K}{2\sigma^2}+2\sigma_{\mathrm{h}}^2\mathrm{trace}\left\{\left(\underline{\tilde{\mathbf{H}}}_{\mathrm{u},n_{\mathrm{B}},n_{\mathrm{F}}}^{*\mathrm{T}}\underline{\tilde{\mathbf{H}}}_{\mathrm{u},n_{\mathrm{B}},n_{\mathrm{F}}}\right)^{-1}\right\}\right) \\
&\quad+2\sigma_{\mathrm{h}}^2\left(K_{\mathrm{B}}-K\right)\left(\underline{\tilde{\mathbf{H}}}_{\mathrm{u},n_{\mathrm{B}},n_{\mathrm{F}}}^{*\mathrm{T}}\underline{\tilde{\mathbf{H}}}_{\mathrm{u},n_{\mathrm{B}},n_{\mathrm{F}}}\right)^{-2}.
\end{aligned}
\tag{8.74}
$$

For the special full–loaded case that the number K_{B} of APs per SA is equal to the number K of MTs per SA, the last term $2\sigma_{\mathrm{h}}^2\left(K_{\mathrm{B}}-K\right)\left(\underline{\tilde{\mathbf{H}}}_{\mathrm{u},n_{\mathrm{B}},n_{\mathrm{F}}}^{*\mathrm{T}}\underline{\tilde{\mathbf{H}}}_{\mathrm{u},n_{\mathrm{B}},n_{\mathrm{F}}}\right)^{-2}$ on the right hand of (8.74) becomes zero so that (8.74) can be rewritten as

$$
\begin{aligned}
\mathbf{R}_{\mathbf{\Delta}_{\mathrm{u}}} &\approx 2\sigma^2\left(\underline{\tilde{\mathbf{H}}}_{\mathrm{u},n_{\mathrm{B}},n_{\mathrm{F}}}^{*\mathrm{T}}\underline{\tilde{\mathbf{H}}}_{\mathrm{u},n_{\mathrm{B}},n_{\mathrm{F}}}\right)^{-1} \\
&\quad\cdot\underbrace{\left(1+\frac{2E_{\mathrm{d}}\cdot2\sigma_{\mathrm{h}}^2\cdot K}{2\sigma^2}+2\sigma_{\mathrm{h}}^2\mathrm{trace}\left\{\left(\underline{\tilde{\mathbf{H}}}_{\mathrm{u},n_{\mathrm{B}},n_{\mathrm{F}}}^{*\mathrm{T}}\underline{\tilde{\mathbf{H}}}_{\mathrm{u},n_{\mathrm{B}},n_{\mathrm{F}}}\right)^{-1}\right\}\right)}_{\xi_{\mathrm{u},n_{\mathrm{F}}}},
\end{aligned}
\tag{8.75}
$$

where $\xi_{\mathrm{u},n_{\mathrm{F}}}$ is a factor greater than one. Consequently, with (8.18), (8.24) and (8.75) the SNR

$$
\begin{aligned}
\gamma_{\mathrm{u},n_{\mathrm{B}},n_{\mathrm{F}}}^{(k)} &= \frac{E_{\mathrm{d}}}{\sigma^2\cdot\xi_{\mathrm{u},n_{\mathrm{F}}}\left[\left(\underline{\tilde{\mathbf{H}}}_{\mathrm{u},n_{\mathrm{B}},n_{\mathrm{F}}}^{*\mathrm{T}}\underline{\tilde{\mathbf{H}}}_{\mathrm{u},n_{\mathrm{B}},n_{\mathrm{F}}}\right)^{-1}\right]_{k,k}} \\
&= \frac{\gamma_{\mathrm{u},n_{\mathrm{B}},n_{\mathrm{F}}}^{(k)}}{\xi_{\mathrm{u},n_{\mathrm{F}}}}
\end{aligned}
\tag{8.76}
$$

of the data symbol $\underline{\tilde{d}}_{\mathrm{u},n_{\mathrm{B}},n_{\mathrm{F}}}^{(k)}$ in the UL can be obtained in the case of imperfect CSI. It can be seen that the CTF estimation error matrix $\underline{\tilde{\mathbf{E}}}_{n_{\mathrm{B}},n_{\mathrm{F}}}$ of (8.67) acts like the additional noise, which makes the system performance worse. If QPSK is applied, with (8.76) the bit error probability of (8.25) can be rewritten as

$$
\begin{aligned}
P_{\mathrm{b},\mathrm{u},n_{\mathrm{B}},n_{\mathrm{F}}}^{(k)} &= \frac{1}{2}\mathrm{erfc}\left(\sqrt{\frac{\gamma_{\mathrm{u},n_{\mathrm{B}},n_{\mathrm{F}}}^{(k)}}{2}}\right) \\[2em]
&= \frac{1}{2}\mathrm{erfc}\left(\sqrt{\frac{\frac{T_{\mathrm{u},n_{\mathrm{B}},n_{\mathrm{F}}}^{(k)}}{\sigma^2}}{2\xi_{\mathrm{u},n_{\mathrm{F}}}\left[\left(\underline{\tilde{\mathbf{H}}}_{\mathrm{u},n_{\mathrm{B}},n_{\mathrm{F}}}^{*\mathrm{T}}\underline{\tilde{\mathbf{H}}}_{\mathrm{u},n_{\mathrm{B}},n_{\mathrm{F}}}\right)^{-1}\right]_{k,k}}}\right).
\end{aligned}
\tag{8.77}
$$

8.3.2.3   Impact on the downlink data transmission

At the CU only the CTF estimation matrix $\underline{\hat{\tilde{\mathbf{H}}}}_{\mathrm{u},n_{\mathrm{B}},n_{\mathrm{F}}}$ of (8.67) is available for the TxZF JT of the DL. Therefore, the modulation matrix $\underline{\tilde{\mathbf{M}}}_{\mathrm{d},n_{\mathrm{B}},n_{\mathrm{F}}}$ of (8.29) of the time slot n_{B} has to be constructed with the CTF estimation matrix $\underline{\hat{\tilde{\mathbf{H}}}}_{\mathrm{u},n_{\mathrm{B}},n_{\mathrm{F}}}$ of (8.67), i.e.,

$$
\begin{aligned}
\underline{\tilde{\mathbf{M}}}_{\mathrm{d},n_{\mathrm{B}},n_{\mathrm{F}}} &= \underline{\hat{\tilde{\mathbf{H}}}}_{\mathrm{d},n_{\mathrm{B}},n_{\mathrm{F}}}^{*\mathrm{T}}\left(\underline{\hat{\tilde{\mathbf{H}}}}_{\mathrm{d},n_{\mathrm{B}},n_{\mathrm{F}}}\underline{\hat{\tilde{\mathbf{H}}}}_{\mathrm{d},n_{\mathrm{B}},n_{\mathrm{F}}}^{*\mathrm{T}}\right)^{-1} = \underline{\hat{\tilde{\mathbf{H}}}}_{\mathrm{u},n_{\mathrm{B}},n_{\mathrm{F}}}^{*}\left(\underline{\hat{\tilde{\mathbf{H}}}}_{\mathrm{u},n_{\mathrm{B}},n_{\mathrm{F}}}^{\mathrm{T}}\underline{\hat{\tilde{\mathbf{H}}}}_{\mathrm{u},n_{\mathrm{B}},n_{\mathrm{F}}}^{*}\right)^{-1} \\[1em]
&= \left(\underline{\tilde{\mathbf{H}}}_{\mathrm{u},n_{\mathrm{B}},n_{\mathrm{F}}} + \underline{\tilde{\mathbf{E}}}_{n_{\mathrm{B}},n_{\mathrm{F}}}\right)^{*}\left(\left(\underline{\tilde{\mathbf{H}}}_{\mathrm{u},n_{\mathrm{B}},n_{\mathrm{F}}} + \underline{\tilde{\mathbf{E}}}_{n_{\mathrm{B}},n_{\mathrm{F}}}\right)^{\mathrm{T}}\left(\underline{\tilde{\mathbf{H}}}_{\mathrm{u},n_{\mathrm{B}},n_{\mathrm{F}}} + \underline{\tilde{\mathbf{E}}}_{n_{\mathrm{B}},n_{\mathrm{F}}}\right)^{*}\right)^{-1}.
\end{aligned}
\tag{8.78}
$$

It can be seen that the modulator matrix $\underline{\tilde{\mathbf{M}}}_{\mathrm{d},n_{\mathrm{B}},n_{\mathrm{F}}}$ of (8.78) is a nonlinear function of the error matrix $\underline{\tilde{\mathbf{E}}}_{n_{\mathrm{B}},n_{\mathrm{F}}}$ of (8.67). Similarly as in the UL, with the assumption of small CTF estimation errors $\left[\underline{\tilde{\mathbf{E}}}_{n_{\mathrm{B}},n_{\mathrm{F}}}\right]_{k_{\mathrm{B}},k}$, i.e., with a small variance σ_{h}^2 of (8.68), the modulator matrix $\underline{\tilde{\mathbf{M}}}_{\mathrm{d},n_{\mathrm{B}},n_{\mathrm{F}}}$ of (8.78) can be approximated by a linear function of the error matrix $\underline{\tilde{\mathbf{E}}}_{n_{\mathrm{B}},n_{\mathrm{F}}}$ of (8.67) by truncating the Taylor series of $\underline{\tilde{\mathbf{M}}}_{\mathrm{d},n_{\mathrm{B}},n_{\mathrm{F}}}$ of (8.78) after

the linear terms [WM03]. Therefore,

$$
\begin{aligned}
\tilde{\underline{\mathbf{M}}}_{\mathrm{d},n_{\mathrm{B}},n_{\mathrm{F}}} &\approx \tilde{\underline{\mathbf{H}}}^{*}_{\mathrm{u},n_{\mathrm{B}},n_{\mathrm{F}}} \left(\tilde{\underline{\mathbf{H}}}^{\mathrm{T}}_{\mathrm{u},n_{\mathrm{B}},n_{\mathrm{F}}} \tilde{\underline{\mathbf{H}}}^{*}_{\mathrm{u},n_{\mathrm{B}},n_{\mathrm{F}}} \right)^{-1} \\
&+ \sum_{k_{\mathrm{B}}=1}^{K_{\mathrm{B}}} \sum_{k=1}^{K} \frac{\partial \tilde{\underline{\mathbf{M}}}_{\mathrm{d},n_{\mathrm{B}},n_{\mathrm{F}}}}{\partial \mathrm{Re}\left\{ \left[\tilde{\underline{\mathbf{E}}}_{n_{\mathrm{B}},n_{\mathrm{F}}} \right]_{k_{\mathrm{B}},k} \right\}} \Bigg|_{\tilde{\underline{\mathbf{E}}}_{n_{\mathrm{B}},n_{\mathrm{F}}}=0} \mathrm{Re}\left\{ \left[\tilde{\underline{\mathbf{E}}}_{n_{\mathrm{B}},n_{\mathrm{F}}} \right]_{k_{\mathrm{B}},k} \right\} \\
&+ \sum_{k_{\mathrm{B}}=1}^{K_{\mathrm{B}}} \sum_{k=1}^{K} \frac{\partial \tilde{\underline{\mathbf{M}}}_{\mathrm{d},n_{\mathrm{B}},n_{\mathrm{F}}}}{\partial \mathrm{Im}\left\{ \left[\tilde{\underline{\mathbf{E}}}_{n_{\mathrm{B}},n_{\mathrm{F}}} \right]_{k_{\mathrm{B}},k} \right\}} \Bigg|_{\tilde{\underline{\mathbf{E}}}_{n_{\mathrm{B}},n_{\mathrm{F}}}=0} \mathrm{Im}\left\{ \left[\tilde{\underline{\mathbf{E}}}_{n_{\mathrm{B}},n_{\mathrm{F}}} \right]_{k_{\mathrm{B}},k} \right\} \\
&\approx \tilde{\underline{\mathbf{H}}}^{*}_{\mathrm{u},n_{\mathrm{B}},n_{\mathrm{F}}} \left(\tilde{\underline{\mathbf{H}}}^{\mathrm{T}}_{\mathrm{u},n_{\mathrm{B}},n_{\mathrm{F}}} \tilde{\underline{\mathbf{H}}}^{*}_{\mathrm{u},n_{\mathrm{B}},n_{\mathrm{F}}} \right)^{-1} + \tilde{\underline{\mathbf{E}}}^{*}_{n_{\mathrm{B}},n_{\mathrm{F}}} \left(\tilde{\underline{\mathbf{H}}}^{\mathrm{T}}_{\mathrm{u},n_{\mathrm{B}},n_{\mathrm{F}}} \tilde{\underline{\mathbf{H}}}^{*}_{\mathrm{u},n_{\mathrm{B}},n_{\mathrm{F}}} \right)^{-1} \\
&- \tilde{\underline{\mathbf{H}}}^{*}_{\mathrm{u},n_{\mathrm{B}},n_{\mathrm{F}}} \left(\tilde{\underline{\mathbf{H}}}^{\mathrm{T}}_{\mathrm{u},n_{\mathrm{B}},n_{\mathrm{F}}} \tilde{\underline{\mathbf{H}}}^{*}_{\mathrm{u},n_{\mathrm{B}},n_{\mathrm{F}}} \right)^{-1} \\
&\cdot \left(\tilde{\underline{\mathbf{H}}}^{\mathrm{T}}_{\mathrm{u},n_{\mathrm{B}},n_{\mathrm{F}}} \tilde{\underline{\mathbf{E}}}^{*}_{n_{\mathrm{B}},n_{\mathrm{F}}} + \tilde{\underline{\mathbf{E}}}^{\mathrm{T}}_{n_{\mathrm{B}},n_{\mathrm{F}}} \tilde{\underline{\mathbf{H}}}^{*}_{\mathrm{u},n_{\mathrm{B}},n_{\mathrm{F}}} \right) \left(\tilde{\underline{\mathbf{H}}}^{\mathrm{T}}_{\mathrm{u},n_{\mathrm{B}},n_{\mathrm{F}}} \tilde{\underline{\mathbf{H}}}^{*}_{\mathrm{u},n_{\mathrm{B}},n_{\mathrm{F}}} \right)^{-1} \quad (8.79)
\end{aligned}
$$

can be obtained after some simplifications.

Consequently, with (8.7), (8.28) and (8.79) the DL data estimation vector

$$
\begin{aligned}
\hat{\tilde{\underline{\mathbf{d}}}}_{n_{\mathrm{B}},n_{\mathrm{F}}} &= \tilde{\underline{\mathbf{H}}}_{\mathrm{d},n_{\mathrm{B}},n_{\mathrm{F}}} \tilde{\underline{\mathbf{M}}}_{\mathrm{d},n_{\mathrm{B}},n_{\mathrm{F}}} \tilde{\underline{\mathbf{d}}}_{n_{\mathrm{B}},n_{\mathrm{F}}} + \tilde{\underline{\mathbf{n}}}_{\mathrm{d},n_{\mathrm{B}},n_{\mathrm{F}}} \\
&= \tilde{\underline{\mathbf{H}}}^{\mathrm{T}}_{\mathrm{u},n_{\mathrm{B}},n_{\mathrm{F}}} \tilde{\underline{\mathbf{M}}}_{\mathrm{d},n_{\mathrm{B}},n_{\mathrm{F}}} \tilde{\underline{\mathbf{d}}}_{n_{\mathrm{B}},n_{\mathrm{F}}} + \tilde{\underline{\mathbf{n}}}_{\mathrm{d},n_{\mathrm{B}},n_{\mathrm{F}}} \quad (8.80)
\end{aligned}
$$

can be obtained. With (8.80) the DL data estimation error vector reads

$$
\begin{aligned}
\underline{\boldsymbol{\Delta}}_{\mathrm{d},n_{\mathrm{B}},n_{\mathrm{F}}} &= \hat{\tilde{\underline{\mathbf{d}}}}_{n_{\mathrm{B}},n_{\mathrm{F}}} - \tilde{\underline{\mathbf{d}}}_{n_{\mathrm{B}},n_{\mathrm{F}}} \\
&\approx \tilde{\underline{\mathbf{E}}}^{*}_{n_{\mathrm{B}},n_{\mathrm{F}}} \tilde{\underline{\mathbf{H}}}^{*}_{\mathrm{u},n_{\mathrm{B}},n_{\mathrm{F}}} \left(\tilde{\underline{\mathbf{H}}}^{\mathrm{T}}_{\mathrm{u},n_{\mathrm{B}},n_{\mathrm{F}}} \tilde{\underline{\mathbf{H}}}^{*}_{\mathrm{u},n_{\mathrm{B}},n_{\mathrm{F}}} \right)^{-1} \tilde{\underline{\mathbf{d}}}_{n_{\mathrm{B}},n_{\mathrm{F}}} + \tilde{\underline{\mathbf{n}}}_{\mathrm{d},n_{\mathrm{B}},n_{\mathrm{F}}}. \quad (8.81)
\end{aligned}
$$

It can be seen that the unbiased estimation in the DL is destroyed by the CTF estimation error matrix $\tilde{\underline{\mathbf{E}}}_{n_{\mathrm{B}},n_{\mathrm{F}}}$ of (8.67), i.e., the DL data estimation error vector $\underline{\boldsymbol{\Delta}}_{\mathrm{d},n_{\mathrm{B}},n_{\mathrm{F}}}$ consists of not only the noise part $\tilde{\underline{\mathbf{n}}}_{\mathrm{d},n_{\mathrm{B}},n_{\mathrm{F}}}$ of (8.81), but contains also the interference part, which is the first term on the right side of (8.81). With (8.10) and (8.11) the covariance matrix

$$
\underline{\mathbf{R}}_{\boldsymbol{\Delta}_{\mathrm{d}}} \approx \left(2\sigma^2 + 2E_{\mathrm{d}} \cdot 2\sigma_{\mathrm{h}}^2 \cdot \mathrm{trace}\left\{ \left(\tilde{\underline{\mathbf{H}}}^{\mathrm{T}}_{\mathrm{u},n_{\mathrm{B}},n_{\mathrm{F}}} \tilde{\underline{\mathbf{H}}}^{*}_{\mathrm{u},n_{\mathrm{B}},n_{\mathrm{F}}} \right)^{-1} \right\} \right) \cdot \mathbf{I}^{K} \quad (8.82)
$$

of the DL data estimation error vector $\underline{\boldsymbol{\Delta}}_{\mathrm{d},n_{\mathrm{B}},n_{\mathrm{F}}}$ of (8.81) can be obtained.

The transmit energy $T^{(k)}_{\mathrm{d},n_{\mathrm{B}},n_{\mathrm{F}}}$ of (8.30) invested for the data symbol $\tilde{\underline{d}}^{(k)}_{n_{\mathrm{B}},n_{\mathrm{F}}}$ in the DL is also influenced by imperfect CSI. With (8.30) and (8.79) the transmit energy reads

$$
\begin{aligned}
T^{(k)}_{\mathrm{d},n_{\mathrm{B}},n_{\mathrm{F}}} &= E_{\mathrm{d}} \left[\tilde{\underline{\mathbf{M}}}^{*\mathrm{T}}_{\mathrm{d},n_{\mathrm{B}},n_{\mathrm{F}}} \tilde{\underline{\mathbf{M}}}_{\mathrm{d},n_{\mathrm{B}},n_{\mathrm{F}}} \right]_{k,k} \\
&= E_{\mathrm{d}} \left[\left(\tilde{\underline{\mathbf{H}}}^{\mathrm{T}}_{\mathrm{u},n_{\mathrm{B}},n_{\mathrm{F}}} \tilde{\underline{\mathbf{H}}}^{*}_{\mathrm{u},n_{\mathrm{B}},n_{\mathrm{F}}} \right)^{-1} \right]_{k,k} \cdot \left(1 + 2\sigma_{\mathrm{h}}^2 \cdot \mathrm{trace}\left\{ \left(\tilde{\underline{\mathbf{H}}}^{\mathrm{T}}_{\mathrm{u},n_{\mathrm{B}},n_{\mathrm{F}}} \tilde{\underline{\mathbf{H}}}^{*}_{\mathrm{u},n_{\mathrm{B}},n_{\mathrm{F}}} \right)^{-1} \right\} \right) \\
&+ E_{\mathrm{d}} \cdot 2\sigma_{\mathrm{h}}^2 \cdot (K_{\mathrm{B}} - K) \left[\left(\tilde{\underline{\mathbf{H}}}^{\mathrm{T}}_{\mathrm{u},n_{\mathrm{B}},n_{\mathrm{F}}} \tilde{\underline{\mathbf{H}}}^{*}_{\mathrm{u},n_{\mathrm{B}},n_{\mathrm{F}}} \right)^{-2} \right]_{k,k}. \quad (8.83)
\end{aligned}
$$

It can be seen that imperfect CSI leads to an increased transmit energy $T_{\mathrm{d},n_\mathrm{B},n_\mathrm{F}}^{(k)}$ of (8.83). In the full–loaded case of K_B equal to K the last term on the right side of (8.83) becomes zero. In such a case with (8.82) and (8.83) the SNR

$$
\begin{aligned}
\gamma_{\mathrm{d},n_\mathrm{B},n_\mathrm{F}}^{(k)} &= \frac{E_\mathrm{d}}{\sigma^2 \left(1 + \frac{2E_\mathrm{d} \cdot 2\sigma_\mathrm{h}^2}{2\sigma^2} \mathrm{trace}\left\{ \left(\tilde{\underline{\mathbf{H}}}_{\mathrm{u},n_\mathrm{B},n_\mathrm{F}}^{\mathrm{T}} \tilde{\underline{\mathbf{H}}}_{\mathrm{u},n_\mathrm{B},n_\mathrm{F}}^{*} \right)^{-1} \right\} \right)} \\[2mm]
&\approx \frac{\frac{T_{\mathrm{d},n_\mathrm{B},n_\mathrm{F}}^{(k)}}{\sigma^2}}{\left[\left(\tilde{\underline{\mathbf{H}}}_{\mathrm{u},n_\mathrm{B},n_\mathrm{F}}^{\mathrm{T}} \tilde{\underline{\mathbf{H}}}_{\mathrm{u},n_\mathrm{B},n_\mathrm{F}}^{*} \right)^{-1} \right]_{k,k}} \cdot \frac{1}{\left(1 + \frac{2E_\mathrm{d} \cdot 2\sigma_\mathrm{h}^2}{2\sigma^2} \mathrm{trace}\left\{ \left(\tilde{\underline{\mathbf{H}}}_{\mathrm{u},n_\mathrm{B},n_\mathrm{F}}^{\mathrm{T}} \tilde{\underline{\mathbf{H}}}_{\mathrm{u},n_\mathrm{B},n_\mathrm{F}}^{*} \right)^{-1} \right\} \right)} \\[2mm]
&\quad \cdot \frac{1}{\left(1 + 2\sigma_\mathrm{h}^2 \cdot \mathrm{trace}\left\{ \left(\tilde{\underline{\mathbf{H}}}_{\mathrm{u},n_\mathrm{B},n_\mathrm{F}}^{\mathrm{T}} \tilde{\underline{\mathbf{H}}}_{\mathrm{u},n_\mathrm{B},n_\mathrm{F}}^{*} \right)^{-1} \right\} \right)} \\[2mm]
&= \frac{\frac{T_{\mathrm{d},n_\mathrm{B},n_\mathrm{F}}^{(k)}}{\sigma^2}}{\xi_{\mathrm{d},n_\mathrm{F}} \left[\left(\tilde{\underline{\mathbf{H}}}_{\mathrm{u},n_\mathrm{B},n_\mathrm{F}}^{\mathrm{T}} \tilde{\underline{\mathbf{H}}}_{\mathrm{u},n_\mathrm{B},n_\mathrm{F}}^{*} \right)^{-1} \right]_{k,k}}
\end{aligned} \tag{8.84}
$$

of the data symbol $\underline{d}_{\mathrm{d},n_\mathrm{B},n_\mathrm{F}}^{(k)}$ in the DL can be obtained, where

$$
\begin{aligned}
\xi_{\mathrm{d},n_\mathrm{F}} &= \left(1 + \frac{2E_\mathrm{d} \cdot 2\sigma_\mathrm{h}^2}{2\sigma^2} \mathrm{trace}\left\{ \left(\tilde{\underline{\mathbf{H}}}_{\mathrm{u},n_\mathrm{B},n_\mathrm{F}}^{\mathrm{T}} \tilde{\underline{\mathbf{H}}}_{\mathrm{u},n_\mathrm{B},n_\mathrm{F}}^{*} \right)^{-1} \right\} \right) \\[2mm]
&= \quad \cdot \left(1 + 2\sigma_\mathrm{h}^2 \cdot \mathrm{trace}\left\{ \left(\tilde{\underline{\mathbf{H}}}_{\mathrm{u},n_\mathrm{B},n_\mathrm{F}}^{\mathrm{T}} \tilde{\underline{\mathbf{H}}}_{\mathrm{u},n_\mathrm{B},n_\mathrm{F}}^{*} \right)^{-1} \right\} \right)
\end{aligned} \tag{8.85}
$$

holds. It can be seen that the degradation factor $\xi_{\mathrm{d},n_\mathrm{F}}$ of (8.85) is greater than one. (8.84) shows that the worse system performance in the DL results from the interference, see (8.82), and the increased transmit energy $T_{\mathrm{d},n_\mathrm{B},n_\mathrm{F}}^{(k)}$ of (8.83) is due to the existence of the CTF estimation error matrix $\tilde{\underline{\mathbf{E}}}_{n_\mathrm{B},n_\mathrm{F}}$ of (8.67).

It is assumed that the QPSK modulation is applied. The bit error probability of (8.32) can be rewritten as

$$
\begin{aligned}
P_{\mathrm{b},\mathrm{d},n_\mathrm{B},n_\mathrm{F}}^{(k)} &= \frac{1}{2}\mathrm{erfc}\left(\sqrt{\frac{\gamma_{\mathrm{d},n_\mathrm{B},n_\mathrm{F}}^{(k)}}{2}} \right) \tag{8.86} \\[4mm]
&= \frac{1}{2}\mathrm{erfc}\left(\sqrt{\frac{\frac{T_{\mathrm{d},n_\mathrm{B},n_\mathrm{F}}^{(k)}}{\sigma^2}}{2\xi_{\mathrm{d},n_\mathrm{F}} \left[\left(\tilde{\underline{\mathbf{H}}}_{\mathrm{u},n_\mathrm{B},n_\mathrm{F}}^{\mathrm{T}} \tilde{\underline{\mathbf{H}}}_{\mathrm{u},n_\mathrm{B},n_\mathrm{F}}^{*} \right)^{-1} \right]_{k,k}}} \right).
\end{aligned}
$$

8.4 Numerical results

8.4.1 Fixed channel snapshot

In order to visualize the analysis in the previous sections an exemplary single–SA scenario with a fixed CTF matrix

$$\underline{\tilde{\mathbf{H}}}_{\mathrm{u},n_{\mathrm{B}},n_{\mathrm{F}}} = \underline{\tilde{\mathbf{H}}}_{\mathrm{d},n_{\mathrm{B}},n_{\mathrm{F}}}^{\mathrm{T}} = \begin{pmatrix} 1 & 2 & 3 \\ 3 & 1 & 1 \\ 2 & 2 & 0 \end{pmatrix}, \tag{8.87}$$

with

$$K_{\mathrm{B}} = K = 3, \tag{8.88}$$

is considered in the present subsection. K equal to 3 data symbols $\underline{\tilde{d}}_{\mathrm{u},n_{\mathrm{B}},n_{\mathrm{F}}}^{(k)}$ and $\underline{\tilde{d}}_{\mathrm{d},n_{\mathrm{B}},n_{\mathrm{F}}}^{(k)}$ are transmitted in the UL and in the DL, which result in the individual bit error probabilities $P_{\mathrm{b},\mathrm{u},n_{\mathrm{B}},n_{\mathrm{F}}}^{(k)}$ in the UL and the bit error probabilities $P_{\mathrm{b},\mathrm{d},n_{\mathrm{B}},n_{\mathrm{F}}}^{(k)}$ in the DL, respectively. For the sake of simplicity and clarity, in the following the bit error probabilities $P_{\mathrm{b},\mathrm{u},n_{\mathrm{B}},n_{\mathrm{F}}}^{(1)}$ and $P_{\mathrm{b},\mathrm{d},n_{\mathrm{B}},n_{\mathrm{F}}}^{(1)}$ of the data symbols $\underline{\tilde{d}}_{\mathrm{u},n_{\mathrm{B}},n_{\mathrm{F}}}^{(1)}$ and $\underline{\tilde{d}}_{\mathrm{d},n_{\mathrm{B}},n_{\mathrm{F}}}^{(1)}$ are depicted.

Firstly, as depicted in Fig. 8.3, the fact that the simulation results with perfect CSI match the theoretical results perfectly illustrates the duality of the UL and the DL performances of JOINT in the case that perfect CSI is available.

Secondly, it is assumed that only the noise plays a role in causing the CTF estimation error $\underline{\tilde{\mathbf{E}}}_{n_{\mathrm{B}},n_{\mathrm{F}}}$ of (8.67). Therefore, with (8.51) the variance σ_{h}^2 of (8.68) is only proportional to the variance σ^2 of the noise, i.e.,

$$\sigma_{\mathrm{h}}^2 = \sigma_{\mathrm{h,n}}^2 \propto \sigma^2. \tag{8.89}$$

In such a case with (8.77) and (8.86) the equality

$$P_{\mathrm{b},\mathrm{u},n_{\mathrm{B}},n_{\mathrm{F}}}^{(1)} = P_{\mathrm{b},\mathrm{d},n_{\mathrm{B}},n_{\mathrm{F}}}^{(1)} \tag{8.90}$$

still holds. As depicted in Fig. 8.3 the simulation results match the theoretical results obtained by (8.77) and (8.86) well. This means that the analysis based on the Taylor series (8.77) and (8.86) are good approximations. The bit error probability curves in such cases are shifted versions of the MF bound, and parallel to the curves of the case with perfect CSI. This shows that the CTF estimation error matrix $\underline{\tilde{\mathbf{E}}}_{n_{\mathrm{B}},n_{\mathrm{F}}}$ of (8.67) caused by the noise only acts like additional noise.

Finally, it is assumed that only the time variance of channels is to be considered to cause the CTF estimation error matrix $\underline{\tilde{\mathbf{E}}}_{n_{\mathrm{B}},n_{\mathrm{F}}}$ of (8.67). In such a case the variance

$$\sigma_{\mathrm{h}}^2 = \sigma_{\mathrm{h,tv}}^2 \tag{8.91}$$

of (8.68) only depends on the time–variant channels according to (8.63). For the fixed channel snapshot of (8.87), the fixed value $\sigma_{\rm h}^2$ equal to 0.09 is simply assumed for the variance $\sigma_{\rm h}^2$ of (8.91), which corresponds to large errors since the standard deviation $\sigma_{\rm h}$ equal to 0.3 is rather high. Due to the fixed variance $\sigma_{\rm h}^2$, which is independent of the variance σ^2 of the noise, the equality of (8.90) does not hold any more. As the ratio $T_{{\rm u},n_{\rm B},n_{\rm F}}^{(k)}/\sigma^2$ increases to very large values, the bit error probability $P_{{\rm b},{\rm u},n_{\rm F}}^{(k)}$ of (8.77) converges to

$$
\begin{aligned}
P_{{\rm b},{\rm u},\infty,n_{\rm B},n_{\rm F}}^{(k)} &= \lim_{\frac{T_{{\rm u},n_{\rm B},n_{\rm F}}^{(k)}}{\sigma^2}\to\infty} P_{{\rm b},{\rm u},n_{\rm B},n_{\rm F}}^{(k)} \\
&\approx \frac{1}{2}{\rm erfc}\left(\sqrt{\frac{1}{4\sigma_{\rm h}^2\cdot K\left[\left(\tilde{\underline{\mathbf{H}}}_{{\rm u},n_{\rm B},n_{\rm F}}^{*{\rm T}}\tilde{\underline{\mathbf{H}}}_{{\rm u},n_{\rm B},n_{\rm F}}\right)^{-1}\right]_{k,k}}}\right).
\end{aligned}
\tag{8.92}
$$

Similarly, as the ratio $T_{{\rm d},n_{\rm B},n_{\rm F}}^{(k)}/\sigma^2$ increases to very large values, the bit error probability $P_{{\rm b},{\rm d},n_{\rm B},n_{\rm F}}^{(k)}$ of (8.86) converges to

$$
\begin{aligned}
P_{{\rm b},{\rm d},\infty,n_{\rm B},n_{\rm F}}^{(k)} &= \lim_{\frac{T_{{\rm d},n_{\rm B},n_{\rm F}}^{(k)}}{\sigma^2}\to\infty} P_{{\rm b},{\rm d},n_{\rm B},n_{\rm F}}^{(k)} \\
&\approx \frac{1}{2}{\rm erfc}\left(\sqrt{\frac{1}{4\sigma_{\rm h}^2\cdot{\rm trace}\left\{\left(\tilde{\underline{\mathbf{H}}}_{{\rm u},n_{\rm B},n_{\rm F}}^{*{\rm T}}\tilde{\underline{\mathbf{H}}}_{{\rm u},n_{\rm B},n_{\rm F}}\right)^{-1}\right\}}}\right).
\end{aligned}
\tag{8.93}
$$

According to (8.92) and (8.93) the bit error probability curves of the UL and of the DL converge to different error floors. This means as well, that (8.90) cannot be satisfied any more for the fixed $\sigma_{\rm h}^2$ of the CTF error $\tilde{\underline{\mathbf{E}}}_{n_{\rm B},n_{\rm F}}$ of (8.67). In other words, imperfect CSI caused by the time–variant channels leads to different error floors of the bit error probability curves in the UL and in the DL. In Fig. 8.4 the mentioned phenomenon can be seen.

8.4.2 Rayleigh fading channel

The influence of imperfect CSI on the individual bit error probabilities $P_{{\rm b},{\rm u},n_{\rm B},n_{\rm F}}^{(1)}$ of (8.77) in the UL and the bit error probabilities $P_{{\rm b},{\rm d},n_{\rm B},n_{\rm F}}^{(1)}$ of (8.86) in the DL with a snapshot of the CTF matrix $\tilde{\underline{\mathbf{H}}}_{{\rm u},n_{\rm B},n_{\rm F}}$ of (8.87) has been analyzed in detail. In the present subsection the average bit error probability performance in a scenario with living Rayleigh fading channels is focused.
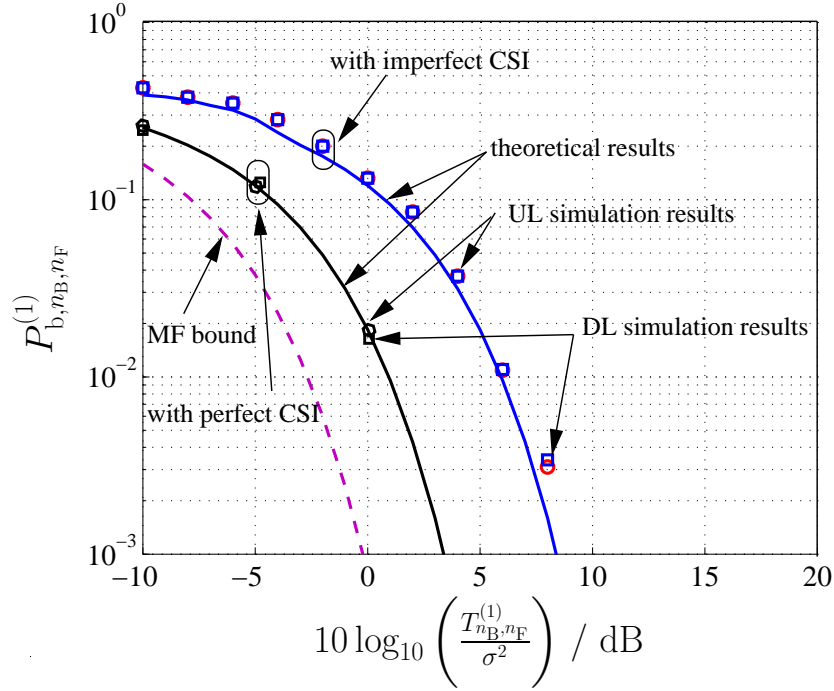
Fig. 8.3. Individual bit error probability $P_{\mathrm{b},n_{\mathrm{B}},n_{\mathrm{F}}}^{(1)}$, if only the noise plays a role in the CTF estimation error $\tilde{\underline{\mathbf{E}}}_{n_{\mathrm{B}},n_{\mathrm{F}}}$, $E_{\mathrm{p}}/E_{\mathrm{d}} = 1$

JCE is applied in the simulations. Both factors, the noise and the time variance of the channels, are taken into account. In order to achieve different degrees of the time variance, different maximum velocities v_{max} of the MTs are assumed. In the simulations, the OFDM frame is assumed to consist of N_{BU} equal to five slots for the UL transmission, N_{BP} equal to one slot for the UL pilot transmission and N_{BD} equal to five slots for the DL transmission. For the other simulation parameters, refer to Table. 3.1.

The average bit error probability $\bar{P}_{\mathrm{b}}$ is obtained by averaging over the fast fading channels, the multiple slots in the UL or in the DL, and the corresponding MTs. T represents the average transmit energy of the data symbols $\underline{\tilde{d}}_{\mathrm{u},n_{\mathrm{F}}}^{(k)}$ for the UL or $\underline{\tilde{d}}_{\mathrm{d},n_{\mathrm{F}}}^{(k)}$ for the DL. As depicted in Fig. 8.5, the $\bar{P}_{\mathrm{b}}$ curves of the UL cases are plotted with solid lines, and the $\bar{P}_{\mathrm{b}}$ curves of the DL cases are plotted with marks. The following conclusions can be drawn from these curves:

- The $\bar{P}_{\mathrm{b}}$ curves in the UL and in the DL are almost the same for the cases with perfect CSI or imperfect CSI.
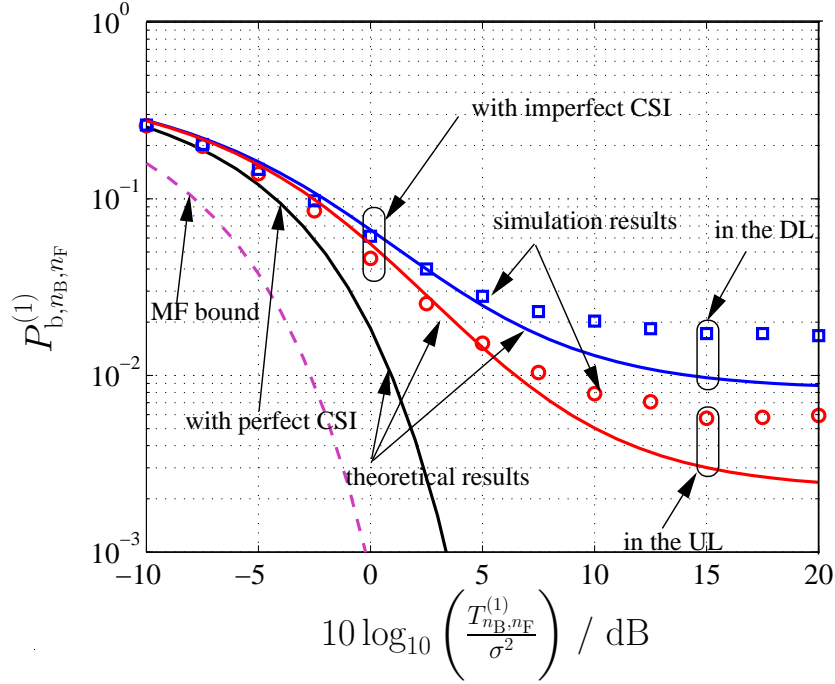
Fig. 8.4. Individual bit error probability $P_{\mathrm{b},n_{\mathrm{B}},n_{\mathrm{F}}}^{(1)}$, if only time variance of channels plays a role in the CTF estimation error $\tilde{\underline{\mathbf{E}}}_{n_{\mathrm{B}},n_{\mathrm{F}}}$

- The noise and the time variance of the channels play a joint role in influencing the JCE performance and the $\bar{P}_{\mathrm{b}}$ performance. For instance, when the noise vanishes, the time variance of channels dominates. Therefore, the $\bar{P}_{\mathrm{b}}$ curves of the cases with imperfect CSI converge to the error floors finally.

- The value of the maximum velocity v_{max} significantly influences the error floors in the cases with imperfect CSI. Different maximum velocities v_{max} correspond to different degrees of the time variance. The greater the maximum velocity v_{max} is, the more significant the time variance of channels appears, and the worse performance becomes, for the fixed frame structure. Therefore, if the MTs move very fast, it should be considered to adjust the frame structure and to process JCE more frequently in order to track the time–variant channels accurately.
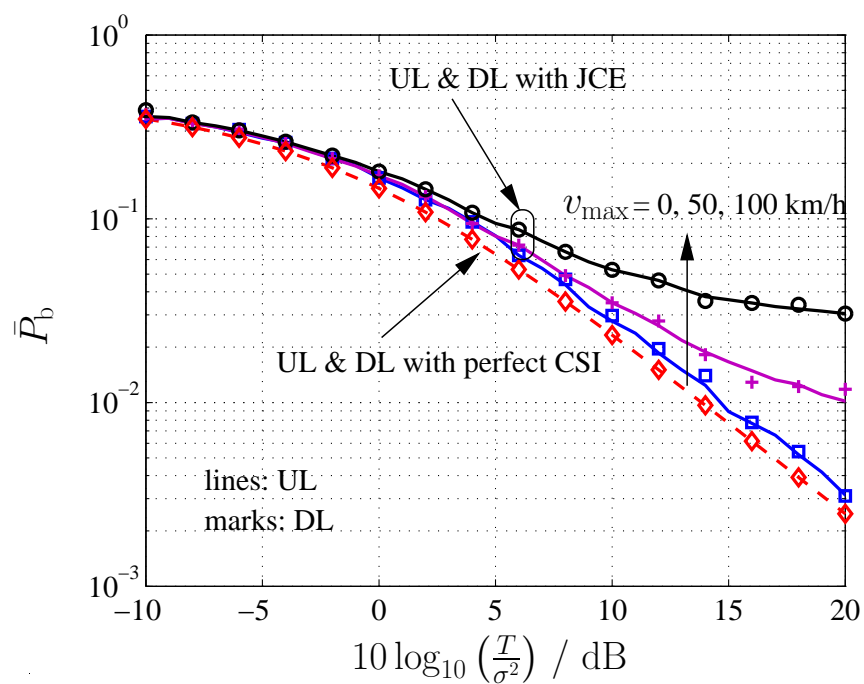
Fig. 8.5. Average bit error probability $\bar{P}_\mathrm{b}$, with the Raleigh fading channel, $K_\mathrm{B} = K = 2$, $N_\mathrm{BU} = N_\mathrm{BD} = 5$, $\Delta t = 32\mu\mathrm{s}$, $N_\mathrm{F} = 512$, $E_\mathrm{p}/E_\mathrm{d} = 1$

Chapter 9

Performance of JOINT in a multiple–service–area scenario

9.1 Preliminary remarks

In Chapter 8 the system performance of JOINT, especially in the single–SA scenario, in which the inter–SA MAI is provisionally not taken into consideration, has been investigated. In reality mobile radio systems are usually interference–limited. Therefore, it is necessary to investigate the performance of JOINT in a multiple–SA scenario, in which not only the noise but also the MAI, including the intra–SA MAI and the inter–SA MAI, are taken into account [LWZ04].

In the present chapter, first the multiple–SA scenario is described. Then the system performance, in terms of the average BERs and the BER statistics, are analyzed based on simulation results carried out with the JOINT simulation chain described in Chapter 7. Moreover, according to some given system criterion the spectrum efficiency of JOINT is studied.

It is assumed that the perfect SA–specific CSI data are available at the corresponding CU for the UL and the DL in the simulations. Since great amounts of simulations have to be carried out, the computational effort is a critical problem. Thanks to the application of OFDM the subcarrierwise processing is possible, see Section 3.2. In the present chapter only an arbitrary subcarrier is considered without loss of generality.

9.2 Multiple–service–area scenario

In order to investigate the advantages of JOINT over conventional cellular systems in the interference elimination, it is necessary to define a multiple–SA scenario, which is comparable to the cellular scenario [LWZ04].

In contrast to cellular systems, the basic entity of JOINT is the SA, consisting of several neighboring sub–areas, which are equivalent to cells in cellular systems. For the sake of simplicity, it is assumed that there is one AP located at the center of each sub–area, and there is at most one active MT randomly distributed in each sub–area.
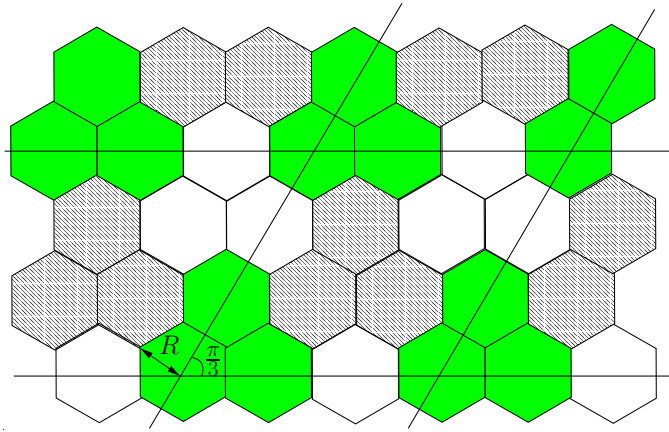
Fig. 9.1. An example of the SA based system architecture with
the SA size $K_{\mathrm{B}} = 3$ and the reuse factor $r = 3$

As depicted in Fig. 9.1, the hexagons represent the sub–areas with radius R, and the APs and the MTs are located in the corresponding hexagonal sub–areas. The radius

$$R = 250 \, \mathrm{m} \tag{9.1}$$

of the hexagonal sub–area is assumed in the following investigations.

The number K_{B} of APs per SA also represents the SA size, indicating how many sub–areas there are per SA. A SA is a cluster of neighboring sub–areas, which share the same frequency resource. Neighboring SAs, which form a cluster of SAs, may use different frequency resources, i.e., the frequency resources can be reused among the different clusters of SAs. The size of the cluster of SAs is described by the reuse factor r. Fig. 9.1 depicts an excerpt of the area, which is covered by the multiple SAs. The neighboring hexagonal sub–areas with the same pattern form a SA using the same frequency resource. The neighboring SAs with different patterns form a cluster of SAs using different frequency resources. The SAs with the same pattern represent the co–channel SAs, in which we are interested. In the case of K_{B} equal to one, i.e., each SA comprising only a single sub–area, the SA–based system architecture is equivalent to the cellular system.

Due to the hexagonal shape of the sub–areas, in most cases the SAs are non–hexagonal, except for the SA size K_{B} equal to one. Because of different combinations of the SA size K_{B} and the reuse factor r, it is difficult to define a scenario with fixed dimensions, in which the SA based system architectures are applied. Fortunately, it is found that, whatever the SAs look like, if one of the APs in one SA is chosen as the reference AP, the reference APs of the neighboring four co–channel SAs always form a diamond,
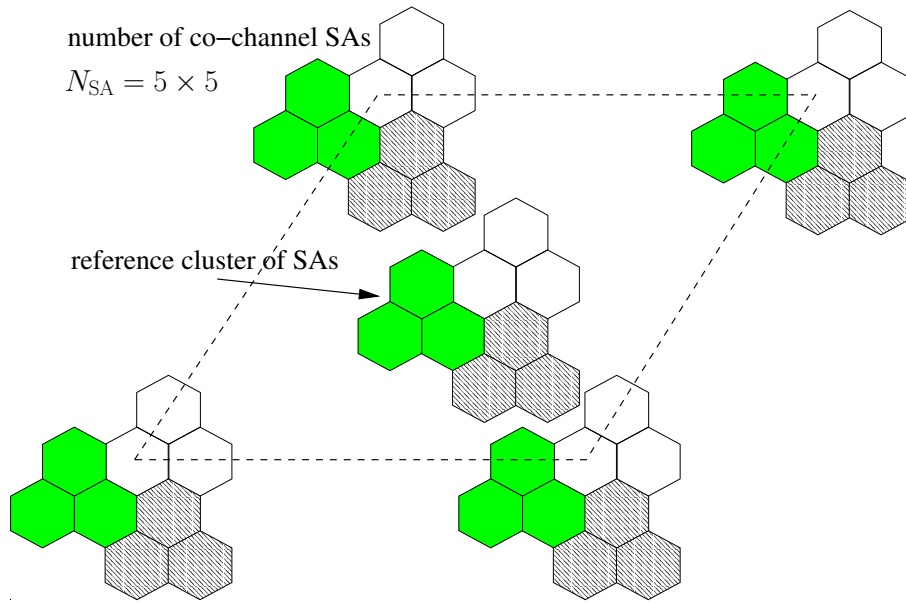
number of co–channel SAs
$N_{\text{SA}} = 5 \times 5$

reference cluster of SAs

Fig. 9.2. Considered area with the SA size $K_{\text{B}} = 3$ and the reuse
factor $r = 3$

as depicted in Fig. 9.1. In other words, the reference APs of the co–channel SAs are
located along a parallelogram grid. In the following simulations, instead of a scenario
with fixed dimensions, the quasi–parallelogram scenario with the fixed number N_{SA} of
the co–channel SAs, e.g.,

$$N_{\text{SA}} = 5 \times 5, \tag{9.2}$$

are investigated. As shown in Fig. 9.2, the reference cluster of SAs is at the center of the
given scenario. Most co–channel interfering SAs, which have the dominant influence
on the reference SA are included so that with a finite scenario we can approximate the
ideal infinite scenario.

The random channel with Rayleigh fading and log–normal fading described in Subsec-
tion 2.3.2 is assumed in the investigation. Concerning the slow fading, the dual–slope
model [XBMLS92] is applied. For the corresponding channel parameters, refer to Table
3.1 in Section 3.4.

In the multiple–SA scenario described above, the distances between the MTs and APs
play a role to determine the CTFs between the MTs and the APs since slow fading
is taken into account. Therefore, the positions of the APs and the MTs are critical
concerning the scenario realizations. Unlike conventional cellular systems, the challenge
of implementation of such a multiple–SA scenario lies in locating the APs and the MTs
based on the SA concept. For the details on the positions of the APs and the MTs,
refer to Appendix A.

9.3 Modified system model

9.3.1 Uplink system model in a multiple–service–area scenario

The UL and DL system models introduced in Sections 5.2 and 6.2 have to be extended to adapt to the multiple–SA scenario [LWZ04]. On the considered subcarrier n_F, the total UL data vector of dimension KN_SA reads

$$
\begin{aligned}
\underline{\tilde{\mathbf{d}}}_{\mathrm{u,mul},n_\mathrm{F}} &= \left({\underline{\tilde{\mathbf{d}}}_{\mathrm{u},n_\mathrm{F}}^{(1)}}^{\mathrm{T}} \cdots \underline{\tilde{\mathbf{d}}}_{\mathrm{u},n_\mathrm{F}}^{(N_\mathrm{SA})\mathrm{T}} \right)^{\mathrm{T}} \\
&= \left(\underline{\tilde{d}}_{\mathrm{u},n_\mathrm{F}}^{(1)} \cdots \underline{\tilde{d}}_{\mathrm{u},n_\mathrm{F}}^{(K)} \cdots \underline{\tilde{d}}_{\mathrm{u},n_\mathrm{F}}^{((N_\mathrm{SA}-1)K+1)} \cdots \underline{\tilde{d}}_{\mathrm{u},n_\mathrm{F}}^{((N_\mathrm{SA}-1)K+K)} \right)^{\mathrm{T}} .
\end{aligned}
\tag{9.3}
$$

The total UL CTF matrix

$$
\underline{\tilde{\mathbf{H}}}_{\mathrm{u,mul},n_\mathrm{F}} = \begin{pmatrix} \underline{\tilde{\mathbf{H}}}_{n_\mathrm{F}}^{(1,1)} & \cdots & \underline{\tilde{\mathbf{H}}}_{n_\mathrm{F}}^{(N_\mathrm{SA},1)} \\ \vdots & & \vdots \\ \underline{\tilde{\mathbf{H}}}_{n_\mathrm{F}}^{(1,N_\mathrm{SA})} & \cdots & \underline{\tilde{\mathbf{H}}}_{n_\mathrm{F}}^{(N_\mathrm{SA},N_\mathrm{SA})} \end{pmatrix}
\tag{9.4}
$$

of the whole scenario consists of $N_\mathrm{SA} \times N_\mathrm{SA}$ submatrices

$$
\underline{\tilde{\mathbf{H}}}_{n_\mathrm{F}}^{(n_\mathrm{SA},n'_\mathrm{SA})} = \begin{pmatrix} \underline{\tilde{h}}_{n_\mathrm{F}}^{((n_\mathrm{SA}-1)K+1,(n'_\mathrm{SA}-1)K_\mathrm{B}+1)} & \cdots & \underline{\tilde{h}}_{n_\mathrm{F}}^{((n_\mathrm{SA}-1)K+K,(n'_\mathrm{SA}-1)K_\mathrm{B}+1)} \\ \vdots & & \vdots \\ \underline{\tilde{h}}_{n_\mathrm{F}}^{((n_\mathrm{SA}-1)K+1,(n'_\mathrm{SA}-1)K_\mathrm{B}+K_\mathrm{B})} & \cdots & \underline{\tilde{h}}_{n_\mathrm{F}}^{((n_\mathrm{SA}-1)K+K,(n'_\mathrm{SA}-1)K_\mathrm{B}+K_\mathrm{B})} \end{pmatrix} , \tag{9.5}
$$

each of dimensions $K_\mathrm{B} \times K$ including the CTFs between the K MTs in the SA n_SA, $n_\mathrm{SA} = 1 \ldots N_\mathrm{SA}$, and the K_B APs in the SA n'_SA, $n'_\mathrm{SA} = 1 \ldots N_\mathrm{SA}$. With (9.4) and the total UL noise vector

$$
\begin{aligned}
\underline{\tilde{\mathbf{n}}}_{\mathrm{u,mul},n_\mathrm{F}} &= \left({\underline{\tilde{\mathbf{n}}}_{\mathrm{u},n_\mathrm{F}}^{(1)}}^{\mathrm{T}} \cdots \underline{\tilde{\mathbf{n}}}_{\mathrm{u},n_\mathrm{F}}^{(N_\mathrm{SA})\mathrm{T}} \right)^{\mathrm{T}} \\
&= \left(\underline{\tilde{n}}_{\mathrm{u},n_\mathrm{F}}^{(1)} \cdots \underline{\tilde{n}}_{\mathrm{u},n_\mathrm{F}}^{(K_\mathrm{B})} \cdots \underline{\tilde{n}}_{\mathrm{u},n_\mathrm{F}}^{((N_\mathrm{SA}-1)K_\mathrm{B}+1)} \cdots \underline{\tilde{n}}_{\mathrm{u},n_\mathrm{F}}^{((N_\mathrm{SA}-1)K_\mathrm{B}+K_\mathrm{B})} \right)^{\mathrm{T}}
\end{aligned}
\tag{9.6}
$$

of dimension $K_\mathrm{B}N_\mathrm{SA}$ the total UL receive vector

$$
\begin{aligned}
\underline{\tilde{\mathbf{e}}}_{\mathrm{u,mul},n_\mathrm{F}} &= \left({\underline{\tilde{\mathbf{e}}}_{\mathrm{u},n_\mathrm{F}}^{(1)}}^{\mathrm{T}} \cdots \underline{\tilde{\mathbf{e}}}_{\mathrm{u},n_\mathrm{F}}^{(N_\mathrm{SA})\mathrm{T}} \right)^{\mathrm{T}} \\
&= \left(\underline{\tilde{e}}_{\mathrm{u},n_\mathrm{F}}^{(1)} \cdots \underline{\tilde{e}}_{\mathrm{u},n_\mathrm{F}}^{(K_\mathrm{B})} \cdots \underline{\tilde{e}}_{\mathrm{u},n_\mathrm{F}}^{((N_\mathrm{SA}-1)K_\mathrm{B}+1)} \cdots \underline{\tilde{e}}_{\mathrm{u},n_\mathrm{F}}^{((N_\mathrm{SA}-1)K_\mathrm{B}+K_\mathrm{B})} \right)^{\mathrm{T}}
\end{aligned}
\tag{9.7}
$$

of dimension $K_\mathrm{B}N_\mathrm{SA}$ becomes

$$
\underline{\tilde{\mathbf{e}}}_{\mathrm{u,mul},n_\mathrm{F}} = \underline{\tilde{\mathbf{H}}}_{\mathrm{u,mul},n_\mathrm{F}} \underline{\tilde{\mathbf{d}}}_{\mathrm{u,mul},n_\mathrm{F}} + \underline{\tilde{\mathbf{n}}}_{\mathrm{u,mul},n_\mathrm{F}}
\tag{9.8}
$$

according to (3.17) and (5.4). Concerning the SA n_{SA}, with the application of the linear RxZF JD [Kle96, Skl04] the SA–specific data estimate vector $\hat{\tilde{\underline{\mathbf{d}}}}_{\mathrm{u},n_{\mathrm{F}}}^{(n_{\mathrm{SA}})}$ of (5.11) can be rewritten as [LWZ04]

$$
\begin{aligned}
\hat{\tilde{\underline{\mathbf{d}}}}_{\mathrm{u},n_{\mathrm{F}}}^{(n_{\mathrm{SA}})} \;=\;& \left(\tilde{\underline{\mathbf{H}}}_{n_{\mathrm{F}}}^{(n_{\mathrm{SA}},n_{\mathrm{SA}})*\mathrm{T}} \tilde{\underline{\mathbf{H}}}_{n_{\mathrm{F}}}^{(n_{\mathrm{SA}},n_{\mathrm{SA}})} \right)^{-1} \tilde{\underline{\mathbf{H}}}_{n_{\mathrm{F}}}^{(n_{\mathrm{SA}},n_{\mathrm{SA}})*\mathrm{T}} \tilde{\underline{\mathbf{e}}}_{\mathrm{u},n_{\mathrm{F}}}^{(n_{\mathrm{SA}})} \\[2mm]
\;=\;& \tilde{\underline{\mathbf{d}}}_{\mathrm{u},n_{\mathrm{F}}}^{(n_{\mathrm{SA}})} + \underbrace{\left(\tilde{\underline{\mathbf{H}}}_{n_{\mathrm{F}}}^{(n_{\mathrm{SA}},n_{\mathrm{SA}})*\mathrm{T}} \tilde{\underline{\mathbf{H}}}_{n_{\mathrm{F}}}^{(n_{\mathrm{SA}},n_{\mathrm{SA}})} \right)^{-1} \tilde{\underline{\mathbf{H}}}_{n_{\mathrm{F}}}^{(n_{\mathrm{SA}},n_{\mathrm{SA}})*\mathrm{T}} \sum_{n_{\mathrm{SA}}'\neq n_{\mathrm{SA}}} \tilde{\underline{\mathbf{H}}}_{\mathrm{u},n_{\mathrm{F}}}^{(n_{\mathrm{SA}}',n_{\mathrm{SA}})} \tilde{\underline{\mathbf{d}}}_{n_{\mathrm{F}}}^{(n_{\mathrm{SA}}')}}_{\mathrm{inter-SA\ MAI}} \\[2mm]
& + \underbrace{\left(\tilde{\underline{\mathbf{H}}}_{n_{\mathrm{F}}}^{(n_{\mathrm{SA}},n_{\mathrm{SA}})*\mathrm{T}} \tilde{\underline{\mathbf{H}}}_{n_{\mathrm{F}}}^{(n_{\mathrm{SA}},n_{\mathrm{SA}})} \right)^{-1} \tilde{\underline{\mathbf{H}}}_{n_{\mathrm{F}}}^{(n_{\mathrm{SA}},n_{\mathrm{SA}})*\mathrm{T}} \tilde{\underline{\mathbf{n}}}_{n_{\mathrm{F}}}^{(n_{\mathrm{SA}})}}_{\mathrm{enhanced\ noise}} .
\end{aligned} \tag{9.9}
$$

It can be seen that the data estimate vector $\hat{\tilde{\underline{\mathbf{d}}}}_{\mathrm{u},n_{\mathrm{F}}}^{(n_{\mathrm{SA}})}$ of (9.9) is not unbiased any more, since the RxZF detector matrix $\left(\tilde{\underline{\mathbf{H}}}_{n_{\mathrm{F}}}^{(n_{\mathrm{SA}},n_{\mathrm{SA}})*\mathrm{T}} \tilde{\underline{\mathbf{H}}}_{n_{\mathrm{F}}}^{(n_{\mathrm{SA}},n_{\mathrm{SA}})} \right)^{-1} \tilde{\underline{\mathbf{H}}}_{n_{\mathrm{F}}}^{(n_{\mathrm{SA}},n_{\mathrm{SA}})*\mathrm{T}}$ of (9.9), which is designed for the SA n_{SA}, cannot counteract the interfering signals $\sum_{n_{\mathrm{SA}}'\neq n_{\mathrm{SA}}} \tilde{\underline{\mathbf{H}}}_{\mathrm{u},n_{\mathrm{F}}}^{(n_{\mathrm{SA}}',n_{\mathrm{SA}})} \tilde{\underline{\mathbf{d}}}_{n_{\mathrm{F}}}^{(n_{\mathrm{SA}}')}$ of (9.9) from the other co–channel SAs n_{SA}'. Both the inter–SA MAI $\left(\tilde{\underline{\mathbf{H}}}_{n_{\mathrm{F}}}^{(n_{\mathrm{SA}},n_{\mathrm{SA}})*\mathrm{T}} \tilde{\underline{\mathbf{H}}}_{n_{\mathrm{F}}}^{(n_{\mathrm{SA}},n_{\mathrm{SA}})} \right)^{-1} \tilde{\underline{\mathbf{H}}}_{n_{\mathrm{F}}}^{(n_{\mathrm{SA}},n_{\mathrm{SA}})*\mathrm{T}} \sum_{n_{\mathrm{SA}}'\neq n_{\mathrm{SA}}} \tilde{\underline{\mathbf{H}}}_{\mathrm{u},n_{\mathrm{F}}}^{(n_{\mathrm{SA}}',n_{\mathrm{SA}})} \tilde{\underline{\mathbf{d}}}_{n_{\mathrm{F}}}^{(n_{\mathrm{SA}}')}$ of (9.9) and the enhanced noise $\left(\tilde{\underline{\mathbf{H}}}_{n_{\mathrm{F}}}^{(n_{\mathrm{SA}},n_{\mathrm{SA}})*\mathrm{T}} \tilde{\underline{\mathbf{H}}}_{n_{\mathrm{F}}}^{(n_{\mathrm{SA}},n_{\mathrm{SA}})} \right)^{-1} \tilde{\underline{\mathbf{H}}}_{n_{\mathrm{F}}}^{(n_{\mathrm{SA}},n_{\mathrm{SA}})*\mathrm{T}} \tilde{\underline{\mathbf{n}}}_{n_{\mathrm{F}}}^{(n_{\mathrm{SA}})}$ of (9.9) account for the UL data estimation error vector [LWZ04]

$$
\begin{aligned}
\hat{\tilde{\underline{\mathbf{d}}}}_{\mathrm{u},n_{\mathrm{F}}}^{(n_{\mathrm{SA}})} - \tilde{\underline{\mathbf{d}}}_{\mathrm{u},n_{\mathrm{F}}}^{(n_{\mathrm{SA}})} \;=\;& \underbrace{\left(\tilde{\underline{\mathbf{H}}}_{n_{\mathrm{F}}}^{(n_{\mathrm{SA}},n_{\mathrm{SA}})*\mathrm{T}} \tilde{\underline{\mathbf{H}}}_{n_{\mathrm{F}}}^{(n_{\mathrm{SA}},n_{\mathrm{SA}})} \right)^{-1} \tilde{\underline{\mathbf{H}}}_{n_{\mathrm{F}}}^{(n_{\mathrm{SA}},n_{\mathrm{SA}})*\mathrm{T}} \sum_{n_{\mathrm{SA}}'\neq n_{\mathrm{SA}}} \tilde{\underline{\mathbf{H}}}_{\mathrm{u},n_{\mathrm{F}}}^{(n_{\mathrm{SA}}',n_{\mathrm{SA}})} \tilde{\underline{\mathbf{d}}}_{n_{\mathrm{F}}}^{(n_{\mathrm{SA}}')}}_{\mathrm{inter-SA\ MAI}} \\[2mm]
& + \underbrace{\left(\tilde{\underline{\mathbf{H}}}_{n_{\mathrm{F}}}^{(n_{\mathrm{SA}},n_{\mathrm{SA}})*\mathrm{T}} \tilde{\underline{\mathbf{H}}}_{n_{\mathrm{F}}}^{(n_{\mathrm{SA}},n_{\mathrm{SA}})} \right)^{-1} \tilde{\underline{\mathbf{H}}}_{n_{\mathrm{F}}}^{(n_{\mathrm{SA}},n_{\mathrm{SA}})*\mathrm{T}} \tilde{\underline{\mathbf{n}}}_{n_{\mathrm{F}}}^{(n_{\mathrm{SA}})}}_{\mathrm{enhanced\ noise}}
\end{aligned} \tag{9.10}
$$

in the corresponding SA n_{SA}.

9.3.2 Downlink system model in a multiple–service–area scenario

On the subcarrier n_{F}, the total DL data vector of dimension KN_{SA} reads

$$
\begin{aligned}
\tilde{\underline{\mathbf{d}}}_{\mathrm{d,mul},n_{\mathrm{F}}} \;=\;& \left(\tilde{\underline{\mathbf{d}}}_{\mathrm{d},n_{\mathrm{F}}}^{(1)\,\mathrm{T}} \ldots \tilde{\underline{\mathbf{d}}}_{\mathrm{d},n_{\mathrm{F}}}^{(N_{\mathrm{SA}})\mathrm{T}} \right)^{\mathrm{T}} \\[2mm]
\;=\;& \left(\tilde{\underline{d}}_{\mathrm{d},n_{\mathrm{F}}}^{(1)} \ldots \tilde{\underline{d}}_{\mathrm{d},n_{\mathrm{F}}}^{(K)} \ldots \tilde{\underline{d}}_{\mathrm{d},n_{\mathrm{F}}}^{((N_{\mathrm{SA}}-1)K+1)} \ldots \tilde{\underline{d}}_{\mathrm{d},n_{\mathrm{F}}}^{((N_{\mathrm{SA}}-1)K+K)} \right)^{\mathrm{T}} .
\end{aligned} \tag{9.11}
$$

Concerning the SA n_{SA}, with the application of the linear TxZF JT [MBW$^+$00, TWMB01, Skl04], the SA–specific DL transmit vector of (6.2) reads

$$\underline{\tilde{\mathbf{s}}}_{\mathrm{d},n_{\mathrm{F}}}^{(n_{\mathrm{SA}})} = \underbrace{\underline{\tilde{\mathbf{H}}}_{n_{\mathrm{F}}}^{(n_{\mathrm{SA}},n_{\mathrm{SA}})^*} \left(\underline{\tilde{\mathbf{H}}}_{n_{\mathrm{F}}}^{(n_{\mathrm{SA}},n_{\mathrm{SA}})^{\mathrm{T}}} \underline{\tilde{\mathbf{H}}}_{n_{\mathrm{F}}}^{(n_{\mathrm{SA}},n_{\mathrm{SA}})^*} \right)^{-1}}_{\underline{\tilde{\mathbf{M}}}_{\mathrm{TxZF},n_{\mathrm{F}}}^{(n_{\mathrm{SA}})}} \underline{\tilde{\mathbf{d}}}_{\mathrm{d},n_{\mathrm{F}}}^{(n_{\mathrm{SA}})}. \tag{9.12}$$

With the total UL CDF matrix $\underline{\tilde{\mathbf{H}}}_{\mathrm{u,mul},n_{\mathrm{F}}}$ of (9.4), with the total DL transmit vector

$$\underline{\tilde{\mathbf{s}}}_{\mathrm{d,mul},n_{\mathrm{F}}} = \left(\underline{\tilde{\mathbf{s}}}_{\mathrm{d},n_{\mathrm{F}}}^{(1)^{\mathrm{T}}} \cdots \underline{\tilde{\mathbf{s}}}_{\mathrm{d},n_{\mathrm{F}}}^{(N_{\mathrm{SA}})^{\mathrm{T}}} \right)^{\mathrm{T}} \tag{9.13}$$

of dimension $K_{\mathrm{B}}N_{\mathrm{SA}}$ consisting of N_{SA} SA–specific transmit vector $\underline{\tilde{\mathbf{s}}}_{\mathrm{d},n_{\mathrm{F}}}^{(n_{\mathrm{SA}})}$ of (9.13) and with the total DL noise vector

$$
\begin{aligned}
\underline{\tilde{\mathbf{n}}}_{\mathrm{d,mul},n_{\mathrm{F}}} &= \left(\underline{\tilde{\mathbf{n}}}_{\mathrm{d},n_{\mathrm{F}}}^{(1)^{\mathrm{T}}} \cdots \underline{\tilde{\mathbf{n}}}_{\mathrm{d},n_{\mathrm{F}}}^{(N_{\mathrm{SA}})^{\mathrm{T}}} \right)^{\mathrm{T}} \\
&= \left(\underline{\tilde{n}}_{\mathrm{d},n_{\mathrm{F}}}^{(1)} \cdots \underline{\tilde{n}}_{\mathrm{d},n_{\mathrm{F}}}^{(K)} \cdots \underline{\tilde{n}}_{\mathrm{d},n_{\mathrm{F}}}^{((N_{\mathrm{SA}}-1)K+1)} \cdots \underline{\tilde{n}}_{\mathrm{d},n_{\mathrm{F}}}^{((N_{\mathrm{SA}}-1)K+K)} \right)^{\mathrm{T}}
\end{aligned} \tag{9.14}
$$

of dimension KN_{SA} the total DL receive vector

$$
\begin{aligned}
\underline{\tilde{\mathbf{e}}}_{\mathrm{d,mul},n_{\mathrm{F}}} &= \left(\underline{\tilde{\mathbf{e}}}_{\mathrm{d},n_{\mathrm{F}}}^{(1)^{\mathrm{T}}} \cdots \underline{\tilde{\mathbf{e}}}_{\mathrm{d},n_{\mathrm{F}}}^{(N_{\mathrm{SA}})^{\mathrm{T}}} \right)^{\mathrm{T}} \\
&= \left(\underline{\tilde{e}}_{\mathrm{d},n_{\mathrm{F}}}^{(1)} \cdots \underline{\tilde{e}}_{\mathrm{d},n_{\mathrm{F}}}^{(K)} \cdots \underline{\tilde{e}}_{\mathrm{d},n_{\mathrm{F}}}^{((N_{\mathrm{SA}}-1)K+1)} \cdots \underline{\tilde{e}}_{\mathrm{d},n_{\mathrm{F}}}^{((N_{\mathrm{SA}}-1)K+K)} \right)^{\mathrm{T}}
\end{aligned} \tag{9.15}
$$

of dimension KN_{SA} is constructed as

$$\underline{\tilde{\mathbf{e}}}_{\mathrm{d,mul},n_{\mathrm{F}}} = \underline{\tilde{\mathbf{H}}}_{\mathrm{u,mul},n_{\mathrm{F}}}^{\mathrm{T}} \underline{\tilde{\mathbf{s}}}_{\mathrm{d,mul},n_{\mathrm{F}}} + \underline{\tilde{\mathbf{n}}}_{\mathrm{d,mul},n_{\mathrm{F}}}. \tag{9.16}$$

Consequently, the SA–specific data estimate vector

$$
\begin{aligned}
\underline{\hat{\tilde{\mathbf{d}}}}_{\mathrm{d},n_{\mathrm{F}}}^{(n_{\mathrm{SA}})} &= \underline{\tilde{\mathbf{e}}}_{\mathrm{d},n_{\mathrm{F}}}^{(n_{\mathrm{SA}})} \\
&= \underline{\tilde{\mathbf{d}}}_{\mathrm{d},n_{\mathrm{F}}}^{(n_{\mathrm{SA}})} + \underline{\tilde{\mathbf{n}}}_{\mathrm{d},n_{\mathrm{F}}}^{(n_{\mathrm{SA}})} \\
&\quad + \underbrace{\sum_{n_{\mathrm{SA}}' \neq n_{\mathrm{SA}}} \underline{\tilde{\mathbf{H}}}_{n_{\mathrm{F}}}^{(n_{\mathrm{SA}},n_{\mathrm{SA}}')^{\mathrm{T}}} \underline{\tilde{\mathbf{H}}}_{n_{\mathrm{F}}}^{(n_{\mathrm{SA}}',n_{\mathrm{SA}}')^*} \left(\underline{\tilde{\mathbf{H}}}_{n_{\mathrm{F}}}^{(n_{\mathrm{SA}}',n_{\mathrm{SA}}')^{\mathrm{T}}} \underline{\tilde{\mathbf{H}}}_{n_{\mathrm{F}}}^{(n_{\mathrm{SA}}',n_{\mathrm{SA}}')^*} \right)^{-1} \underline{\tilde{\mathbf{d}}}_{\mathrm{d},n_{\mathrm{F}}}^{(n_{\mathrm{SA}}')}}_{\mathrm{inter-SA\ MAI}}
\end{aligned} \tag{9.17}
$$

of the SA–specific data vector $\underline{\tilde{\mathbf{d}}}_{\mathrm{d},n_{\mathrm{F}}}^{(n_{\mathrm{SA}})}$ of (9.11) is obtained.

It can be seen that the SA–specific data estimate vector $\underline{\hat{\tilde{\mathbf{d}}}}_{\mathrm{d},n_{\mathrm{F}}}^{(n_{\mathrm{SA}})}$ of (9.17) is not unbiased any more due to the inter–SA MAI $\sum_{n_{\mathrm{SA}}' \neq n_{\mathrm{SA}}} \underline{\tilde{\mathbf{H}}}_{n_{\mathrm{F}}}^{(n_{\mathrm{SA}},n_{\mathrm{SA}}')^{\mathrm{T}}} \underline{\tilde{\mathbf{H}}}_{n_{\mathrm{F}}}^{(n_{\mathrm{SA}}',n_{\mathrm{SA}}')^*} \left(\underline{\tilde{\mathbf{H}}}_{n_{\mathrm{F}}}^{(n_{\mathrm{SA}}',n_{\mathrm{SA}}')^{\mathrm{T}}} \underline{\tilde{\mathbf{H}}}_{n_{\mathrm{F}}}^{(n_{\mathrm{SA}}',n_{\mathrm{SA}}')^*} \right)^{-1} \underline{\tilde{\mathbf{d}}}_{\mathrm{d},n_{\mathrm{F}}}^{(n_{\mathrm{SA}}')}$ of (9.17)

coming from the other co–channel SAs n'_{SA}. The inter–SA MAI $\sum_{n'_{\mathrm{SA}} \neq n_{\mathrm{SA}}} \tilde{\underline{\mathbf{H}}}_{n_{\mathrm{F}}}^{(n_{\mathrm{SA}},n'_{\mathrm{SA}})\mathrm{T}} \tilde{\underline{\mathbf{H}}}_{n_{\mathrm{F}}}^{(n'_{\mathrm{SA}},n'_{\mathrm{SA}})*} \left(\tilde{\underline{\mathbf{H}}}_{n_{\mathrm{F}}}^{(n'_{\mathrm{SA}},n'_{\mathrm{SA}})\mathrm{T}} \tilde{\underline{\mathbf{H}}}_{n_{\mathrm{F}}}^{(n'_{\mathrm{SA}},n'_{\mathrm{SA}})*} \right)^{-1} \tilde{\underline{\mathbf{d}}}_{\mathrm{d},n_{\mathrm{F}}}^{(n'_{\mathrm{SA}})}$ of (9.17) and the noise $\tilde{\underline{\mathbf{n}}}_{\mathrm{d},n_{\mathrm{F}}}^{(n_{\mathrm{SA}})}$ of (9.17) account for the DL data estimation error vector

$$\hat{\tilde{\underline{\mathbf{d}}}}_{\mathrm{d},n_{\mathrm{F}}}^{(n_{\mathrm{SA}})} - \tilde{\underline{\mathbf{d}}}_{\mathrm{d},n_{\mathrm{F}}}^{(n_{\mathrm{SA}})} = \tilde{\underline{\mathbf{n}}}_{\mathrm{d},n_{\mathrm{F}}}^{(n_{\mathrm{SA}})} \qquad (9.18)$$
$$+ \underbrace{\sum_{n'_{\mathrm{SA}} \neq n_{\mathrm{SA}}} \tilde{\underline{\mathbf{H}}}_{n_{\mathrm{F}}}^{(n_{\mathrm{SA}},n'_{\mathrm{SA}})\mathrm{T}} \tilde{\underline{\mathbf{H}}}_{n_{\mathrm{F}}}^{(n'_{\mathrm{SA}},n'_{\mathrm{SA}})*} \left(\tilde{\underline{\mathbf{H}}}_{n_{\mathrm{F}}}^{(n'_{\mathrm{SA}},n'_{\mathrm{SA}})\mathrm{T}} \tilde{\underline{\mathbf{H}}}_{n_{\mathrm{F}}}^{(n'_{\mathrm{SA}},n'_{\mathrm{SA}})*} \right)^{-1} \tilde{\underline{\mathbf{d}}}_{\mathrm{d},n_{\mathrm{F}}}^{(n'_{\mathrm{SA}})}}_{\mathrm{inter-SA\ MAI}}$$

in the corresponding SA n_{SA}.

9.4 Average bit error rate

In the system where the noise and the MAI are considered, the average BERs $\bar{P}_{\mathrm{b}}$ versus the pseudo SNR, i.e., the ratio T/σ^2 of the average transmit energy T of the data symbols $\tilde{\underline{d}}_{\mathrm{u},n_{\mathrm{F}}}^{(k)}$ or $\tilde{\underline{d}}_{\mathrm{d},n_{\mathrm{F}}}^{(k)}$ to the variance σ^2 of the noise reveal the performance, especially from the viewpoint of the energy transmission, as discussed in Subsection 8.2.2. Thermal noise is assumed at the receiver. Described by the noise figure F [Cou97], which is an inherent property of the receiver device, the noise variance σ^2 of (4.12), (5.6) and (6.7), reads [Cou97]

$$\sigma^2 = \kappa\, T_0\, B\, F, \qquad (9.19)$$

where κ is Boltzmann's constant equal to 1.38×10^{-23} J/K, T_0 is the absolute temperature, e.g., equal to 290 K, and the bandwidth B of the considered system is equal to the subcarrier spacing $\Delta f_{n_{\mathrm{F}}}$ of Table 3.1, since only a single subcarrier is considered in the following investigation. With (9.19) the logarithmic ratio

$$\begin{aligned} 10 \log_{10} \left(\frac{T}{\sigma^2} \right) &= 10 \log_{10} \left(\frac{T}{10^{-3}\,\mathrm{w}} \right) - 10 \log_{10} F + 10 \log_{10} \left(\frac{10^{-3}\,\mathrm{w}}{\kappa\, T_0\, B} \right) \\ &= T_{\mathrm{dBm}} - F_{\mathrm{dB}} + \mathrm{const} \end{aligned} \qquad (9.20)$$

depends only on the difference between the logarithmic average transmit energy T_{dBm} in dBm and the logarithmic noise figure F_{dB} in dB. The average BERs $\bar{P}_{\mathrm{b}}$ are averaged over all the individual BERs P_{b} in the UL and in the DL, respectively, in the reference SA, which is the considered SA in the central cluster of SAs, as depicted in Fig. 9.2. In the present section the simulation results are plotted as the curves of the average BERs $\bar{P}_{\mathrm{b}}$ versus the difference $T_{\mathrm{dBm}}/\mathrm{dBm} - F_{\mathrm{dB}}/\mathrm{dB}$. In the real system with a limit of total transmit power 30 dBm [Cou97], the typical values

$$T_{\mathrm{dBm}} = 30\,\mathrm{dBm} - 10 \log_{10} N_{\mathrm{F}} = 30\,\mathrm{dBm} - 10 \log_{10} 512 = 3\,\mathrm{dBm} \qquad (9.21)$$

and

$$F_{\mathrm{dB}} = 5\,\mathrm{dB} \qquad (9.22)$$

are usually valid.

Fig. 9.3 depicts the average BER performances of the equivalent cellular system, i.e., of the cases of

$$K_{\mathrm{B}} = K = 1, \qquad (9.23)$$

for different reuse factors r in the UL and in the DL, respectively. The average BER $\bar{P}_{\mathrm{b}}$ curves in the UL are plotted with solid lines, and the $\bar{P}_{\mathrm{b}}$ curves in the DL are plotted with marks. It is seen that the average $\bar{P}_{\mathrm{b}}$ curves perform almost the same in the UL and in the DL for the different reuse factors $r = 1, 3, 4, 7$, respectively. It proves that the prices paid for the interference elimination with the application of linear ZF [Kle96, Skl04] are the same in the UL and in the DL. This phenomenon is consistent with the conclusion drawn in Section 8.2 concerning the duality of the UL and the DL with perfect CSI.
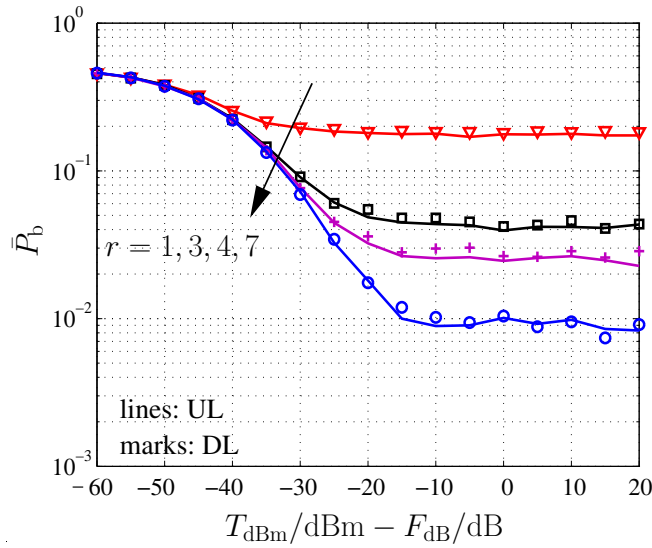
Fig. 9.3. Average BERs $\bar{P}_{\mathrm{b}}$ in the reference SA, $K_{\mathrm{B}} = K = 1$

Figs. 9.3 to 9.6 depict the average BER performances of JOINT with different combinations of the number K of MTs per SA, the number K_{B} of APs per SA and the reuse factor r, in the UL and in the DL, respectively. The $\bar{P}_{\mathrm{b}}$ curves of the equivalent cellular system for the corresponding reuse factors r are plotted with dashed lines as references. The following can be stated:

- The $\bar{P}_{\mathrm{b}}$ curves converge to error floors [LWZ04]. Since either the RxZF JD [Kle96, Skl04] or the TxZF JT [MBL$^+$00, TWMB01, Skl04] at the CU is applied
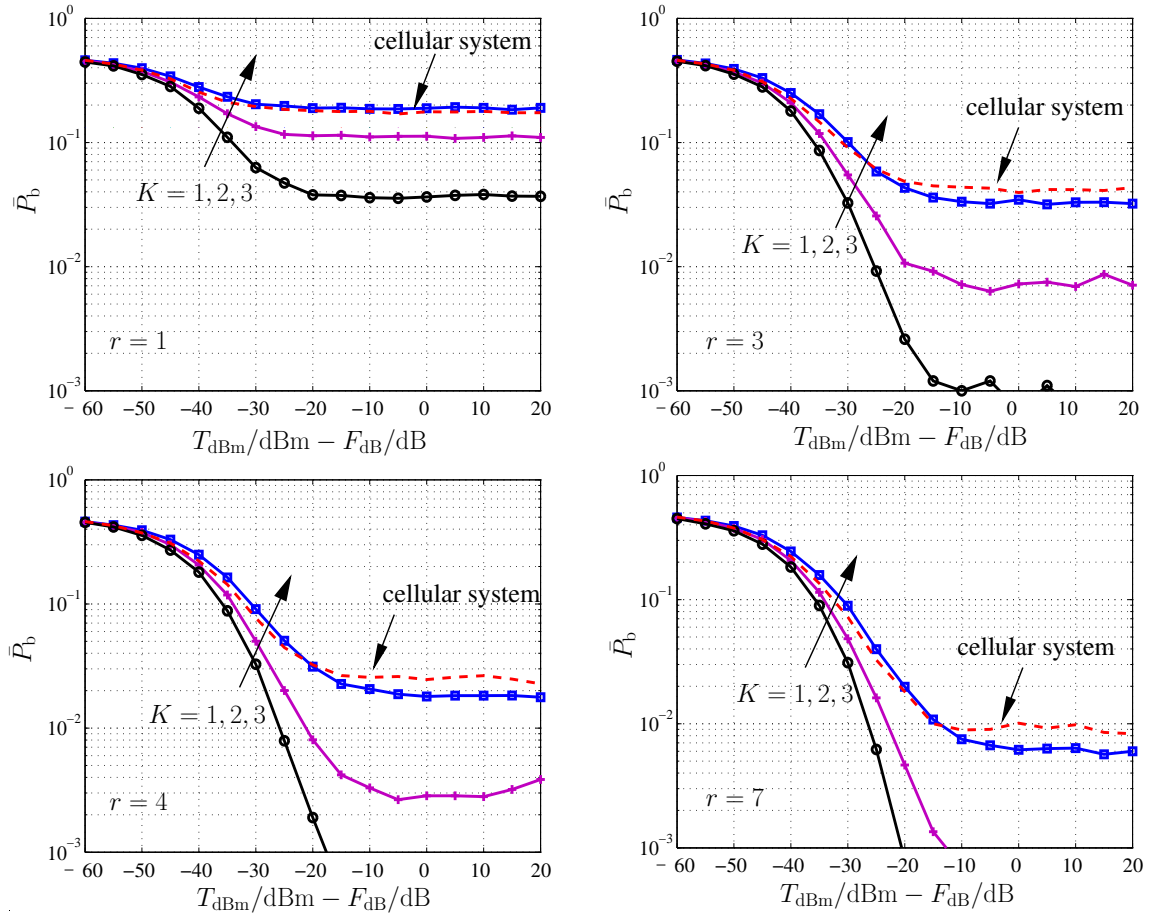
Fig. 9.4. Average BERs $\bar{P}_\mathrm{b}$ in the reference SA in the UL, $K_\mathrm{B} = 3$

based on the knowledge of the CTF matrix $\tilde{\underline{\mathbf{H}}}_{n_\mathrm{F}}^{(n_\mathrm{SA}, n_\mathrm{SA})}$ of (9.5) of the corresponding SA n_SA regardless of the other co–channel SAs n'_SA, the intra–SA MAI is eliminated, while the inter–SA MAI in the multiple–SA scenario remains as a factor degrading the UL or the DL performance, as well as the noise. Meanwhile, the impact of the inter–SA MAI on the average BER performance, which greatly depends on the average transmit energy T_dBm of (9.20) for the given channel model described in Subsection 2.3.2, does not change as the noise varies. Therefore, when the logarithmic noise figure F_dB of (9.20) is very small or the average transmit energy T_dBm of (9.20) is very large, i.e., T_dBm of (9.20) dominates the difference $T_\mathrm{dBm}/\mathrm{dBm} - F_\mathrm{dB}/\mathrm{dB}$ of (9.20), the error floors occur, in the UL and in the DL, respectively.

- It becomes obvious from Figs. 9.4 to 9.6 that as the increase of the number K of MTs per SA the UL performance becomes worse due to the enlarged inter–SA MAI and the extra enhanced noise to eliminate the increased intra–SA MAI
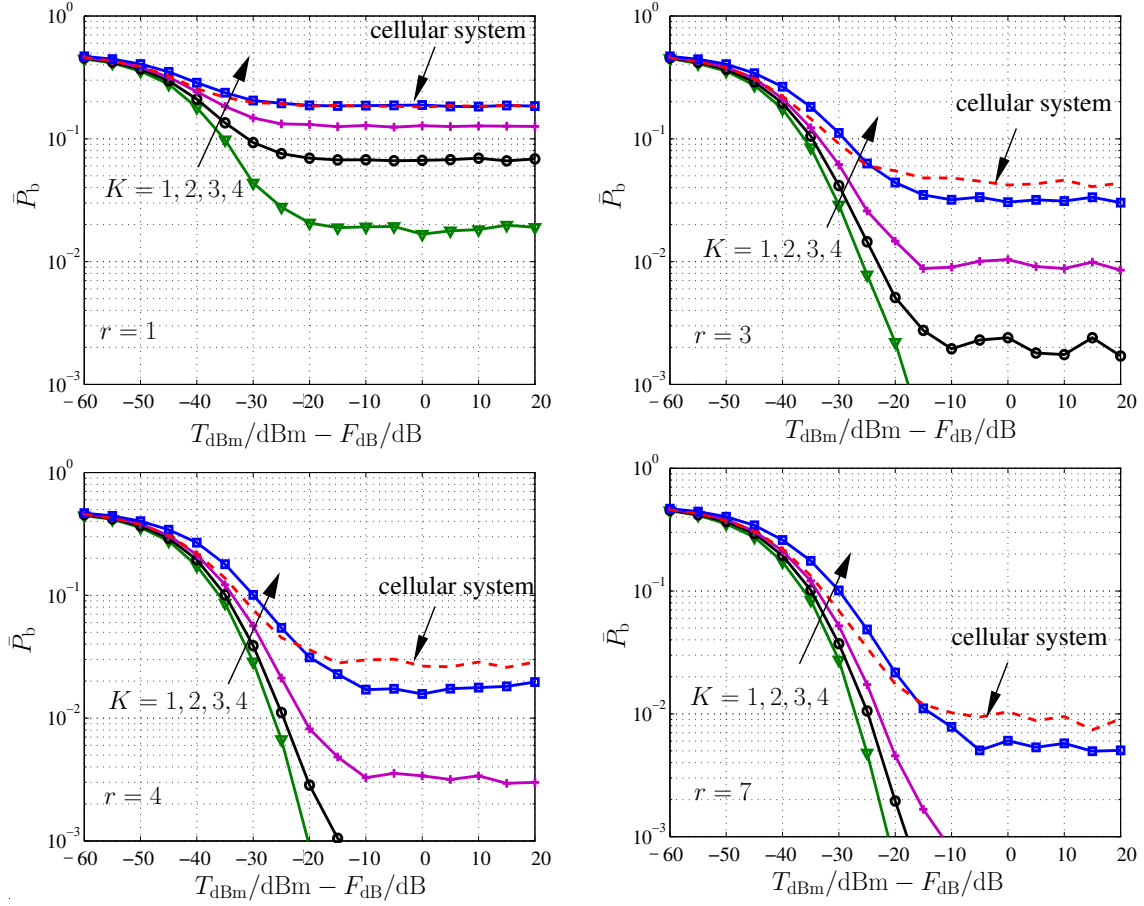
Fig. 9.5. Average BERs $\bar{P}_\mathrm{b}$ in the reference SA in the UL, $K_\mathrm{B} = 4$

[LWZ04] according to (9.9). The DL performance is degraded as well due to the enlarged inter–SA MAI according to (9.17).

- As the increase of the reuse factor r, the average distances between the interferers of the co–channel SAs and the receivers in the reference SA correspondingly increase so that the received inter–SA MAI decreases as well. Consequently the system performance is greatly improved.

- It can bee seen in Figs. 9.4 to 9.6 that for the same number K of MTs per SA and the same reuse factor r, a larger SA size K_B corresponds to a better average BER performance in the UL [LWZ04] as well as in the DL.

- Through the performance comparison of the case of full load, i.e., K equal K_B, of JOINT and the cellular system, whose simulation results are plotted with dashed curves in Figs. 9.4 to 9.6, it is found that with the small–value reuse factor, e.g., r equal to one, the differences between the SA based system performances and
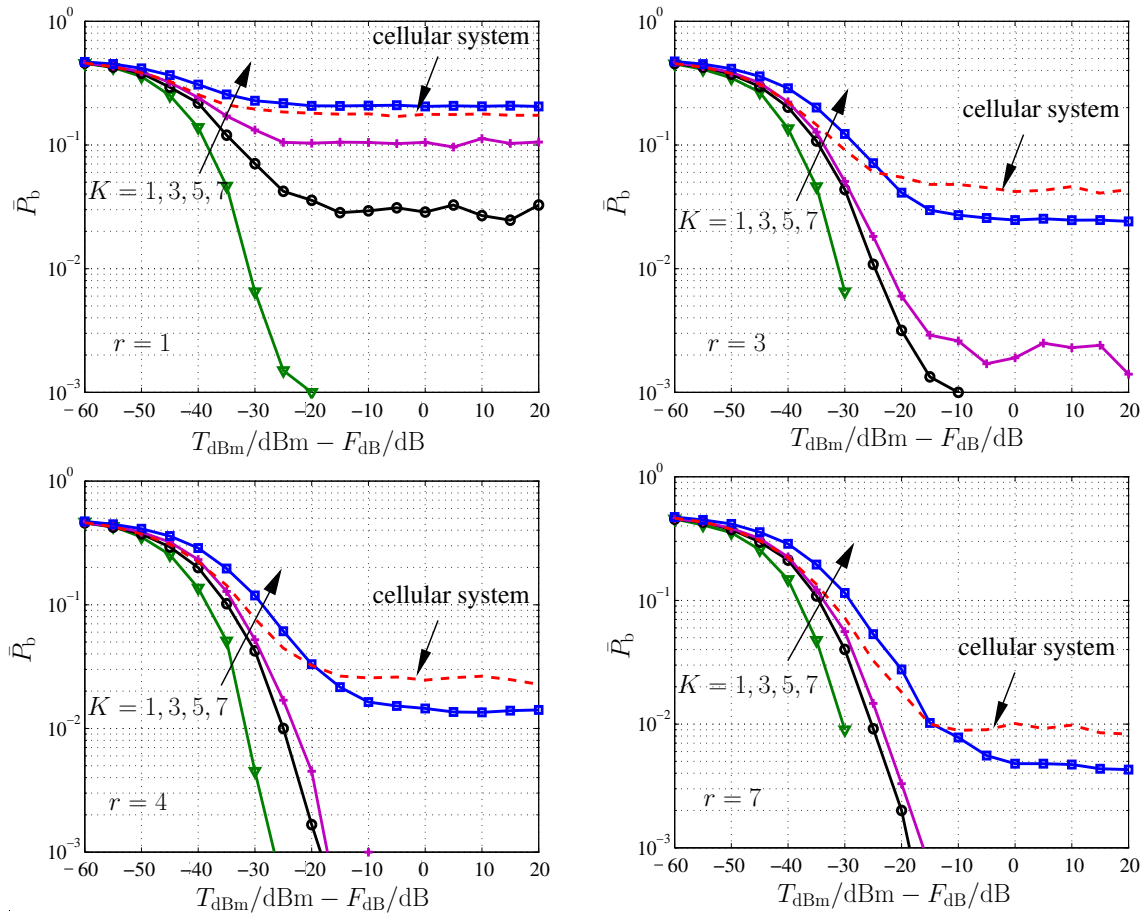
Fig. 9.6. Average BERs $\bar{P}_b$ in the reference SA in the DL, $K_B = 7$

the cellular system performances are very small. In other words, the SA based JOINT does not show advantages over the conventional cellular system for the reuse factor r equal to one. However, as the reuse factor r increases, the $\bar{P}_b$ curves of the SA based system and of the cellular system cross, and the $\bar{P}_b$ curves of the cellular system converge to higher error floors. Moreover, the larger the SA size K_B becomes, the larger the gaps between the error floors of JOINT and the error floors of the cellular system. At the given values of the logarithmic average transmit energy T_{dBm} of (9.21) and of the logarithmic noise figure F_{dB} of (9.22) in the real system, the advantages of JOINT, which is based on the SA concept, over the conventional cellular system in interference elimination is manifested.

9.5   Bit error rate statistics

In Section 9.4 the system performances, in terms of the average BERs, have been discussed for the UL and the DL. However, the $\bar{P}_b$ curves only give us a rough assessment of the system performance of JOINT. Instead of the average BERs, the outage probability P_{out} [FGS03] is a more meaningful quality criterion to evaluate the system performance. The outage probability P_{out} [FGS03] is the probability that the outage occurs if the MT–specific BER P_b, which is the BER averaged only over the noise and the fast fading for the corresponding MT, is greater than a given outage threshold, i.e., a given maximum acceptable BER P_{max}. In order to comprehensively assess JOINT the statistics of the MT–specific BERs P_b in the reference SA are discussed in the following.

Usually for the uncoded transmission, the maximum acceptable BER

$$P_{max} = 0.01 \tag{9.24}$$

is assumed [FGS03]. The outage probability

$$P_{out} = \mathrm{Prob}\,(P_b \geq P_{max} = 0.01) \tag{9.25}$$

not greater than 0.05 [FGS03] is chosen as the quality criterion, e.g., for the system with the given values of the logarithmic average transmit energy T_{dBm} of (9.21) and of the logarithmic noise figure F_{dB} of (9.22).

Fig. 9.7 depicts the BER statistics, in terms of complementary cumulative distribution function (CCDF) curves of the equivalent cellular system, see (9.23), for different reuse factors r in the UL and in the DL, respectively. The UL results are plotted with dashed lines, and the DL results are plotted with solid lines. It can be seen that the CCDF curves in the UL are very close to the CCDF curves in the DL for different reuse factors r. This phenomenon is consistent with the conclusion of Section 8.2 concerning the duality of the UL and the DL with perfect CSI.

Figs. 9.8 to 9.10 depict the CCDF curves of the MT–specific BERs P_b in the reference SA. In each figure, the vertical dashed line indicates the maximum acceptable BER P_{max} of (9.24), and the horizontal dashed line represents the outage probability P_{out} of (9.25). Concerning the CCDF curves, the flatter the curve, the better the system performs. The following points can be seen in Figs. 9.8 to 9.10:

- To fulfill the quality criterion of (9.25) for each case there exists an upper limit of the system load K/K_B, which may be smaller than the full system load K/K_B equal to one.
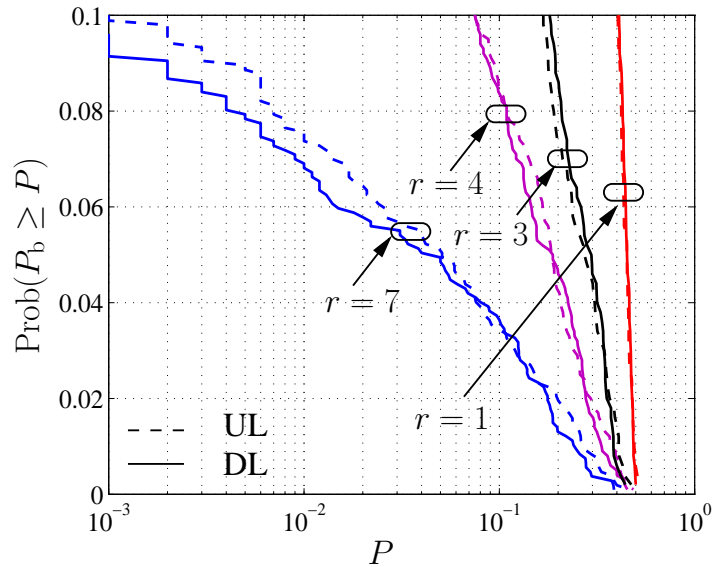
Fig. 9.7. CCDF curves of the BERs P_b, $K_\mathrm{B} = K = 1$

- At the given values of T_dBm of (9.21) and of F_dB of (9.22) the SA based JOINT shows advantages over the cellular system in the interference elimination. Moreover, the larger the SA size K_B becomes, the greater performance improvement can be obtained.

- Increasing the reuse factor r can improve the system performance, however, the usage of frequency resources becomes less efficient.

9.6 Spectrum efficiency

Based on the analysis in Sections 9.4 and 9.5 it is seen that the improved performances of JOINT, in terms of the average BERs and the BER statistics, can be obtained through increasing the SA size r, increasing the reuse factor r or reducing the system load K/K_B, i.e., the system performance could be further improved with the sacrifice of capacity. High capacity is a major challenge for future mobile radio systems. A trade–off between the performance and the capacity has to be made for the system design.

Spectrum efficiency η_c [Ste92, DB96] is a good measure, which links the system performance and the capacity. In conventional cellular system the spectrum efficiency η_c is defined as the ratio of the total data rate per cell and the corresponding bandwidth
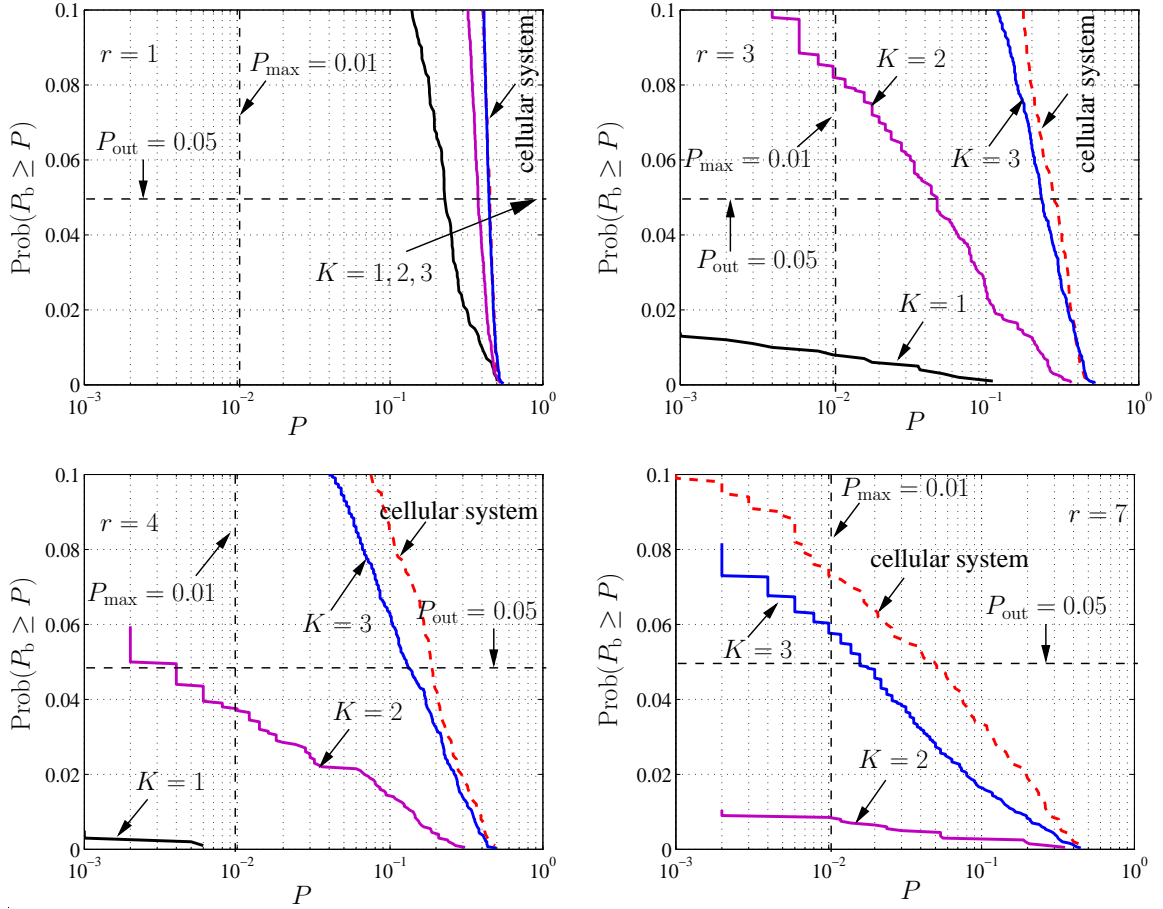
Fig. 9.8. CCDF curves of the BERs P_b in the UL, $K_\mathrm{B} = 3$

used [Ste92, DB96]. To adapt the definition to the SA concept it is fair to consider the spectrum efficiency per AP. With the maximum system load K/K_B fulfilling the quality criterion of (9.25) and the corresponding reuse factor r, with the data rate

$$R_\mathrm{d} = \frac{\text{No. of bits per OFDM symbol}}{\text{OFDM symbol duration}} = \frac{2}{T_\mathrm{s}} = 62.5\,\text{kBits/s} \tag{9.26}$$

per MT per subcarrier and with the bandwidth B equal to the subcarrier spacing Δf_{n_F} of a single subcarrier, the spectrum efficiency

$$\eta_\mathrm{c} = \frac{R_\mathrm{d}\frac{K}{K_\mathrm{B}}}{\Delta f_{n_\mathrm{F}} r} \tag{9.27}$$

is defined based on the analysis of the BER statistics in Section 9.5.

According to (9.27) the spectrum efficiencies η_c are calculated for different combinations of the SA size K_B, the number K of MTs per SA and the reuse factor r. The corresponding results are listed in Tables. 9.1 and 9.2. The symbol "-" in the tables
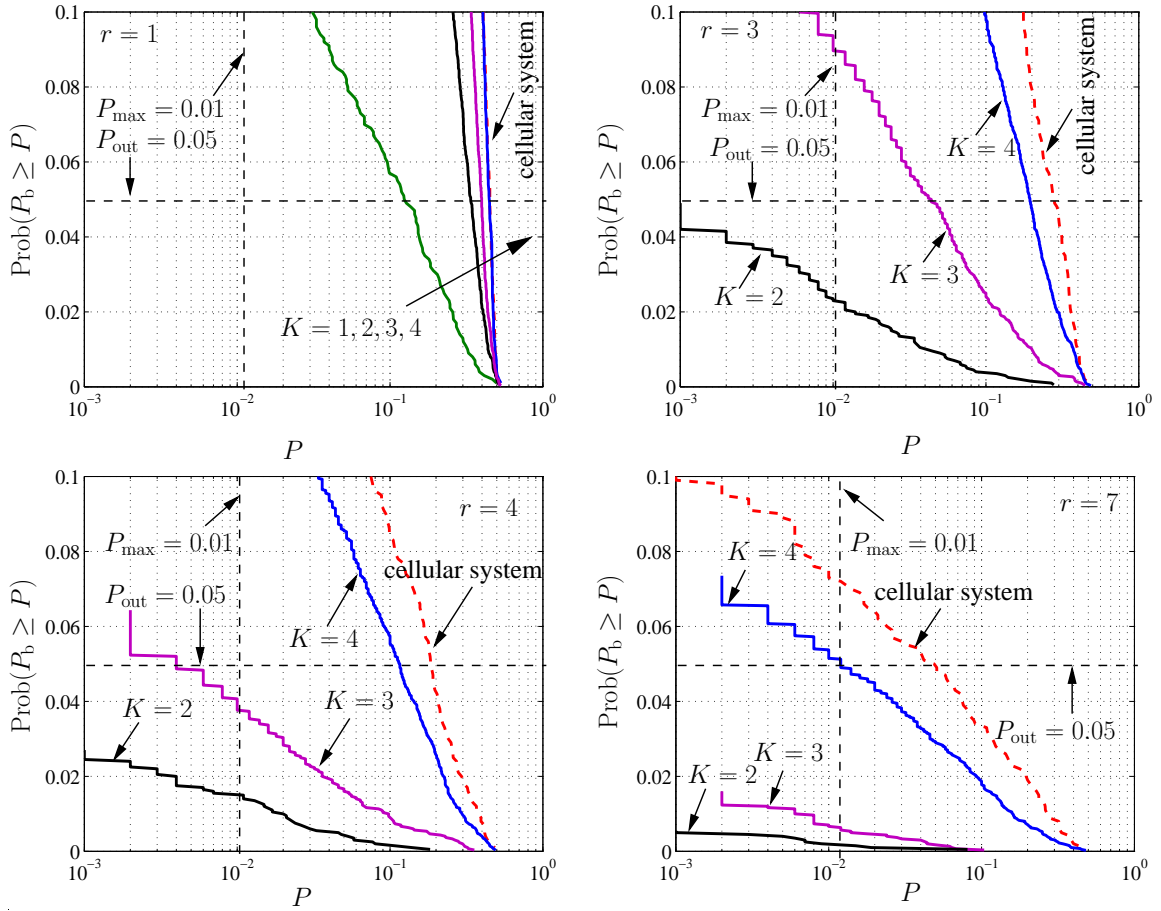
Fig. 9.9. CCDF curves of the BERs P_b in the DL, $K_\mathrm{B} = 4$

means that the corresponding case does not fulfill the criterion of (9.25). For the optimum spectrum efficiency follows

$$\eta_{\mathrm{c,op}} = \max_{\frac{K}{K_\mathrm{B}},r} \eta_\mathrm{c}, \ K_\mathrm{B} = 1, 3, 4, 7, \dots \tag{9.28}$$

for each case of K_B. As listed in Table. 9.3, it can be seen that the SA based JOINT has a great potential for improving the spectrum efficiency η_c compared to the conventional cellular system.
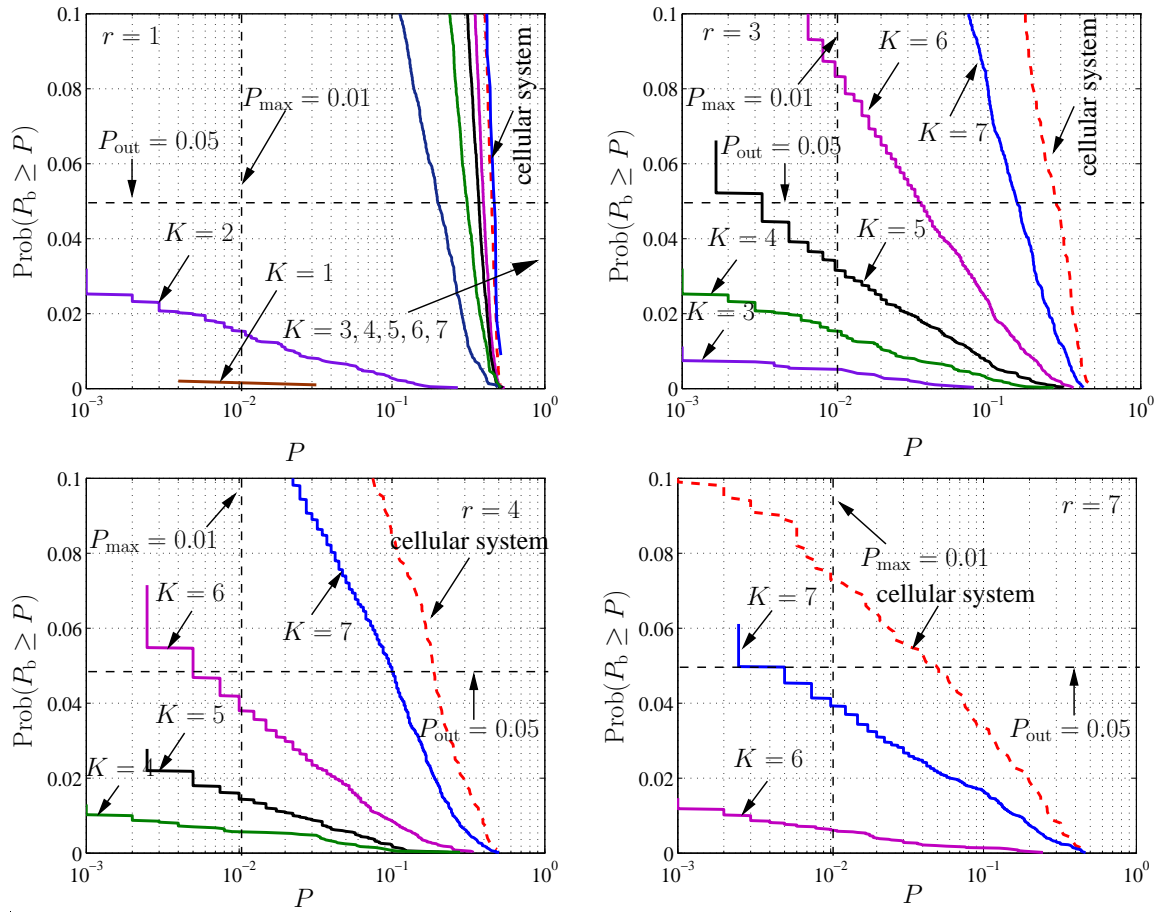
Fig. 9.10. CCDF curves of the BERs P_b in the DL, $K_\text{B} = 7$

Table 9.1. Spectrum efficiencies η_c of the reference system of $K_\text{B} =$ 1 and $K = 1$

	$r = 1$	$r = 3$	$r = 4$	$r = 7$	$r = 9$	$r = 12$
$\frac{\eta_\text{c}}{\text{bits/s/Hz}}$	-	-	-	-	-	0.1333

Table 9.2. Spectrum efficiencies η_c of JOINT

$\frac{K}{K_B} = \frac{1}{3}$	$r = 1$	$r = 3$	$r = 4$	$r = 7$
$\frac{\eta_c}{\text{bits/s/Hz}}$	-	0.1778	0.1333	0.0762
$\frac{K}{K_B} = \frac{2}{3}$	$r = 1$	$r = 3$	$r = 4$	$r = 7$
$\frac{\eta_c}{\text{bits/s/Hz}}$	-	-	0.2667	0.1524
$\frac{K}{K_B} = \frac{3}{3}$	$r = 1$	$r = 3$	$r = 4$	$r = 7$
$\frac{\eta_c}{\text{bits/s/Hz}}$	-	-	-	-
$\frac{K}{K_B} = \frac{1}{4}$	$r = 1$	$r = 3$	$r = 4$	$r = 7$
$\frac{\eta_c}{\text{bits/s/Hz}}$	-	0.1333	0.1	0.0571
$\frac{K}{K_B} = \frac{2}{4}$	$r = 1$	$r = 3$	$r = 4$	$r = 7$
$\frac{\eta_c}{\text{bits/s/Hz}}$	-	0.2667	0.2	0.1143
$\frac{K}{K_B} = \frac{3}{4}$	$r = 1$	$r = 3$	$r = 4$	$r = 7$
$\frac{\eta_c}{\text{bits/s/Hz}}$	-	-	0.3	0.1714
$\frac{K}{K_B} = \frac{4}{4}$	$r = 1$	$r = 3$	$r = 4$	$r = 7$
$\frac{\eta_c}{\text{bits/s/Hz}}$	-	-	-	0.2286
$\frac{K}{K_B} = \frac{1}{7}$	$r = 1$	$r = 3$	$r = 4$	$r = 7$
$\frac{\eta_c}{\text{bits/s/Hz}}$	0.2286	0.0762	0.0571	0.0327
$\frac{K}{K_B} = \frac{2}{7}$	$r = 1$	$r = 3$	$r = 4$	$r = 7$
$\frac{\eta_c}{\text{bits/s/Hz}}$	0.4571	0.1524	0.1143	0.0653
$\frac{K}{K_B} = \frac{3}{7}$	$r = 1$	$r = 3$	$r = 4$	$r = 7$
$\frac{\eta_c}{\text{bits/s/Hz}}$	-	0.2286	0.1714	0.098
$\frac{K}{K_B} = \frac{4}{7}$	$r = 1$	$r = 3$	$r = 4$	$r = 7$
$\frac{\eta_c}{\text{bits/s/Hz}}$	-	0.3048	0.2286	0.1306
$\frac{K}{K_B} = \frac{5}{7}$	$r = 1$	$r = 3$	$r = 4$	$r = 7$
$\frac{\eta_c}{\text{bits/s/Hz}}$	-	0.381	0.2857	0.1633
$\frac{K}{K_B} = \frac{6}{7}$	$r = 1$	$r = 3$	$r = 4$	$r = 7$
$\frac{\eta_c}{\text{bits/s/Hz}}$	-	-	0.3429	0.1960
$\frac{K}{K_B} = \frac{7}{7}$	$r = 1$	$r = 3$	$r = 4$	$r = 7$
$\frac{\eta_c}{\text{bits/s/Hz}}$	-	-	-	0.2286

Table 9.3. Optimum spectrum efficiencies $\eta_{c,op}$

	$K_B = 1$	$K_B = 3$	$K_B = 4$	$K_B = 7$
$\frac{\eta_{c,op}}{\text{bits/s/Hz}}$	0.1333	0.2667	0.3	0.4571

Chapter 10
Summaries

10.1 English

The thesis is focused on modelling and simulation of a Joint Transmission and Detection Integrated Network (JOINT), a novel air interface concept for B3G mobile radio systems. Besides the utilization of the OFDM transmission technique, which is a promising candidate for future mobile radio systems, and of the duplexing scheme time division duplexing (TDD), the subdivision of the geographical domain to be supported by mobile radio communications into service areas (SAs) is a highlighted concept of JOINT. A SA consists of neighboring sub-areas, which correspond to the cells of conventional cellular systems. The signals in a SA are jointly processed in a Central Unit (CU) in each SA. The CU performs joint channel estimation (JCE) and joint detection (JD) in the form of the receive-zero-forcing (RxZF) Filter for the uplink (UL) transmission and joint transmission (JT) in the form of the transmit-zero-forcing (TxZF) Filter for the downlink (DL) transmission. By these algorithms intra-SA multiple access interference (MAI) can be eliminated within the limits of the used model so that unbiased data estimates are obtained, and most of the computational effort is moved from mobile terminals (MTs) to the CU so that the MTs can do with low complexity. A simulation chain of JOINT has been established in the software MLDesigner by the author based on time discrete equivalent lowpass modelling. In this simulation chain, all key functionalities of JOINT are implemented. The simulation chain is designed for link level investigations. A number of channel models are implemented both for the single-SA scenario and the multiple-SA scenario so that the system performance of JOINT can be comprehensively studied. It is shown that in JOINT a duality or a symmetry of the MAI elimination in the UL and in the DL exists. Therefore, the typical noise enhancement going along with the MAI elimination by JD and JT, respectively, is the same in both links. In the simulations also the impact of channel estimation errors on the system performance is studied. In the multiple-SA scenario, due to the existence of the inter-SA MAI, which cannot be suppressed by the algorithms of JD and JT, the system performance in terms of the average bit error rate (BER) and the BER statistics degrades. A collection of simulation results show the potential of JOINT with respect to the improvement of the system performance and the enhancement of the spectrum efficiency as compared to conventional cellular systems.

10.2   Deutsch

Obwohl Mobilfunksysteme der dritten Generation (3G) derzeit noch nicht auf Front im Einsatz sind, sind bereits heute in vielen Teilen der Welt Forschungsaktivitäten in Richtung von Mobilfunksystemen jenseits von 3G (Beyond 3G Systems, B3G) angelaufen. Diese Aktivitäten sind nicht als verfrüht zu bezeichnen, weil erfahrungsgemäß zwischen den ersten Schritten zur Entstehung eines neuen Mobilfunksystems bis zu dessen endgültiger Inbetriebnahme durchaus ein Jahrzehnt oder mehr verstreichen können. Ein wichtiger Aspekt bei der Konzeption von B3G-Mobilfunksystemen ist das Ermöglichen wesentlich höherer Datenraten als es die 2G- und 3G-Systeme gestatten. Zunächst liegt es nahe, das Unterstützen solch höherer Datenraten ausschließlich durch den Einsatz breiterer Frequenzbänder zu ermöglichen. Weil allerdings Übertragungsbandbreite auch künftig ein kostbares Gut sein wird, erfordert das Unterstützen solch höherer Datenraten eine möglichst effiziente Nutzung der Ressource Frequenzbereich, d.h. eine möglichst hohe spektrale Effizienz. Die spektrale Effizienz kann durch Maßnahmen auf verschiedenen Ebenen des ISO/OSI-Referenzmodells gesteigert werden. Grundsätzlich kann man unterscheiden zwischen Maßnahmen auf der physikalischen Ebene, die in vorteilhafter Weise auf die Phänomene der Wellenausbreitung eingehen und diese ausnutzen, und Maßnahme auf höheren Ebenen, die auf eine möglichst optimale Nutzung der von der physikalischen Schicht bereitgestellten Ressourcen abzielen. Bei einem ausgewogenen Systementwurf kommt es auf ein harmonisches Zusammenspiel dieser beiden Klassen von Maßnahmen an, wobei die physikalische Ebene als Basis des Ganzen eine besondere Bedeutung hat. Die vorliegende Dissertation befaßt sich mit einer neuen Architektur der physikalischen Ebene für B3G-Mobilfunksysteme.

Bei der herkömmlichen zellularen Struktur, wie man sie bei den heutigen 2G- und 3G-Systemen vorfindet, sind die mobilen Terminale (MT) einer jeden Zelle im allgemeinen exklusiv der Basisstation (BS) der betreffenden Zelle zugeordnet, wenn man von dem gelegentlich verwendeten Verfahren der "weichen" Übergabe (engl. Soft Handoff) absieht. Diese strukturell einfache Art der Zuordnung ist vorteilhaft hinsichtlich des erforderlichen Signalisierungsaufwands, hat jedoch einige gravierende Nachteile:

- In der Aufwärtsstrecke treffen die von den MTs einer Zelle abgestrahlten Signale nicht nur an der BS der eigenen Zelle ein, sondern unerwünschterweise auch an den BSs anderer Zellen.

- In der Abwärtsstrecke treten die von der BS abgestrahlten Signale nicht nur an den der betreffenden BS zugeordneten MTs auf, sondern unerwünschterweise auch an den MTs anderer BSs.
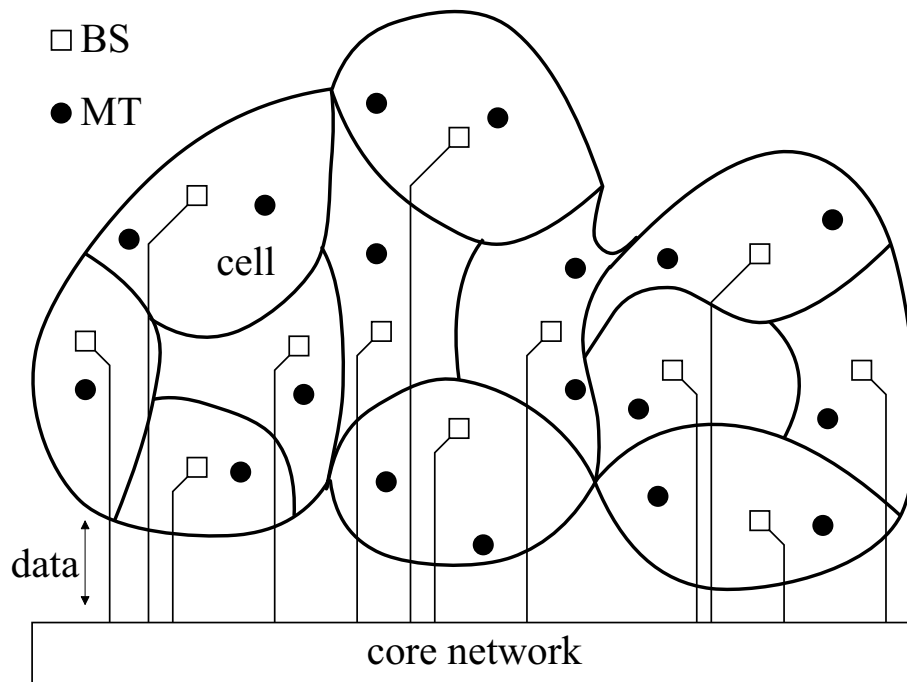
Bild 10.1. Conventionalle zellulare Architektur, Beispiel mit 12 Zellen

Die genannten unerwünschten Signale wirken als Störung und werden als Vielfachzugriffsinterenferenz (engl. Multiple Access Interference, MAI) bezeichnet. Bei herkömmlichen Systemen kann die MAI aus anderen Zellen, die auch als Interzell-MAI bezeichnet wird, nicht unterdrückt oder gar nutzbringend ausgewertet werden, was sich letzten Endes schädlich auf die spektrale Effizienz auswirkt.

In der neuen Architektur, die in dieser Arbeit vorgeschlagen und untersucht wird, geht es um die Milderung des genannten schädlichen Effekts der Interzell-MAI. Hierzu werden in dem System anstelle der individuellen BSs Radiozugangspunkte (engl. Access Point, AP) eingeführt, und Gruppen solcher APs werden mit einer der jeweiligen Gruppe zugeordneten Zentraleinheit (engl. Central Unit, CU) verbunden, z.B. über Leitungen, Glasfasern oder mit Richtfunk. Der geographische Bereich um eine solche Gruppe von APs bildet ein Servicegebiet (engl. Service Area, SA), und die MTs einer jeden SA können mit der CU der SA über die APs der SA kommunizieren. In den Bildern 10.1 und 10.2 sind die konventionelle zellulare bzw. die neue SA-basierte Architektur dargestellt, so daß ein Vergleich dieser beiden Architekturen möglich wird. In der konventionelle zellularen Architektur nach Bild 10.1 kommunizieren die MTs einer Zelle nur mit der BS ihrer Zelle, d.h. nur mit einem einzigen Funkzugangspunkt.

Die grundsätzliche Arbeitsweise der SA-basierten Architektur nach Bild 10.2 kann folgendermaßen charakterisiert werden:
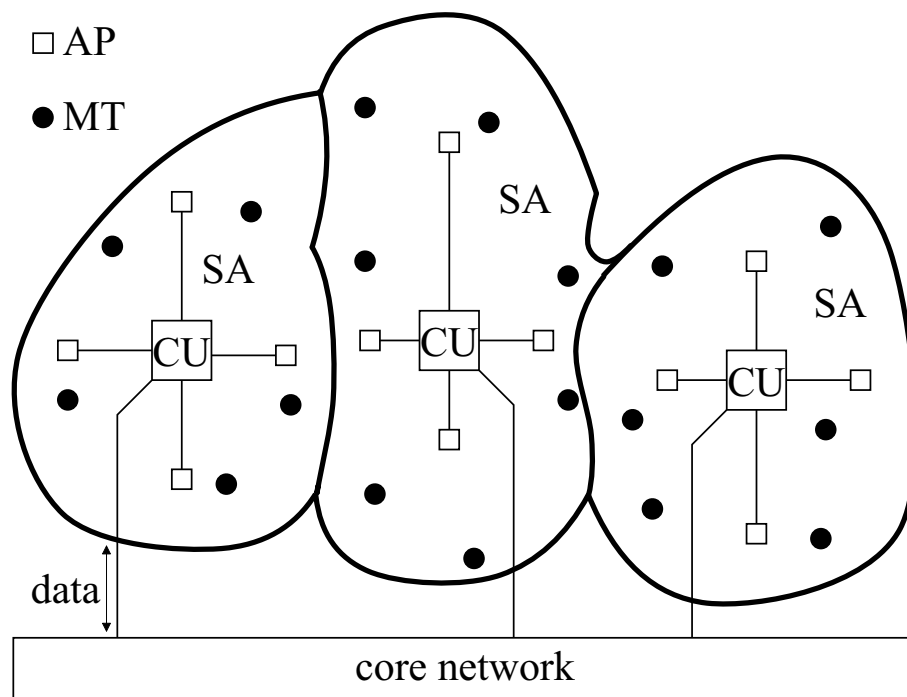
Bild 10.2. Neue SA-basierte Architektur, Beispiel mit drei SAs

- In der Aufwärtsstrecke werden die Sendesignale der MTs der SA von allen APs
  der SA empfangen und zur CU weitergeleitet, wo sie gemeinsam verarbeitet wer-
  den. Das Ziel einer solchen gemeinsamen Verarbeitung besteht im Ausnutzen der
  Empfangsleistungen aller APs derart, daß die gesamte abgestrahlte Leistung in
  der SA und die Komplexität der MTs klein gehalten werden können. Eine solche
  gemeinsame Signalverarbeitung ist unter der Bezeichnung gemeinsame Detektion
  (engl. Joint Detection, JD) bekannt und wird in abgewandelter Form auch schon
  bei manchen 3G-Konzepten eingesetzt.

- In der Abwärtsstrecke wird jede MT der SA durch die Sendesignale aller APs der
  SA unterstützt. Diese Signale werden in der CU gemeinsam erzeugt, und zwar
  derart, daß die gesamte von den APs der SA abgestrahlte Sendeleistung möglichst
  klein wird. Ein hierbei in der CU anwendbares Verfahren der Signalerzeugung
  ist unter der Bezeichnung gemeinsames Senden (engl. Joint Transmission, JT)
  bekannt und ist derzeit in verschiedenen Versionen ein weltweiter Gegenstand der
  Forschung.

Weil der Einsatz von JD und JT wichtige Merkmale der vorgeschlagenen neuen SA-
basierten Architektur sind, wurde für diese die Bezeichnung „ Joint Transmission and
Detection Integrated Network (JOINT)" eingeführt.

Bei der herkömmlichen zellularen Architektur nach Bild 10.1 kann man die MTs einer Zelle durch den Einsatz entsprechender Vielfachzugriffsverfahren so versorgen, daß keine gegenseitigen Störungen innerhalb der Zelle auftreten, d.h. daß es keine Intrazell-MAI gibt. Bei dem Konzept JOINT können die MTs einer ganzen SA so versorgt werden, daß man innerhalb einer jeden SA keine gegenseitigen Störungen durch Interferenz hat, d.h. es gibt keine Intrazell-MAI. Ein Vergleich der Strukturen nach Bild 10.1 und 10.2 zeigt nun, daß bei der SA-basierten Architektur die Anzahl der interferenzfrei versorgbaren MTs wesentlich größer ist als bei der herkömmlichen zellularen Architektur. Dieser Sachverhalt ist der Grund für die im SA-basierten Konzept erwartete höhere spektrale Effizienz.

Im Rahmen der oben beschriebenen SA-basierten Architektur von JOINT hat man beim Systementwurf zahlreiche Freiheitsgrade, z.B. hinsichtlich

- des Vielfachzugriffsverfahrens (FDMA, TDMA, CDMA, SDMA),

- des Übertragungsmodus (Einzelträger- oder Mehrträgerübertragung),

- des Duplexverfahrens (TDD oder FDD), und

- der Antennenanordnungen an den APs und den MTs (Einelement- oder Mehrelementantennen).

Vor dem Hintergrund dieser Freiheitsgrade wird in der vorliegenden Arbeit eine gewisse Auswahl getroffen, die sich an den Rahmenbedingungen orientiert, die sich derzeit in der B3G-Standardisierung abzeichnen. Folgendes wird für die Untersuchungen in dieser Arbeit ausgewählt:

- Vielfachzugriffsverfahren: SDMA,

- Übertragungsmodus: Mehrträgerübertragung, speziell OFDM,

- Duplexverfahren:TDD,

- Antennenanordnung: Ein- oder Mehrelementantennen an den APs, Einelementantennen an den MTs.

Im folgenden wird diese Auswahl kurz begründet. Das Vielfachzugriffsverfahren SDMA ist ein naheliegendes Trennverfahren für räumlich dislozierte MTs, die mit einer Anzahl räumlich ebenfalls dislozierter APs kommunizieren, wie es bei JOINT der Fall ist. Auf den Übertragungsmodus OFDM, der im übrigen ganz generell ein Favorit

im Bereich B3G ist, fiel die Wahl wegen seiner Flexibilität und seines Potentials einer niedrigen Sender- und Empfängerkomplexität. Das Duplexverfahren TDD wurde ausgewählt, weil es Anwendungen mit stark unterschiedlicher Datenraten in Auf- und Abwärtsstrecke unterstützt; mit FDD könnte man solche Asymmetrien nicht ohne weiteres bewältigen. Überdies ermöglicht TDD Vereinfachungen beim Beschaffen der in der CU für die Algorithmen JD und JT erforderlichen Kanalinformation, weil man die Reziprozität der gleichfrequenten Funkkanäle von Auf- und Abwärtsstrecke ausnutzen kann.

Der Entwurf und die Entwicklung von Mobilfunksystemen auf der Grundlage des Konzepts JOINT ist aufgrund der zu bewältigenden Komplexität, der vielfältigen Möglichkeiten der Parameterwahl und der vielen zu beachtenden Randbedingungen eine sehr anspruchsvolle Aufgabe. Diese Aufgabe kann weder allein durch geschlossene Systemberechnungen noch durch Messungen an realisierten Hardware-Funktionsmustern bewältigt werde. Vielmehr ist als eine wesentliche Komponente bei solchen Arbeiten die Systemsimulation auf dem Rechner erforderlich. Hierzu benötigt man hinreichend genaue mathematische Modelle handhabbarer Komplexität aller Systemkomponenten wie z.B. Sender, Empfänger, Antennen, Übertragungskanäle etc. Weiterhin benötigt man, um den eigenen Programmieraufwand in Grenzen zu halten, ein möglichst komfortables und flexibles kommerzielles Simulationswerkzeug. Gegenstand der vorliegenden Arbeit sind die Modellierung und Simulation SA-basierter Übertragungssysteme nach dem Konzept JOINT. Als Werkzeug zum Lösen dieser Aufgaben hat die Verfasserin das Werkzeug MLDesigner ausgewählt. Mit den Ergebnissen ihrer Arbeit hat sie auch zur Weiterentwicklung von JOINT beigetragen, wobei erwähnt werden sollte, daß die Grundlagen der in JOINT verwendeten Algorithmen für die Kanalschätzung sowie zum Durchführen von JD und JT in zwei anderen Promotionsvorhaben gelegt wurden. Das primäres Anliegen in der vorliegenden Arbeit ist das Aufbereiten von JOINT für die Simulationen und das Gewinnen quantitativer Ergebnisse zur Performanzevaluierung und günstigen Parametrisierung von JOINT.

In Systemen wie JOINT senden und empfangen eine Vielzahl von MTs informationstragende Signale über die zeitvarianten und frequenzselektiven Übertragungskanäle zwischen den MTs und den APs. Die daraus resultierende gegenseitige Störung der einzelnen Verbindungen (engl. Muliple Access Interference, MAI) ist der wesentliche Grund für die Begrenztheit der spektralen Effizienz. Bei der Modellierung und Simulation von JOINT spielen deshalb das quantitative Ermitteln und möglichst weitgehende Eliminieren solcher Interferenzen durch JD bzw. JT eine zentrale Rolle. Wichtige durch die Simulation zu beantwortende Fragen betreffen

- die Performanz von JOINT in Auf- und Abwärtsstrecke einer isolierten SA unter

der Voraussetzung perfekter Kanalkenntnis,

- die Auswirkungen nicht perfekter Kanalkenntnis auf die Performanz einer isolierten SA,

- die Auswirkungen von Inter-SA-MAI im Falle eines Verbandes von mehreren SAs.

Kapitel 1 ist die Einleitung der Arbeit. In Kapitel 2 werden die für die Simulation erstellten Kanalmodelle vorgestellt. Kapitel 3 ist der detaillierten mathematischen Modellierung von JOINT gewidmet. Zum Beschreiben von Signalen und Operationen im zeitdiskreten äquivalenten Tiefpaßbereich werden hierbei Vektoren bzw. Matrizen eingeführt. In diesem Kapitel werden auch die bei den späteren Simulationen gewählten Parametersätze zusammengestellt. Kapitel 4 ist speziell dem Problem der Kanalschätzung in JOINT und der Modellierung des entsprechenden Algorithmus JCE (Joint Channel Estimation) gewidmet. Kapitel 5 befaßt sich mit der mathematischen Modellierung des in der Aufwärtsstrecke von JOINT zu wählenden Signalverarbeitungsalgorithmus JD. Hierbei wird auch das Performanzkriterium SNR-Degradation eingeführt, das zum quantitativen Bewerten des durch die Simulationen ermittelten Systemverhaltens geeignet ist. In Kapitel 6 wird in entsprechender Weise der in der Abwärtsstrecke von JOINT zu wählende Algorithmus JT mathematisch modelliert; weiterhin wird in diesem Kapitel ein der SNR-Degradation der Aufwärtsstrecke entsprechendes Performanzkriterium eingeführt. Dieses Kriterium wird als Sendeeffizienz bezeichnet und ist ein Maß für die zum Erzielen einer bestimmten Empfangsqualität erforderliche Sendeleistung in der SA. Kapitel 7 gibt einen umfassenden Überblick über die Implementierung der JOINT-Simulationskette mit dem Werkzeug MLDesigner. Hierbei wird auf möglichst große Flexibilität der Simulationskette abgehoben. Flexibiltät wird durch eine konsequente modulare Anordnung und komfortable Parametereinstellmöglichkeiten erzielt, so daß eine leichte Austauschbarkeit von Simulationsmodulen und ein müheloser Wechsel von Parametern gewährleistet. In Kapitel 8 werden umfangreiche Simulationsergebnisse zur Performanz der Aufwärtstrecke und der Abwärtsstrecke in einer isolierten SA von JOINT präsentiert. Besonderes Augenmerk wird hierbei auf den Einfluß einer fehlerbehafteten Kanalschätzung auf das Systemverhalten gelegt. Kapitel 9 ist schließlich Simulationsergebnissen zum Verhalten von JOINT in einem Verbund mehrerer SAs gewidmet. Es werden Fehlerwahrscheinlichkeiten sowie Wahrscheinlichkeitsdichteverteilungen von Fehlerwahrscheinlichkeiten ermittelt. Auf der Grundlage dieser Ergebnisse kann dann die spektrale Effizienz konventioneller zellularer Systeme und SA-basierter Systeme nach dem Konzept JOINT vergleichen werden. Bei den Simulationen zeigte sich, daß die spektrale Effizienz beim Konzept JOINT je nach Parametrisierung zwei bis drei mal höher ist als beim konventionellen zellularen Konzept. Dieser Vergleich zeigt eindrucksvoll das vorteilhafte

Abschneiden von JOINT.

10.3　Chinese

本篇论文的重点是对 JOINT(Joint Transmission and Detection Integrated Network)，即
联合传输与检测集成网络系统，进行建模与仿真。JOINT 着眼于超三代(Beyond 3G,
B3G)移动通讯系统，是一项崭新的空间接口技术。在性能优越的正交频分复用
(Orthogonal Frequency Division Multiplexing, OFDM)传输技术的基础上，JOINT 采用
了时分复用(Time Devision Duplex, TDD)模式。另外，JOINT 以传统的蜂窝小区(cell)
的概念为基础，对移动通讯系统所覆盖的区域重新进行划分，所形成的服务区
(service areas, SAs)的概念，在 JOINT 中最为引人注目。一个 SA 由相邻的若干子服
务区(sub-areas)构成，其中，sub-areas 在概念上对应于传统蜂窝移动系统中的 cells。
在同一个 SA 内的信号将由该 SA 中的中央控制区(central unit, CU)联合处理。在上行
链路(uplink, UL)中，CU 执行联合信道检测(joint channel estimation, JCE)算法以及联
合数据检测(joint detection, JD)算法；在下行链路(downlink, DL)中，CU 执行联合数
据传输(joint transmission, JT)算法。其中，处于接收端的 JD 和处于发送端的 JT 都采
用了强制归零(zero forcing, ZF)算法。通过上述技术在系统中的应用，可以有效地抑
制同一 SA 内多址干扰(intra-SA multiple access interference, intra-SA MAI)的影响，从
而实现无偏数据估计。与此同时，主要的、复杂的信号处理任务都由 CU 承担，因
此移动终端(mobile terminals, MTs)可以保持轻便的设计。作者在仿真软件
MLDesigner 中完成了对 JOINT 系统的设计与实现。全部关键组件都是建立在时域离
散等效低通的模型基础上，为链路层仿真所设计，适用于单服务区(single-SA)与多
服务区(multiple-SA)、以及不同的信道模型的情况。通过研究发现，在 single-SA 的
情况下，系统在 UL 和 DL 中呈现出某种对称性，即在抑制 intra-SA MAI 方面，JD
和 JT 要付出相同的代价。另外，本文还研究了信道估计的误差对系统性能造成的影
响。针对 multiple-SA 的情况，由于来自其他同频服务区的干扰(inter-SA MAI)无法
通过上述 JD 和 JT 算法消除，系统性能将会有所降低。对仿真结果，特别是关于平
均误码率(bit error rate, BER)和 BER 的统计特性的分析表明，与传统的蜂窝式系统结
构相比，基于 SA 概念上的 JOINT 系统，在提高系统性能和增进频谱利用率等方面
具有很大的潜力，具有非常好的研究与开发前景。

Appendix A

Positions of access points and mobile terminals of Section 9.2

A.1 Preliminary remarks

The method to implement the multiple–SA scenarios described in Section 9.2 is discussed in the following. Since the shape of the sub–areas, which form the SA, is hexagonal, the shape of the SAs might become non–hexagonal. Moreover, the shape of the clusters of the SAs might be non–hexagonal as well. These facts will make the implementation of the scenarios more difficult, especially to locate the APs and the MTs of the co–channel SAs. In the following, with the aid of hierarchical–diamond grids, the positions of the APs and the MTs in the co–channel SAs are generated step by step.

A.2 Positions of access points

A.2.1 Positions of reference access points in co–channel service areas

The positions of the APs in the sub–areas, of the reference APs in the SAs, and of the reference APs in the co–channels SAs are located along three hierarchical–diamond grids, respectively.

At the first level, the APs of all the hexagonal sub–areas are located along the diamond grid, as depicted in Fig. A.1. With R denoting the radius of the hexagonal sub–areas the distance

$$D_1 = \sqrt{3}R \tag{A.1}$$

between the neighboring points along the grid can be obtained for the first–level grid. The rotation angle φ_1 is defined as the angle between the unit vector $\overrightarrow{l_1}$ of the first–level grid and the dashed reference line (RL). E.g., in Fig. A.1 with the initial angle θ_1

$$\varphi_1 = \theta_1 \tag{A.2}$$

holds, where θ_1 is usually assumed to be zero. With (A.1) and (A.2) the two unit vectors of the grid can be expressed as

$$\vec{l_1} = \begin{pmatrix} D_1 \cos \varphi_1 \\ D_1 \sin \varphi_1 \end{pmatrix} = \begin{pmatrix} \sqrt{3}R \cos \theta_1 \\ \sqrt{3}R \sin \theta_1 \end{pmatrix} \tag{A.3}$$

and

$$\vec{l_2} = \begin{pmatrix} D_1 \cos \left(\varphi_1 + \frac{\pi}{3}\right) \\ D_1 \sin \left(\varphi_1 + \frac{\pi}{3}\right) \end{pmatrix} = \begin{pmatrix} \sqrt{3}R \cos \left(\theta_1 + \frac{\pi}{3}\right) \\ \sqrt{3}R \sin \left(\theta_1 + \frac{\pi}{3}\right) \end{pmatrix} \tag{A.4}$$

so that the first–level grid can be totally determined.
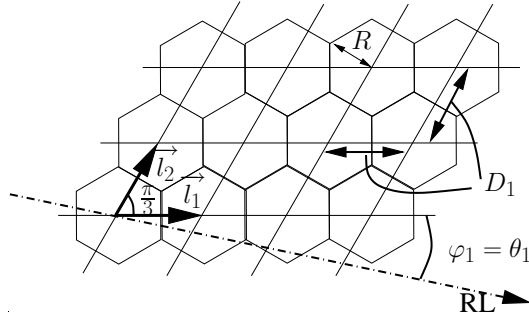
Fig. A.1. First–level grid of all the APs in the sub–areas
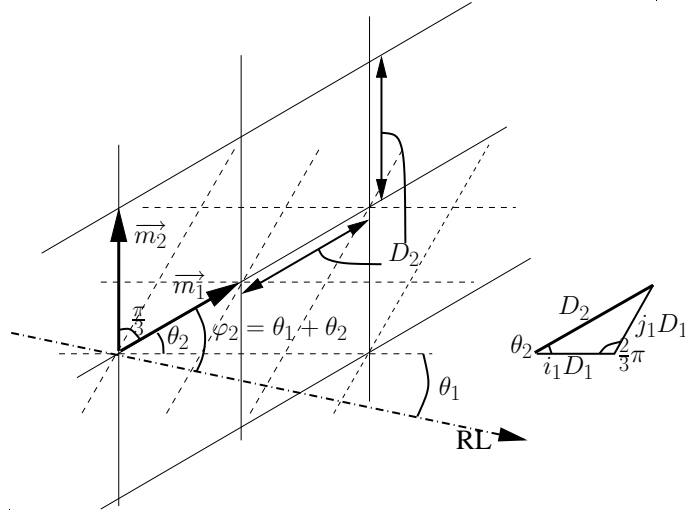

Fig. A.2. Second–level grid of the reference APs in all the SAs

On the second level, the grid, along which the reference APs of all the SAs are located, can be obtained based on the first–level grid. In the scenarios with the hexagonal sub–areas the SA size reads

$$K_{\mathrm{B}} = i_1^2 + j_1^2 + i_1 j_1, \ \ \text{with } i_1, j_1 \in \mathbb{N}_0, i_1 + j_1 \neq 0. \tag{A.5}$$
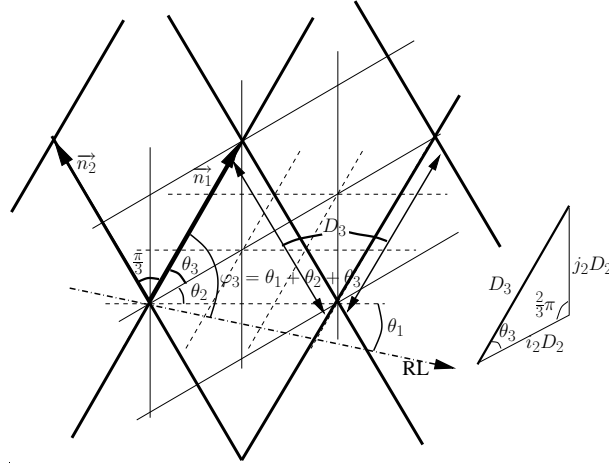
Fig. A.3. Third–level grid of the reference APs in the co–channel
SAs

With (A.1) the distance

$$D_2 = \sqrt{K_\mathrm{B}} D_1 = \sqrt{3K_\mathrm{B}} R \qquad (A.6)$$

between the neighboring points along the grid can be obtained for the second–level grid.
In the triangle depicted on the right of Fig. A.2, according to the geometry property of
triangles [Ton56],

$$(j_1 D_1)^2 = D_2^2 + (i_1 D_1)^2 - 2D_2 \cdot i_1 D_1 \cos \theta_2 \qquad (A.7)$$

holds. With (A.7) the additional rotation angle

$$\theta_2 = \arccos \left(\frac{2i_1 + j_1}{2\sqrt{i_1^2 + j_1^2 + i_1 j_1}} \right) \qquad (A.8)$$

is obtained. For the rotation angle on the second level follows

$$\varphi_2 = \theta_1 + \theta_2. \qquad (A.9)$$

Therefore, with (A.6) and (A.9), the two unit vectors of the second level grid can be
expressed as

$$\vec{m_1} = \left(\begin{array}{c} D_2 \cos \varphi_2 \\ D_2 \sin \varphi_2 \end{array} \right) = \left(\begin{array}{c} \sqrt{3K_\mathrm{B}} R \cos (\theta_1 + \theta_2) \\ \sqrt{3K_\mathrm{B}} R \sin (\theta_1 + \theta_2) \end{array} \right) \qquad (A.10)$$

and

$$\vec{m_2} = \left(\begin{array}{c} D_2 \cos \left(\varphi_2 + \frac{\pi}{3} \right) \\ D_2 \sin \left(\varphi_2 + \frac{\pi}{3} \right) \end{array} \right) = \left(\begin{array}{c} \sqrt{3K_\mathrm{B}} R \cos \left(\theta_1 + \theta_2 + \frac{\pi}{3} \right) \\ \sqrt{3K_\mathrm{B}} R \sin \left(\theta_1 + \theta_2 + \frac{\pi}{3} \right) \end{array} \right) \qquad (A.11)$$

so that the second–level grid can be totally determined.
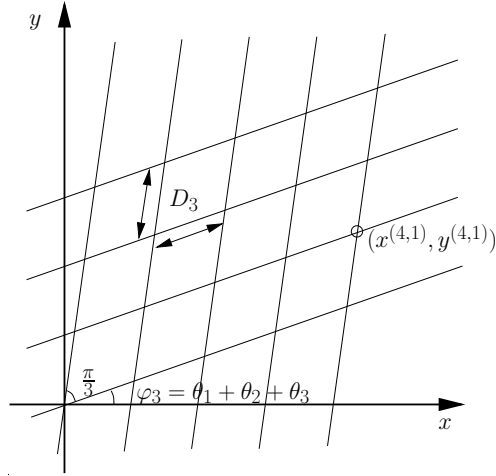
Fig. A.4. Positions $(x^{(i,j)}, y^{(i,j)})$ of the reference APs in the co–channel SAs

On the third level, the grid, along which the reference APs of the co–channel SAs are located, can be obtained based on the second–level grid. In the scenarios with the hexagonal sub–areas the reuse factor reads

$$r = i_2^2 + j_2^2 + i_2 j_2, \quad \text{with} \ i_2, j_2 \in \mathbb{N}_0, i_2 + j_2 \neq 0. \tag{A.12}$$

Therefore, with (A.6) the distance

$$D_3 = \sqrt{r} D_2 = \sqrt{3 K_{\mathrm{B}} r} R \tag{A.13}$$

between the neighboring points along the grid can be obtained for the third–level grid. In the triangle depicted on the right of Fig. A.2, according to the geometry property of triangles [Ton56],

$$(j_2 D_2)^2 = D_3^2 + (i_2 D_2)^2 - 2 D_3 \cdot i_2 D_2 \cos \theta_3 \tag{A.14}$$

holds. With (A.14) the additional rotation angle

$$\theta_3 = \arccos \left(\frac{2 i_2 + j_2}{2 \sqrt{i_2^2 + j_2^2 + i_2 j_2}} \right) \tag{A.15}$$

on the third level is obtained. For the rotation angle on the third level follows

$$\varphi_3 = \theta_1 + \theta_2 + \theta_3. \tag{A.16}$$

With (A.13) and (A.16), the two unit vectors of the third level grid can be expressed as

$$\overrightarrow{n_1} = \begin{pmatrix} D_3 \cos \varphi_3 \\ D_3 \sin \varphi_3 \end{pmatrix} = \begin{pmatrix} \sqrt{3 K_{\mathrm{B}} r} R \cos (\theta_1 + \theta_2 + \theta_3) \\ \sqrt{3 K_{\mathrm{B}} r} R \sin (\theta_1 + \theta_2 + \theta_3) \end{pmatrix} \tag{A.17}$$

and

$$\vec{n_2} = \begin{pmatrix} D_3 \cos\left(\varphi_3 + \frac{\pi}{3}\right) \\ D_3 \sin\left(\varphi_3 + \frac{\pi}{3}\right) \end{pmatrix} = \begin{pmatrix} \sqrt{3K_{\mathrm{B}}r}R \cos\left(\theta_1 + \theta_2 + \theta_3 + \frac{\pi}{3}\right) \\ \sqrt{3K_{\mathrm{B}}r}R \sin\left(\theta_1 + \theta_2 + \theta_3 + \frac{\pi}{3}\right) \end{pmatrix} \tag{A.18}$$

so that the third–level grid can be totally determined.

An arbitrary reference AP, as well as the corresponding SA, can be denoted by a pair of integers (i, j) on the third–level grid, e.g., the indicated reference AP in Fig. A.4 is denoted by $(4, 1)$. With (A.13) and (A.16) the reference AP (i, j) on the third–level grid can be represented with the Cartesian coordinates

$$\begin{aligned} \begin{pmatrix} x^{(i,j)} \\ y^{(i,j)} \end{pmatrix} &= jD_3 \begin{pmatrix} \sin(\frac{\pi}{6} - \varphi_3) \\ \cos(\frac{\pi}{6} - \varphi_3) \end{pmatrix} + iD_3 \begin{pmatrix} \cos\varphi_3 \\ \sin\varphi_3 \end{pmatrix} \\ &= \sqrt{3K_{\mathrm{B}}r}R \begin{pmatrix} j\sin(\frac{\pi}{6} - \varphi_3) + i\cos\varphi_3 \\ j\cos(\frac{\pi}{6} - \varphi_3) + i\sin\varphi_3 \end{pmatrix}. \end{aligned} \tag{A.19}$$

A.2.2 Positions of other access points in co–channel service areas

To locate all the APs in the co–channel SAs, it is necessary to know first the positions of the APs $k_{\mathrm{B}}, k_{\mathrm{B}} = 1 \ldots K_{\mathrm{B}}$, in the SA $(0,0)$. Fig. A.5 depicts the positions of the K_{B} APs in some cases of different SA sizes K_{B}. With (A.19) the position of the AP $k_{\mathrm{B}}, k_{\mathrm{B}} = 1 \ldots K_{\mathrm{B}}$, in the co–channel SA (i, j) can be calculated by

$$\begin{pmatrix} x_{\mathrm{AP}}^{(i,j,k_{\mathrm{B}})} \\ y_{\mathrm{AP}}^{(i,j,k_{\mathrm{B}})} \end{pmatrix} = \begin{pmatrix} x_{\mathrm{AP}}^{(0,0,k_{\mathrm{B}})} \\ y_{\mathrm{AP}}^{(0,0,k_{\mathrm{B}})} \end{pmatrix} + \begin{pmatrix} x^{(i,j)} \\ y^{(i,j)} \end{pmatrix}. \tag{A.20}$$

A.3 Positions of mobile terminals

In [Meu98] the algorithm of generating a random position with uniform distribution in a hexagon was introduced. In this algorithm, a random position $(x_{\mathrm{rand}}, y_{\mathrm{rand}})$, which is uniformly distributed in an equilateral triangle, one of the six components forming the hexagon, is first generated, as depicted in Fig. A.6. Then, by rotation five positions in the other five equilateral triangles can be obtained. Finally, one of the six positions is chosen as the random desired position.

With the aid of the random position $(x_{\mathrm{rand}}, y_{\mathrm{rand}})$ generated by

$$y_{\mathrm{rand}} = \frac{\sqrt{3}}{2}R(1 - \sqrt{u}), \ u \in [0, 1], \tag{A.21}$$
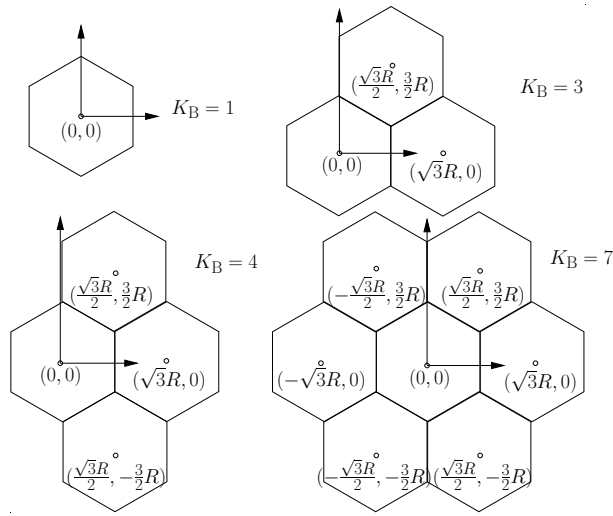
Fig. A.5. Positions $(x_{\mathrm{AP}}^{(0,0,k_{\mathrm{B}})}, y_{\mathrm{AP}}^{(0,0,k_{\mathrm{B}})})$ of the APs k_{B}, $k_{\mathrm{B}} = 1 \ldots K_{\mathrm{B}}$, in the SA (0,0), for different SA sizes K_{B}
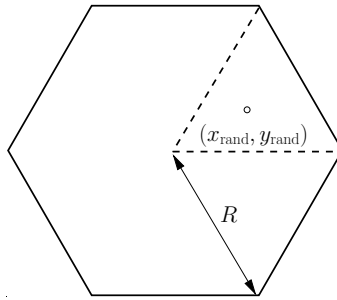
Fig. A.6. Generation of random positions in a hexagon with the aid of a random position $(x_{\mathrm{rand}}, y_{\mathrm{rand}})$ in the dashed–line triangle

and

$$x_{\mathrm{rand}} = \frac{R}{2} + \left(v - \frac{1}{2}\right)\left(R - \frac{2}{\sqrt{3}} y_{\mathrm{rand}}\right), \ v \in [0,1], \qquad (\mathrm{A.22})$$

in the equilateral triangle depicted in Fig. A.6, where random variables u and v are uniformly distributed in the interval $[0, 1]$, with m denoting an integer randomly distributed in the set $\{0, 1, 2, 3, 4, 5\}$ [Meu98] and with (A.20), a possible position

$$\begin{pmatrix} x_{\mathrm{MT}}^{(i,j,k)} \\ y_{\mathrm{MT}}^{(i,j,k)} \end{pmatrix} = \begin{pmatrix} \cos(m\frac{\pi}{3} + \frac{\pi}{6}) & -\sin(m\frac{\pi}{3} + \frac{\pi}{6}) \\ \sin(m\frac{\pi}{3} + \frac{\pi}{6}) & \cos(m\frac{\pi}{3} + \frac{\pi}{6}) \end{pmatrix} \begin{pmatrix} x_{\mathrm{rand}} \\ y_{\mathrm{rand}} \end{pmatrix} + \begin{pmatrix} x_{\mathrm{AP}}^{(i,j,k_{\mathrm{B}})} \\ y_{\mathrm{AP}}^{(i,j,k_{\mathrm{B}})} \end{pmatrix} \quad (\mathrm{A.23})$$

of the MT k, in the sub–area, at whose center the AP k_{B} is located, in the co–channel SA (i, j) [Meu98].

List of frequently used abbreviations and symbols

Abbreviations

2G / 3G	2nd Generation / 3rd Generation
AP	access point
B3G	beyond 3 Generation
BER	bit error rate
CCDF	complementary cumulative distribution function
CDMA	code division multiple access
CIR	channel impulse response
CSI	channel state information
CTF	channel transfer function
CU	central unit
DL	downlink
JCE	joint channel estimation
JD	joint detection
JOINT	Joint Transmission and Detection Integrated Network
JT	joint transmission
LTS	linear transmission system
MA	multiple access
MAI	multiple access interference
MF	matched filter
MIMO	multiple input multiple output
ML	maximum likelihood
MT	mobile terminal
MUD	multiuser detection
OFDM	orthogonal frequency division multiplexing
SA	service area
SNR	signal–to–noise ratio
TDD	Time Division Duplexing
TxZF	transmit zero forcing
UL	uplink
ZF	zero forcing

Symbols

B	system bandwidth
B_{c}	coherence bandwidth
c_0	speed of light in the vacuum
$\underline{\tilde{d}}_{n_{\mathrm{F}}}^{(k)}$	data symbol of the MT k on the subcarrier n_{F} in the general transmission model
$\underline{\hat{\tilde{d}}}_{n_{\mathrm{F}}}^{(k)}$	estimate of the data symbol $\underline{\tilde{d}}_{n_{\mathrm{F}}}^{(k)}$
$\underline{\tilde{d}}_{\mathrm{d},\,n_{\mathrm{F}}}^{(k)}$	DL data symbol of the MT k on the subcarrier n_{F}
$\underline{\hat{\tilde{d}}}_{\mathrm{d},\,n_{\mathrm{F}}}^{(k)}$	estimate of the data symbol $\underline{\tilde{d}}_{\mathrm{d},\,n_{\mathrm{F}}}^{(k)}$
$\underline{\tilde{d}}_{\mathrm{d},\,n_{\mathrm{B}},\,n_{\mathrm{F}}}^{(k)}$	DL data symbol of the MT k on the subcarrier n_{F} at the time slot n_{B}
$\underline{\tilde{d}}_{\mathrm{u},\,n_{\mathrm{F}}}^{(k)}$	UL data symbol of the MT k on the subcarrier n_{F}
$\underline{\hat{\tilde{d}}}_{\mathrm{u},\,n_{\mathrm{F}}}^{(k)}$	estimate of the data symbol $\underline{\tilde{d}}_{\mathrm{u},\,n_{\mathrm{F}}}^{(k)}$
$\underline{\tilde{d}}_{\mathrm{u},\,n_{\mathrm{B}},\,n_{\mathrm{F}}}^{(k)}$	UL data symbol of the MT k on the subcarrier n_{F} at the time slot n_{B}
$\underline{\tilde{\mathbf{d}}}_{n_{\mathrm{F}}}$	subcarrier–specific data vector in the general transmission model
$\underline{\hat{\tilde{\mathbf{d}}}}_{n_{\mathrm{F}}}$	estimate vector of the subcarrier–specific data vector $\underline{\tilde{\mathbf{d}}}_{n_{\mathrm{F}}}$ in the general transmission model
$\underline{\tilde{\mathbf{d}}}_{\mathrm{d}}$	DL total data vector
$\underline{\tilde{\mathbf{d}}}_{\mathrm{d},\,n_{\mathrm{F}}}$	subcarrier–specific DL data vector
$\underline{\hat{\tilde{\mathbf{d}}}}_{\mathrm{d},\,n_{\mathrm{F}}}$	estimate vector of the subcarrier–specific DL data vector $\underline{\tilde{\mathbf{d}}}_{\mathrm{d},\,n_{\mathrm{F}}}$
$\underline{\tilde{\mathbf{d}}}_{\mathrm{d},\,\mathrm{mul},\,n_{\mathrm{F}}}$	subcarrier–specific DL data vector in the multiple–SA scenario
$\underline{\tilde{\mathbf{d}}}_{\mathrm{d},\,n_{\mathrm{B}},\,n_{\mathrm{F}}}$	slot–subcarrier–specific DL data vector
$\underline{\tilde{\mathbf{d}}}_{\mathrm{d},\,n_{\mathrm{F}}}^{(n_{\mathrm{SA}})}$	subcarrier–specific DL data vector of the SA n_{SA}
$\underline{\hat{\tilde{\mathbf{d}}}}_{\mathrm{d},\,n_{\mathrm{F}}}^{(n_{\mathrm{SA}})}$	estimate vector of the subcarrier–specific DL data vector $\underline{\tilde{\mathbf{d}}}_{\mathrm{d},\,n_{\mathrm{F}}}^{(n_{\mathrm{SA}})}$
$\underline{\tilde{\mathbf{d}}}_{\mathrm{u}}$	total UL data vector
$\underline{\tilde{\mathbf{d}}}_{\mathrm{u},\,n_{\mathrm{F}}}$	subcarrier–specific UL data vector
$\underline{\hat{\tilde{\mathbf{d}}}}_{\mathrm{u},\,n_{\mathrm{F}}}$	estimate vector of the subcarrier–specific UL data vector $\underline{\tilde{\mathbf{d}}}_{\mathrm{u},\,n_{\mathrm{F}}}$
$\underline{\tilde{\mathbf{d}}}_{\mathrm{u},\,\mathrm{mul},\,n_{\mathrm{F}}}$	subcarrier–specific UL data vector in the multiple–SA scenario
$\underline{\tilde{\mathbf{d}}}_{\mathrm{u},\,n_{\mathrm{B}},\,n_{\mathrm{F}}}$	slot–subcarrier–specific UL data vector
$\underline{\tilde{\mathbf{d}}}_{\mathrm{u},\,n_{\mathrm{F}}}^{(n_{\mathrm{SA}})}$	subcarrier–specific UL data vector of the SA n_{SA}
$\underline{\hat{\tilde{\mathbf{d}}}}_{\mathrm{u},\,n_{\mathrm{F}}}^{(n_{\mathrm{SA}})}$	estimate vector of the subcarrier–specific UL data vector $\underline{\tilde{\mathbf{d}}}_{\mathrm{u},\,n_{\mathrm{F}}}^{(n_{\mathrm{SA}})}$
$\underline{\tilde{\mathbf{D}}}_{n_{\mathrm{F}}}$	subcarrier–specific detector matrix in the general transmission model
$\underline{\tilde{\mathbf{D}}}_{\mathrm{d},\,n_{\mathrm{F}}}$	subcarrier–specific DL detector matrix
$\underline{\tilde{\mathbf{D}}}_{\mathrm{u},\,n_{\mathrm{F}}}$	subcarrier–specific UL detector matrix
$\underline{\tilde{e}}_{\mathrm{d},\,n_{\mathrm{F}}}^{(k_{\mathrm{B}})}$	DL receive value of the AP k_{B} on the subcarrier n_{F}
$\underline{\tilde{e}}_{\mathrm{u},\,n_{\mathrm{F}}}^{(k)}$	UL data symbol of the MT k on the subcarrier n_{F}
$\underline{\tilde{\mathbf{e}}}_{\mathrm{d}}$	total DL receive vector

$\tilde{\underline{\mathbf{e}}}_{\mathrm{d},\,n_{\mathrm{F}}}$	subcarrier–specific DL receive vector
$\tilde{\underline{\mathbf{e}}}_{\mathrm{d},\,n_{\mathrm{F}}}^{(n_{\mathrm{SA}})}$	subcarrier–specific DL receive vector of the SA n_{SA}
$\tilde{\underline{\mathbf{e}}}_{\mathrm{d},\,\mathrm{mul},\,n_{\mathrm{F}}}$	subcarrier–specific DL receive vector in the multiple–SA scenario
$\tilde{\underline{\mathbf{e}}}_{\mathrm{u}}$	total UL receive vector
$\tilde{\underline{\mathbf{e}}}_{\mathrm{u},\,n_{\mathrm{F}}}$	subcarrier–specific UL receive vector
$\tilde{\underline{\mathbf{e}}}_{\mathrm{u},\,n_{\mathrm{F}}}^{(n_{\mathrm{SA}})}$	subcarrier–specific UL receive vector of the SA n_{SA}
$\tilde{\underline{\mathbf{e}}}_{\mathrm{u},\,\mathrm{mul},\,n_{\mathrm{F}}}$	subcarrier–specific UL receive vector in the multiple–SA scenario
E_{d}	data symbol energy
E_{p}	pilot symbol energy
$\tilde{\underline{\mathbf{E}}}_{n_{\mathrm{B}},\,n_{\mathrm{F}}}$	CTF estimation error matrix of the time slot n_{B} on the subcarrier n_{F}
f_{c}	carrier frequency
$f_{\mathrm{d},\,\mathrm{max}}$	maximum Doppler frequency
$\Delta f_{n_{\mathrm{F}}}$	subcarrier spacing
F	noise figure
F_{dB}	logarithmic noise figure
$\tilde{\boldsymbol{\mathcal{F}}}$	Fourier transform matrix
$\tilde{\boldsymbol{\mathcal{F}}}_{W,\,\mathrm{tot}}$	total Fourier transform matrix
$g(t)$	linear path gain
$G(t)$	logarithmic path gain
$\bar{G}$	average logarithmic path gain
g_{R}	antenna gain at the receiver
g_{T}	antenna gain at the transmitter
$\underline{h}_{w}^{(k,\,k_{\mathrm{B}})}$	w–th tap CIR between the MT k and the AP k_{B}
$\underline{\hat{h}}_{w}^{(k,\,k_{\mathrm{B}})}$	estimate of the CIR $\underline{h}_{w}^{(k,\,k_{\mathrm{B}})}$
$\underline{\tilde{h}}_{n_{\mathrm{F}}}^{(k,\,k_{\mathrm{B}})}$	CTF between the MT k and the AP k_{B} on the subcarrier n_{F}
$\underline{\hat{\tilde{h}}}_{n_{\mathrm{F}}}^{(k,\,k_{\mathrm{B}})}$	estimate of the CTF $\underline{\tilde{h}}_{n_{\mathrm{F}}}^{(k,\,k_{\mathrm{B}})}$
$\underline{\tilde{h}}_{n_{\mathrm{B}},\,n_{\mathrm{F}}}^{(k,\,k_{\mathrm{B}})}$	slot–specific CTF between the MT k and the AP k_{B} on the subcarrier n_{F}
$\underline{\hat{\tilde{h}}}_{n_{\mathrm{B}},\,n_{\mathrm{F}}}^{(k,\,k_{\mathrm{B}})}$	estimate of the slot–specific CTF $\underline{\tilde{h}}_{n_{\mathrm{B}},\,n_{\mathrm{F}}}^{(k,\,k_{\mathrm{B}})}$ the subcarrier n_{F}
$\underline{\mathbf{h}}(t)$	time continuous CIR vector
$\underline{\tilde{\mathbf{h}}}(t)$	time continuous CTF vector
$\underline{\mathbf{h}}^{(k_{\mathrm{B}})}$	AP–specific CIR vector
$\underline{\hat{\mathbf{h}}}^{(k_{\mathrm{B}})}$	estimate vector of the AP–specific CIR vector $\underline{\mathbf{h}}^{(k_{\mathrm{B}})}$
$\underline{\tilde{\mathbf{h}}}^{(k_{\mathrm{B}})}$	AP–specific CTF vector
$\underline{\hat{\tilde{\mathbf{h}}}}^{(k_{\mathrm{B}})}$	estimate vector of the AP–specific CTF vector $\underline{\tilde{\mathbf{h}}}^{(k_{\mathrm{B}})}$
$\underline{\tilde{\mathbf{H}}}_{n_{\mathrm{F}}}$	subcarrier–specific CTF matrix in the general transmission model
$\underline{\tilde{\mathbf{H}}}_{\mathrm{d}}$	DL CTF matrix

$\tilde{\underline{\mathbf{H}}}_{\mathrm{d},\,n_{\mathrm{F}}}$	subcarrier–specific DL CTF matrix
$\tilde{\underline{\mathbf{H}}}_{\mathrm{u}}$	UL CTF matrix
$\tilde{\underline{\mathbf{H}}}_{\mathrm{u},\,n_{\mathrm{F}}}$	subcarrier–specific UL CTF matrix
$\hat{\tilde{\underline{\mathbf{H}}}}_{\mathrm{u},\,n_{\mathrm{F}}}$	estimate matrix of the subcarrier–specific UL CTF matrix $\tilde{\underline{\mathbf{H}}}_{\mathrm{u},n_{\mathrm{F}}}$
$\tilde{\underline{\mathbf{H}}}_{\mathrm{u},\,\mathrm{mul},\,n_{\mathrm{F}}}$	subcarrier–specific UL CTF matrix in the multiple–SA scenario
$\tilde{\underline{\mathbf{H}}}_{n_{\mathrm{B}}}$	slot–specific total UL CTF matrix
$\tilde{\underline{\mathbf{H}}}_{n_{\mathrm{B}},\,n_{\mathrm{F}}}$	slot–subcarrier–specific total UL TF matrix
$\tilde{\underline{\mathbf{H}}}_{n_{\mathrm{F}}}^{(n_{\mathrm{SA}},\,n'_{\mathrm{SA}})}$	subcarrier–specific UL CTF matrix between the MTs of the SA n_{SA} and the APs of the SA n'_{SA}
$\tilde{\underline{\mathbf{H}}}_{n_{\mathrm{B}},n_{\mathrm{F}}}^{(n_{\mathrm{SA}},\,n'_{\mathrm{SA}})}$	slot–subcarrier–specific UL CTF matrix between the MTs of the SA n_{SA} and the APs of the SA n'_{SA}
K	number of MTs per SA
K_{B}	number of APs per SA
K_{I}	number of the inputs of the MIMO channel
K_{O}	number of the outputs of the MIMO channel
$\tilde{\underline{\mathbf{M}}}_{n_{\mathrm{F}}}$	subcarrier–specific modulator matrix in the general transmission model
$\tilde{\underline{\mathbf{M}}}_{\mathrm{d},\,n_{\mathrm{F}}}$	subcarrier–specific DL modulator matrix
$\tilde{\underline{\mathbf{M}}}_{\mathrm{u},\,n_{\mathrm{F}}}$	subcarrier–specific UL modulator matrix
$\tilde{\underline{\mathbf{M}}}_{\mathrm{TxMF},\,n_{\mathrm{F}}}$	subcarrier–specific TxMF modulator matrix
$\tilde{\underline{\mathbf{M}}}_{\mathrm{TxZF},\,n_{\mathrm{F}}}$	subcarrier–specific TxZF modulator matrix
N_{AP}	number of the considered APs in the multiple–SA scenario
N_{MT}	number of the considered MTs in the multiple–SA scenario
N_{SA}	number of the co–channel SAs in the multiple–SA scenario
N_{B}	number of OFDM slots per frame
N_{F}	number of subcarriers
N_{BD}	number of OFDM slots per frame for the DL data transmission
N_{BP}	number of OFDM slots per frame for the pilot transmission
N_{BU}	number of OFDM slots per frame for the UL data transmission
N_{SA}	number of co–channel SAs
$\tilde{\underline{n}}_{\mathrm{d},\,n_{\mathrm{F}}}^{(k_{\mathrm{B}})}$	DL noise value of the MT k_{B} on the subcarrier n_{F}
$\tilde{\underline{n}}_{\mathrm{u},\,n_{\mathrm{F}}}^{(k_{\mathrm{B}})}$	UL noise value of the MT k_{B} on the subcarrier n_{F}
$\tilde{\underline{\mathbf{n}}}_{\mathrm{d}}$	total DL noise vector
$\tilde{\underline{\mathbf{n}}}_{\mathrm{d},n_{\mathrm{F}}}$	subcarrier–specific DL noise vector
$\tilde{\underline{\mathbf{n}}}_{\mathrm{d},\,n_{\mathrm{F}}}^{(n_{\mathrm{SA}})}$	subcarrier–specific DL noise vector of the SA n_{SA}
$\tilde{\underline{\mathbf{n}}}_{\mathrm{d},\,\mathrm{mul},\,n_{\mathrm{F}}}$	subcarrier–specific DL noise vector in the multiple–SA scenario
$\tilde{\underline{\mathbf{n}}}_{\mathrm{u}}$	total DL noise vector
$\tilde{\underline{\mathbf{n}}}_{\mathrm{u},\,n_{\mathrm{F}}}$	subcarrier–specific UL noise vector
$\tilde{\underline{\mathbf{n}}}_{\mathrm{u},\,n_{\mathrm{F}}}^{(n_{\mathrm{SA}})}$	subcarrier–specific UL noise vector of the SA n_{SA}
$\tilde{\underline{\mathbf{n}}}_{\mathrm{u},\,\mathrm{mul},\,n_{\mathrm{F}}}$	subcarrier–specific UL noise vector in the multiple–SA scenario

$\tilde{\underline{p}}_{n_F}^{(k)}$	pilot symbol for the MT k on the subcarrier n_F
$\tilde{\underline{\mathbf{p}}}^{(k)}$	MT–specific pilot vector
$\tilde{\underline{\mathbf{P}}}^{(k)}$	MT–specific pilot matrix
$\tilde{\underline{\mathbf{P}}}$	total pilot matrix
$P_{b,d,n_F}^{(k)}$	bit error probability of the DL data symbol $\tilde{\underline{d}}_{d,n_F}^{(k)}$
$P_{b,d,n_B,n_F}^{(k)}$	bit error probability of the DL data symbol $\tilde{\underline{d}}_{d,n_B,n_F}^{(k)}$
$P_{b,u,n_F}^{(k)}$	bit error probability of the UL data symbol $\tilde{\underline{d}}_{u,n_F}^{(k)}$
$P_{b,u,n_B,n_F}^{(k)}$	bit error probability of the UL data symbol $\tilde{\underline{d}}_{u,n_B,n_F}^{(k)}$
r	reuse factor
R	radius of the hexagonal sub–area
R_d	data rate per MT per subcarrier
$R_{d,n_F}^{(k)}$	useful receive energy of the DL data symbol $\tilde{\underline{d}}_{d,n_F}^{(k)}$
$R_{TxMF,n_F}^{(k)}$	useful receive energy of the DL data symbol $\tilde{\underline{d}}_{d,n_F}^{(k)}$ with TxMF
$R_{TxZF,n_F}^{(k)}$	useful receive energy of the DL data symbol $\tilde{\underline{d}}_{d,n_F}^{(k)}$ with TxZF
$\underline{\mathbf{R}}_{d,d}$	covariance matrix of the data vector $\tilde{\underline{\mathbf{d}}}_{d,n_F}$
$\underline{\mathbf{R}}_{d,u}$	covariance matrix of the data vector $\tilde{\underline{\mathbf{d}}}_{u,n_F}$
$\underline{\mathbf{R}}_{n,d}$	covariance matrix of the noise vector $\tilde{\underline{\mathbf{n}}}_{d,n_F}$
$\underline{\mathbf{R}}_{n,u}$	covariance matrix of the noise vector $\tilde{\underline{\mathbf{n}}}_{u,n_F}$
$\underline{\mathbf{R}}_{\mathbf{\Delta}}$	covariance matrix of the data estimation error vector $\underline{\mathbf{\Delta}}_{n_F}$ in the general transmission model
$\underline{\mathbf{R}}_{\mathbf{\Delta},d}$	covariance matrix of the DL data estimation error vector $\underline{\mathbf{\Delta}}_{d,n_B,n_F}$
$\underline{\mathbf{R}}_{\mathbf{\Delta},u}$	covariance matrix of the UL data estimation error vector $\underline{\mathbf{\Delta}}_{u,n_B,n_F}$
$\tilde{\underline{s}}_{d,n_F}^{(k_B)}$	DL transmit symbol of the AP k_B on the subcarrier n_F
$\tilde{\underline{s}}_{u,n_F}^{(k)}$	UL transmit symbol of the MT k on the subcarrier n_F
$\tilde{\underline{\mathbf{s}}}_d$	DL total transmit vector
$\tilde{\underline{\mathbf{s}}}_{d,n_F}$	subcarrier–specific DL transmit vector
$\tilde{\underline{\mathbf{s}}}_{d,mul,n_F}$	subcarrier–specific DL transmit vector in the multiple–SA scenario
$\tilde{\underline{\mathbf{s}}}_{d,n_F}^{(n_{SA})}$	subcarrier–specific DL transmit vector of the SA n_{SA}
$\tilde{\underline{\mathbf{s}}}_u$	UL total transmit vector
$\tilde{\underline{\mathbf{s}}}_{u,n_F}$	subcarrier–specific UL transmit vector
$\tilde{\underline{\mathbf{s}}}_{u,mul,n_F}$	subcarrier–specific UL transmit vector in the multiple–SA scenario
$\tilde{\underline{\mathbf{s}}}_{u,n_F}^{(n_{SA})}$	subcarrier–specific UL transmit vector of the SA n_{SA}
T	average transmit data symbol energy
T_{dBm}	average transmit data symbol energy in dBm
T_{cp}	cyclic prefix duration
T_s	OFDM symbol duration
T_{oss}	OFDM symbol slot duration
T_{fr}	OFDM frame duration

T_{d}	total transmit anergy
T_{k}	correlation duration
$T_{n_{\mathrm{F}}}^{(k)}$	transmit energy invested for the data symbol $\underline{\tilde{d}}_{n_{\mathrm{F}}}^{(k)}$ in the general transmission model
$T_{\mathrm{d},\,n_{\mathrm{F}}}^{(k)}$	transmit energy invested for the DL data symbol $\underline{\tilde{d}}_{\mathrm{d},\,n_{\mathrm{F}}}^{(k)}$
$T_{\mathrm{u},\,n_{\mathrm{F}}}^{(k)}$	transmit energy invested for the UL data symbol $\underline{\tilde{d}}_{\mathrm{u},\,n_{\mathrm{F}}}^{(k)}$
$T_{\mathrm{TxMF},\,n_{\mathrm{F}}}^{(k)}$	transmit energy invested for the DL data symbol $\underline{\tilde{d}}_{\mathrm{d},\,n_{\mathrm{F}}}^{(k)}$ with TxMF
$T_{\mathrm{TxZF},\,n_{\mathrm{F}}}^{(k)}$	transmit energy invested for the DL data symbol $\underline{\tilde{d}}_{\mathrm{d},\,n_{\mathrm{F}}}^{(k)}$ with TxZF
$v_{\max}$	maximum velocity of MTs
W	dimension of the CIR vector
α_1	the first attenuation exponent in the dual–slope model
α_2	the second attenuation exponent in the dual–slope model
$\gamma_{n_{\mathrm{F}}}^{(k)}$	SNR of the data symbol $\underline{\tilde{d}}_{n_{\mathrm{F}}}^{(k)}$ in the general transmission model
$\gamma_{\mathrm{d},\,n_{\mathrm{F}}}^{(k)}$	SNR of the DL data symbol $\underline{\tilde{d}}_{\mathrm{d},\,n_{\mathrm{F}}}^{(k)}$
$\gamma_{\mathrm{u},\,n_{\mathrm{F}}}^{(k)}$	SNR of the UL data symbol $\underline{\tilde{d}}_{\mathrm{u},\,n_{\mathrm{F}}}^{(k)}$
$\gamma_{\mathrm{MF},\,n_{\mathrm{F}}}^{(k)}$	SNR of the UL data symbol $\underline{\tilde{d}}_{\mathrm{u},\,n_{\mathrm{F}}}^{(k)}$ with RxMF
$\gamma_{\mathrm{ZF},\,n_{\mathrm{F}}}^{(k)}$	SNR of the UL data symbol $\underline{\tilde{d}}_{\mathrm{u},\,n_{\mathrm{F}}}^{(k)}$ with RxZF
$\delta_{n_{\mathrm{F}}}^{(k)}$	SNR degradation of the data symbol $\underline{\tilde{d}}_{n_{\mathrm{F}}}^{(k)}$ in the general transmission model
$\underline{\boldsymbol{\Delta}}_{\mathrm{h},\,\mathrm{n}}^{(k_{\mathrm{B}})}$	AP–specific CTF estimation error vector due to the noise
$\underline{\boldsymbol{\Delta}}_{\mathrm{h},\,n_{\mathrm{B}}}^{(k_{\mathrm{B}})}$	AP–specific CTF estimation error vector due to the time variance
$\underline{\boldsymbol{\Delta}}_{\mathrm{d},\,n_{\mathrm{B}},\,n_{\mathrm{F}}}$	subcarrier–specific DL data estimation error vector
$\underline{\boldsymbol{\Delta}}_{\mathrm{u},\,n_{\mathrm{B}},\,n_{\mathrm{F}}}$	subcarrier–specific UL data estimation error vector
η_{c}	spectral efficiency
$\eta_{\mathrm{c},\,\mathrm{op}}$	optimum spectral efficiency
$\eta_{\mathrm{Tx},\,n_{\mathrm{F}}}^{(k)}$	efficiency of the data symbol $\underline{\tilde{d}}_{n_{\mathrm{F}}}^{(k)}$ at the transmitter side in the general transmission model
$\eta_{\mathrm{Rx},\,n_{\mathrm{F}}}^{(k)}$	efficiency of the data symbol $\underline{\tilde{d}}_{n_{\mathrm{F}}}^{(k)}$ at the receiver side in the general transmission model
$\eta_{\mathrm{Tx},\,\mathrm{d},\,n_{\mathrm{F}}}^{(k)}$	efficiency of the DL data symbol $\underline{\tilde{d}}_{\mathrm{d},\,n_{\mathrm{F}}}^{(k)}$ at the transmitter side
$\eta_{\mathrm{Tx},\mathrm{u},\,n_{\mathrm{F}}}^{(k)}$	efficiency of the UL data symbol $\underline{\tilde{d}}_{\mathrm{u},\,n_{\mathrm{F}}}^{(k)}$ at the transmitter side
$\eta_{\mathrm{Rx},\mathrm{d},\,n_{\mathrm{F}}}^{(k)}$	efficiency of the DL data symbol $\underline{\tilde{d}}_{\mathrm{d},\,n_{\mathrm{F}}}^{(k)}$ at the receiver side
$\eta_{\mathrm{Rx},\mathrm{u},\,n_{\mathrm{F}}}^{(k)}$	efficiency of the UL data symbol $\underline{\tilde{d}}_{\mathrm{u},\,n_{\mathrm{F}}}^{(k)}$ at the receiver side
$\varepsilon_{n_{\mathrm{F}}}^{(k)}$	overall energy efficiency of the data symbol $\underline{\tilde{d}}_{n_{\mathrm{F}}}^{(k)}$ in the general transmission model
$\varepsilon_{\mathrm{d},\,n_{\mathrm{F}}}^{(k)}$	overall energy efficiency of the DL data symbol $\underline{\tilde{d}}_{\mathrm{d},\,n_{\mathrm{F}}}^{(k)}$
$\varepsilon_{\mathrm{u},\,n_{\mathrm{F}}}^{(k)}$	overall energy efficiency of the UL data symbol $\underline{\tilde{d}}_{\mathrm{u},\,n_{\mathrm{F}}}^{(k)}$

κ	Bolzmann's constant
ρ	distance between the transmitter and the receiver
ρ_{B}	break–even–point distance
σ^2	variance of real and imaginary parts of noise
$\sigma^2_{\mathrm{h,n}}$	variance of the CTF estimation errors due to the noise
$\sigma^2_{\mathrm{h,tv}}$	variance of the CTF estimation errors due to the time variance
ρ_{B}	break–even–point distance
$\tau_{\max}$	maximum delay
$\tau_{\min}$	minimum delay
τ_{h}	excess delay
$\tau_{\sup}$	supremum of maximum delays

Literature

[BARY96]   Bach Andersen, J.; Rappaport, T. S.; Yoshida, S.: Propagation measurements and models for wireless communications channels. *IEEE Communications Magazine*, vol. 34, 1996, pp. 42–49.

[Bin90]   Bingham, J. A. C.: Multicarrier modulation for data transmission: An idea whose time has come. *IEEE Communications Magazine*, vol. 28, 1990, pp. 5–14.

[Bin91]   Bingham, J.: *ADSL, VDSL and Multicarrier Modulation*. New York: John Wiley & Sons, 1991.

[Bla98]   Blanz, J. J.: *Empfangsantennendiversität in CDMA-Mobilfunksystemen mit gemeinsamer Detektion der Teilnehmersignale*. Fortschrittberichte VDI, Reihe 10, No. 535. Düsseldorf: VDI-Verlag, 1998.

[BMWT00]   Baier, P. W.; Meurer, M.; Weber, T.; Tröger, H.: Joint transmission (JT), an alternative rationale for the downlink of time division CDMA using multi-element transmit antennas. *Proc. IEEE 6th International Symposium on Spread Spectrum Techniques & Applications (ISSSTA'00)*, vol. 1, Parsippany, 2000, pp. 1–5.

[Cim85]   Cimini, L.: Analysis and simulation of a digital mobile channel using orthogonal division frequency multiplexing. *IEEE Transactions on Communications*, vol. 33, 1985, pp. 665–675.

[COS89]   *COST 207: Digital land mobile radio communications*. Final Report, Office for Official Publications of the European Communities, Luxemburg, 1989.

[COS91]   *COST 231: Urban Transmission Loss Models for Mobile Radio in the 900- and 1800- MHz Bands*. Technical Report COST 231 TD (91) (119, Rev. 2), COST 231, 1991.

[Cou97]   Couch, L. W.: *Digital and Analog Communication Systems, 5th Edition*. Prentice-Hall International, 1997.

[CTC91]   Chow, P.; Tu, J.; Cioffi, J.: Performance evaluation of a multichannel tranceiver system for ADSL and VHDSL services. *IEEE Journal on Selected Areas in Communications*, vol. 9, 1991, pp. 909–919.

[CWKS97]   Chow, P.; Widjada, I.; Kim, J.; Sakai, P.: IEEE 802.11 wireless local area networks. *IEEE Communications Magazine*, vol. 9, 1997, pp. 116–126.

[DB96]   David, K.; Benkner, T.: *Digitale Mobilfunksysteme*. Stuttgart: B. G. Teubner, 1996.

[Doe57]   Doelz, M.: Binary Data Transmission Technique for Linear Systems. *Proc. IRE*, 1957, pp. 656–661.

[EF86]   Effelsberg, W.; Fleischmann, A.: Das ISO-Referenzmodell für offene Systeme und seine sieben Schichten. *Informatik-Spektrum*, vol. 9, 1986, pp. 280–299.

[EKLG+03] El-Khazen, K.; Lefevre, F.; Garrec, D.; Guiraudou, M.; Benali, O.: Beyond 3G demonstrator for enhanced service signaling, discovery and management. *Proc. IEEE Symposium on Computers and Communications (ISCC'2003)*, vol. 2, Kemer-Antalya, 2003, pp. 1367–1372.

[ETS96]   *Radio equipment and systems, high performance radio local area network (HIPERLAN) Type 1*. Technical Report EN 300–652, European Telecommunication and Standardization Institute (ETSI), 1996.

[ETS97a]   *Universal Mobile Telecommunications System (UMTS); Selection procedures for the choice of radio transmission technologies of the UMTS (UMTS 30.03 version 3.1.0)*. Technical Report TR 101 112, European Telecommunication and Standardization Institute (ETSI), 1997.

[ETS97b]   *Digital video broadcasting: Framing structure, channel coding, and modulation for digital terrestial television*. Technical Report EN 300–744, European Telecommunication and Standardization Institute (ETSI), 1997.

[ETS97c]   *Radio broadcasting systems; digital audio broadcasting (DAB) to mobile, portable and fixed receivers*. Technical Report EN 300–401, ed. 2, European Telecommunication and Standardization Institute (ETSI), 1997.

[ETS99]   *Broadband radio access networks (BRAN) HIPERLAN Type 2 technical specification Part 1 – physical layer*. Technical Report DTS/BRAN030003–1, European Telecommunication and Standardization Institute (ETSI), 1999.

[EV97]   Eberspächer, J.; Vögel, H. J.: *GSM Global System for Mobile Communication*. Stuttgart: B. G. Teubner, 1997.

[FGS03]   Fischione, C.; Graziosi, F.; Santucci, F.: Outage performance of power controlled DS-CDMA wireless systems with heteroheneous traffic sources. *Wireless Personal Communications*, vol. 24, 2003, pp. 171–187.

[FK03]   Fazel, K.; Kaiser, S.: *Multi-Carrier and Spread Spectrum Systems*. Chichester: John Wiley & Sons, 2003.

[For72]   Forney, Jr, G. D.: Maximum-likelihood sequence estimation of digital sequences in the presence of intersymbol interference. *IEEE Transactions on Information Theory*, vol. 18, 1972, pp. 363–378.

[Gib99]   Gibson, J. D. (Ed.): *The Mobile Communications Handbook*. Heidelberg: Springer-Verlag, 1999.

[GJM91]   Ghezzi, C.; Jazayeri, M.; Mandrioli, D. (Ed.): *Fundamentals of Software Engineering*. Englewood Cliffs, NJ.: PRENTICE HALL, 1991.

[Hay01]   Haykin, S. (Ed.): *Communication Systems.* Chichester: John Wiley & Sons, 2001.

[HN80]   Hata, M.; Nagatsu, T.: Mobile location using signal strength measurements in a cellular systems. *IEEE Transactions on Vehicular Technology*, vol. 29, 1980, pp. 245–252.

[IEE99]   *IEEE standard for wireless LAN medium access control (MAC) and physical layer (PHY) specifications, High-speed Physical Layer (PHY) in the 5GHz Band.* Technical Report ISO/IEC 8802–11:1999/Amd 1:2000(E), IEEE, 1999.

[Jon95]   Jones, D.: Frequency domain echo cancellation for discrete multitone asymmetric digital subscriber lines tranceivers. *IEEE Transactions on Communications*, vol. 43, 1995, pp. 1663–1672.

[Kam96]   Kammeyer, K. D.: *Nachrichtenübertragung.* Stuttgart: B. G. Teubner, 1996.

[Kle96]   Klein, A.: *Multi-user Detection of CDMA Signals – Algorithms and Their Application to Cellular Mobile Radio.* Fortschrittberichte VDI, Reihe 10, No. 423. Düsseldorf: VDI-Verlag, 1996.

[KMH98]   Kapoor, S.; Marchok, D.; Huang, Y.-F.: Pilot assisted synchronization for wireless OFDM systems over fast time varying fading channels. *Proc. IEEE 48th Vehicular Technology Conference (VTC'98)*, vol. 3, Ottawa, 1998, pp. 2077–2080.

[KS01]   Kammeyer, K.-D.; Schmidt, H.: OFDM: An old idea solves new problems. *Proc. International Symposium on Theoretical Electrical Engineering (ISTET01)*, Linz, 2001, pp. K1–K9.

[LR99]   Liberti, J. C.; Rappaport, T. S.: *Smart Antennas for Wireless Communications: IS-95 and Third Generation CDMA Applications.* Upper Saddle River: Prentice Hall, 1999.

[Lu01]   Lu, Y.: *Contributions to the application of adaptive antennas and CDMA in the TD-CDMA downlink.* Dissertation, Lehrstuhl für hochfrequente Signalübertragung und -verarbeitung, Universität Kaiserslautern, 2001.

[LWZ04]   Liu, Y.; Weber, T.; Zirwas, W.: Uplink performance of a service area based multiuser mobile rario system. *Proc. 9th International OFDM-Workshop (InOWo'04)*, Dresden, 2004, pp. 17–21.

[Man04]   Maniatis, I.: *Joint channel estimation in service area based OFDM air interfaces for beyond 3G mobile radio systems.* Dissertation, Lehrstuhl für hochfrequente Signalübertragung und -verarbeitung, Universität Kaiserslautern, 2004.

[MBL+00]   Meurer, M.; Baier, P. W.; Lu, Y.; Papathanassiou, A.; Weber, T.:
            TD-CDMA downlink: Optimum transmit signal design reduces receiver
            complexity and enhances system performance. *Proc. 7th International
            Conference on Telecommunications (ICT'00)*, vol. 1, Acapulco, 2000, pp.
            300–305.

[MBW+00]   Meurer, M.; Baier, P. W.; Weber, T.; Lu, Y.; Papathanassiou, A.: Joint
            transmission: advantageous downlink concept for CDMA mobile radio
            systems using time division duplexing. *IEE Electronics Letters*, vol. 36,
            2000, pp. 900–901.

[MD79]   Mac Donald, V. H.: The cellular concept. *The Bell System Technical
            Journal*, vol. 58, 1979, pp. 15–41.

[Meu98]   Meurer, M.: Simulatives ermitteln des träger- zu interferenzverhältnisses
            eines digitalen zellularen mobilfunksystems unter ber"ucksichtigung der
            gror"aumigen teilnehmerbewegung. Diplomarbeit, Universität Kaiser-
            slautern, 1998.

[MT03]   MLDesigner Technologies, I.: *MLDesigner Document*. Technical Docu-
            ment, MLDesigner Technologies, Inc, 2003.

[MWSL02]   Maniatis, I.; Weber, T.; Sklavos, A.; Liu, Y.: Pilots for joint channel
            estimation in multi-user OFDM mobile radio systems. *Proc. IEEE 7th
            International Symposium on Spread Spectrum Techniques & Applications
            (ISSSTA'02)*, vol. 1, Prague, 2002, pp. 44–48.

[Nat03]   Natarajan, N.: On systems beyond 3G: requirements and approaches.
            *Proc. International Conference on Communication Technology 2003
            (ICCT2003)*, vol. 2, Beijing, 2003, pp. 1305–1309.

[Ous90]   Ousterhout, J. K.: Tcl: An embeddable command language. *Proc. Pro-
            cessing of USENIX Conference*, Washington, DC., 1990, pp. 133–146.

[Ous94]   Ousterhout, J. K.: *An Introduction to Tcl and Tk*. Redwood City, CA:
            Addison-Wesley Publishing, 1994.

[Pap00]   Papathanassiou, A.: *Adaptive antennas for mobile radio systems using
            Time Division CDMA and joint detection*. Dissertation, Lehrstuhl für
            hochfrequente Signalübertragung und -verarbeitung, Universität Kaiser-
            slautern, 2000.

[Par92]   Parsons, J. D.: *The Mobile Radio Propagation Channel*. London: Pentech
            Press, 1992.

[PR80]   Peled, A.; Ruiz, A.: Frequency Domain Data Transmission Using
            Reduced Computational Complexity Algorithms. vol. 5, Denver, 1980,
            pp. 964–967.

[Pra98]   Prasad, R.: *Universal Wireless Personal Communications*. Boston:
            Artech House, 1998.

[Pro95]   Proakis, J. G.: *Digital Communications.* New York: McGraw-Hill, 1995.

[RCLF89]   Rault, J.; Castelain, D.; Le Floch, B.: The coded orthogonal division multiplexing (COFDM) technique, and its application to digital radio broadcasting towards mobile receivers. *Proc. IEEE Global Telecommunications Conference (GLOBECOM'89)*, vol. 1, Dallas, 1989, pp. 428–432.

[RGG01]   Rohling, H.; Grünheid, R.; Galda, D.: OFDM transmission technique for the 4th generation of mobile communication systems. *Proc. 6th International OFDM-Workshop (InOWo'01)*, Hamburg, 2001, pp. 0–1–0–28.

[Rom95]   Rombach, H. (Ed.): *Software Engineering I, Skript zur Vorlesung.* Kaiserslautern: Universität Kaiserslautern, 1995.

[RS95]   Russel, M.; Stüber, G.: Terrestrial digital video broadcasting for mobile reception using OFDM. *Wireless Personal Communications*, vol. 2, 1995, pp. 45–66.

[RW95]   Redl, S.; Weber, M.: *GSM-Technik und Meßpraxis, Netzeigenschaften, Übertragungsverfahren, praktische Meßtechnik.* München: Franzis-Verlag, 1995.

[SJ67]   Stein, S.; Jones, J. J.: *Modern Communication Principles.* New York: McGraw-Hill, 1967.

[Skl04]   Sklavos, A.: *Service area based OFDM air interfaces for beyond 3G mobile radio systems.* Dissertation, Lehrstuhl für hochfrequente Signalübertragung und -verarbeitung, Universität Kaiserslautern, 2004.

[SMWB01]   Sklavos, A.; Maniatis, I.; Weber, T.; Baier, P. W.: Joint channel estimation in multi-user OFDM systems. *Proc. 6th International OFDM-Workshop (InOWo'01)*, Hamburg, 2001, pp. 3–1–3–4.

[Ste92]   Steele, R.: *Mobile Radio Communications.* London: Pentech Press, 1992.

[Ste96]   Steil, A.: *Spektrale Effizienz digitaler CDMA–Mobilfunksysteme mit gemeinsamer Detektion.* Fortschrittberichte VDI, Reihe 10, No. 437. Düsseldorf: VDI-Verlag, 1996.

[TL97]   Thibault, L.; Le, M.: Performance evaluation of COFDM for digital audio broadcasting part I: Parametric study. *IEEE Transaction On Broadcasting*, vol. 43, 1997, pp. 64–75.

[TNA+01]   Tjelta, T.; Nordbotten, A.; Annoni, M.; Scarrone, E.; Bizzarri, S.; Tokarchuk, L.; Adams, C.; Craig, K.; Dinis, M.: Future broadband radio access systems for integrated services and flexible resource management. *IEEE Communications Magazine*, vol. 39, 2001, pp. 56–63.

[Ton56]   Tonndorf, R.: Englische Aussprache mathematischer Formeln. *Elektronische Rundschau*, vol. 4, 1956, pp. 107–112.

[TWMB01]   Tröger, H.; Weber, T.; Meurer, M.; Baier, P. W.: Performance assessment of joint transmission (JT) multi-user downlinks with multi-element transmit antennas. *European Transactions on Telecommunications*, vol. 12, 2001, pp. 407–415.

[vdBBB+99] van de Beek, J.-J.; Borjesson, P.; Boucheret, M.-L.; Landstrom, D.; Arenas, J.; Odling, P.; Ostberg, C.; Wahlqvist, M.; Wilson, S.: A time and frequency synchronization scheme for multiuser OFDM. *IEEE Journal on Selected Areas in Communications*, vol. 17, 1999, pp. 1900–1914.

[Ver86]   Verdú, S.: Minimum probability of error for asynchronous gaussian multiple-access channels. *IEEE Transactions on Information Theory*, vol. 32, 1986, pp. 85–96.

[Ver98]   Verdú, S.: *Multiuser Detection*. Cambridge: Cambridge University Press, 1998.

[vNAM+99]   van Nee, R.; Awater, G.; Morikura, M.; Takanashi, H.; Webster, M.: Near high-rate wireless LAN standards. *IEEE Communications Magazine*, vol. 12, 1999, pp. 82–88.

[vNP00]   van Nee, R. D. J.; Prasad, R.: *OFDM for Wireless Multimedia Communications*. Boston: Artech House, 2000.

[Wal98]   Walke, B.: *Mobilfunknetze und ihre Protokolle: Grundlagen, GSM, UMTS und andere zellulare Mobilfunknetze*. vol. 1. Stuttgart: B. G. Teubner, 1998.

[WE71]   Weinstein, S. B.; Ebert, P. M.: Data transmission by frequency-division multiplexing using the discrete Fourier transform. *IEEE Transactions on Communications*, vol. 19, 1971, pp. 628–634.

[Wes02]   Wesołowski, K.: *Mobile Communication Systems*. New York: John Wiley & Sons, 2002.

[WLM+03]   Weber, T.; Liu, Y.; Maniatis, I.; Meurer, M.; Costa, E.: Performance of a Multiuser OFDM Mobile Rario System with Joint Detection. *Proc. 8th International OFDM-Workshop (InOWo'03)*, Hamburg, 2003, pp. 191–195.

[WM02]   Wisely, D.; Mitjana, E.: Paving the road to systems beyond 3G - the IST MIND project. *Proc. IEEE 3rd International Symposium on Personal, Indoor and Mobile Radio Communications (PIMRC'02)*, vol. 3, Lisbon, 2002, pp. 1042–1046.

[WM03]   Weber, T.; Meurer, M.: Potential of optimum joint transmission. *Proc. 1. Diskussionssitzung der ITG-Fachgruppe Angewandte Informationstheorie*, Erlangen, 2003.

[WMSL02]   Weber, T.; Maniatis, I.; Sklavos, A.; Liu, Y.:   Joint transmission and detection integrated network (JOINT), a generic proposal for beyond 3G systems. *Proc. 9th International Conference on Telecommunications (ICT'02)*, vol. 3, Beijing, 2002, pp. 479–483.

[WMZ04]   Weber, T.; Meurer, M.; Zirwas, W.:   COST 273 TD (04) 008: Transmit nonlinear zero forcing for OFDM multiuser downlinks. *Proc. COST 273 Workshop*, Athens, Greece, 2004, pp. 2077–2080.

[WSLW03]   Weber, T.; Sklavos, A.; Liu, Y.; Weckerle, M.: The air interface concept JOINT for beyond 3G mobile radio networks. *Proc. 15th International Conference on Wireless Communications (WIRELESS 2003)*, vol. 1, Calgary, 2003, pp. 25–33.

[XBMLS92]   Xia, H.; Bertoni, H.; Macial, L.; Lindsay-Stewart, A.: Radio propagation measurements and modelling for line-of-sight microcellular systems. *Proc. IEEE 42th Vehicular Technology Conference (VTC'92)*, vol. 1, Denver, 1992, pp. 349–354.

Tabellarischer Lebenslauf

Name:	Yin Liu
Adresse:	Kurt-Schumacher-Str. 46
	67663 Kaiserslautern
Geburtsdatum:	26 Oktober 1975
Familienstand:	verheiratet
Staatsangehörigkeit:	chinesisch
Schulausbildung:	September 1982 – Juli 1988 Grundschule in Beijing
	September 1988 – Juli 1994 Gymnasium in Beijing
Hochschulaufnahmenprüfung:	Juli 1994
1. Studium:	September 1994 – Juli 1999
	Studium der Automation
	an der Tsinghua University, Beijing, China
Studienabschluß:	Bachelor of Engineering
2. Studium:	Oktober 1999 – Oktober 2001
	Studium der Elektrotechnik
	an der Technischen Universität Kaiserslautern
Studienabschluß:	Master of Science
Berufstätigkeit:	seit November 2001
	wissenschaftlicher Mitarbeiterin
	am Lehrstuhl für hochfrequente Signalübertragung
	und–verarbeitung der Technischen Universität
	Kaiserslautern